

UNIVERSITY OF OKLAHOMA  
GRADUATE COLLEGE

HARNESSING SMALL-MOLECULE PROTEIN STIMULATION TO DEVELOP NEW  
LEADS FOR RETINAL AND INFECTIOUS DISEASES

A DISSERTATION  
SUBMITTED TO THE GRADUATE FACULTY  
in partial fulfillment of the requirements for the  
Degree of  
DOCTOR OF PHILOSOPHY

By

XIAOZHENG DOU  
Norman, Oklahoma  
2020

HARNESSING SMALL-MOLECULE PROTEIN STIMULATION TO DEVELOP NEW  
LEADS FOR RETINAL AND INFECTIOUS DISEASES

A DISSERTATION APPROVED FOR THE  
DEPARTMENT OF CHEMISTRY AND BIOCHEMISTRY

BY THE COMMITTEE CONSISTING OF

Dr. Adam S. Duerfeldt, Chair

Dr. Helen I. Zgurskaya

Dr. Indrajeet Sharma

Dr. Mark A. Nanny



## Acknowledgements

It has been five years since I started this wonderful journey in the Department of Chemistry at the University of Oklahoma. I remember the joy of starting graduate school and the warm welcome from the department. I have met so many incredible people and had the honor of working in an amazing laboratory that I will forever appreciate.

I must start by thanking my mentor, Dr. Adam Duerfeldt. From taking me into his lab and trusting in me after failure, to reading my terrible manuscripts and correcting my scientific communication so I could mature as a scientist. I learned from Dr. Duerfeldt, not only passion about science but also thinking smart. Dr. Duerfeldt has provided a supportive, transparent, and productive working environment, which is better than what I dreamt of. I also want to thank everyone I have met in the Duerfeldt lab for their encouragement and friendship. Special thanks to Dr. Dinesh Nath for working together on the PPAR project, Dr. Ziwei Hu for guiding me in work and life, and Dr. Catherine Bishop for patiently editing my writing. The memory and spirit of the Duerfeldt lab will always be cherished.

Secondly, I want to thank my committee members, Dr. Indrajeet Sharma, Dr. Elena Zgurskaya, and Dr. Mark Nanny. They were incredible advisors for my academic research and helped me understand my potential. Thank you so much for leading me to where I am now.

Finally, I would like to thank my family and friends for their love, support, and companionship. I must give a special thank you to my parents who have supported me in every aspect of life and having them is my biggest fortune. Also, my wife, Ellen Dou, has been a wonderful and amazing person that has supported me and is currently carrying our first child.

## Table of Contents

### Chapter 1 An Introduction to Small Molecule Agonism of PPARs - A Promising Approach to Treat Retinal Diseases

1.1	Abstract .....	1
1.2	Introduction .....	2
1.2.1	Age-related Macular Degeneration (AMD).....	2
1.2.2	Diabetic Retinopathy (DR) .....	4
1.2.3	Retinopathy of Prematurity (ROP) .....	6
1.2.4	Retinal Diseases: State of Treatment .....	7
1.3	A Case for Targeting PPARs .....	8
1.3.1	PPAR $\beta/\delta$ .....	10
1.3.2	PPAR $\gamma$ .....	11
1.3.3	PPAR $\alpha$ .....	13
1.4	Strategic Promiscuity .....	19
1.4.1	Dual PPAR Regulation .....	19
1.4.2	PPAR and FABP.....	19
1.4.3	PPAR and RXR.....	22
1.5	Conclusion.....	24
1.6	References .....	25

### Chapter 2 First-generation SAR Study of New PPAR $\alpha$ Agonists

2.1	Abstract .....	40
2.2	Rationale for the Development of Y-0452.....	41
2.3	Synthesis and Results of First-generation Analogs.....	44

2.4	Conclusion.....	52
2.5	Methods and Experimental.....	52
2.6	References .....	62
	Appendix 1 Supporting Information to Chapter 2 .....	66
<b>Chapter 3 Pharmacology and Second-generation SAR Studies of Selective PPAR<math>\alpha</math> Agonists</b>		
3.1	Abstract .....	80
3.2	Introduction .....	81
3.3	Results and Discussion.....	81
3.3.1	PK/PD Profile of First-generation Lead .....	81
3.3.2	<i>In vivo</i> Efficacy of First-generation Lead .....	84
3.3.3	Stage I SAR: Linker Extension, C-ring Modification, Carboxylate Location.....	88
3.3.4	Stage II SAR: Strategic Methylation, Metabolism Blocking, Carboxylate Isosteric Replacement .....	93
3.3.5	Additional Assessment of 3.4u .....	97
3.3.6	Stage III SAR: Combining Lessons Learned.....	99
3.3.7	Thermodynamic Binding Profiles.....	101
3.4	Conclusion.....	103
3.5	Experimental Section .....	104
3.5.1	General Synthetic Information.....	104
3.5.2	Biological Assay Protocols.....	133
3.5.3	Pharmacokinetic Analyses .....	134
3.5.4	Docking Protocols.....	138
3.6	References .....	140

Appendix 2 Supporting Information to Chapter 3 .....	143
--	-----

**Chapter 4 Design and Total Synthesis of a Methylene-linked ADEP Analog**

4.1 Caseinolytic Peptidase Proteolytic Subunit (ClpP).....	202
4.2 Acyldepsipeptide (ADEP).....	205
4.3 Addressing the Hydrolysis Issue of ADEP .....	207
4.4 Total Synthesis of Designed Analog .....	208
4.5 Conclusion.....	215
4.6 Experimental Section .....	216
4.7 References .....	224

## List of Figures

<b>Figure 1.1</b> Location of macular damage in diseased eye. -----	3
<b>Figure 1.2</b> Pathology of nonproliferative retinopathy and proliferative retinopathy. -----	5
<b>Figure 1.3</b> ROP results from the abnormal growth of blood vessels, which causes scars and eventually leads to retinal detachment. The position of ROP can be divided into 3 zones. ---	6
<b>Figure 1.4</b> Functional domains and secondary structures of PPARs. -----	9
<b>Figure 1.5</b> Well-known synthetic PPAR $\beta/\delta$ agonists and antagonist. -----	10
<b>Figure 1.6</b> Representative natural product PPAR $\gamma$ ligands. -----	11
<b>Figure 1.7</b> Representative synthetic PPAR $\gamma$ ligands. -----	12
<b>Figure 1.8</b> Synthetic PPAR $\alpha$ agonists -----	14
<b>Figure 1.9</b> Pema fibrate (green) co-crystallized with PPAR $\alpha$ . Binding pocket indicated with gray surface and interacting amino acid depicted in orange. -----	17
<b>Figure 1.10</b> Mechanism of FABP mediated PPAR activation. -----	20
<b>Figure 1.11</b> Compounds listed in <b>Table 1.2</b> . -----	22
<b>Figure 1.12</b> Compounds mentioned for PPAR-RXR interaction. -----	23
<b>Figure 2.1</b> PPAR $\alpha$ agonists referenced in this chapter. -----	41
<b>Figure 2.2</b> General approach of this work -----	42
<b>Figure 2.3</b> Initial evaluation results of <b>2.9-2.14</b> and <b>2.21-2.24</b> for hPPAR $\alpha$ agonism. -----	45
<b>Figure 2.4</b> Biochemical analysis of <b>2.10</b> . -----	47
<b>Figure 2.5</b> A) Co-crystallized (green) and docked (cyan) GW590735. B) Predicted binding pose of <b>2.10</b> . C) Predicted binding pose of <b>2.28</b> . Binding pocket cavity depicted by surface representation, PDBID: 2P54. -----	49



<b>Figure 2.6</b> Compound <b>2.22</b> (blue molecule) docked into the LBD of PPAR $\delta$ (PDBID: 3TKM) and PPAR $\gamma$ (PDBID: 2VV0). -----	51
<b>Figure 3.1</b> Overall strategy for hit optimization and the objective of the studies presented herein. -----	81
<b>Figure 3.2</b> Pharmacokinetic profile of A91 ( <b>3.4a</b> ). -----	83
<b>Figure 3.3</b> Animal studies of A91. -----	84
<b>Figure 3.4</b> Multi-stage approach to structural improvement of A91. Model depicts <b>3.4a</b> (A91) docked to PDBID 2P54. -----	85
<b>Figure 3.5</b> Dose-response curves for <b>3.4u</b> (blue squares, solid line) against PPAR $\alpha$ , PPAR $\delta$ , and PPAR $\gamma$ . Respective controls are provided as black circles/dashed line. -----	93
<b>Figure 3.6</b> Predicted binding modes of <b>3.4b</b> , <b>3.4t</b> , and <b>3.4u</b> , demonstrating the possible effects of methyl installation on the 2- or 3-position of the B ring. -----	94
<b>Figure 3.7</b> Cellular thermal shift assay results for A91 and <b>3.4u</b> . -----	96
<b>Figure 3.8</b> Pharmacokinetic profile of <b>3.4u</b> . -----	98
<b>Figure 3.9</b> Thermodynamic binding profiles of select ligands. -----	102
<b>Figure 3.10</b> Summary of current SAR on the 4-benxyloxy-benzylamino chemotype for PPAR $\alpha$ agonism.-----	103
<b>Figure 4.1</b> Activation: turning on an enzyme or pathway with a small molecule. -----	202
<b>Figure 4.2</b> Structural overview of ClpP and ClpP modulation. -----	204
<b>Figure 4.3</b> ADEP structure and mechanism of action. -----	205
<b>Figure 4.4</b> Overall strategy for the total synthesis. -----	208
<b>Figure 4.5</b> Synthesis of linkage fragment. -----	209
<b>Figure 4.6</b> Synthesis of fragment and assembly of linkage and tripeptide fragment. -----	210

<b>Figure 4.7</b> Comparison of $^1\text{H}$ NMR spectrum between Boc and Cbz protected compounds. --	212
<b>Figure 4.9</b> Cyclization and completion of compound <b>4.4</b> .-----	213
<b>Figure 4.8</b> Selected HMBC correlation for <b>4.16</b> and key correlation between H4 and C23 of <b>4.16</b> optimized for 5.0 Hz.-----	214

## List of Tables

<b>Table 1.1</b> Current anti-VEGF agents-----	4
<b>Table 1.2</b> PPAR ligands interact with FABPs -----	21
<b>Table 2.1</b> Human PPAR agonism of select analogs.-----	46
<b>Table 3.1</b> In vitro activity of <b>3.4a-1<sup>a</sup></b> -----	87
<b>Table 3.2</b> In vitro activity of <b>3.5a, 3.5b, 3.5b*, 3.5f<sup>a</sup></b> -----	88
<b>Table 3.3</b> In vitro activity of <b>3.4m-3.4o</b> -----	89
<b>Table 3.4</b> <i>In vitro</i> activity of <b>3.4p-3.4s</b> -----	90
<b>Table 3.5</b> In vitro activity of <b>3.4t-3.4z</b> -----	92
<b>Table 3.6</b> In vitro activity of carboxylate isosteres <b>3.19a-3.19f</b> -----	95
<b>Table 3.7</b> In vitro activity of phase III analogues -----	100
<b>Table 3.8</b> Thermodynamic Binding Profiles of Selected Ligands with the Ligand Binding Domain of PPAR $\alpha^a$ -----	101
<b>Table 4.1</b> Structure of designed ADEP analogs and activity comparison between ADEP analogs -----	207
<b>Table 4.2</b> NMR Data (500 MHz, CD <sub>3</sub> CN) of <b>4.16<sup>a</sup></b> -----	211

## List of Schemes

<b>Scheme 2.1</b> Synthesis of benzoic acid derivatives <b>2.9-2.14</b> .-----	43
<b>Scheme 2.2</b> Synthesis of <b>2.21-2.24</b> .-----	44
<b>Scheme 2.3</b> Synthesis of derivatives <b>2.26</b> and <b>2.27</b> .-----	48
<b>Scheme 3.1</b> Synthesis of stage I analogues.-----	86
<b>Scheme 3.2</b> Synthesis of <b>3.4p-3.4s</b> .-----	89
<b>Scheme 3.3</b> Synthesis of methylated derivatives <b>3.4t-3.4z</b> .-----	91
<b>Scheme 3.4</b> Synthesis of isostere containing derivatives <b>3.19a-3.19f</b> .-----	94
<b>Scheme 3.5</b> Synthesis of isostere containing derivatives <b>3.20-3.33</b> .-----	99

## List of Abbreviation

ACADM = acyl-CoA dehydrogenase medium chain  
ACCORD = Action to Control Cardiovascular Risk in Diabetes  
AD = Alzheimer's disease  
ADEP = acyldepsipeptide  
AGE = advanced glycation product  
AMD = age-related macular degeneration  
ANGPTL4 = angiopoietin-like-4  
ABCA1 = ATP binding cassette subfamily A member 1

CAR = constitutive androstane receptor  
CBZ = benzyloxycarbonyl  
CCL8 = chemokine ligand 8  
CCL17 = chemokine ligand 17  
CDC = Centers for Disease Control and Prevention  
CETSA = cellular thermal shift assay  
CI = confidence interval  
CLPP = Caseinolytic peptidase proteolytic subunit  
CNS = central nervous system  
CNV = choroidal neovascularization  
CPT1A = carnitine palmitoyltransferase 1A  
CXCL10 = C-X-C motif chemokine 10

DBD = DNA-binding domain  
DHA = docosahexaenoic acid  
DME = diabetic macular edema  
DR = diabetic retinopathy

ETDRS = early treatment diabetic retinopathy study  
ENPEP = glutamyl aminopeptidase  
ERG = electroretinogram

FA = fatty acid  
FABP = fatty acid binding protein  
FENO = fenofibrate  
FENOFA = fenofibric acid  
FGF21 = fibroblast growth factor 21  
FIELD = Fenofibrate Intervention and Event Lowering in Diabetes  
FXR = farnesoid X receptor

HDL-C = high-density lipoprotein cholesterol  
hERG = human ether-á-go-go  
hPPAR = human PPAR  
HRCEC = human retinal capillary endothelial cell  
HRCP = human retinal capillary pericyte

HRMEC = human retinal microvascular endothelial cell  
HUVEC = human umbilical vein endothelial cell

ICAM-1 = intercellular cell adhesion molecule-1  
IL6 = interleukin 6  
ITC = isothermal titration calorimetry

LBD = ligand-binding domain  
LCFA = long-chain fatty acid  
LDL = low-density lipoprotein  
LXR = liver X receptor

MBL2 = mannose-binding lectin 2  
MCP-1 = monocyte chemoattractant protein-1  
MIC = minimal inhibitory concentration  
MRSA = methicillin-resistant *Staphylococcus aureus*  
MS = multiple sclerosis

NCoR1 = nuclear receptor co-repressor 1  
NCoR2 = nuclear receptor co-repressor 2  
NF $\kappa$ B = nuclear factor-kappa B  
NOX4 = NADPH oxidase 4  
NPDR = non-proliferative diabetic retinopathy

OIR = oxygen-induced retinopathy  
OPFB = para-fluorobenzyl

PDR = proliferative diabetic retinopathy  
PEDF = pigment epithelial-derived factor  
PGF = placenta growth factor  
PMB = p-methoxybenzyl  
PPAR = peroxisome proliferator-activated receptor  
PPRE = peroxisome proliferator response element  
PROMINENT = pemafibrate to reduce cardiovascular outcomes by reducing triglycerides in patients with diabetes  
PRSP = penicillin-resistant *Streptococcus pneumoniae*

Rb1 = ginsenoside-Rb1  
RLU = relative light unit  
ROP = retinopathy of prematurity  
ROS = reactive oxygen species  
RPE = retinal pigment epithelium  
RR = risk ratio  
RXR = retinoid X receptor

SAR = structure-activity relationship

Slc25a20 = solute carrier family 25 member 20

SPPARM = selective peroxisome proliferator-activated receptor modulator

STZ = streptozotocin

T2D = type II diabetes

TNF- $\alpha$  = tumor necrosis factor- $\alpha$

TZD = thiazolidinedione

UPLC = Ultra-high-pressure liquid chromatography

VCAM-1 = vascular cell adhesion molecule 1

VEGF = vascular endothelial growth factor

VLDLR = very-low-density lipoprotein receptor

VRE = vancomycin-resistant *Enterococcus faecalis*

WHO = World Health Organization

**Abstract:** This dissertation describes the development of new therapeutic leads for retinal (chapter 1-3) and infectious diseases (chapter 4).

**Development of non-invasive drug leads for retinal diseases.** More than 40% of patients with retinal inflammatory diseases are refractory to the standard of care treatment, direct intraocular injection of anti-VEGF antibodies. The inability to effectively treat these diseases accounts for >20% of healthcare expenditures and impacts the quality of life of >30 million people in the United States alone. Considering population growth rates and aging demographics, the prevalence of retinal diseases continues to increase. Frontline approaches require frequent injections, are destructive, demand specialized facilities, suffer from poor response rates, and produce significant burdens on the healthcare system. Fenofibrate, one of two approved drugs known to agonize peroxisome proliferative-activated receptor alpha (PPAR $\alpha$ ), has demonstrated beneficial effects on DR in several experimental and clinical studies (FIELD and ACCORD). Fenofibrate, however, is a relatively weak PPAR $\alpha$  agonist, exhibits poor selectivity over other PPAR isoforms, exhibits poor distribution to the eye, and suffers from dose-limiting side effects, all of which will preclude its use as a viable therapy for DR. I was charged with developing small molecules with improved potency and selectivity for PPAR $\alpha$  as potential treatments for DR.

Our collaborator identified a 4-carboxy-quinoline (Y-0452) as a chemically distinct PPAR $\alpha$  agonist and inducer. My initial optimization efforts on Y-0452 produced novel PPAR $\alpha$  agonists that exhibit better potency (~10-fold) and efficacy (~1.5-fold increase in agonism) than both fenofibric acid (FA, the active metabolite of fenofibrate) and Y-0452 in our primary luciferase assay. More detailed biochemical evaluation of A91, the top lead from these first-generation studies, by our collaborator confirms typical downstream responses of PPAR $\alpha$  agonism, including PPAR $\alpha$  upregulation, induction of target genes, and inhibition of cell migration. A91 reduces



retinal vascular leakage in diabetic rats – a major culprit behind diabetic macular edema and consequential vision loss. Interestingly, A91 seems to lack signs of hepatomegaly, a common side-effect of fenofibrate that may impose dose-limiting toxicity. These results provide proof-of-concept that the A91 chemotype 1) demonstrates *in vivo* efficacy in a relevant DR model following systemic (i.p) administration, 2) is bioavailable, 3) survives first-pass metabolism and clearance mechanisms well enough to maintain efficacy, and 4) demonstrates a relatively safe profile (no observable toxicity) after daily i.p. injection for one-month. Initial pharmacokinetic assessment of A91 reveals 1) good stability in human and rat microsomes, 2) low clearance, 3) no evidence of irreversible inhibition of any of the five major drug metabolizing CYP450s, and 4) low risk of hERG inhibition. Leveraging our structural modification approach, I developed second generation analogs that exhibit EC<sub>50</sub> values <50 nM with >2,700-fold selectivity for PPAR $\alpha$  over other PPAR isoforms in cellular luciferase assays. To date >200 analogs have been designed, synthesized, and evaluated for PPAR $\alpha$  agonistic properties. This work sets the stage for future SAR campaigns on the developed and new chemotypes and sets a foundation for detailed PK/PD and preclinical assessment.

**Acyldepsipeptide alteration through total synthesis.** Currently, the *status quo* for antibiotic development is to inhibit essential processes in bacteria, thus leading to cell death. The development of chemical probes and antimicrobial agents that operate through pathway/enzyme activation, rather than inhibition, thus provides a clearly differentiated avenue to uncover new biology and represents an innovative therapeutic strategy. In this regard, caseinolytic protease P (ClpP) represents a promising new antibacterial target, as ClpP chemo-activation leads to uncontrolled proteolysis and bactericidal activity. Activation of ClpP has been validated and proven safe *in vivo* as an antibacterial strategy against systemic lethal infections of *Enterococcus*

*faecium*, *E. faecalis*, *Staphylococcus aureus*, and *Streptococcus pneumonia*. In each case, activation of ClpP with a small molecule acyldepsipeptide (ADEP) outperforms clinically utilized antibiotics, including linezolid and ampicillin. Although potent ClpP activators have been identified, the structural diversity of compounds is limited. In addition, poor physicochemical properties, a limited spectrum of utility, and/or susceptibility to drug efflux pumps have hindered the clinical development of known activators. ClpP is a promising target, but new compounds are needed to allow for pre-clinical and clinical validation.

Structure-activity relationship studies of the ADEP scaffold have produced extremely potent analogs against Gram-positive pathogens. However, several physicochemical liabilities have hindered the clinical development of this class. Specifically, hydrolysis of the ADEP depsipeptide ester under basic or acidic conditions has been a major concern regarding this natural product family. One approach to address depsipeptide stability is to replace the ester linkage. Previously, our group provided direct evidence that ester to amide linkage substitution maintained the *in vitro* biochemical activity but resulted in a significant drop in the whole-cell activity, likely due to a disruption of a key intramolecular hydrogen bond interaction thought to influence membrane permeability.

To provide more insight into the influence of the depsipeptide core on whole-cell activity, we hypothesized that a -CH<sub>2</sub>- substitution will improve stability while maintaining the intramolecular hydrogen bond interaction. This new family of ADEP was envisioned to be accessible through a convergent approach comprised of three fragments: tripeptide, linkage, and F-Phe-heptenamide fragments. In a little over 8-months, several synthetic challenges were addressed in order to complete the total synthesis.

# **Chapter 1    An Introduction to Small Molecule Agonism of PPARs - A Promising Approach to Treat Retinal Diseases**

## **1.1    Abstract**

Retinal diseases dramatically impact people's lives and create a substantial burden on the health-care system. Age-related macular degeneration, diabetic retinopathy, and retinopathy of prematurity are leading causes of irreversible blindness. In recent years, the scientific community has made great progress in understanding the pathology of these diseases and recent discoveries have identified promising new treatment strategies. Specifically, compelling biochemical and clinical evidence is arising that small-molecule modulation of peroxisome proliferator-activated receptors (PPARs) represents a promising approach to simultaneously address many of the pathological drivers of these diseases. This has excited academic and pharmaceutical researchers towards developing new and potent PPAR ligands. This dissertation introduction highlights recent developments in PPAR ligand discovery and discusses the molecular implications of targeting PPARs as a therapeutic approach to treating retinal diseases. In addition, we introduce the concept of PPAR/FABP strategic promiscuity as an approach worth considering for improving small-molecule PPAR modulation. The emphasis of this introductory chapter is placed on PPAR $\alpha$  to provide a foundation of knowledge necessary to place the dissertation work in context.

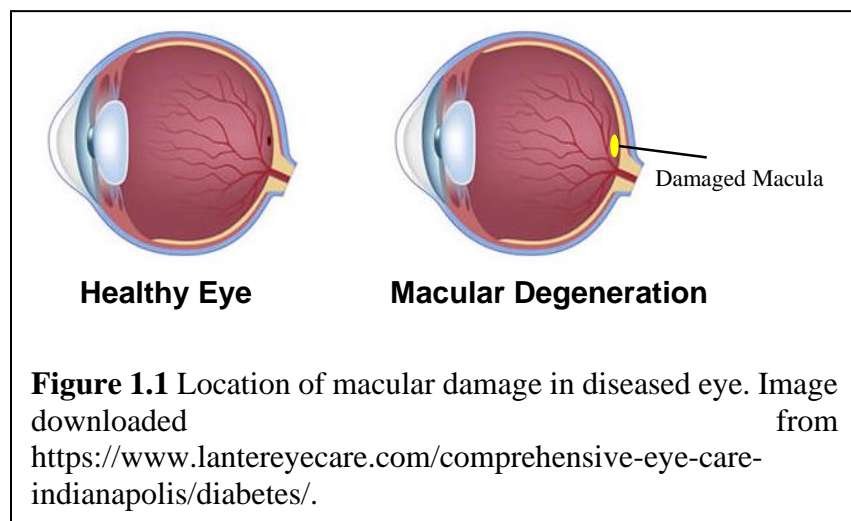
## 1.2 Introduction

Vision provides approximately 80% of the information we acquire from the environment and is arguably the most important sensory function for maintaining a high quality of life. Progressive irreversible blindness or significant visual impairment results in drastic changes to lifestyle that can lead to additional hardships (e.g., financial, familial, logistical), especially in the working-age population. Thus, although visual impairment produces a substantial burden to the health-care system (a total of \$5.8 billion was reimbursed for ophthalmology in 2013 in U.S.), the overall impact is immeasurable.<sup>1</sup> Two diseases that contribute the most to pathological blindness are diabetic retinopathy (DR) and age-related macular degeneration (AMD), both of which result from retinal damage. Additionally, retinopathy of prematurity (ROP), a condition driven by similar pathological features, is becoming a large burden in the neonatal population. The goal of this chapter is to summarize the evidence that small molecule modulation of peroxisome proliferator-activated receptors (PPARs) represents a promising approach to identify new treatments for retinal diseases.

### 1.2.1 Age-related Macular Degeneration (AMD)

AMD is caused by deterioration of photoreceptor cells in the macula due to abnormalities within the retinal pigment epithelium (RPE), leading to central vision loss (**Figure 1.1**).<sup>2-4</sup> Currently, AMD is estimated to affect ~196 million people worldwide. Due to an aging population, this number is expected to climb to ~288 million by 2040.<sup>2,5</sup> Genetic and/or environmental factors are both thought to play significant roles in AMD. During the earliest stages of AMD, insoluble extracellular aggregates, called drusen, form in the retina but no signs of RPE abnormalities or vision loss are apparent.<sup>3,4</sup> In the intermediate stages of AMD, drusen enlarge, resulting in RPE abnormalities and increasing the risk for progression to late AMD.<sup>3,4,6</sup> Patients with late stage

AMD have one of two forms, geographic atrophy (i.e., dry AMD), or neovascular (i.e., wet AMD), either of which results in progressive vision loss. In dry AMD, degeneration of RPE cells leads to the destruction of light-sensing retinal photoreceptors, resulting in gradual vision loss.<sup>3,5,6</sup> In contrast, acute vision loss resulting from wet AMD arises from the abnormal growth of blood vessels in choroids, termed choroidal neovascularization (CNV).<sup>2,3,6</sup> Overall, the pathobiology of AMD is multi-faceted and involves: oxidative damage, lipofuscin accumulation, impaired activity or function of the RPE, increased apoptosis, abnormal immune system activation, senescent loss of homeostatic control, and/or abnormalities in Bruch's membrane.<sup>3,5</sup>



In 2006, the US Food and Drug Administration approved Ranibizumab (Lucentis, Genentech), a vascular endothelial growth factor A (VEGF-A) antibody, providing a breakthrough for the treatment of AMD.

VEGF is a signaling protein produced by cells that stimulates the formation of blood vessels and is comprised of five members VEGF-A, VEGF-B, VEGF-C, VEGF-D, and placenta growth factor (PGF).<sup>7</sup> Specifically, VEGF-A has been implicated in CNV and the increased vascular permeability that results in eventual loss of vision, and thus is recognized as a central contributor to the pathology of wet AMD.<sup>3</sup> FDA-approved anti-VEGF agents now include pegaptanib sodium (Macugen, Eyetech/Pfizer), ranibizumab (Lucentis, Genentech/Roche), aflibercept (Eylea,

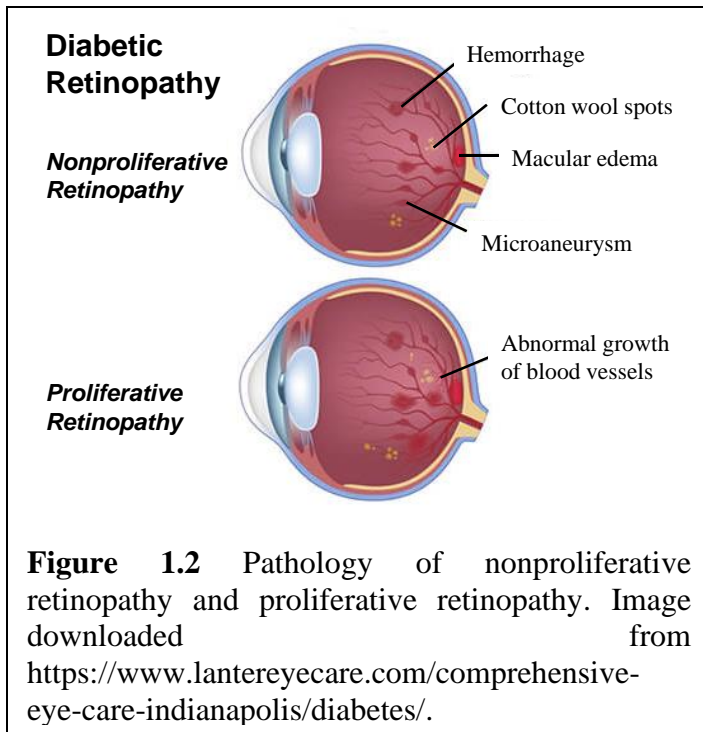
<b>Drug (brand name)</b>	<b>Sponsor</b>	<b>Indications</b>
<b>Pegaptanib sodium (Macugen)</b>	Eyetechnology/Pfizer	Neovascular AMD
<b>Ranibizumab (Lucentis)</b>	Genentech/Roche	Neovascular AMD
<b>Aflibercept (Eylea)</b>	Regeneron	AMD, macular edema, and DR
<b>Bevacizumab (Avastin)</b>	Genentech	Neovascular AMD

Regeneron) and bevacizumab (Avastin, Genentech) (**Table 1.1**).<sup>3</sup> It is interesting to note that bevacizumab is much cheaper (\$50/dose) than ranibizumab (\$2000/dose) and exhibits a similar improvement of visual acuity (7.8% compared to ranibizumab as 8.8%), but is only considered an “off-label” treatment by the FDA.<sup>8</sup>

Although anti-VEGF approaches have drastically improved the quality of life for many patients with wet AMD, patients with dry AMD remain refractory to this strategy.<sup>5</sup> In fact, there is no treatment available to prevent or reverse the progression of dry AMD. Moreover, long-term anti-VEGF treatment has now revealed various complications, such as endophthalmitis, retinal and retinal pigment epithelial detachment, retinal pigment epithelial tears, anterior chamber inflammation, increased intraocular pressure, and intraocular hemorrhage.<sup>9</sup>

### **1.2.2 Diabetic Retinopathy (DR)**

DR is one of the most common comorbidities of diabetes and the primary reason for vision impairment worldwide. The number of patients globally with DR is estimated to exceed 160 million people.<sup>10,11</sup> Considering the growing prevalence of diabetes, DR will continue to produce a large burden on healthcare until new countermeasures are developed. To this point, the World Health Organization (WHO) has called for global action to halt the increase of diabetes by 2025 and improve care for complications arising from diabetes.<sup>12</sup> Diabetic macular edema (DME), caused by retinal vascular leakage and neovascularization, is the major pathological feature responsible for DR-induced vision loss (**Figure 1.2**).<sup>13</sup> DME leads to retinal ischemia and increased levels of VEGF, which results in the development of aberrant neovascularization. The



severity of DR is classified into two categories, non-proliferative diabetic retinopathy (NPDR) and proliferative diabetic retinopathy (PDR). NPDR comprises the early stage of DR and is characterized by micro-aneurysms, retinal hemorrhages, and exudates. Abnormal retinal blood vessel formation synergizes with an increase of intraocular VEGF-levels, eventually leading to PDR, characterized by

aberrant neovascularization. If neovascularization is left untreated, vitreous hemorrhage and retinal detachment occurs, eventually producing extensive retinal damage and blindness. Accumulating evidence suggests that DR is also a chronic inflammatory disorder, as multiple pro-inflammatory factors such as tumor necrosis factor- $\alpha$  (TNF- $\alpha$ ), intercellular cell adhesion molecule-1 (ICAM-1), and VEGF are over-expressed in the diabetic retina.<sup>13</sup> Retinal inflammation plays a causative role in impaired vascular endothelium, pericyte loss, vascular leakage and later retinal neovascularization.<sup>13-15</sup>

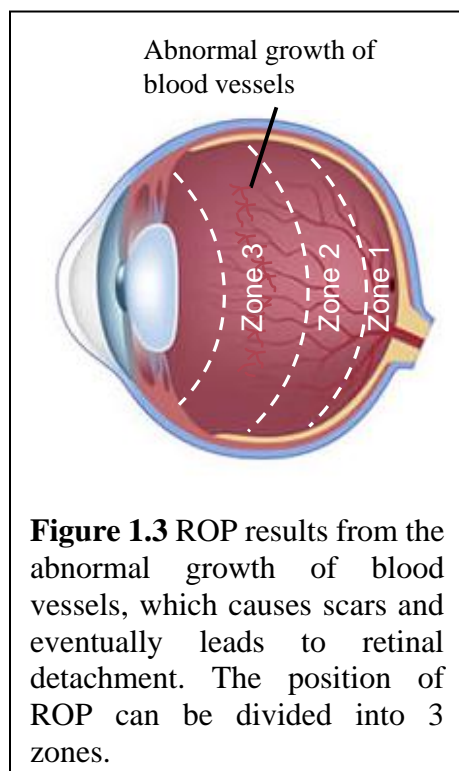
Despite standard treatment options, including laser photocoagulation, glucose-lowering treatments, and intravitreal injection of corticosteroids and anti-VEGF antibodies, the ability to address the complex nature of DR remains a challenge.<sup>14</sup> In fact, >40% of the DR patient population fails to respond to the gold-standard anti-VEGF treatment.<sup>16</sup> As mentioned in the context of AMD, evidence is mounting that chronic anti-VEGF therapy can lead to cataracts,

infection, vitreous hemorrhage, fibrosis, and even retinal detachment.<sup>17</sup> Additional studies that define possible complications (i.e., hypertension, proteinuria, ischemic cardiovascular disease) by anti-VEGF agents due to systemic exposure arising from long term administration are still needed.<sup>18</sup> Another common treatment, laser photocoagulation, suffers from its destructive nature that leads to the exacerbation or development of macular edema, vision loss, peripheral vision defects, and night vision loss.

### 1.2.3 Retinopathy of Prematurity (ROP)

Due to modern medical advances, we are now able to save exceedingly premature neonates. Premature infants are at a higher than average risk for developing ROP, a condition resulting from eye vascular abnormalities that can lead to blindness.<sup>19</sup> The National Eye Institute estimates that nearly 16,000 of the 3.9 million infants born in the U.S. suffer from some degree of ROP each year.<sup>20</sup> Of the ROP diagnosed infants, ~10% will require medical treatment and ~4% will become legally blind due to ROP related issues, with low- and middle-income countries exhibiting blindness prevalence of ~40%.

Scarring and retinal detachment are caused by disorganized growth of retinal blood vessels during premature development in ROP. The first phase starts from vaso-obliteration of the developing retinal capillaries due to decreased levels of cytoprotective factors. This leads to hypoxic vasoproliferation in the second phase, wherein the hypoxic retina overproduces hormones, (e.g., VEGF) resulting in the growth of anarchic vessel formation at the immature nonperfused area of the retina. Eventually,





abnormal neovascularization accumulates in the retina leading to final invasion into the vitreous, which cause blindness.<sup>19,21</sup> According to the International Classification of ROP definitions, ROP is categorized by location (3 zones, **Figure 1.3**), severity (mild, moderate, or severe), extent (12 clock hours), and vascular dilatation and tortuosity (a + symbol).<sup>22</sup>

The current gold-standard treatments for ROP are cryotherapy and laser photocoagulation. The two approaches destroy the portion of the avascular retina that is the source of growth factors, which promote neovascularization.<sup>23</sup> This results in permanent damage to the peripheral retina and significantly reduces vision. Additionally, laser photocoagulation has been shown to be a major contributor to the development of corneal edema, myopia, intraocular hemorrhage, and cataract formation.

As expected, anti-vascular endothelial growth factor (anti-VEGF) has recently been pursued as a preventative and less destructive therapy for ROP.<sup>24</sup> While anti-VEGF reduces the risk of the recurrence in infants with zone I ROP, an increase of recurrence in infants with zone II ROP has been observed.<sup>25</sup> Moreover, when anti-VEGF agents were used as monotherapy, neither bevacizumab or ranibizumab reduce the risk of retinal detachment, mortality before discharge, corneal opacity requiring corneal transplant, or lens opacity requiring cataract removal.<sup>25</sup> Furthermore, recent evidence suggests that anti-VEGF treatments give rise to not only ocular issues but also result in systemic complications in premature infants.<sup>26</sup> Therefore, in addition to potential ethical issues of this treatment on infants, the safety and efficacy of anti-VEGF agents raise significant concerns.

#### **1.2.4 Retinal Diseases: State of Treatment**

Despite a number of treatment options, the ability to address the complex nature of retinal diseases like DR, AMD, and ROP remains a significant challenge.<sup>14</sup> Frontline approaches require

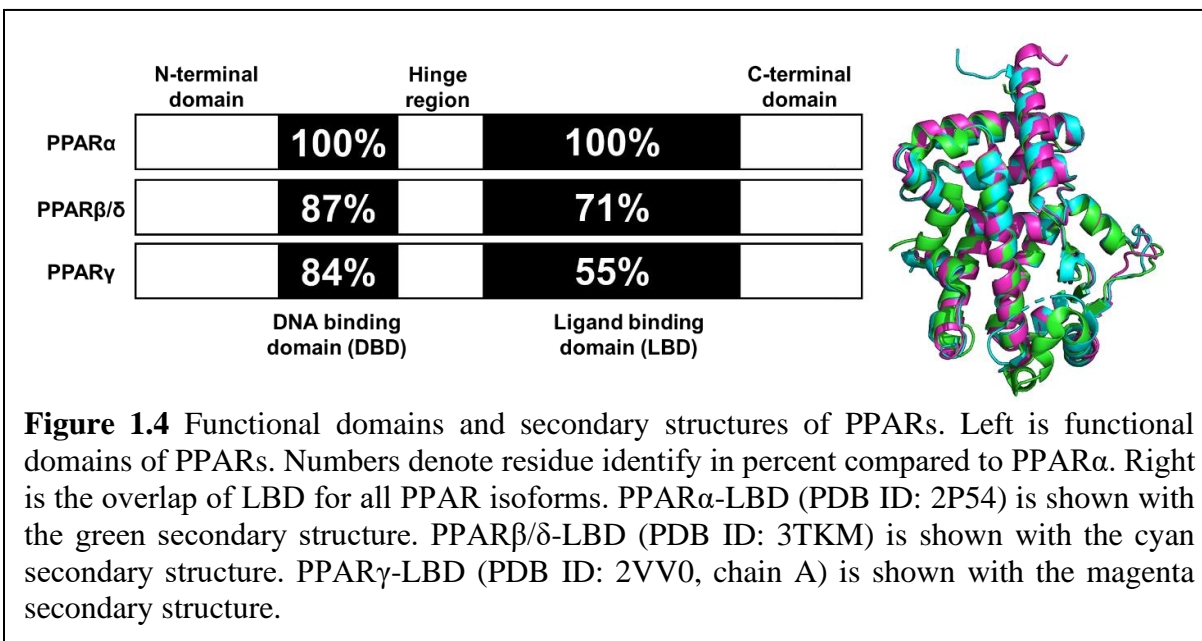
frequent injections, are destructive, demand specialized facilities, suffer from limited response rates, and produce significant financial burdens on the healthcare system. Not unexpected, since VEGF-A has been reported to have an orthogonal physiologic cytoprotective role in the retina and VEGF inhibition is toxic to multiple cell types in rodent retinae.<sup>3,14,27-31</sup> Thus, a critical need exists to develop new treatments.

Looking forward to the future of retinal disease treatment, emerging paradigms should diverge from the conventional approaches of simply preventing angiogenesis. For example, therapeutic mechanisms that synergistically protect the retina from inflammation, cell death, leakage, and angiogenesis, are worthy of pursuit in retinal-disease prevention and treatment. Unlike current options, these new approaches should be non-invasive (to the eye), safe, readily available, affordable, and capable of being administered without specialized facilities. New therapies that are either superior to or synergistic with current approaches, allow the treatment of a wider population demographic, and address those not suitable for current approaches, will be of great value to patients.

### **1.3 A Case for Targeting PPARs**

Peroxisome proliferator-activated receptors (PPARs) are a group of ligand dependent nuclear transcription factors that play essential roles in regulating energy balance and metabolic processes. As such, PPARs have received a significant amount of attention as drug targets for diseases ranging from dyslipidemia to Alzheimer's.<sup>32,33</sup> Three PPAR subtypes exist and are the products of distinct genes, commonly identified as PPAR $\alpha$  [NR1C1], PPAR $\beta/\delta$  [NR1C2] and PPAR $\gamma$  [NR1C3]. All PPARs exhibit a prototypical domain architecture including 1) an N-terminal region, 2) a highly conserved DNA-binding domain (DBD), 3) a flexible hinge region, 4) a ligand-binding domain (LBD), and 5) a C-terminal region (**Figure 1.4**). To regulate gene

expression, PPARs often form a heterodimeric complex with retinoid X receptor (RXR). The heterodimer is activated by binding of a ligand to PPAR and/or RXR. Activation results in corepressor dissociation and binding of the heterodimer to the peroxisome proliferator response elements (PPREs) on the promoter domain of the target genes, subsequently leading to gene transcription. Due to different expression patterns, tissue distributions, and pharmacological profiles, each PPAR subtype regulates different metabolic pathways.



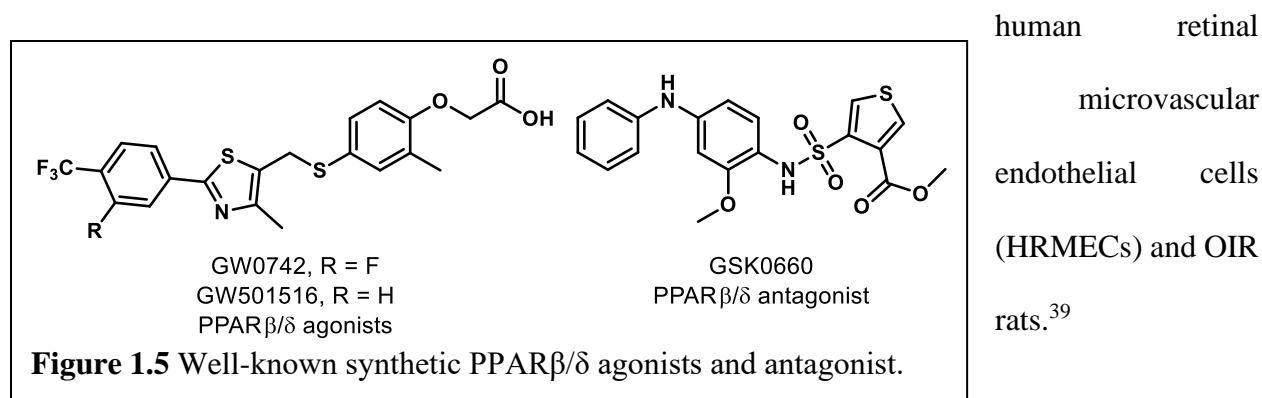
The last decade has witnessed increasing evidence that the regulation of PPARs play roles in angiogenesis, fibrosis, inflammation, and oxidative effects for various organs. As mentioned earlier, the pathological mechanism of major blinding diseases, such as AMD, DR, and ROP, often involve neovascularization, and inflammation- and oxidative stress-mediated cell death. This suggests that PPAR modulation represents an opportunity to affect these vision-threatening diseases through simultaneous regulation of many etiological features, thus predicting a higher rate of patient response.

### 1.3.1 PPAR $\beta/\delta$

PPAR $\beta/\delta$  is the least understood isoform in the PPAR family and is ubiquitously expressed (PPAR $\delta$  will be used for short). This receptor regulates fatty acid catabolism, energy metabolism, and reverse cholesterol transport.<sup>34</sup> Activation of PPAR $\delta$  was initially thought to be a therapeutic target for dyslipidemia, diabetes, and cardiovascular disease, but the beneficial effects in primate models were not reproducible.<sup>35</sup> Recently, a growing body of evidence suggests that PPAR $\delta$  is also involved in angiogenesis, inflammation, lipid metabolism, and extracellular matrix remodeling, which are central to the pathogenesis of retinal diseases such as AMD.<sup>36-38</sup> However, that more studies demonstrating the effects of PPAR $\delta$  modulation in ophthalmology are warranted.

Aged PPAR $\delta$ -knockdown mice exhibit several phenotypic features of dry AMD including hypo- and hyper-pigmentation, loss of basal infoldings, thickened Bruch's membrane, and a higher frequency of abnormal sub-RPE deposits.<sup>36</sup> This suggests that PPAR $\delta$  plays an essential role in the early development of dry AMD and that PPAR $\delta$  agonism may provide a complementary approach to anti-VEGF injections for different clinical sub-types of AMD.

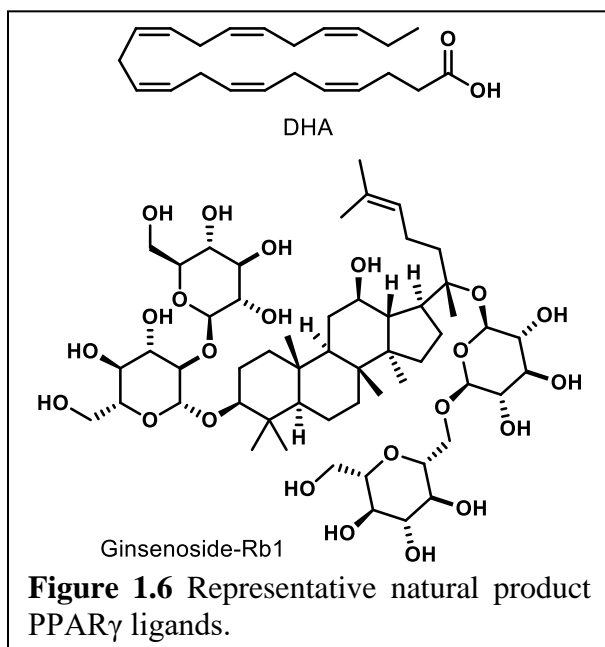
Investigation surrounding the molecular effects of PPAR $\delta$  agonism however, revealed that PPAR $\delta$  activation aggravates angiogenic cell behaviors and oxygen-induced retinopathy (OIR). In fact, administration of PPAR $\delta$  agonists, GW0742 and GW501516 (**Figure 1.5**), significantly increased the level of angiopoietin-like-4 (angptl4) mRNA that aggravates the tubulogenesis in



On the other hand, pharmacological antagonism of PPAR $\delta$  by GSK0660 (**Figure 1.5**) was reported to decrease the level of angptl4 mRNA that reduced proliferation and tubulogenesis in HRMECs.<sup>39</sup> Moreover, GSK0660 treatment reduced the expression of angptl4 and preretinal neovascularization in OIR rats.<sup>39</sup> Similar results were reported by Choudhary et al., which showed that pharmacological antagonism of PPAR $\delta$  inhibited choroidal endothelial cell migration *in vitro* and attenuated CNV lesions in laser-induced CNV Ppar $\delta^{+/+}$  mice.<sup>36</sup> Suarez et al. provided further evidence that PPAR $\delta$  antagonism exhibits promises, as studies demonstrate that administration of GSK0660 decreases phosphorylation of extracellular signal-regulated protein kinases and expression of VEGF in HRMECs, and reduces retinal vascular permeability and retinal VEGF level in a mouse model.<sup>40</sup> With these promising results, studies were conducted on the mechanism of vascular inflammation and PPAR $\delta$  antagonism. It was determined that GSK0660 prevents upregulation of TNF $\alpha$ -induced transcription, such as chemokine ligand 8 (CCL8), chemokine ligand 17 (CCL17), and C-X-C motif chemokine 10 (CXCL10), which inhibits leukocyte recruitment in HRMECs.<sup>41</sup> Although the evidence suggests that ubiquitously expressed PPAR $\delta$  has multiple effects on retinal diseases, the functional studies of PPAR $\delta$  are still in their infancy and the results are controversial.

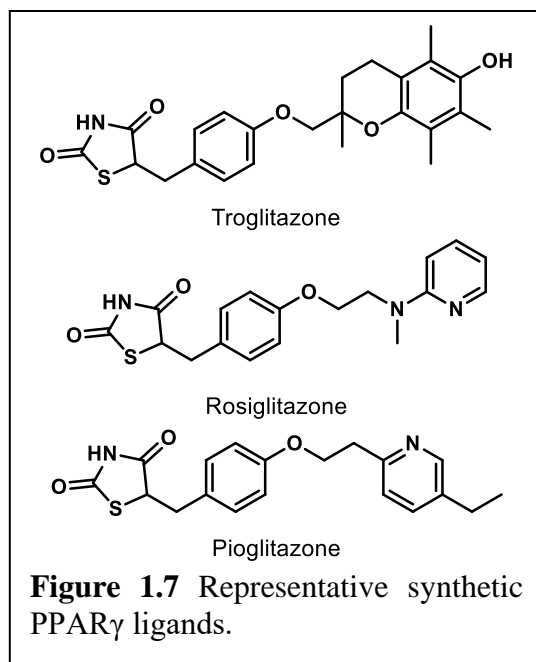
### 1.3.2 PPAR $\gamma$

PPAR $\gamma$  is arguably the most widely investigated PPAR subtype. It is expressed predominantly in adipose tissue, kidney, stomach, heart, liver, spleen, and brain. The functions of PPAR $\gamma$  are to regulate energy storage and utilization, inflammatory and



immunological responses, and adipocyte differentiation. Recently, moderate levels of PPAR $\gamma$  have been found in cultured primary RPE cells and ARPE19 cells (a human immortalized RPE cell line).<sup>42</sup> Molecular implications of PPAR $\gamma$  in retinal diseases have been reported thoroughly in previous communications.<sup>43-46</sup> Activation of PPAR $\gamma$  provides a neuroprotective effect and inhibits microvascular abnormalities in DR.<sup>45</sup> Moreover, research clearly demonstrates that PPAR $\gamma$  activation inhibits CNV, attenuates retinal and choroidal angiogenesis, and renews photoreceptor processes corrupted by oxidants in AMD.<sup>43</sup> Subsequent studies show that up-regulation of PPAR $\gamma$  induces anti-fibrogenic effects for AMD.<sup>47</sup> Therefore, continued investigation into PPAR $\gamma$  and its therapeutic potential through pharmacological modulation is a worthwhile endeavor; one that is certain to, at the very least, reveal new molecular insights into disease pathology.

Docosahexaenoic acid (DHA), an omega-3-fatty acid (**Figure 1.6**), is a natural ligand of PPAR $\gamma$ . DHA activates PPAR $\gamma$  to decrease nuclear factor-kappa B (NF $\kappa$ B) activity leading to inhibition of advanced glycation products (AGEs) induced microglia activation in retinal cells from newborn Sprague-Dawley rats.<sup>48</sup> Ginsenoside-Rb1 (Rb1, **Figure 1.6**) is the most abundant ginsenoside isolated from *Panax ginseng*. Lu et. al reported Rb1 to exhibit an anti-angiogenesis effect by increasing pigment epithelial-derived factor (PEDF) expression and reducing miR-33 through a PPAR $\gamma$ -dependent pathway in human umbilical vein endothelial cells (HUVECs). These results demonstrate that PPAR $\gamma$  activation regulates multiple pathways to provide benefits that might be used for treating retinal diseases.



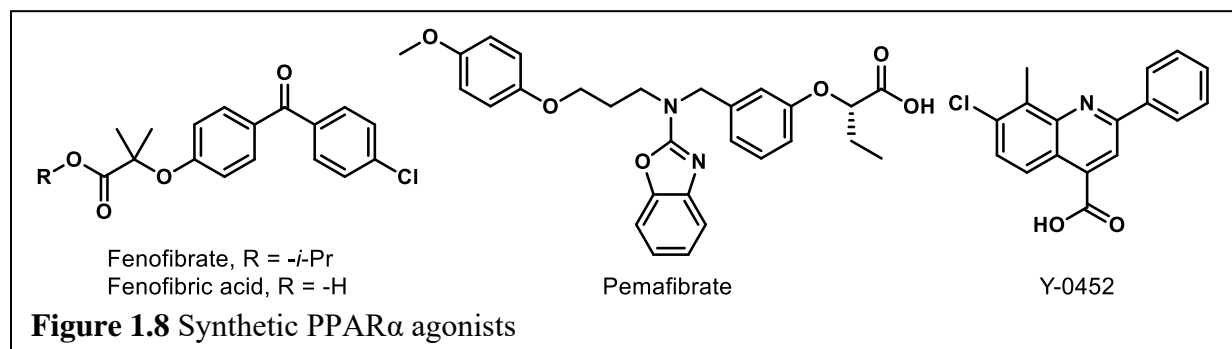
Although natural products as PPAR $\gamma$  ligands have only been assessed at the cellular level, synthetic PPAR $\gamma$  agonists have been applied in clinical studies. In fact, an article reported the association of thiazolidinediones (TZDs, **Figure 1.7**), a group of synthetic PPAR $\gamma$  agonists including rosiglitazone, troglitazone, and pioglitazone, with DR in human subjects.<sup>49</sup> However, the most recent clinical study found no benefits from using TZD to improve vision or reduce DME progression.<sup>50</sup> Additionally, it is well known that the US FDA reviews TZDs more rigorously due to their adverse effects. Therefore, either selective PPAR $\gamma$  agonists or dual PPAR agonists containing PPAR $\gamma$  activation are likely to continue to face a precarious journey for drug development.

### **1.3.3 PPAR $\alpha$**

PPAR $\alpha$  is the most studied PPAR isoform for retinal diseases, with publication tracking back to 1969. It is highly expressed in all types of retinal cells and plays essential roles in multiple factors, such as regulation of VEGF expression, regulation of mitochondrial function, inflammation, apoptosis, and angiogenesis. Multiple animal models demonstrate that inefficient PPAR $\alpha$  function (e.g., PPAR $\alpha^{-/-}$  mice) results in apoptosis of retinal and pericyte cells, activation of retinal glia, and formation of retinal acellular capillaries.<sup>51-53</sup> Diabetic PPAR $\alpha$  knockout mice exhibit increased expression of several inflammatory factors including VEGF, TNF- $\alpha$ , and ICAM-1, thus leading to more severe retinal inflammation and neovascularization.<sup>51</sup> Furthermore, deficiency of PPAR $\alpha$  in diabetic mice seems to aggravate the severity of fibronectin and inflammation as well as increase the level of fatty acids and renal triglycerides.<sup>54,55</sup> On the other hand, PPAR $\alpha$  overexpression in streptozotocin (STZ)-diabetic rats reduces vascular leakage and retinal inflammation by decreasing adherent leukocytes and expression levels of VEGF, TNF- $\alpha$ ,

and ICAM-1.<sup>51</sup> These studies reveal PPAR $\alpha$  agonism to play an important role in providing multiple beneficial effects such as, anti-apoptosis, anti-inflammation, and anti-oxidation.

The benefits of PPAR $\alpha$  activation have also been confirmed at the cellular level. Overexpression of PPAR $\alpha$  in human retinal capillary endothelial cells (HRCECs) inhibits cell migration and proliferation to provide an antiangiogenic effect.<sup>51</sup> In another study, protection of human retinal capillary pericytes (HRCP) was demonstrated by overexpression of PPAR $\alpha$ , which resulted in a decrease in oxidative stress-induced apoptosis, a reduction in the production of reactive oxygen species (ROS), and a down-regulation of NADPH oxidase 4 (NOX4) expression in cultured cells.<sup>52</sup> Mitochondrial dysfunction of HRCP was also ameliorated by the overexpression of PPAR $\alpha$ , which reduces ROS production and thus provides protective effects.<sup>52</sup> PPAR $\alpha$  overexpression inhibits the Wnt pathway that provides anti-inflammatory and anti-fibrosis effects.<sup>54</sup> Taken collectively, the multidimensional benefits of enhanced PPAR $\alpha$  activity provide compelling evidence that PPAR $\alpha$  agonism is capable of addressing the complex nature of common retinal diseases.<sup>52-54</sup> Two different mechanisms can be envisioned to enhance PPAR $\alpha$  activity: 1) genetic modified PPAR $\alpha$  overexpression and 2) ligand-binding induced PPAR $\alpha$  activation. The latter option has generated excitement from academic and pharmaceutical labs, as it represents an obvious option for small molecule drug development. Herein, we summarize recent findings for PPAR $\alpha$  agonists in the therapeutic treatment of retinal diseases.





### 1.3.3.1 Fenofibrate/Fenofibric acid

Fenofibrate (**Figure 1.8**) is the most studied PPAR $\alpha$  agonist for treating retinal diseases. Fibrates are amphipathic (one end is hydrophobic, and one end is hydrophilic) carboxylic acids that are employed to lower plasma triglyceride levels. Fenofibrate is hydrolyzed *in vivo* by hepatic esterase to its active PPAR $\alpha$  agonizing form, fenofibric acid (**Figure 1.8**). Experimental and clinical studies suggest that fenofibric acid has beneficial effects for treating DR. Two of the most predominant studies are the Fenofibrate Intervention and Event Lowering in Diabetes (FIELD) study and the Action to Control Cardiovascular Risk in Diabetes (ACCORD)-Eye study.<sup>56,57</sup>

The FIELD study evaluated the ability of long-term fenofibrate (200 mg/day for 5 years) to treat DR in a research cohort of 9,795 diabetic patients.<sup>57,58</sup> A significant reduction in the need for the first laser treatment of all retinopathy was observed compared to the placebo group, and the ophthalmology substudy showed significant reduction in the progression of retinopathy and the prevalence of macular edema in the patients with pre-existing retinopathy.<sup>57,59</sup> The ACCORD-Eye study explored the potential of fenofibrate (160 mg/day) plus simvastatin (simvastatin reduces low-density lipoprotein [LDL] cholesterol and triglyceride levels) in a research cohort of 2,856 diabetic retinopathy patients over a 4-year span.<sup>56,60</sup> The combination of fenofibrate and simvastatin slowed the progression of DR, an improvement not provided by simvastatin alone.

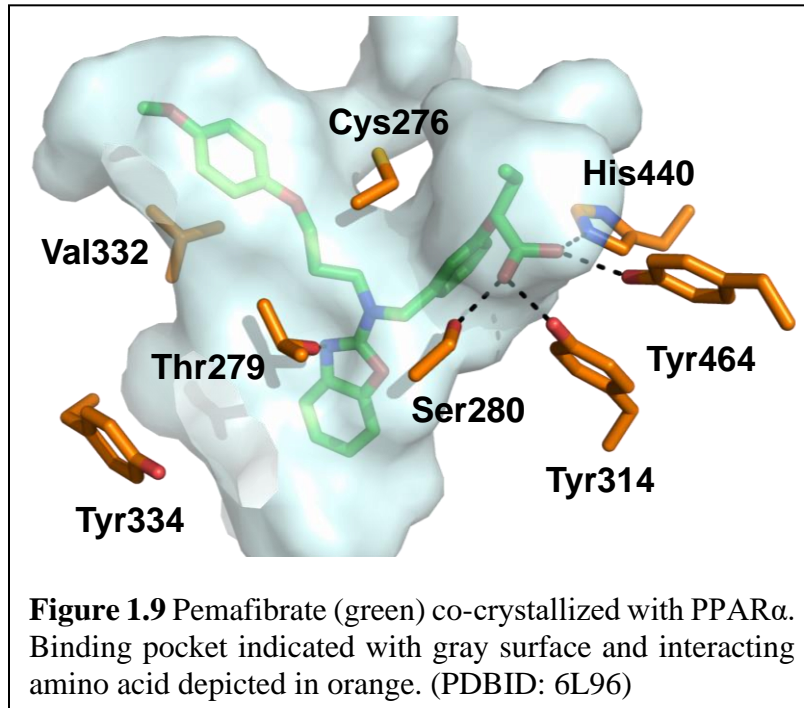
Since these clinical trials, the therapeutic effects of fenofibrate on DR have been found to be unrelated to its lipid-lowering activity, but rather result from its agonism and upregulation of PPAR $\alpha$ . Given the pleiotropic role of PPAR $\alpha$ , as described previously, it is not surprising that fenofibrate and fenofibric acid demonstrate protective effects against retinal neurodegeneration, pericyte dropout, inflammation, vascular leakage, and neovascularization in OIR and type 1 diabetic models.<sup>51-53,61</sup> Furthermore, the Takahashi group reported that administration of

fenofibrate prevented up-regulation of proinflammatory cytokines and monocyte chemoattractant protein-1 (MCP-1) and inhibited inflammatory cell infiltration into the injured cornea of the rats.<sup>62</sup> Therefore, fenofibrate treatment produces beneficial effects on various pathological driver of DR and related conditions through the activation of PPAR $\alpha$ .

However, fenofibric acid is a weak PPAR $\alpha$  agonist and has a poor selectivity for PPAR $\alpha$  over other two isoforms. In fact, more than 100 mg/kg of fenofibrate are required to reach meaningful effects in mice studies.<sup>63</sup> Moreover, poor efficacy by fenofibrate to reduce cardiovascular events has resulted in fewer medical physicians prescribing it for dyslipidemia or using it off-label for treating diabetic retinopathy.<sup>64</sup> Although fenofibrate experiments provide compelling evidence that small-molecule activation of PPAR $\alpha$  represents a new avenue for the treatment of retinal disease, new PPAR $\alpha$  agonists are necessary. This realization has captured the attention of pharmaceutical and academic drug discovery teams.

### 1.3.3.2 Pemafibrate

Pemafibrate (K-877, Parmodia<sup>TM</sup>, **Figure 1.8**) is a newly approved fibrate drug in Japan (2017) indicated for the treatment of atherogenic dyslipidemia. It was developed as a novel selective peroxisome proliferator-activated receptor  $\alpha$  modulator (SPPARM $\alpha$ ) and exhibits an excellent potency ( $EC_{50} = 1.5$  nM) and a high selectivity (>2000-fold) for PPAR $\alpha$  over other isoforms in cell-based transactivation assays.<sup>63</sup> Pemafibrate contains an acidic region similar to other PPAR $\alpha$  agonists and has a Y-shape structure including a 2-aminobenzoxazolic ring and a phenoxyalkyl chain to fit the ligand-binding pocket of PPAR $\alpha$ , thereby increasing its activity and selectivity.<sup>65-67</sup> Co-crystallization studies reveal the Y-shaped pemafibrate binds to the entire cavity region, which has been demonstrated by computational docking. (**Figure 1.9**).<sup>67,68</sup>



Pemaifibrate upregulates 11 of the top 20 genes involved in carbohydrate and lipid metabolism, such as very-low-density lipoprotein receptor (VLDLR), ATP binding cassette subfamily A member 1 (ABCA1), nuclear receptor co-repressor 1 and 2 (NCoR1 and NCoR2), vascular cell adhesion

molecule 1 (VCAM-1), and MCP-1, but to a much greater extent than fenofibric acid.<sup>63,69</sup> Moreover, unique genes that are involved in regulation of the innate immune system and inflammation, such as mannose-binding lectin 2 (MBL2), glutamyl aminopeptidase (ENPEP), and fibroblast growth factor 21 (FGF21), are induced by administration of pemaifibrate.<sup>70</sup>

Similar to fenofibrate, pemaifibrate exhibits beneficial effects on lipid metabolism and inflammation through activation of PPAR $\alpha$ .<sup>71,72</sup> Administration of pemaifibrate in LDL receptor knockout mice results in a reduction of plasma triglycerides and total cholesterol, and a concomitant increase in high-density lipoprotein cholesterol (HDL-C) as a result of regulation of PPAR $\alpha$ -related genes.<sup>71</sup> In human apolipoprotein E2 knock-in mice, pemaifibrate reduces biomarkers for inflammation and macrophage, such as MCP1, VCAM-1, and interleukin 6 (IL6).<sup>72</sup> Moreover, the low therapeutic dose of pemaifibrate (0.2-0.4 mg/day) is unlikely to induce peroxisome proliferation or liver toxicity in clinical use.<sup>72</sup> In fact, pemaifibrate showed a 25% increase in liver weight compared to 44% increase of fenofibrate in rats.<sup>65</sup>

Inspired by the fenofibrate FIELD and ACCORD studies, pemafibrate was scheduled to undergo a phase III clinical trial, called Pemafibrate to Reduce Cardiovascular Outcomes by Reducing Triglycerides in Patients with Diabetes (PROMINENT), which began in the United States and Europe in March 2017.<sup>73</sup> The PROMINENT study was not only expected to investigate effects of pemafibrate on the residual cardiovascular risk remaining after treatment but also the ability of pemafibrate to reduce DR in diabetic patients through an ancillary study.<sup>74</sup> Unfortunately, the initial recruiting period failed to reach required enrollment and the trial has been postponed. Recent studies show that pemafibrate, but not fenofibrate, inhibits pathological angiogenesis of the retina in animal studies. Surprisingly it has been suggested that systemically administered pemafibrate elicit this effects through the agonism of liver PPAR $\alpha$  rather than from stimulating PPAR $\alpha$  in the retina.<sup>75</sup> Although more studies are needed, pemafibrate represents a promising therapeutic lead to treat neovascular retinal diseases.

### 1.3.3.3 Y-0452

Recently, a new PPAR $\alpha$  agonist, 7-chloro-8-methyl-2-phenylquinoline-4-carboxylic acid (Y-0452, **Figure 1.8**), was reported by the Ma Lab at the University of Oklahoma Health Science Center. Y-0452 was identified from a virtual screen as a chemically distinct chemotype predicted to exhibit PPAR $\alpha$  agonism. Experimentally, the compound exhibits anti-apoptosis, anti-angiogenic, and neuroprotective effects in R28 (a cell line derived from photoreceptor precursors) and HRCECs. Additionally, the compound significantly reduces retinal inflammation and apoptosis without signs of toxicity in the retinas of mice and diabetic rats.<sup>76</sup> Y-0452 exhibits efficacy in DR animal models after systemic (i.p.) administration, providing a new lead for development. Although Y-0452 is an attractive molecule, it exhibits only weak on-target activity in biochemical PPAR $\alpha$  assays ( $EC_{50} \approx 25-50 \mu M$ ), and manifests a low level of agonism compared

to known PPAR- $\alpha$  agonists.<sup>76</sup> Additionally, the highly functionalized quinoline core of Y-0452 presents significant synthetic challenges regarding comprehensive structure-activity relationship (SAR) studies. These aspects inspired us to investigate the SAR of Y-0452 through molecular simplification with a goal of enhancing synthetic tractability, target engagement, selectivity, and level of PPAR $\alpha$  agonism. Towards this initiative, we utilized *in silico* approaches to design a series of derivatives, which were then synthesized and evaluated for PPAR $\alpha$  agonism. The results from these studies comprise chapters 2 and 3 of this dissertation.

## **1.4 Strategic Promiscuity**

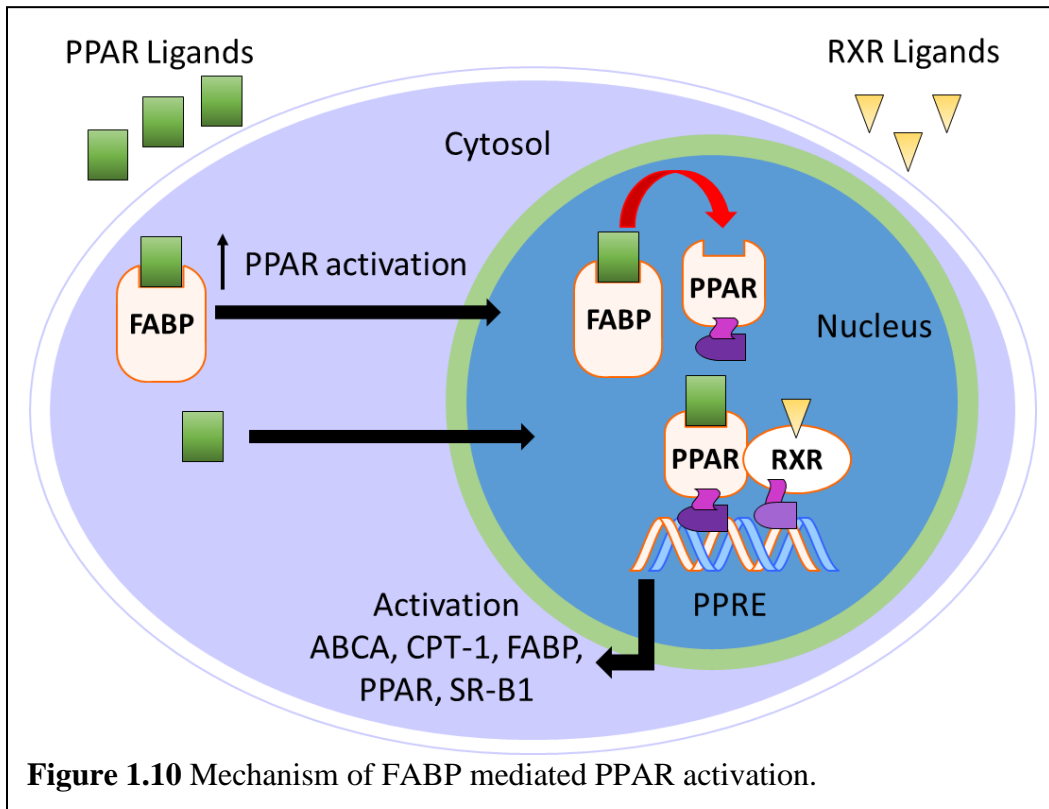
### **1.4.1 Dual PPAR Regulation**

Various PPAR dual agonists, especially PPAR $\alpha/\gamma$  dual agonists, and PPAR pan( $\alpha/\delta/\gamma$ ) agonists have emerged in last couple years, including lobeglitazone sulfate (approved in Korean), aleglitazar (Roche), ragaglitazar (Novo Nordisk), imiglitazar (Takeda), peliglitazar (Bristol-Myers Squibb), and farglitazar (GlaxoSmithKline).<sup>77</sup> Recently, it has been reported that the PPAR $\alpha/\gamma$  dual agonist saroglitazar, developed by Zydus cadila and approved in India, is patented for treating retinal diseases caused by inflammation, macular degeneration, and neovascularization.<sup>78</sup> However, the development of dual PPAR agonists has not yet achieved the anticipated success in the United State, due to the side effects such as increased cardiovascular risk (muraglitazar), carcinogenicity (ragaglitazar and MK-767), liver toxicity (imiglitazar), and renal injury (tesaglitazar).<sup>79</sup>

### **1.4.2 PPAR and FABP**

Fatty acid binding proteins (FABPs) are a group of intracellular lipid-binding proteins, which are 14-15 kDa cytosolic proteins. Research on FABPs and their biological importance have attracted many academic and industrial researchers.<sup>80-83</sup> The FABPs facilitate the transport of free

fatty acids to many specific compartments in the cell for storage, signaling, and/or metabolism (Figure 1.10).<sup>83</sup> The most significant thing to our work is that FABP transports hydrophobic ligands to PPAR, thereby enhancing transcriptional regulation.<sup>84</sup> Without FABP shuttling, the hydrophobic nature of PPAR ligands would preclude interactions with PPARs.



At least 9 different FABPs (FABP1-9) have been identified in humans. Studies have shown that FABPs coexist in

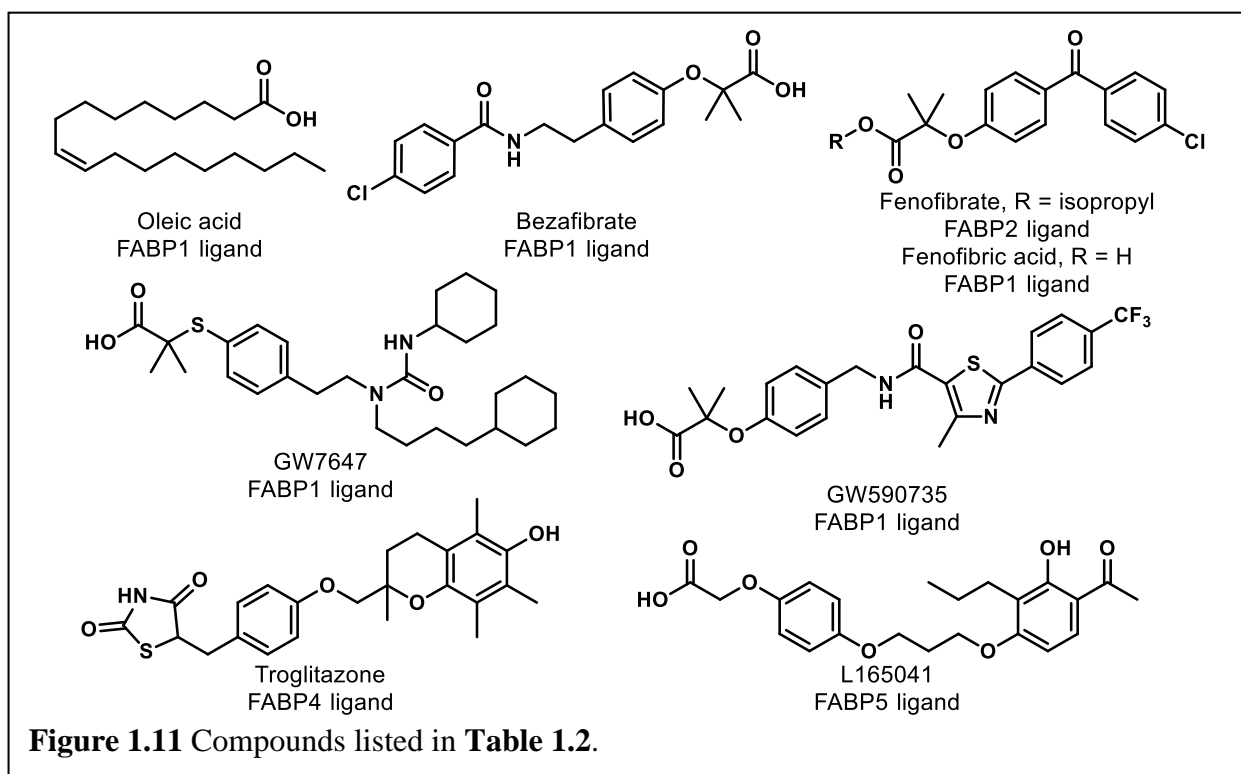
tissue or cells, so the numbered nomenclature is preferred over the traditional tissue-related names, FABP1 (liver/L-), FABP2 (intestinal/I-), FABP3 (heart/H-), FABP4 (adipocyte/A-), FABP5 (epidermal/E-), FABP6 (ileal/Il-), FABP7 (brain/B-), FABP8 (myelin/M-), and FABP9 (testis/T-).<sup>82,83</sup> Recently, a new FABP isoform, FABP12, was found mainly in the retina including in ganglion cells and the inner nuclear layer of adult rats.<sup>85</sup> Other FABPs, such as FABP7, have also been found in the retina and play an important role in maintenance of retinal vasculature.<sup>86</sup>

This suggests that FABPs are likely to play an important role in the PPAR ligand shuttling in the retina, and thus are involved in the pathology of retinal diseases.

Research shows that FABPs promote the uptake and transportation of long-chain fatty acids or synthetic ligands to the PPARs, thereby enhancing the ability of these ligands to interact with PPARs.<sup>87</sup> Interestingly, studies have suggested that FABPs are fairly selective for specific PPARs as well as ligands (**Table 1.2**).<sup>87,88</sup> For example, multiple groups have demonstrated that FABP1 interacts with PPAR $\alpha$  and PPAR $\gamma$  but not with PPAR $\delta$ .<sup>87,89,90</sup> More specifically, FABP1 and FABP2 enhance the transcriptional activation of PPAR $\alpha$  for oleic acid and hypolipidemic drugs, such as fenofibric acid and GW7647 (**Figure 1.11**).<sup>91</sup> The activations of PPAR $\gamma$  and PPAR $\delta$  are increased by FABP4 and FABP5, respectively.<sup>92</sup> Moreover, genes expressing FABPs are

<b>Ligand</b>	<b>PPARs</b>	<b>FABPs</b>	<b>Note</b>	<b>Refs</b>
<b>Oleic acid</b>	PPAR $\alpha$	FABP1	A linear correlation is shown between transactivation and FABP1 concentration. Binding affinity of h-FABP1 is 0.15 $\mu$ M. Binding of PPAR $\alpha$ is 0.21 $\mu$ M.	86, 88, 89
<b>Bezafibrate</b>	PPAR $\alpha$	FABP1	Linear correlation is shown between transactivation and FABP1 concentration.	86
<b>Fenofibrate</b>	PPAR $\alpha$	FABP2	2-fold increase	90
<b>Fenofibric acid</b>	PPAR $\alpha$	FABP1	Binding affinity of h-FABP1 is 1.0 $\mu$ M. Binding affinity of PPAR $\alpha$ is 10 $\mu$ M.	89, 90
<b>GW7647</b>	PPAR $\alpha$	FABP1	Binding affinity of h-FABP1 is 0.32 $\mu$ M. Binding affinity of PPAR $\alpha$ is 0.035 $\mu$ M.	88, 89
<b>GW590735</b>	PPAR $\alpha$	FABP1	Binding affinity of h-FABP1 is 20 $\mu$ M. Binding affinity of PPAR $\alpha$ is 0.06 $\mu$ M	89
<b>Troglitazone</b>	PPAR $\gamma$	FABP4	Linear correlation between transactivation and FABP4 concentration. 1.5-fold increase was improved with 0.3 $\mu$ g of FABP4. Binding affinity of FABP4 is 47.3 nM. Binding affinity of PPAR $\gamma$ is 50.7 nM.	91
<b>L165041</b>	PPAR $\beta$	FABP5	Liner correlation between transactivation and FABP5 concentration. 3-fold increase was improved with 0.3 $\mu$ g of FABP5. Binding affinity of FABP5 is 45.9 nM. Binding affinity of PPAR $\beta$ is 33.1 nM.	89, 91

transcribed by the activation of PPARs.<sup>93,94</sup> This provides an additional mechanism (along with ligand design) to improve the activity of a certain PPAR isoform. Thus, the hypothesis arises that ligand affinity should be optimized for both targets (i.e., FABP and PPAR) if one wants to optimize PPAR agonism. For PPAR $\alpha$ , for example, one might focus on optimizing affinity for FABP1 and PPAR $\alpha$  simultaneously to achieve the optimal efficiency of activation. This strategy has yet to be employed in literature, as far as we can tell, and represents an exciting unexplored avenue for our future studies.

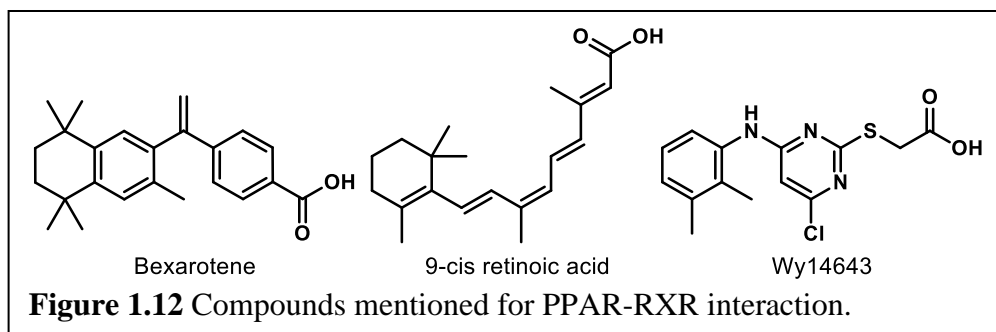


### 1.4.3 PPAR and RXR

RXRs are well known as the heterodimerization partner of many nuclear receptors such as constitutive androstane receptor (CAR), farnesoid X receptor (FXR), liver X receptor (LXR), and PPAR.<sup>95,96</sup> There are three subtypes of RXR including RXR $\alpha$ , RXR $\beta$ , and RXR $\gamma$ . Although activation of RXRs elicits beneficial effects for inflammation,<sup>97</sup> central nervous system (CNS)



remyelination,<sup>98</sup>  
multiple sclerosis  
(MS),<sup>99,100</sup>  
Alzheimer's  
disease (AD),<sup>101</sup>



and cancer.<sup>102</sup> However, RXR agonism as a therapeutic approach is still at a relatively preliminary stage. The only market-approved RXR agonist, bexarotene, faces safety issues including skin dryness, hypothyroidism and hypertriglyceridemia.<sup>103-105</sup> Gemfibrozil, a fibrate drug that is used to improve cholesterol and triglyceride levels, was originally intended to reduce the side effects of bexarotene, but resulted in a worsened condition due to an increase of bexarotene in plasma level.<sup>103</sup>

Dual RXR and PPAR (especially PPAR $\alpha$ ) agonism, however, might provide new avenues for PPAR mediated treatments. Wy14643, a known PPAR $\alpha$  agonist, was found to be more potent for RXR than PPARs, which could be the reason that Wy14643 has unique biological activities compared to other PPAR $\alpha$  agonists, such as clofibrate.<sup>106</sup> The dual RXR/PPAR $\alpha$  agonism did not trigger the sources of side effects in bexarotene therapy from the *in vitro* and *in vivo* studies.<sup>106</sup> Moreover, research shows that activation of RXR improves the transcription by PPARs in a permissive way.<sup>96</sup> PPAR mediated gene expression was increased more than 3-fold by the addition of RXR when PPAR was activated by clofibric acid and 9-cis retinoic acid.<sup>107</sup> Therefore, the combination of PPAR and RXR activation in a dual RXR/PPAR agonist could open a new pathway for PPAR mediated therapy, which might also be beneficial for the treatment of retinal diseases.

## 1.5 Conclusion

Retinal diseases, such as AMD, DR, and ROP have become widespread and serious medical conditions. However, the current treatments are still insufficient, lack efficacy in certain stages of the disease (as in the case for AMD), or exhibit detrimental side effects (such as for DR or ROP). The development of new treatments is necessary.

The pathology of retinal diseases spans an extensive web of molecular pathways and networks, such as lipid accumulation or oxidative stress induced inflammation, upregulated angiogenic factors (e.g. VEGF) causing aberrant angiogenesis, and neovascularization, leading to retinal detachments.<sup>5</sup> Diverse higher order physiological activities such as Bruch's membrane homeostasis, protein and lipid turnover, energy metabolism and complement regulation are involved in the formation of diseases. Also, the complex anatomical microenvironments in the retina is a critical consideration to address retinal diseases (e.g., blood-retina barrier).

New approaches should be able to address the complex interplay of pathogenic factors, be mechanistically differentiated from current strategies, provide superior and or synergistic effects on current treatments, and be capable of being employed as prophylactics for high risk population. New diagnostic tools that can identify preclinical risk factors or subtypes of retinal disease to prevent and/or predict the progression at early stages are also crucial for the development of new approaches. Activation of PPAR by small molecules is a promising approach to treat various retinal diseases. Development of newly discovered PPAR $\alpha$  agonists for treating retinal diseases will provide patients a safe, readily available, affordable treatment. While the work communicated in this dissertation describes my efforts towards contributing to the development of new therapeutic leads for retinal (chapters 1-3) and infectious diseases (chapter 4), the majority of the work focuses on developing novel PPAR $\alpha$  agonists to fill this need.

## 1.6 References

1. Han, E.; Baisiwala, S.; Jain, A.; Bundorf, M. K.; Pershing, S., An Analysis of Medicare Reimbursement to Ophthalmologists: Years 2012 to 2013. *Am J Ophthalmol* **2017**, *182*, 133-140.
2. Del, V. C. M.; Gehlbach, P. L., Ppar-Alpha Ligands as Potential Therapeutic Agents for Wet Age-Related Macular Degeneration. *PPAR Res.* **2008**, *2008*, No. 18401454.
3. Ambati, J.; Fowler, B. J., Mechanisms of Age-Related Macular Degeneration. *Neuron* **2012**, *75*, 26-39.
4. Ferris, F. L., 3rd; Wilkinson, C. P.; Bird, A.; Chakravarthy, U.; Chew, E.; Csaky, K.; Sadda, S. R.; Beckman Initiative for Macular Research Classification, C., Clinical Classification of Age-Related Macular Degeneration. *Ophthalmology* **2013**, *120*, 844-851.
5. Handa, J. T.; Bowes Rickman, C.; Dick, A. D.; Gorin, M. B.; Miller, J. W.; Toth, C. A.; Ueffing, M.; Zarbin, M.; Farrer, L. A., A Systems Biology Approach Towards Understanding and Treating Non-Neovascular Age-Related Macular Degeneration. *Nat. Commun.* **2019**, *10*, No. 3347.
6. Hernandez-Zimbron, L. F.; Zamora-Alvarado, R.; Ochoa-De la Paz, L.; Velez-Montoya, R.; Zenteno, E.; Gullias-Canizo, R.; Quiroz-Mercado, H.; Gonzalez-Salinas, R., Age-Related Macular Degeneration: New Paradigms for Treatment and Management of Amd. *Oxid Med Cell Longev* **2018**, *2018*, No. 8374647.
7. Holmes, D. I. R.; Zachary, I., The Vascular Endothelial Growth Factor (Vegf) Family: Angiogenic Factors in Health and Disease. *Genome Biol.* **2005**, *6*, No. 209.
8. Martin, D. F.; Maguire, M. G.; Fine, S. L.; Ying, G. S.; Jaffe, G. J.; Grunwald, J. E.; Toth, C.; Redford, M.; Ferris, F. L., 3rd, Ranibizumab and Bevacizumab for Treatment of Neovascular Age-Related Macular Degeneration: Two-Year Results. *Ophthalmology* **2012**, *119*, 1388-1398.

9. van der Reis, M. I.; La Heij, E. C.; De Jong-Hesse, Y.; Ringens, P. J.; Hendrikse, F.; Schouten, J. S., A Systematic Review of the Adverse Events of Intravitreal Anti-Vascular Endothelial Growth Factor Injections. *Retina* **2011**, *31*, 1449-1469.
10. Yau, J. W.; Rogers, S. L.; Kawasaki, R.; Lamoureux, E. L.; Kowalski, J. W.; Bek, T.; Chen, S. J.; Dekker, J. M.; Fletcher, A.; Grauslund, J.; Haffner, S.; Hamman, R. F.; Ikram, M. K.; Kayama, T.; Klein, B. E.; Klein, R.; Krishnaiah, S.; Mayurasakorn, K.; O'Hare, J. P.; Orchard, T. J.; Porta, M.; Rema, M.; Roy, M. S.; Sharma, T.; Shaw, J.; Taylor, H.; Tielsch, J. M.; Varma, R.; Wang, J. J.; Wang, N.; West, S.; Xu, L.; Yasuda, M.; Zhang, X.; Mitchell, P.; Wong, T. Y.; Meta-Analysis for Eye Disease Study, G., Global Prevalence and Major Risk Factors of Diabetic Retinopathy. *Diabetes Care* **2012**, *35*, 556-564.
11. Antonetti, D. A.; Klein, R.; Gardner, T. W., Diabetic Retinopathy. *N Engl J Med* **2012**, *366*, 1227-1239.
12. World Health Organization, World Health Day 2016: Who Calls for Global Action to Halt Rise in and Improve Care for People with Diabetes. <https://www.who.int/news-room/detail/06-04-2016-world-health-day-2016-who-calls-for-global-action-to-halt-rise-in-and-improve-care-for-people-with-diabetes>, (accessed October 31, 2019).
13. Sapiaha, P.; Hamel, D.; Shao, Z.; Rivera, J. C.; Zaniolo, K.; Joyal, J. S.; Chemtob, S., Proliferative Retinopathies: Angiogenesis That Blinds. *Int. J. Biochem. Cell Biol.* **2010**, *42*, 5-12.
14. Cai, X.; McGinnis, J. F., Diabetic Retinopathy: Animal Models, Therapies, and Perspectives. *J. Diabetes Res.* **2016**, *2016*, No. 3789217.
15. Singh, A.; Stewart, J. M., Pathophysiology of Diabetic Macular Edema. *Int. Ophthalmol. Clin.* **2009**, *49*, 1-11.

16. Simo, R.; Hernandez, C., Novel Approaches for Treating Diabetic Retinopathy Based on Recent Pathogenic Evidence. *Prog. Retin. Eye Res.* **2015**, *48*, 160-180.
17. Falavarjani, K. G.; Nguyen, Q. D., Adverse Events and Complications Associated with Intravitreal Injection of Anti-Vegf Agents: A Review of Literature. *Eye* **2013**, *27*, 787-794.
18. Simó, R.; Sundstrom, J. M.; Antonetti, D. A., Ocular Anti-Vegf Therapy for Diabetic Retinopathy: The Role of Vegf in the Pathogenesis of Diabetic Retinopathy. *Diabetes Care* **2014**, *37*, No. 893.
19. Rivera, J. C.; Sapiha, P.; Joyal, J. S.; Duhamel, F.; Shao, Z.; Sitaras, N.; Picard, E.; Zhou, E.; Lachapelle, P.; Chemtob, S., Understanding Retinopathy of Prematurity: Update on Pathogenesis. *Neonatology* **2011**, *100*, 343-353.
20. National Eye Institute, Retinopathy of Prematurity. <https://www.nei.nih.gov/learn-about-eye-health/eye-conditions-and-diseases/retinopathy-prematurity>, (accessed April 23, 2020).
21. Rivera, J. C.; Holm, M.; Austeng, D.; Morken, T. S.; Zhou, T. W.; Beaudry-Richard, A.; Sierra, E. M.; Dammann, O.; Chemtob, S., Retinopathy of Prematurity: Inflammation, Choroidal Degeneration, and Novel Promising Therapeutic Strategies. *J. Neuroinflamm.* **2017**, *14*, No. 165.
22. Gole, G. A.; Ells, A. L.; Holmstrom, G.; Fielder, A. R.; Jr, A. C.; Flynn, J. T.; Good, W. G.; Holmes, J. M.; McNamara, J. A.; Palmer, E. A.; Quinn, G. E.; Shapiro, M. J.; Trese, M. G. J.; Wallace, D. K., The International Classification of Retinopathy of Prematurity Revisited. *Arch. Ophthalmol.* **2005**, *123*, 991-999.
23. Aranda, J. V.; Qu, J.; Valencia, G. B.; Beharry, K. D., Pharmacologic Interventions for the Prevention and Treatment of Retinopathy of Prematurity. *Semin. Perinatol.* **2019**, *43*, 360-366.
24. Pertl, L.; Steinwender, G.; Mayer, C.; Hausberger, S.; Pöschl, E.-M.; Wackernagel, W.; Wedrich, A.; El-Shabrawi, Y.; Haas, A., A Systematic Review and Meta-Analysis on the Safety

of Vascular Endothelial Growth Factor (Vegf) Inhibitors for the Treatment of Retinopathy of Prematurity. *PLOS ONE* **2015**, *10*, e0129383.

25. Sankar, M. J.; Sankar, J.; Chandra, P., Anti-Vascular Endothelial Growth Factor (Vegf) Drugs for Treatment of Retinopathy of Prematurity. *Cochrane Database Syst Rev* **2018**, *1*, CD009734.

26. McCloskey, M.; Wang, H.; Jiang, Y.; Smith, G. W.; Strange, J.; Hartnett, M. E., Anti-Vegf Antibody Leads to Later Atypical Intravitreal Neovascularization and Activation of Angiogenic Pathways in a Rat Model of Retinopathy of Prematurity. *Invest Ophthalmol Vis Sci* **2013**, *54*, 2020-2026.

27. Cheung, N.; Wong, I. Y.; Wong, T. Y., Ocular Anti-Vegf Therapy for Diabetic Retinopathy: Overview of Clinical Efficacy and Evolving Applications. *Diabetes Care* **2014**, *37*, 900-905.

28. Global Report on Diabetes. *World Health Organization* <http://www.who.int/diabetes/global-report/en/>, (accessed May 26, 2020).

29. Treacy, M. P.; Hurst, T. P., The Case for Intraocular Delivery of Ppar Agonists in the Treatment of Diabetic Retinopathy. *BMC Ophthalmol.* **2012**, *12*, No. 46.

30. Wong, T. Y.; Simo, R.; Mitchell, P., Fenofibrate - a Potential Systemic Treatment for Diabetic Retinopathy? *Am. J. Ophthalmol.* **2012**, *154*, 6-12.

31. Nentwich, M. M.; Ulbig, M. W., Diabetic Retinopathy - Ocular Complications of Diabetes Mellitus. *World J. Diabetes* **2015**, *6*, 489-499.

32. Kliewer, S. A.; Lehmann, J. M.; Willson, T. M., Orphan Nuclear Receptors: Shifting Endocrinology into Reverse. *Science* **1999**, *284*, 757-760.

33. Willson, T. M.; Brown, P. J.; Sternbach, D. D.; Henke, B. R., The Ppars: From Orphan Receptors to Drug Discovery. *Journal of Medicinal Chemistry* **2000**, *43*, 527-550.

34. Pirat, C.; Farce, A.; Lebegue, N.; Renault, N.; Furman, C.; Millet, R.; Yous, S.; Speca, S.; Berthelot, P.; Desreumaux, P.; Chavatte, P., Targeting Peroxisome Proliferator-Activated Receptors (Ppars): Development of Modulators. *J. Med. Chem.* **2012**, *55*, 4027-4061.
35. Berger, J.; Moller, D. E., The Mechanisms of Action of Ppars. *Annu. Rev. Med.* **2002**, *53*, 409-435.
36. Choudhary, M.; Ding, J. D.; Qi, X.; Boulton, M. E.; Yao, P. L.; Peters, J. M.; Malek, G., Pparbeta/Delta Selectively Regulates Phenotypic Features of Age-Related Macular Degeneration. *Aging (Albany NY)* **2016**, *8*, 1952-1978.
37. Malek, G.; Lad, E. M., Emerging Roles for Nuclear Receptors in the Pathogenesis of Age-Related Macular Degeneration. *Cell. Mol. Life Sci.* **2014**, *71*, 4617-4636.
38. Choudhary, M.; Malek, G., Rethinking Nuclear Receptors as Potential Therapeutic Targets for Retinal Diseases. *J Biomol Screen* **2016**, *21*, 1007-1018.
39. Capozzi, M. E.; McCollum, G. W.; Savage, S. R.; Penn, J. S., Peroxisome Proliferator-Activated Receptor-B/ $\Delta$  Regulates Angiogenic Cell Behaviors and Oxygen-Induced Retinopathy. *Invest. Ophthalmol. Vis. Sci.* **2013**, *54*, 4197-4207.
40. Suarez, S.; McCollum, G. W.; Bretz, C. A.; Yang, R.; Capozzi, M. E.; Penn, J. S., Modulation of Vegf-Induced Retinal Vascular Permeability by Peroxisome Proliferator-Activated Receptor-Beta/Delta. *Invest Ophthalmol Vis Sci* **2014**, *55*, 8232-8240.
41. Savage, S. R.; McCollum, G. W.; Yang, R.; Penn, J. S., Rna-Seq Identifies a Role for the Ppar $\beta$ / $\Delta$  Inverse Agonist Gsk0660 in the Regulation of Tnfa-Induced Cytokine Signaling in Retinal Endothelial Cells. *Mol. Vis.* **2015**, *21*, 568-576.

42. Dwyer, M. A.; Kazmin, D.; Hu, P.; McDonnell, D. P.; Malek, G., Research Resource: Nuclear Receptor Atlas of Human Retinal Pigment Epithelial Cells: Potential Relevance to Age-Related Macular Degeneration. *Mol Endocrinol* **2011**, *25*, 360-372.
43. Zhang, S.; Gu, H.; Hu, N., Role of Peroxisome Proliferator-Activated Receptor Gamma in Ocular Diseases. *J Ophthalmol* **2015**, *2015*, No. 275435.
44. Treacy, M. P.; Hurst, T. P., The Case for Intraocular Delivery of Ppar Agonists in the Treatment of Diabetic Retinopathy. *BMC Ophthalmol.* **2012**, *12*, 46.
45. Ciudin, A.; Hernandez, C.; Simo, R., Molecular Implications of the Ppars in the Diabetic Eye. *PPAR Res.* **2013**, *2013*, No. 686525.
46. Song, M. K.; Roufogalis, B. D.; Huang, T. H., Modulation of Diabetic Retinopathy Pathophysiology by Natural Medicines through Ppar-Gamma-Related Pharmacology. *Br. J. Pharmacol.* **2012**, *165*, 4-19.
47. Ramos de Carvalho, J. E.; Verwoert, M. T.; Vogels, I. M. C.; Reits, E. A.; Van Noorden, C. J. F.; Klaassen, I.; Schlingemann, R. O., Involvement of the Ubiquitin-Proteasome System in the Expression of Extracellular Matrix Genes in Retinal Pigment Epithelial Cells. *Biochem Biophys Rep* **2018**, *13*, 83-92.
48. Wang, L.; Chen, K.; Liu, K.; Zhou, Y.; Zhang, T.; Wang, B.; Mi, M., Dha Inhibited Ages-Induced Retinal Microglia Activation Via Suppression of the Ppargamma/Nfkappab Pathway and Reduction of Signal Transducers in the Ages/Rage Axis Recruitment into Lipid Rafts. *Neurochem Res* **2015**, *40*, 713-722.
49. Shen, L. Q.; Child, A.; Weber, G. M.; Folkman, J.; Aiello, L. P., Rosiglitazone and Delayed Onset of Proliferative Diabetic Retinopathy. *Arch. Ophthalmol.* **2008**, *126*, 793-799.



50. Gower, E. W.; Lovato, J. F.; Ambrosius, W. T.; Chew, E. Y.; Danis, R. P.; Davis, M. D.; Goff, D. C., Jr.; Greven, C. M.; Gotto, A. M., Jr.; Bailey, K.; Gohdes, D.; Haffner, S.; Hiss, R.; Jamerson, K.; Lee, K.; Nathan, D.; Sowers, J.; Walters, L., Lack of Longitudinal Association between Thiazolidinediones and Incidence and Progression of Diabetic Eye Disease: The Accord Eye Study. *Am. J. Ophthalmol.* **2018**, *187*, 138-147.
51. Hu, Y.; Chen, Y.; Ding, L.; He, X.; Takahashi, Y.; Gao, Y.; Shen, W.; Cheng, R.; Chen, Q.; Qi, X.; Boulton, M. E.; Ma, J.-x., Pathogenic Role of Diabetes-Induced Ppar-A Down-Regulation in Microvascular Dysfunction. *PNAS* **2013**, *110*, 15401-15406.
52. Ding, L.; Cheng, R.; Hu, Y.; Takahashi, Y.; Jenkins, A. J.; Keech, A. C.; Humphries, K. M.; Gu, X.; Elliott, M. H.; Xia, X.; Ma, J. X., Peroxisome Proliferator-Activated Receptor Alpha Protects Capillary Pericytes in the Retina. *Am J Pathol* **2014**, *184*, 2709-2720.
53. Moran, E.; Ding, L.; Wang, Z.; Cheng, R.; Chen, Q.; Moore, R.; Takahashi, Y.; Ma, J. X., Protective and Antioxidant Effects of Pparalpha in the Ischemic Retina. *Invest Ophthalmol Vis Sci* **2014**, *55*, 4568-4576.
54. Cheng, R.; Ding, L.; He, X.; Takahashi, Y.; Ma, J. X., Interaction of Pparalpha with the Canonic Wnt Pathway in the Regulation of Renal Fibrosis. *Diabetes* **2016**, *65*, 3730-3743.
55. Park, C. W.; Kim, H. W.; Ko, S. H.; Chung, H. W.; Lim, S. W.; Yang, C. W.; Chang, Y. S.; Sugawara, A.; Guan, Y.; Breyer, M. D., Accelerated Diabetic Nephropathy in Mice Lacking the Peroxisome Proliferator-Activated Receptor *Diabetes* **2006**, *55*, 885-893.
56. Chew, E. Y.; Ambrosius, W. T.; Davis, M. D.; Danis, R. P.; Gangaputra, S.; Greven, C. M.; Hubbard, L.; Esser, B. A.; Lovato, J. F.; Perdue, L. H.; Goff, D. C., Jr.; Cushman, W. C.; Ginsberg, H. N.; Elam, M. B.; Genuth, S.; Gerstein, H. C.; Schubart, U.; Fine, L. J., Effects of Medical Therapies on Retinopathy Progression in Type 2 Diabetes. *N. Engl. J. Med.* **2010**, *363*, 233-244.

57. Keech, A. C.; Mitchell, P.; Summanen, P. A.; O'Day, J.; Davis, T. M. E.; Moffitt, M. S.; Taskinen, M. R.; Simes, R. J.; Tse, D.; Williamson, E.; Merrifield, A.; Laatikainen, L. T.; d'Emden, M. C.; Crimet, D. C.; O'Connell, R. L.; Colman, P. G., Effect of Fenofibrate on the Need for Laser Treatment for Diabetic Retinopathy (Field Study): A Randomised Controlled Trial. *The Lancet* **2007**, *370*, 1687-1697.
58. investigators, T. F. s., Effects of Long-Term Fenofibrate Therapy on Cardiovascular Events in 9795 People with Type 2 Diabetes Mellitus (the Field Study): Randomised Controlled Trial. *The Lancet* **2005**, *366*, 1849-1861.
59. Ansquer, J.; Foucher, C.; Aubonnet, P.; Le Malicot, K., Fibrates and Microvascular Complications in Diabetes - Insight from the Field Study. *Current Pharmaceutical Design* **2009**, *15*, 537-552.
60. Chew, E. Y.; Davis, M. D.; Danis, R. P.; Lovato, J. F.; Perdue, L. H.; Greven, C.; Genuth, S.; Goff, D. C.; Leiter, L. A.; Ismail-Beigi, F.; Ambrosius, W. T.; Action to Control Cardiovascular Risk in Diabetes Eye Study Research, G., The Effects of Medical Management on the Progression of Diabetic Retinopathy in Persons with Type 2 Diabetes: The Action to Control Cardiovascular Risk in Diabetes (Accord) Eye Study. *Ophthalmology* **2014**, *121*, 2443-2451.
61. Chen, Y.; Hu, Y.; Lin, M.; Jenkins, A. J.; Keech, A. C.; Mott, R.; Lyons, T. J.; Ma, J. X., Therapeutic Effects of Pparalpha Agonists on Diabetic Retinopathy in Type 1 Diabetes Models. *Diabetes* **2013**, *62*, 261-272.
62. Nakano, Y.; Uchiyama, M.; Arima, T.; Nagasaka, S.; Igarashi, T.; Shimizu, A.; Takahashi, H., Pparalpha Agonist Suppresses Inflammation after Corneal Alkali Burn by Suppressing Proinflammatory Cytokines, Mcp-1, and Nuclear Translocation of Nf-Kappab. *Molecules* **2018**, *24*, No. 114.

63. Raza-Iqbal, S.; Tanaka, T.; Anai, M.; Inagaki, T.; Matsumura, Y.; Ikeda, K.; Taguchi, A.; Gonzalez, F. J.; Sakai, J.; Kodama, T., Transcriptome Analysis of K-877 (a Novel Selective Ppar $\alpha$  Modulator (Spparm $\alpha$ ))-Regulated Genes in Primary Human Hepatocytes and the Mouse Liver. *Journal of Atherosclerosis and Thrombosis* **2015**, *22*, 754-772.
64. Knickelbein, J. E.; Abbott, A. B.; Chew, E. Y., Fenofibrate and Diabetic Retinopathy. *Curr. Diab. Rep.* **2016**, *16*, No. 90.
65. Yamazaki, Y.; Abe, K.; Toma, T.; Nishikawa, M.; Ozawa, H.; Okuda, A.; Araki, T.; Oda, S.; Inoue, K.; Shibuya, K.; Staels, B.; Fruchart, J. C., Design and Synthesis of Highly Potent and Selective Human Peroxisome Proliferator-Activated Receptor Alpha Agonists. *Bioorg Med Chem Lett* **2007**, *17*, 4689-4693.
66. Fruchart, J. C., Selective Peroxisome Proliferator-Activated Receptor Alpha Modulators (Spparm Alpha): The Next Generation of Peroxisome Proliferator-Activated Receptor Alpha-Agonists. *Cardiovas. Diabetol.* **2013**, *12*, No. 82.
67. Yamamoto, Y.; Takei, K.; Arulmozhiraja, S.; Sladek, V.; Matsuo, N.; Han, S. I.; Matsuzaka, T.; Sekiya, M.; Tokiwa, T.; Shoji, M.; Shigeta, Y.; Nakagawa, Y.; Tokiwa, H.; Shimano, H., Molecular Association Model of Pparalpha and Its New Specific and Efficient Ligand, Pemaifibrate: Structural Basis for Spparmalpha. *Biochem. Biophys. Res. Commun.* **2018**, *499*, 239-245.
68. Kawasaki, M.; Kambe, A.; Yamamoto, Y.; Arulmozhiraja, S.; Ito, S.; Nakagawa, Y.; Tokiwa, H.; Nakano, S.; Shimano, H., Elucidation of Molecular Mechanism of a Selective Pparalpha Modulator, Pemaifibrate, through Combinational Approaches of X-Ray Crystallography, Thermodynamic Analysis, and First-Principle Calculations. *Int J Mol Sci* **2020**, *21*.
69. Sasaki, Y.; Raza-Iqbal, S.; Tanaka, T.; Murakami, K.; Anai, M.; Osawa, T.; Matsumura, Y.; Sakai, J.; Kodama, T., Gene Expression Profiles Induced by a Novel Selective Peroxisome

Proliferator-Activated Receptor Alpha Modulator (Spparmalpha) Pemafibrate. *Int J Mol Sci* **2019**, *20*, No. 5682.

70. Fruchart, J. C., Pemafibrate (K-877), a Novel Selective Peroxisome Proliferator-Activated Receptor Alpha Modulator for Management of Atherogenic Dyslipidaemia. *Cardiovas. Diabetol.* **2017**, *16*, No. 124.

71. Takei, K.; Nakagawa, Y.; Wang, Y.; Han, S. I.; Satoh, A.; Sekiya, M.; Matsuzaka, T.; Shimano, H., Effects of K-877, a Novel Selective Pparalpha Modulator, on Small Intestine Contribute to the Amelioration of Hyperlipidemia in Low-Density Lipoprotein Receptor Knockout Mice. *J. Pharmacol. Sci.* **2017**, *133*, 214-222.

72. Hennuyer, N.; Duplan, I.; Paquet, C.; Vanhoutte, J.; Woittrain, E.; Touche, V.; Colin, S.; Vallez, E.; Lestavel, S.; Lefebvre, P.; Staels, B., The Novel Selective Pparalpha Modulator (Spparmalpha) Pemafibrate Improves Dyslipidemia, Enhances Reverse Cholesterol Transport and Decreases Inflammation and Atherosclerosis. *Atherosclerosis* **2016**, *249*, 200-208.

73. Ishibashi, S.; Arai, H.; Yokote, K.; Araki, E.; Suganami, H.; Yamashita, S.; Group, K. S., Efficacy and Safety of Pemafibrate (K-877), a Selective Peroxisome Proliferator-Activated Receptor Alpha Modulator, in Patients with Dyslipidemia: Results from a 24-Week, Randomized, Double Blind, Active-Controlled, Phase 3 Trial. *J. Clin. Lipidol.* **2018**, *12*, 173-184.

74. Pradhan, A. D.; Paynter, N. P.; Everett, B. M.; Glynn, R. J.; Amarenco, P.; Elam, M.; Ginsberg, H.; Hiatt, W. R.; Ishibashi, S.; Koenig, W.; Nordestgaard, B. G.; Fruchart, J. C.; Libby, P.; Ridker, P. M., Rationale and Design of the Pemafibrate to Reduce Cardiovascular Outcomes by Reducing Triglycerides in Patients with Diabetes (Prominent) Study. *Am. Heart J.* **2018**, *206*, 80-93.

75. Tomita, Y.; Ozawa, N.; Miwa, Y.; Ishida, A.; Ohta, M.; Tsubota, K.; Kurihara, T., Pemafibrate Prevents Retinal Pathological Neovascularization by Increasing Fgf21 Level in a Murine Oxygen-Induced Retinopathy Model. *Int J Mol Sci* **2019**, *20*, No. 5878.
76. Deng, G.; Moran, E. P.; Cheng, R.; Matlock, G.; Zhou, K.; Moran, D.; Chen, D.; Yu, Q.; Ma, J. X., Therapeutic Effects of a Novel Agonist of Peroxisome Proliferator-Activated Receptor Alpha for the Treatment of Diabetic Retinopathy. *Invest. Ophthalmol. Vis. Sci.* **2017**, *58*, 5030-5042.
77. Hong, F.; Xu, P.; Zhai, Y., The Opportunities and Challenges of Peroxisome Proliferator-Activated Receptors Ligands in Clinical Drug Discovery and Development. *Int J Mol Sci* **2018**, *19*, No. 2189.
78. Mukul Jain; Amit Arvind Joharapurkar; Patel, V. J. Dual Ppar Modulators for the Treatment of Diabetic Retinopathy and Diabetic Eye Diseases. WO 2017/089980 A1, **2017**.
79. Fievet, C.; Fruchart, J. C.; Staels, B., Pparalpha and Ppargamma Dual Agonists for the Treatment of Type 2 Diabetes and the Metabolic Syndrome. *Curr Opin Pharmacol* **2006**, *6*, 606-614.
80. Wang, Y. T.; Liu, C. H.; Zhu, H. L., Fatty Acid Binding Protein (Fabp) Inhibitors: A Patent Review (2012-2015). *Expert Opin Ther Pat* **2016**, *26*, 767-776.
81. Floresta, G.; Pistara, V.; Amata, E.; Dichiara, M.; Marrazzo, A.; Prezzavento, O.; Rescifina, A., Adipocyte Fatty Acid Binding Protein 4 (Fabp4) Inhibitors. A Comprehensive Systematic Review. *Eur J Med Chem* **2017**, *138*, 854-873.
82. Falomir-Lockhart, L. J.; Cavazzutti, G. F.; Gimenez, E.; Toscani, A. M., Fatty Acid Signaling Mechanisms in Neural Cells: Fatty Acid Receptors. *Front. Cell. Neurosci.* **2019**, *13*, 162.

83. Furuhashi, M., Fatty Acid-Binding Proteins, a Family of Lipid Chaperones. In *Biogenesis of Fatty Acids, Lipids and Membranes*, Geiger, O., Ed. Springer International Publishing: Cham, **2017**; pp 1-16.
84. Schroeder, F.; Petrescu, A. D.; Huang, H.; Atshaves, B. P.; McIntosh, A. L.; Martin, G. G.; Hostetler, H. A.; Vespa, A.; Landrock, D.; Landrock, K. K.; Payne, H. R.; Kier, A. B., Role of Fatty Acid Binding Proteins and Long Chain Fatty Acids in Modulating Nuclear Receptors and Gene Transcription. *Lipids* **2008**, *43*, 1-17.
85. Liu, R. Z.; Li, X.; Godbout, R., A Novel Fatty Acid-Binding Protein (Fabp) Gene Resulting from Tandem Gene Duplication in Mammals: Transcription in Rat Retina and Testis. *Genomics* **2008**, *92*, 436-445.
86. Su, X.; Tan, Q. S.; Parikh, B. H.; Tan, A.; Mehta, M. N.; Sia Wey, Y.; Tun, S. B.; Li, L. J.; Han, X. Y.; Wong, T. Y.; Hunziker, W.; Luu, C. D.; Owada, Y.; Barathi, V. A.; Zhang, S. S.; Chaurasia, S. S., Characterization of Fatty Acid Binding Protein 7 (Fabp7) in the Murine Retina. *Invest Ophthalmol Vis Sci* **2016**, *57*, 3397-3408.
87. Wolfrum, C.; Borrmann, C. M.; Borchers, T.; Spener, F., Fatty Acids and Hypolipidemic Drugs Regulate Peroxisome Proliferator-Activated Receptors Alpha - and Gamma-Mediated Gene Expression Via Liver Fatty Acid Binding Protein: A Signaling Path to the Nucleus. *Proc Natl Acad Sci U S A* **2001**, *98*, 2323-2328.
88. Furuhashi, M.; Hotamisligil, G. S., Fatty Acid-Binding Proteins: Role in Metabolic Diseases and Potential as Drug Targets. *Nat Rev Drug Discov* **2008**, *7*, 489-503.
89. Patil, R.; Mohanty, B.; Liu, B.; Chandrashekar, I. R.; Headey, S. J.; Williams, M. L.; Clements, C. S.; Ilyichova, O.; Doak, B. C.; Genissel, P.; Weaver, R. J.; Vuillard, L.; Halls, M. L.; Porter, C. J. H.; Scanlon, M. J., A Ligand-Induced Structural Change in Fatty Acid-Binding Protein

1 Is Associated with Potentiation of Peroxisome Proliferator-Activated Receptor Alpha Agonists. *J Biol Chem* **2019**, *294*, 3720-3734.

90. Velkov, T., Interactions between Human Liver Fatty Acid Binding Protein and Peroxisome Proliferator Activated Receptor Selective Drugs. *PPAR Res.* **2013**, *2013*, No. 938401.

91. Hughes, M. L.; Liu, B.; Halls, M. L.; Wagstaff, K. M.; Patil, R.; Velkov, T.; Jans, D. A.; Bunnett, N. W.; Scanlon, M. J.; Porter, C. J., Fatty Acid-Binding Proteins 1 and 2 Differentially Modulate the Activation of Peroxisome Proliferator-Activated Receptor Alpha in a Ligand-Selective Manner. *J Biol Chem* **2015**, *290*, 13895-13906.

92. Tan, N. S.; Shaw, N. S.; Vinckenbosch, N.; Liu, P.; Yasmin, R.; Desvergne, B.; Wahli, W.; Noy, N., Selective Cooperation between Fatty Acid Binding Proteins and Peroxisome Proliferator-Activated Receptors in Regulating Transcription. *Mol. Cell. Biol.* **2002**, *22*, 5114-5127.

93. Motojima, K., Differential Effects of Ppara Activators on Induction of Ectopic Expression of Tissue-Specific Fatty Acid Binding Protein Genes in the Mouse Liver. *The International Journal of Biochemistry & Cell Biology* **2000**, *32*, 1085-1092.

94. Schachtrup, C.; Emmler, T.; Bleck, B.; Sandqvist, A.; Spener, F., Functional Analysis of Peroxisome-Proliferator-Responsive Element Motifs in Genes of Fatty Acid-Binding Proteins. *Biochem. J.* **2004**, *382*, 239-245.

95. Evans, R. M.; Mangelsdorf, D. J., Nuclear Receptors, Rxr, and the Big Bang. *Cell* **2014**, *157*, 255-266.

96. Dawson, M. I.; Xia, Z., The Retinoid X Receptors and Their Ligands. *Biochim. Biophys. Acta* **2012**, *1821*, 21-56.

97. Nunez, V.; Alameda, D.; Rico, D.; Mota, R.; Gonzalo, P.; Cedenilla, M.; Fischer, T.; Bosca, L.; Glass, C. K.; Arroyo, A. G.; Ricote, M., Retinoid X Receptor Alpha Controls Innate

Inflammatory Responses through the up-Regulation of Chemokine Expression. *Proc Natl Acad Sci U S A* **2010**, *107*, 10626-10631.

98. Huang, J. K.; Jarjour, A. A.; Nait Oumesmar, B.; Kerninon, C.; Williams, A.; Krezel, W.; Kagechika, H.; Bauer, J.; Zhao, C.; Baron-Van Evercooren, A.; Chambon, P.; Ffrench-Constant, C.; Franklin, R. J. M., Retinoid X Receptor Gamma Signaling Accelerates Cns Remyelination. *Nat. Neurosci.* **2011**, *14*, 45-53.

99. Hanafy, K. A.; Sloane, J. A., Regulation of Remyelination in Multiple Sclerosis. *FEBS Lett.* **2011**, *585*, 3821-3828.

100. Chandraratna, R. A.; Noelle, R. J.; Nowak, E. C., Treatment with Retinoid X Receptor Agonist Irx4204 Ameliorates Experimental Autoimmune Encephalomyelitis. *Am J Transl Res* **2016**, *8*, 1016-1026.

101. Cummings, J. L.; Zhong, K.; Kinney, J. W.; Heaney, C.; Moll-Tudla, J.; Joshi, A.; Pontecorvo, M.; Devous, M.; Tang, A.; Bena, J., Double-Blind, Placebo-Controlled, Proof-of-Concept Trial of Bexarotene in Moderate Alzheimer's Disease. *Alzheimers Res Ther* **2016**, *8*, No. 4.

102. Kiss, M.; Czimmerer, Z.; Nagy, G.; Bieniasz-Krzywiec, P.; Ehling, M.; Pap, A.; Poliska, S.; Boto, P.; Tzerpos, P.; Horvath, A.; Kolostyak, Z.; Daniel, B.; Szatmari, I.; Mazzone, M.; Nagy, L., Retinoid X Receptor Suppresses a Metastasis-Promoting Transcriptional Program in Myeloid Cells Via a Ligand-Insensitive Mechanism. *Proc Natl Acad Sci U S A* **2017**, *114*, 10725-10730.

103. Farol, L. T.; Hymes, K. B., Bexarotene: A Clinical Review. *Expert Rev. Anticancer Ther.* **2004**, *4*, 180-188.

104. Boehm, M. F.; Zhang, L.; Badea, B. A.; White, S. K.; Mais, D. E.; Berger, E.; Suto, C. M.; Goldman, M. E.; Heyman, R. A., Synthesis and Structure-Activity Relationships of Novel Retinoid X Receptor-Selective Retinoids. *J Med Chem* **1994**, *37*, 2930-2941.



105. Boehm, M. F.; Zhang, L.; Zhi, L.; McClurg, M. R.; Berger, E.; Wagoner, M.; Mais, D. E.; Suto, C. M.; Davies, P. J. A.; Heyman, R. A.; Nadzan, A. M., Design and Synthesis of Potent Retinoid X Receptor Selective Ligands That Induce Apoptosis in Leukemia Cells. *Journal of Medicinal Chemistry* **1995**, *38*, 3146-3155.
106. Pollinger, J.; Gellrich, L.; Schierle, S.; Kilu, W.; Schmidt, J.; Kalinowsky, L.; Ohrndorf, J.; Kaiser, A.; Heering, J.; Proschak, E.; Merk, D., Tuning Nuclear Receptor Selectivity of Wy14,643 Towards Selective Retinoid X Receptor Modulation. *J. Med. Chem.* **2019**, *62*, 2112-2126.
107. Kliewer, S. A.; Umesono, K.; Noonan, D. J.; Heyman, R. A.; Evans, R. M., Convergence of 9-Cis Retinoic Acid and Peroxisome Proliferator Signalling Pathways through Heterodimer Formation of Their Receptors. *Nature* **1992**, *358*, 771-774.

## Chapter 2 First-generation SAR Study of New PPAR $\alpha$ Agonists

### 2.1 Abstract

Small molecule agonism of PPAR $\alpha$  represents a promising new avenue for the development of non-invasive treatments for oculo-vascular diseases like diabetic retinopathy and age-related macular degeneration. Herein we report initial SAR for the newly identified quinoline-based PPAR $\alpha$  agonist, Y-0452. Preliminary computational studies led to the hypothesis that carboxylic acid transposition and deconstruction of the Y-0452 quinoline system would enhance ligand-protein interactions and better complement the nature of the binding pocket. A focused subset of analogs was designed, synthesized, and assessed for PPAR $\alpha$  agonism. Two key observations arose from this work 1) contrary to other PPAR $\alpha$  agonists, incorporation of the fibrate “head-group” decreases PPAR $\alpha$  selectivity and instead provides *pan*-PPAR agonists and 2) computational models reveal a relatively unexploited amphiphilic pocket in PPAR $\alpha$  that provides new opportunities to for the development of novel agonists. As an example, compound **2.10** exhibits more potent PPAR $\alpha$  agonism ( $EC_{50} = \sim 6 \mu\text{M}$ ) than Y-0452 ( $EC_{50} = \sim 50 \mu\text{M}$ ) and manifests >20-fold selectivity for PPAR $\alpha$  over the PPAR $\gamma$  and PPAR $\delta$  isoforms. More detailed biochemical analysis of **2.10** confirms typical downstream responses of PPAR $\alpha$  agonism including PPAR $\alpha$  upregulation, induction of target genes, and inhibition of cell migration.

---

Reprinted with permission from: Xiao-Zheng Dou, Dinesh Nath, Younghwa Shin, Jian-Xing Ma, and Adam S. Duerfeldt, “Structure-guided Evolution of a 2-Phenyl-4-carboxyquinoline Chemotype into PPAR $\alpha$  Selective Agonists: New Leads for Oculo-vascular Conditions” *Bioorganic & Medicinal Chemistry Letters* 2018, 28 (16), 2717-2722 DOI: <https://doi.org/10.1016/j.bmcl.2018.03.010>. Copyright © 2020 Elsevier B.V. or its licensors or contributors. X.-Z. D. and D.N. equally conducted all experiments described herein except for western blot analysis, RT-PCR, and HRCEC wound healing assay experiments conducted by Y. Shin. X.-Z. D., D. N., and A.S.D. designed the research studies, analyzed, and interpreted the data, wrote, and reviewed the manuscript. Y. Shin and J.-X. Ma provided critical insight, expertise, personnel, and facilities and reviewed the manuscript.

## 2.2 Rationale for the Development of Y-0452

The promise of PPAR $\alpha$  agonism as a novel strategy for treating retinal diseases was discussed in chapter 1. Although PPAR $\alpha$  agonism was intensely investigated in the 1990s as a therapeutic approach for dyslipidemia, and numerous potent agonists exist in literature, none of the known chemotypes have been evaluated in animal models for efficacy against retinal conditions. Rather than attempting to repurpose known compounds, often lacking full disclosure of physicochemical and pharmacokinetic/pharmacodynamic (PK/PD) profiles, we decided to embark on a discovery process to identify and develop novel PPAR $\alpha$  agonistic chemotypes (**Figure 2.1**) as new compositions for DR and AMD leads.

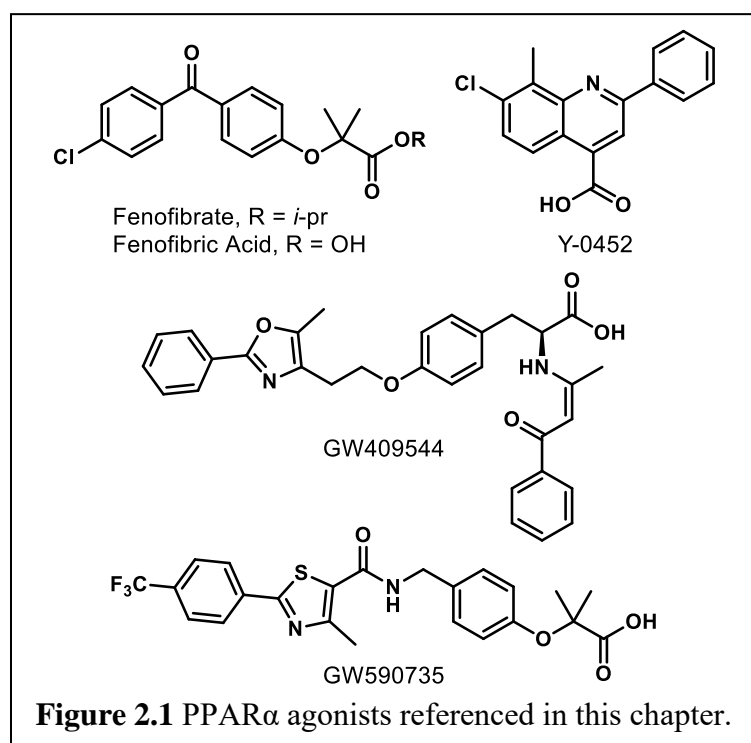


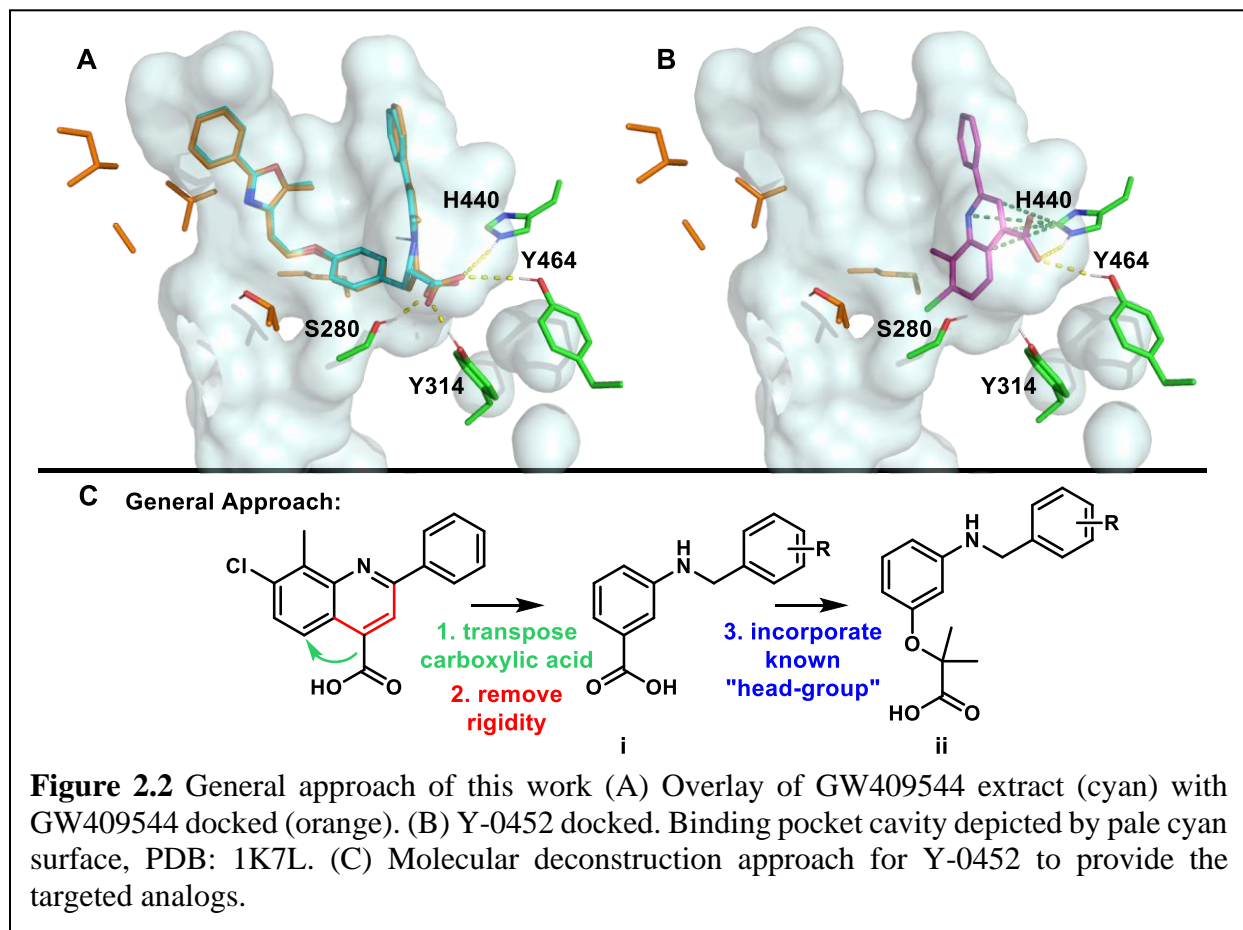
**Figure 2.1** PPAR $\alpha$  agonists referenced in this chapter.

As described in chapter 1, Y-0452 (**Figure 2.1**) was reported as a new PPAR $\alpha$  agonist that has a distinct chemical structure and exhibits protective effects against DR *in vitro* and *in vivo*.<sup>1</sup> With a goal to enhance synthetic tractability, target engagement, selectivity, and level of PPAR $\alpha$  agonism, we embarked on SAR studies of Y-0452 leveraging *in silico* studies for guidance.

To gain insight into the potential binding modes of Y-0452 to PPAR $\alpha$  we conducted docking studies with the Schrodinger Drug Discovery Suite. For these initial computational studies we selected PDB 1K7L, a co-crystal structure of GW409544 (**Figure 2.1**) bound to human PPAR $\alpha$ .

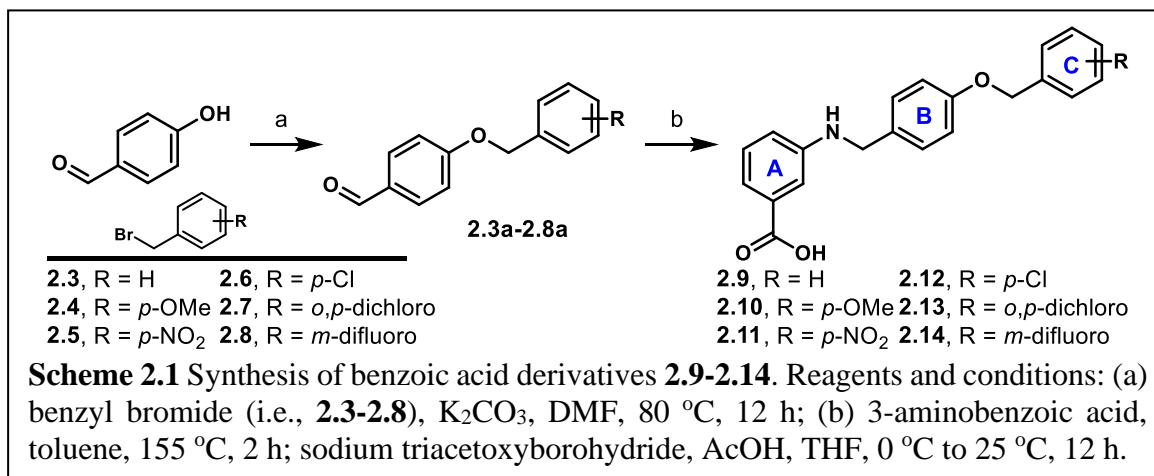
(hPPAR $\alpha$ ).<sup>2</sup> Although GW409544 exhibits 10-fold higher selectivity for hPPAR $\gamma$  ( $EC_{50}$  = 0.28 nM) over hPPAR $\alpha$  ( $EC_{50}$  = 2.3 nM), this structure was selected on the basis that detailed structural analyses of this chemotype and its interactions with different hPPAR isoforms are available for comparison and the data have been well-vetted in subsequent studies.<sup>2</sup>

To validate our docking approach, constraints, and parameters, GW409544 was extracted, exposed to MM2 energy-minimization, and re-docked into the hPPAR $\alpha$  ligand binding domain to ensure that the results reproduced the bound conformation of the ligand. As shown in **Figure 2.2A**, the overlay of co-crystallized (cyan) and docked (orange) GW409544 shows excellent congruence (RMSD = 0.34 Å). Maintaining the same constraints and parameters, Y-0452 was docked into hPPAR $\alpha$  and the results were analyzed for strategies to improve or introduce key interactions. Previous studies have demonstrated the significance of hydrogen bond interactions between



hPPAR $\alpha$  Ser280, Tyr314, His440, and Tyr464 and the carboxylate motif of ligands.<sup>2-9</sup> Interactions with all four of these residues is believed to be responsible for triggering full agonism of hPPAR $\alpha$ .<sup>5</sup> Poorer agonists tend to only interact with some of these hydrogen-bonding partners. As can be seen in **Figure 2.2B**, while the quinoline core of Y-0452 provides a  $\pi$ -system for additional beneficial ligand-protein interactions via edge-to-face stacking with His440, the position of the carboxylate group on Y-0452 is predicted to only allow for two of the four possible hydrogen bonds.

We hypothesized that deconstruction of the quinoline core would 1) provide a more synthetically tractable scaffold amenable to facile assessment of carboxylate location and 2) relieve the rigidity encompassed within the aromatic 2-phenyl-carboxyquinoline chemotype. Although conformational constraint is a common technique used in medicinal chemistry to reduce entropic penalties through conformational bias, we hypothesized that, in this case, the rigidity of Y-0452 may be disadvantageous when the fragment is “grown” to fit the “U-shaped” binding pocket. We anticipated, however, that oversimplification of an already modest hit may lead to inactive compounds, simply due to a reduction in surface area, thus limiting beneficial ligand-protein interactions. Indeed, simple N-benzylated variants of **i** (**Figure 2.2C**) resulted in inactive derivatives (data not included). Docking of the simple N-benzylated analogs, however, revealed a

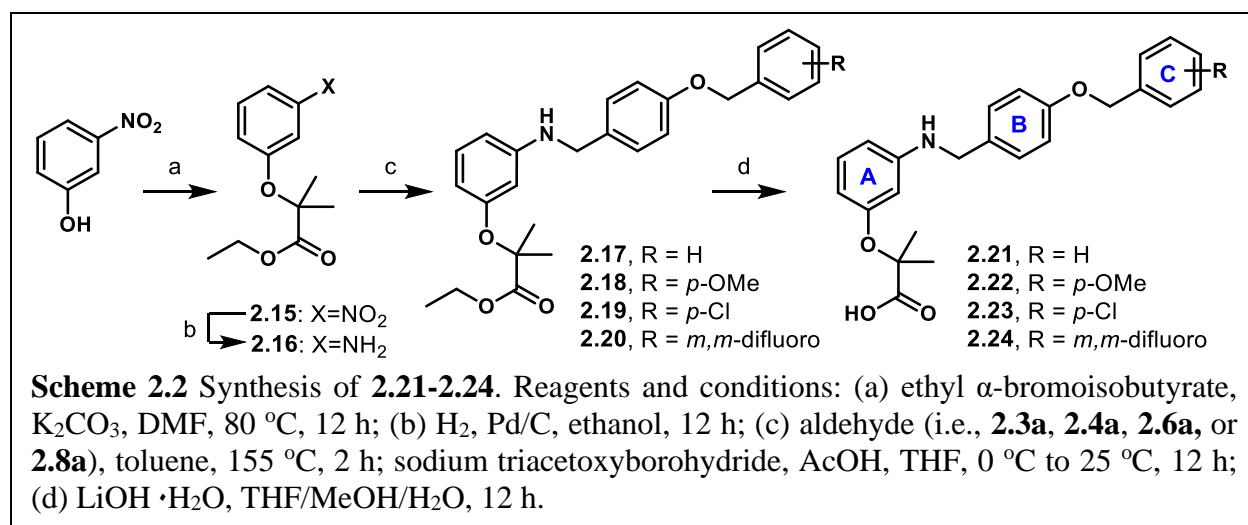


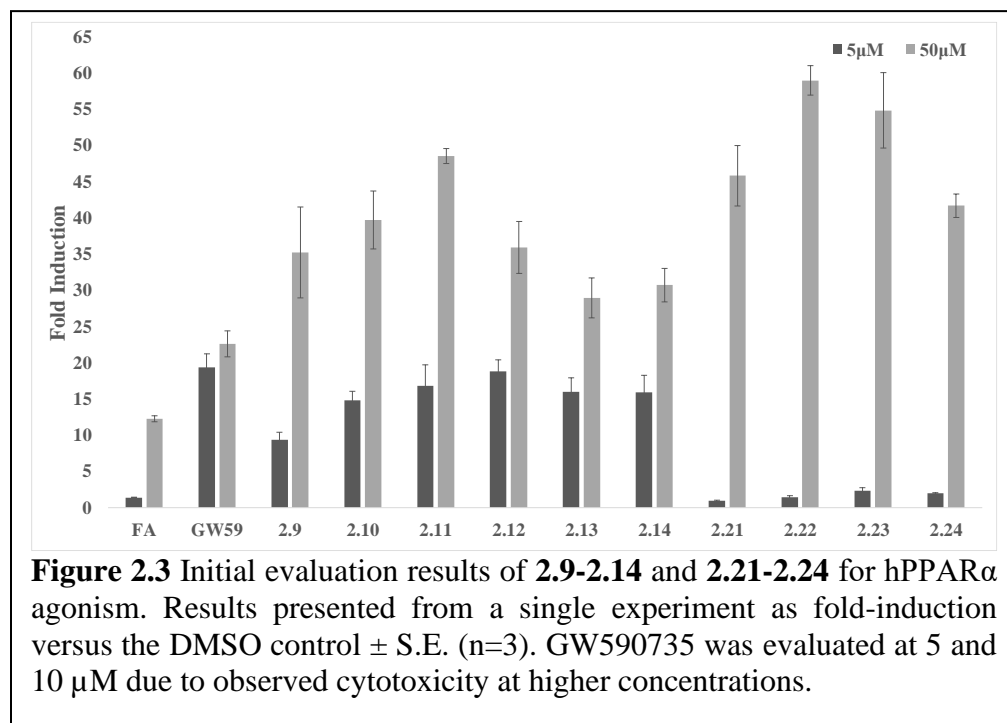
180° rotation of the molecules in the binding pocket, which positioned the substituted benzyl group in the same pocket as the oxazole of GW409544. Taking this into account and recognizing the value in the molecular orientation, we utilized structure-guided design to develop **2.9-2.14** and **2.21-2.24** that filled the hydrophobic binding pocket more efficiently. This focused set of analogs allowed us to test our hypothesis that quinoline deconstruction and transposition of the carboxylic acid would provide improved PPAR $\alpha$  agonists.

### 2.3 Synthesis and Results of First-generation Analogs

Derivatives **2.9-2.14** were synthesized as shown in **Scheme 2.1**. Commercially available 4-hydroxybenzaldehyde was coupled with various benzyl bromides **2.3-2.8** to afford benzaldehydes **2.3a-2.8a**. Treatment of **2.3a-2.8a** with 3-aminobenzoic acid produced the respective imines *in situ*, which were then reduced upon the addition of sodium triacetoxyborohydride to provide **2.9-2.14** in an unoptimized 40-82% yield.

In addition to the benzoic acids derivatives **2.9-2.14**, we wanted to incorporate the classical fibrate “head-group” with an aim to improve potency and instill selectivity for PPAR $\alpha$  over other isoforms.<sup>31</sup> The preparation of these analogs is depicted in **Scheme 2.2**. Commercially available 3-nitrophenol was coupled with ethyl  $\alpha$ -bromoisobutyrate to afford **2.15**, which was then reduced





to the corresponding aniline (**2.16**) under catalytic hydrogenation conditions ( $H_2$  and Pd/C in ethanol). Treatment of **2.16** with **2.3a**,

**2.4a**, **2.6a**, or **2.8a** followed by reduction with sodium triacetoxyborohydride yielded **2.17-2.20**, respectively. Hydrolysis of the pendant ester gave the desired products **2.21-2.24** in an unoptimized 46-88% yield.

With the focused subset of Y-0452 analogs in-hand, our efforts shifted to the evaluation of these derivatives for PPAR $\alpha$  agonism. Preliminary evaluation utilized a commercially available PPAR $\alpha$  luciferase cell reporter assay (Indigo Biosciences). The cell-line employed is engineered to constitutively express high-levels of hPPAR $\alpha$ . Upon interaction with an agonist, hPPAR $\alpha$  translocates to the nucleus, binds to the PPRE, and upregulates gene transcription, including the inserted luciferase gene. Luciferase activity is detected indirectly through quantification of oxyluciferin production. Initially, **2.9-2.14** and **2.21-2.24** were evaluated at 5  $\mu$ M and 50  $\mu$ M to provide an idea of agonism-level at two 10-fold increments. As shown in **Figure 2.3**, a number of compounds exhibited levels of hPPAR $\alpha$  agonism on par with or surpassing the positive control, GW590735 (5  $\mu$ M and 10  $\mu$ M, **Figure 2.1**), at one or both of the concentrations evaluated. Direct

comparison of **2.9/2.21**, **2.10/2.22**, **2.12/2.23**, **2.14/2.24** reveals that incorporation of the fenofibrate “head-group” enhances the level of PPAR $\alpha$  agonism at 50  $\mu$ M. This data also indicates, however, that incorporation of the fibrate “head-group” decreases potency, as **2.21-2.24** fail to elicit appreciable activity at 5  $\mu$ M, whereas the benzoic acid analogs **2.9-2.14** all exhibit significant PPAR $\alpha$  agonism at this lower concentration. Compounds **2.10** and **2.22** were selected for more detailed evaluation, and a more expansive 10-point dose-response assessment was conducted to obtain EC<sub>50</sub> values (**Table 2.1**): **2.10** (5.6  $\mu$ M), and **2.22** (25.3  $\mu$ M).

To further confirm that this 4-benzyloxy-benzylamino chemotype acts as a PPAR $\alpha$  agonist, we evaluated compound **2.10** in various biochemical assays. As expected for a PPAR $\alpha$  agonist, **2.10** induced the expression of PPAR $\alpha$  in a dose-dependent manner (**Figure 2.4A** and **2.4B**), as demonstrated by Western blot analysis using a cell line derived from C57BL/6N mouse photoreceptors (661W). Likewise, RT-PCR studies on the same cell-line confirm PPAR $\alpha$  agonism, as treatment with **2.10** induces the expression of various PPAR $\alpha$  target genes (**Figure 2.4C**),<sup>10</sup> including acyl-CoA dehydrogenase medium chain (*Acadm*), carnitine palmitoyltransferase 1A

(*Cpt1a*), fatty acid binding protein 3 (*Fabp3*), and solute carrier family 25 member 20 (*Slc25a20*). Compound **2.10** was also evaluated in an *in vitro* wound healing assay utilizing HRCEC. PPAR $\alpha$  agonism reduces cell migration<sup>12</sup> and

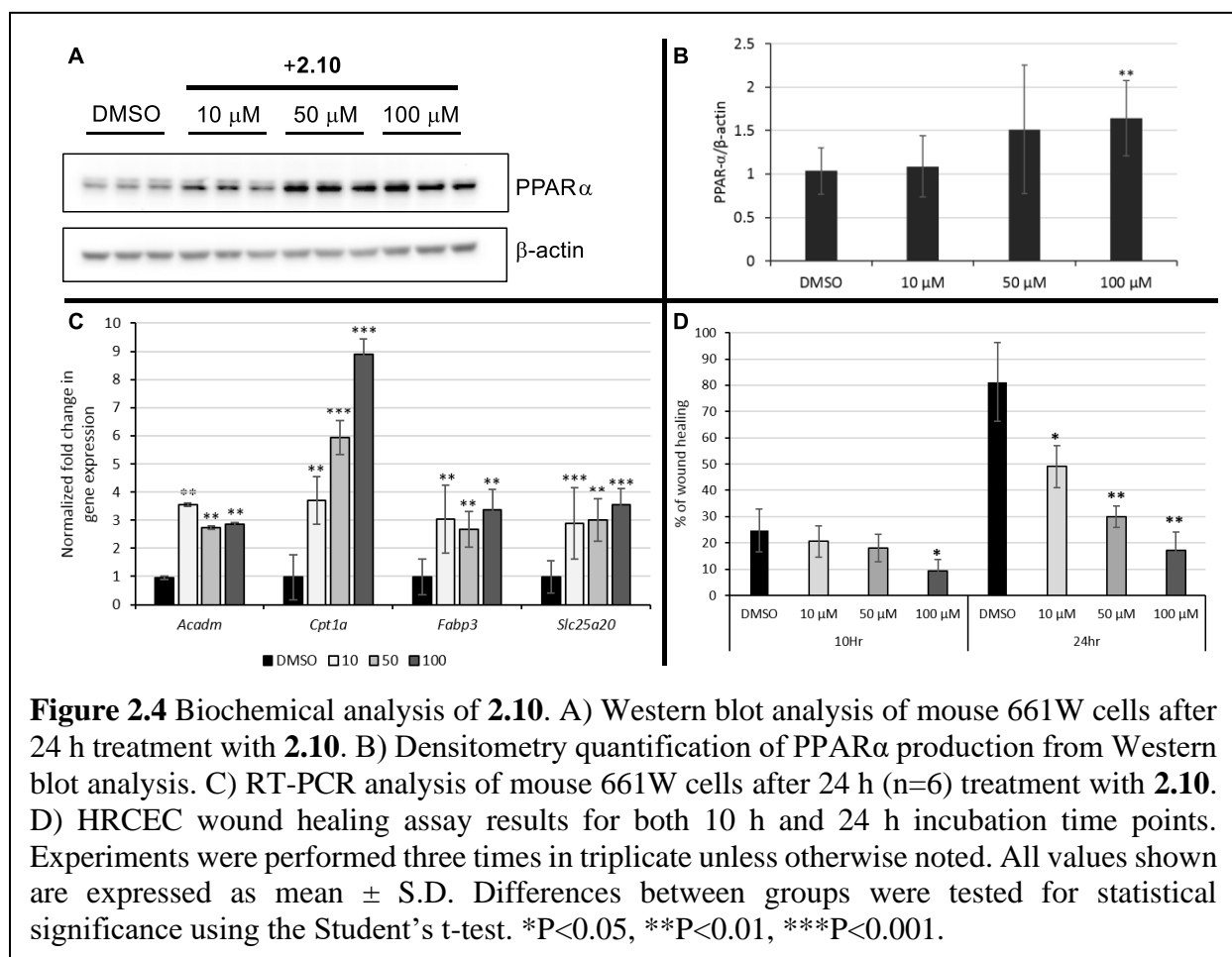
**Table 2.1** Human PPAR agonism of select analogs. Data are represented as the EC<sub>50</sub> ( $\mu$ M) for the agonism of the corresponding luciferase reporter cell-lines (Indigo Biosciences). Dosing was done in triplicate as a single experiment. n.d.=not determined. Values in parentheses indicate the ratio of agonism compared to GW590735.

Compound	EC <sub>50</sub> ( $\mu$ M)		
	hPPAR $\alpha$	hPPAR $\delta$	hPPAR $\gamma$
<b>2.10</b>	5.6 (1.5)	>100	>100
<b>2.22</b>	25.3 (1.7)	38.6	18.3
<b>2.26</b>	5.1 (1.1)	>100	>100
<b>2.28</b>	2.1 (1.4)	8.9	5.6
GW590735	0.012	n.d.	n.d.
Rosiglitazone	n.d.	n.d.	0.083
GW0742	n.d.	0.002	n.d.
Y-0542	52.4 (0.3)	n.d.	n.d.

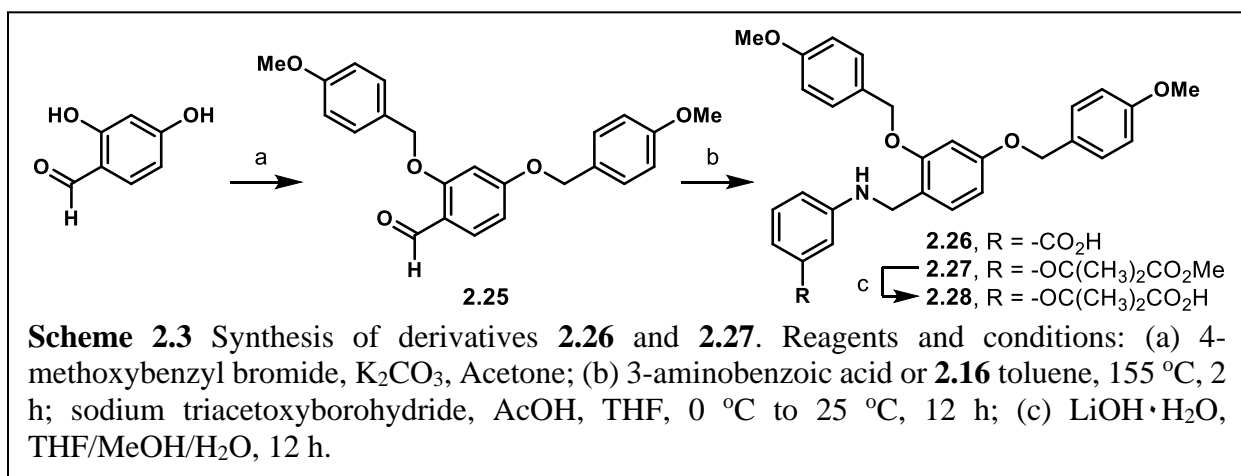


**2.10**, indeed, inhibits wound closure in a dose-dependent fashion (**Figure 2.4D**).

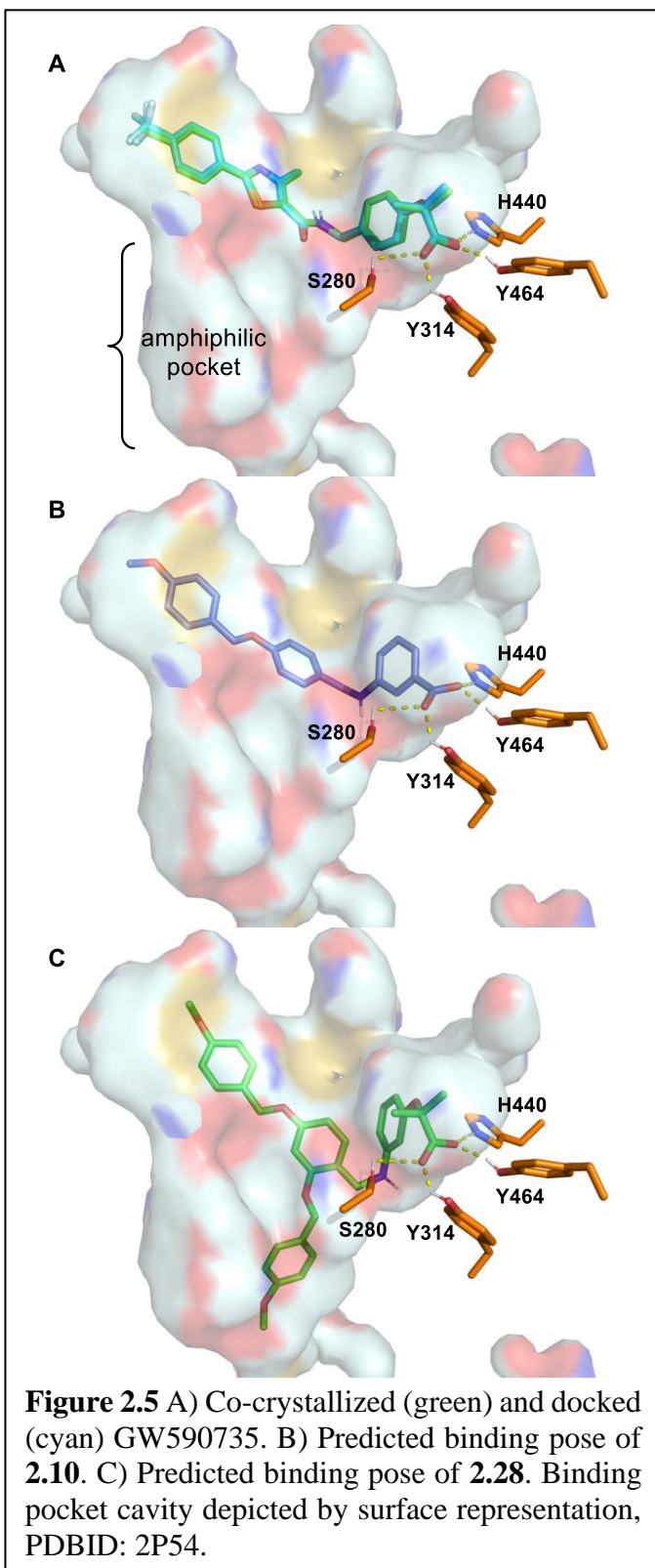
Convinced that 4-benzyloxy-benzylamino derivatives exhibit characteristic PPAR $\alpha$  agonistic activity in several biological settings, the selectivity of **2.10** for PPAR $\alpha$  agonism over PPAR $\delta$  and PPAR $\gamma$  was assessed. Luciferase assays were conducted on isogenic cell-lines engineered to overexpress either PPAR $\delta$  or PPAR $\gamma$  with expression of the requisite luciferase reporter gene dependent upon exogenous activation of each isoform. As shown in **Table 2.1**, compound **2.10** exhibits  $\geq 20$ -fold selectivity for hPPAR $\alpha$  over hPPAR $\delta$  and hPPAR $\gamma$ , whereas **2.22** displays *pan*-agonism. This is interesting, as the fibrate “head-group” has been described as a critical feature for PPAR $\alpha$  selectivity,<sup>10</sup> but with this 4-benzyloxy-benzylamino chemotype it seems to be detrimental.



To better visualize the 4-benzyloxy-benzylamino derivatives in the hPPAR $\alpha$  binding pocket, we utilized PDB 2P54, the GW590735•hPPAR $\alpha$  co-crystal structure, for docking assessment (see Appendix 1). GW590735 is a selective PPAR $\alpha$  agonist that exhibits  $\geq 500$ -fold selectivity for PPAR $\alpha$  over PPAR $\beta$  and PPAR $\gamma$ .<sup>31</sup> As shown in **Figure 2.5A** and **2.5B**, compound **2.10** is predicted to bind in an orientation similar to GW590735. Interestingly, however, **2.10** lacks the gem-dimethyl “head-group” and amide linker domain, both of which have been postulated to be critical determinants in GW590735 selectivity and major enhancers of potency.<sup>31</sup> The acid, however, for **2.10** is predicted to make four hydrogen bonds with Ser280, Tyr314, His440, and Tyr464, consistent with our hypothesis that deconstruction of the Y-0452 quinoline core and transposition of the carboxylic acid would provide a significant improvement in PPAR $\alpha$  agonism. We were interested if this 4-benzyloxy-benzylamino chemotype could be expanded to take advantage of an apparent amphiphilic pocket that lies below GW590735 (**Figure 2.5A**) and is comprised of Met330, Tyr334, Glu282, Thr279, Met320, Val324, Leu321, Ile317, and Met220. We postulated that functionalization of the B-ring *meta* to the ether linkage (**Schemes 2.2** and **2.3**) on **2.10** would provide an optimal trajectory for accessing this amphiphilic pocket. To the best of our knowledge, few PPAR $\alpha$  agonists exploit this pocket and little SAR exists regarding the effect of occupying this domain on the level of agonism and/or isoform selectivity.

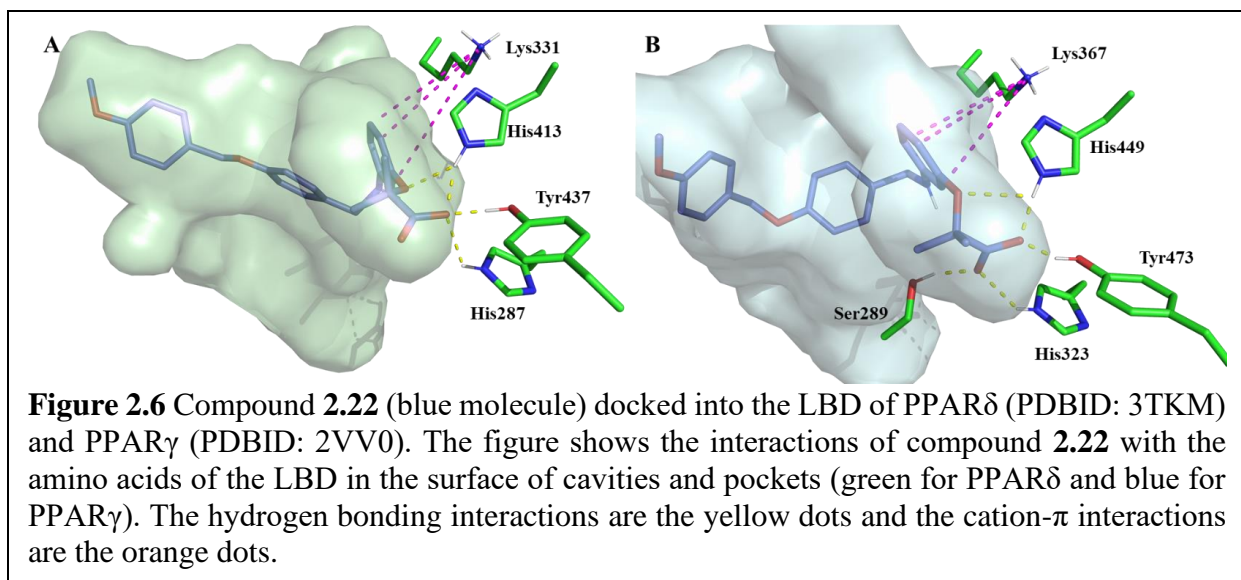


To investigate the possible impact of occupying the amphiphilic pocket, we synthesized two additional derivatives, **2.26** and **2.28** (Scheme 2.3). Briefly, commercially available 2,4-dihydroxybenzaldehyde was treated with 4-methoxybenzaldehyde in the presence of potassium carbonate in acetone to produce the di-*p*-methoxybenzyl (PMB) functionalized resorcinol **2.25**. This intermediate was coupled to either 3-aminobenzoic acid or **2.16** followed by reduction of the resulting imine to provide analog **2.26** and the methyl ester **2.27**, respectively. Following saponification of **2.27**, the desired derivative **2.28** was obtained in 75% yield. Incorporation of the 4-methoxybenzyl motif as the “third-arm” was rather arbitrary at this point and was selected on belief that it 1) would be compatible with the predicted binding environment and 2) could be easily synthesized through dialkylation of an aldehyde already in our chemical inventory.



Derivatives **2.26** and **2.28** were evaluated for hPPAR $\alpha$  agonistic activity and selectivity in the luciferase cell-lines. Analysis of the data suggests that regarding the benzoic acid derivatives (compare **2.10** and **2.26**), the additional 4-methoxybenzyl substituent does not affect potency and maintains the selectivity, at least within the range of doses evaluated. For derivatives containing the fibrate “head-group” (compare **2.22** and **2.28**), however, the addition of the third substituent on the B-ring resulted in a 10-fold improvement in potency, but the *pan*-agonist profile was maintained. Both **2.26** and **2.28** were docked using our previously generated model and as can be seen in **Figure 2.5C** the additional 4-methoxybenzyl group is, indeed, predicted to extend into the amphiphilic pocket. Experimental validation is necessary to confirm the binding mode predicted by *in silico* methods, but thus far the SAR data seem to support the models. Studies are ongoing to optimize each of the three substituents on the B-ring and results will be reported in due course.

In most PPAR $\alpha$  agonists a carboxylic acid acts as the pharmacophore and forms a hydrogen bond network with Ser280, Tyr314, His440, and Tyr464. This interaction is known to play key roles in affinity, selectivity and degree of agonism.<sup>11</sup> The 4-benzyloxy-benzylamino chemotype that we developed contains a benzoic acid, which provides the carboxylic acid necessary to fulfill the critical hydrogen bonding trigger. Previous SAR studies on other PPAR $\alpha$  agonistic chemotypes show that incorporation of the fibrate head-group typically results in improved selectivity and potency for PPAR $\alpha$ .<sup>12</sup> Interestingly, however, the 4-benzyloxy-benzylamino chemotype fails to follow this trend, as incorporation of the fibrate head-group leads to decreases in potency and selectivity but results instead in a higher level of agonism. This is worth noting, as it suggests that the 4-benzyloxy-benzylamino chemotype interacts with the ligand binding domain differently than other reported chemotypes. This is an important observation, because as a transcription factor, it is well known that the specific downstream effects of PPAR $\alpha$  activation are dependent upon ligand



induced conformational changes.<sup>13</sup> Thus, it is very possible that the 4-benzyloxy-benzylamino chemotype may display differential downstream effects and/or produce a unique PPAR $\alpha$  agonistic profile that differentiates it from the well-studied fibrates.

In hopes of rationalizing why the fibrate head-group installation on this scaffold results in pan-agonism of all isoforms, we conducted *in silico* experiments for the rest of the PPAR isoforms, PPAR $\delta$  and PPAR $\gamma$  (**Figure 2.6**). Our models predict that incorporation of the fibrate head-group results in an extra predicted hydrogen bonding interaction with His413 (PPAR $\delta$ ) and His449 (PPAR $\gamma$ ), which may strengthen the binding to these two isoforms. Additionally, inclusion of the fibrate head-group is predicted to cause a slight rotation of the pendant benzene ring in the binding pocket, which is predicted to allow for a cation- $\pi$  interaction with Lys331 (PPAR $\delta$ ) and Lys367 (PPAR $\gamma$ ). These additional interactions are not observed with the 4-benzyloxy-benzylamino chemotype and thus may be a key factor in the observed pan agonism for the fibrate head-group containing analogs.

## 2.4 Conclusion

In conclusion, we have leveraged *in silico* methods to provide structure-guided insight towards the evolution of a new PPAR $\alpha$  agonistic chemotype. The results confirm our hypothesis that transposition of the carboxylic acid and deconstruction of the rigid quinoline core of Y-0452 provides a more synthetically tractable class of analogs that exhibit promising PPAR $\alpha$  agonism levels and selectivity over other isoforms. Two classes of PPAR agonists have emerged from the initial SAR studies; benzoic acid derivatives that exhibit >20-fold selectivity for PPAR $\alpha$  and second class that contains the classical fibrate head-group and exhibits *pan*-PPAR agonism. The preliminary results presented suggest that a relatively unexploited amphiphilic pocket provides a promising avenue to interrogate in future SAR studies. Co-crystallization studies are underway to provide more detailed insight into the specific ligand-protein interactions driving PPAR $\alpha$  potency and selectivity within this 4-benzyloxy-benzylamino chemotype.

## 2.5 Methods and Experimental

### *General procedure A: synthesis of 4-benzyloxy-benzaldehydes (2.3a-2.8a)*

To a stirred solution of 4-hydroxybenzaldehyde (1.0 eq.) in DMF (1 M) was added K<sub>2</sub>CO<sub>3</sub> (2.0 eq.). After 10 min, the reaction was treated with an appropriately substituted benzyl bromide **2.3-2.8** (1.02 eq.) and heated to 80 °C for 16 h. The reaction was monitored by TLC. Upon complete consumption of 4-hydroxybenzaldehyde, the reaction was quenched with 1N aq. HCl and extracted with EtOAc. The combined organic layers were washed with aq. 5% NaOH, water, and brine. The organic layer was dried over anhydrous Na<sub>2</sub>SO<sub>4</sub>, filtered, and concentrated under vacuum. The crude products were used without further purification.

### *General procedure B: reductive amination (2.9-2.14, 2.17-2.20, 2.26, and 2.27)*

To a stirred solution of 3-amino-benzoic acid (1.0 eq.) in toluene (0.01 M), was added the requisite aldehyde **2.3a-2.8a** (1.02 eq.). The reaction mixture was connected to a Dean–Stark apparatus and heated to reflux for 2 h. The solvent and excess aldehyde were removed under vacuum. The resulting crude residue was dissolved in THF (0.01 M) and cooled to 0 °C prior to the addition of sodium triacetoxyborohydride (2.0 eq.). The reaction mixture was stirred for 15 min and then a couple drops of glacial acetic acid were added. The reaction mixture was allowed to warm to ambient temperature and stir 12 h.<sup>14</sup> The reaction was quenched with water after upon completion. The mixture was extracted with EtOAc and the organic layers were combined, dried over Na<sub>2</sub>SO<sub>4</sub>, filtered, and evaporated under vacuum. For **2.9-2.14**, the products were purified by flash column chromatography (SiO<sub>2</sub>, CH<sub>2</sub>Cl<sub>2</sub>/CH<sub>3</sub>OH, 99.5:0.5). For **2.17-2.20**, the crude products were advanced without further purification. All reaction scales indicated below are with respect to the limiting reactant, 3-amino-benzoic acid.

*General procedure C: ester saponification (2.21-2.24, and 2.28)*

To a stirred solution of ethyl ester (1.0 eq.) in THF/MeOH/H<sub>2</sub>O (0.5 M, 3:1:1) was added lithium hydroxide monohydrate (5.0 eq.) and the reaction mixture was stirred for 16 h at room temperature. The reaction mixture was then concentrated by vacuum. The aqueous layer was acidified to pH ~2.0 with 1 N aq. HCl and then extracted with EtOAc. The organic layer was washed with water, brine, dried over Na<sub>2</sub>SO<sub>4</sub>, and filtered. The organics were removed in vacuo. **2.21-2.24** were purified by flash column chromatography (SiO<sub>2</sub>, CH<sub>2</sub>Cl<sub>2</sub>/CH<sub>3</sub>OH, 99:1).<sup>15</sup>

**3-((4-(Benzyloxy)benzyl)amino)benzoic acid (2.9)**: Reaction scale: 100 mg (0.73 mmol). Compound **2.9** was prepared following general procedure B with **2.3a**. The product was purified by flash column chromatography (SiO<sub>2</sub>, CH<sub>2</sub>Cl<sub>2</sub>/CH<sub>3</sub>OH, 99.5:0.5) to give a white amorphous solid (160 mg, 66% yield) <sup>1</sup>H NMR (500 MHz, Methanol-*d*<sub>4</sub>) δ 7.42 (d, *J* = 7.2 Hz, 2H), 7.35 (t,

$J = 7.6, 7.2$  Hz, 2H), 7.32 – 7.29 (m, 1H), 7.29 – 7.29 (m, 2H), 7.29 – 7.27 (m, 1H), 7.25 (ddd,  $J = 7.8, 1.5$  Hz, 1H), 7.15 (dd,  $J = 8.5, 7.8$  Hz, 1H), 6.94 (d,  $J = 8.7$  Hz, 2H), 6.82 (dd,  $J = 7.6, 2.0$  Hz, 1H), 5.05 (s, 2H), 4.26 (s, 2H) ppm;  $^{13}\text{C}$  NMR (101 MHz, Methanol- $d_4$ )  $\delta$  198.9, 187.4, 178.4, 166.9, 161.4, 160.6, 158.0, 157.7, 157.6, 156.9, 156.7, 147.1, 146.5, 144.0, 142.8, 99.1, 76.1 ppm. HRESI  $m/z$ : 356.1240 ( $\text{C}_{21}\text{H}_{19}\text{NO}_3 + \text{Na}^+$  requires 356.1257).

**3-((4-((4-methoxybenzyl)oxy)benzyl)amino)benzoic acid (2.10):** Reaction scale: 100 mg (0.73 mmol). Compound **2.10** was prepared following general procedure B with compound **2.4a**. The product was purified by flash column chromatography ( $\text{SiO}_2$ ,  $\text{CH}_2\text{Cl}_2/\text{CH}_3\text{OH}$ , 99.5:0.5) to give a white amorphous solid (210 mg, 80% yield)  $^1\text{H}$  NMR (400 MHz, Chloroform- $d$ )  $\delta$  7.46 (d,  $J = 7.7$  Hz, 1H), 7.36 (d,  $J = 9.2$  Hz, 3H), 7.27 (q,  $J = 6.3, 4.1$  Hz, 4H), 6.94 (dd,  $J = 14.6, 8.1$  Hz, 4H), 6.84 (d,  $J = 8.3$  Hz, 1H), 4.99 (s, 2H), 4.30 (s, 2H), 3.82 (s, 3H) ppm;  $^{13}\text{C}$  NMR (101 MHz, Chloroform- $d$ )  $\delta$  171.8, 159.6, 158.4, 148.3, 131.1, 130.2, 129.4, 129.3, 129.1, 128.9, 119.4, 118.2, 115.2, 114.1, 114.0, 70.0, 55.4, 47.8 ppm. HRESI  $m/z$ : 364.1449 ( $\text{C}_{22}\text{H}_{21}\text{NO}_4 + \text{H}^+$  requires 364.1543).

**3-((4-((4-Nitrobenzyl)oxy)benzyl)amino)benzoic acid (2.11):** Reaction scale: 50 mg (0.36 mmol scale). Compound **2.11** was prepared following general procedure B with compound **2.5a**. The product was purified by flash column chromatography ( $\text{SiO}_2$ ,  $\text{CH}_2\text{Cl}_2/\text{CH}_3\text{OH}$ , 99.5:0.5) to give a yellow amorphous solid (25 mg, 40% yield).  $^1\text{H}$  NMR (400 MHz, Acetone- $d_6$ )  $\delta$  8.27 (d,  $J = 8.7$  Hz, 2H), 7.77 (d,  $J = 8.4$  Hz, 2H), 7.37 (s, 2H), 7.35 (s, 1H), 7.28 (d,  $J = 7.7$  Hz, 1H), 7.18 (t,  $J = 7.8$  Hz, 1H), 7.01 (d,  $J = 8.6$  Hz, 2H), 6.88 (dd,  $J = 8.1, 2.3$  Hz, 1H), 5.29 (s, 2H), 4.34 (s, 2H) ppm.  $^{13}\text{C}$  NMR (101 MHz, Acetone- $d_6$ )  $\delta$  168.2, 158.3, 149.7, 148.3, 146.2, 133.3, 132.2, 129.7, 129.4, 128.8, 124.3, 118.5, 117.6, 115.6, 114.2, 69.2, 47.3 ppm. HRESI  $m/z$ : 377.1153 ( $\text{C}_{21}\text{H}_{18}\text{N}_2\text{O}_5 + \text{H}^+$  requires 377.1137)



**3-((4-((4-Chlorobenzyl)oxy)benzyl)amino)benzoic acid (2.12):** Reaction scale: 100 mg (0.73 mmol). Compound **2.12** was prepared following general procedure B with compound **2.6a**. The product was purified by flash column chromatography (SiO<sub>2</sub>, CH<sub>2</sub>Cl<sub>2</sub>/CH<sub>3</sub>OH, 99.5:0.5) to give a white amorphous solid (200 mg, 75% yield). <sup>1</sup>H NMR (400 MHz, Methanol-*d*<sub>4</sub>) δ 7.41 (d, *J* = 8.6 Hz, 2H), 7.36 (d, *J* = 8.5 Hz, 2H), 7.30 (s, 1H), 7.28 (s, 2H), 7.25 (ddd, *J* = 7.6, 1.3 Hz, 1H), 7.15 (dd, *J* = 7.8 Hz, 1H), 6.93 (d, *J* = 8.6 Hz, 2H), 6.82 (ddd, *J* = 8.0, 2.5, 1.1 Hz, 1H), 5.03 (s, 2H), 4.26 (s, 3H) ppm. <sup>13</sup>C NMR (101 MHz, Methanol-*d*<sub>4</sub>) δ 170.6, 159.0, 150.2, 137.6, 134.5, 133.4, 132.4, 130.1, 129.8, 129.6, 129.5, 118.9, 118.4, 115.9, 114.6, 70.1, 47.9 ppm. HRESI m/z: 366.0897 (C<sub>21</sub>H<sub>18</sub>ClNO<sub>3</sub> - H<sup>-</sup> requires 366.0897).

**3-((4-((2,4-Dichlorobenzyl)oxy)benzyl)amino)benzoic acid (2.13):** Reaction scale: 100 mg (0.73 mmol). Compound **2.13** was prepared following general procedure B with compound **2.7a**. The product was purified by flash column chromatography (SiO<sub>2</sub>, CH<sub>2</sub>Cl<sub>2</sub>/CH<sub>3</sub>OH, 99.5:0.5) to give a white amorphous solid (240 mg, 82% yield). <sup>1</sup>H NMR (500 MHz, Methanol-*d*<sub>4</sub>) δ 7.54 (d, *J* = 8.3 Hz, 1H), 7.49 (d, *J* = 2.1 Hz, 1H), 7.34 (dd, *J* = 8.3, 2.1 Hz, 1H), 7.31 (d, *J* = 8.6 Hz, 2H), 7.28 (t, *J* = 2.0 Hz, 1H), 7.25 (dt, *J* = 7.6, 1.3 Hz, 1H), 7.15 (t, *J* = 7.9 Hz, 1H), 6.95 (d, *J* = 8.7 Hz, 2H), 6.82 (ddd, *J* = 8.1, 2.5, 1.0 Hz, 1H), 5.11 (s, 2H), 4.27 (s, 2H) ppm. <sup>13</sup>C NMR (101 MHz, Methanol-*d*<sub>4</sub>) δ 170.6, 158.9, 150.2, 135.3, 135.2, 134.8, 133.9, 132.4, 131.5, 130.1, 129.8, 129.7, 128.4, 119.0, 118.4, 116.0, 114.7, 67.9, 48.0 ppm. HRESI m/z: 424.0468 (C<sub>21</sub>H<sub>17</sub>Cl<sub>2</sub>NO<sub>3</sub> + Na<sup>+</sup> requires 424.0478).

**3-((4-((3,5-Difluorobenzyl)oxy)benzyl)amino)benzoic acid (2.14):** Reaction scale: 100 mg (0.73 mmol). Compound **2.14** was prepared following general procedure B with compound **2.8a**. The product was purified by flash column chromatography (SiO<sub>2</sub>, CH<sub>2</sub>Cl<sub>2</sub>/CH<sub>3</sub>OH, 99.5:0.5) to give a white amorphous solid (200 mg, 74% yield). <sup>1</sup>H NMR (500 MHz, Methanol-*d*<sub>4</sub>) δ 7.30 (d, *J* = 8.6

Hz, 2H), 7.28 (t,  $J = 2.0$  Hz, 3H), 7.25 (dt,  $J = 7.5, 1.3$  Hz, 1H), 7.15 (t,  $J = 7.9$  Hz, 1H), 7.07 – 7.00 (m, 2H), 6.94 (d,  $J = 8.6$  Hz, 2H), 6.86 (tt,  $J = 9.2, 2.4$  Hz, 1H), 6.82 (ddd,  $J = 8.1, 2.5, 1.0$  Hz, 1H), 5.08 (s, 2H), 4.27 (s, 2H) ppm.  $^{13}\text{C}$  NMR (101 MHz, Methanol- $d_4$ )  $\delta$  170.6, 165.8 (d,  $J = 12.9$  Hz), 158.7, 150.2, 143.6, 133.7, 132.4, 129.9, 129.7, 119.0, 118.4, 115.9, 114.6, 112.9 – 108.6 (m), 103.6 (t,  $J = 25.8$  Hz), 69.5 (t,  $J = 2.3$  Hz), 48.0 ppm. HRESI  $m/z$ : 368.1120 ( $\text{C}_{21}\text{H}_{16}\text{F}_2\text{NO}_3 - \text{H}^+$  requires 368.1098).

**2-(3-((4-(Benzyloxy)benzyl)amino)phenoxy)-2-methylpropanoic acid (2.21):** Compound **2.21** was prepared following the General Procedure C from compound **2.17** (30 mg, 0.07 mmol). The product was purified by flash column chromatography ( $\text{SiO}_2$   $\text{CH}_2\text{Cl}_2/\text{CH}_3\text{OH}$ , 100:1) to give a white amorphous solid (22 mg, 78% yield).  $^1\text{H}$  NMR (500 MHz, Methanol- $d_4$ )  $\delta$  7.41 (d,  $J = 7.4$  Hz, 2H), 7.35 (t,  $J = 7.6$  Hz, 2H), 7.29 (t,  $J = 7.1$  Hz, 1H), 7.26 (d,  $J = 8.3$  Hz, 2H), 6.96 – 6.92 (m, 2H), 6.92 (d,  $J = 3.5$  Hz, 2H), 6.31 (dd,  $J = 8.1, 2.0$  Hz, 1H), 6.19 (s, 1H), 6.16 (dd,  $J = 8.1, 2.2$  Hz, 1H), 5.05 (d,  $J = 2.1$  Hz, 2H), 4.18 (s, 2H), 1.47 (s, 6H) ppm.  $^{13}\text{C}$  NMR (101 MHz, Methanol- $d_4$ )  $\delta$  178.3, 159.2, 157.7, 151.1, 138.8, 133.5, 130.2, 129.6, 129.4, 128.7, 128.5, 115.8, 109.1, 105.6, 105.5, 79.9, 70.9, 48.2, 25.7 ppm. HRESI  $m/z$ : 392.1060 ( $\text{C}_{24}\text{H}_{25}\text{NO}_4 + \text{H}^+$  requires 392.1856).

**2-(3-((4-((4-Methoxybenzyl)oxy)benzyl)amino)phenoxy)-2-methylpropanoic acid (2.22):** Compound **2.22** was prepared following general procedure C from compound **2.18** (30 mg, 0.07 mmol). The product was purified by flash column chromatography ( $\text{SiO}_2$ ,  $\text{CH}_2\text{Cl}_2/\text{CH}_3\text{OH}$ , 100:1) to give a white amorphous solid (13 mg, 46% yield).  $^1\text{H}$  NMR (400 MHz, Methanol- $d_4$ )  $\delta$  7.34 (d,  $J = 8.6$  Hz, 2H), 7.25 (d,  $J = 8.5$  Hz, 2H), 6.95 – 6.93 (m, 1H), 6.92 (d,  $J = 3.1$  Hz, 5H), 6.90 (d,  $J = 3.1$  Hz, 2H), 6.30 (dd,  $J = 8.2, 1.6$  Hz, 1H), 6.19 (s, 1H), 6.16 (d,  $J = 8.6$  Hz, 2H), 4.97 (s, 2H), 4.18 (s, 2H), 3.79 (s, 3H), 1.47 (s, 6H) ppm.  $^{13}\text{C}$  NMR (101 MHz, Methanol- $d_4$ )  $\delta$  160.9, 159.2,

157.7, 151.1, 133.4, 130.7, 130.2, 130.1, 130.0, 129.5, 115.9, 114.8, 111.4, 109.2, 109.0, 105.6, 70.8, 55.6, 48.2, 25.8 ppm. HRESI m/z: 444.1771 (C<sub>25</sub>H<sub>27</sub>NO<sub>5</sub> + Na<sup>+</sup> requires 444.1781).

**2-(3-((4-((4-Chlorobenzyl)oxy)benzyl)amino)phenoxy)-2-methylpropanoic acid (2.23):**

Compound **2.23** was prepared following general procedure C from compound **2.19** (120 mg, 0.26 mmol). The product was purified by flash column chromatography (SiO<sub>2</sub>, CH<sub>2</sub>Cl<sub>2</sub>/CH<sub>3</sub>OH, 100:1) to give a white amorphous solid (100 mg, 88% yield). <sup>1</sup>H NMR (500 MHz, Chloroform-*d*) δ 7.39 (s, 1H), 7.26 (d, *J* = 2.1 Hz, 2H), 7.26 (s, 2H), 7.16 (d, *J* = 8.1 Hz, 2H), 6.94 (td, *J* = 8.1, 1.3 Hz, 1H), 6.82 (d, *J* = 7.8 Hz, 2H), 6.25 (dd, *J* = 8.2, 2.2 Hz, 1H), 6.20 (dd, *J* = 8.0, 2.3 Hz, 1H), 6.15 (s, 1H), 4.92 (d, *J* = 1.4 Hz, 2H), 4.11 (s, 2H), 1.47 (s, 6H) ppm. <sup>13</sup>C NMR (126 MHz, Chloroform-*d*) δ 178.8, 157.8, 155.8, 149.1, 135.5, 133.7, 131.5, 129.7, 128.9, 128.8, 115.1, 109.4, 108.4, 105.2, 79.3, 69.3, 47.9, 25.2 ppm. HRESI m/z: 424.1328 (C<sub>24</sub>H<sub>24</sub>ClNO<sub>4</sub> - H<sup>-</sup> requires 424.1316).

**2-(3-((4-((3,5-Difluorobenzyl)oxy)benzyl)amino)phenoxy)-2-methylpropanoic acid (2.24):**

Compound **2.24** was prepared following general procedure C from compound **2.20** (180 mg, 0.40 mmol). The product was purified by flash column chromatography (SiO<sub>2</sub>, CH<sub>2</sub>Cl<sub>2</sub>/CH<sub>3</sub>OH, 100:1) to give a white amorphous solid (130 mg, 51% yield). <sup>1</sup>H NMR (500 MHz, Methanol-*d*<sub>4</sub>) δ 7.28 (d, *J* = 8.6 Hz, 2H), 7.07 – 7.00 (m, 2H), 6.97 – 6.93 (m, 2H), 6.92 (d, *J* = 6.6 Hz, 2H), 6.86 (tt, *J* = 9.0, 2.3 Hz, 1H), 6.31 (ddd, *J* = 8.1, 2.2, 0.8 Hz, 1H), 6.18 (t, *J* = 2.2 Hz, 1H), 6.15 (ddd, *J* = 7.9, 2.3, 0.9 Hz, 1H), 5.09 (s, 2H), 4.19 (s, 2H), 1.46 (s, 6H) ppm. <sup>13</sup>C NMR (101 MHz, Methanol-*d*<sub>4</sub>) δ 178.2, 164.5 (dd, *J* = 247.2, 12.7 Hz), 158.6, 157.6, 151.0, 143.6 (d, *J* = 9.1 Hz), 133.9, 130.2, 129.7, 115.8, 112.9 – 108.5 (m), 109.2, 109.0, 105.5, 103.6 (t, *J* = 25.8 Hz), 79.8, 69.3 (t, *J* = 2.3 Hz), 48.1, 25.7 ppm. HRESI m/z: 426.1542 (C<sub>24</sub>H<sub>23</sub>F<sub>2</sub>NO<sub>4</sub> - H<sup>-</sup> requires 426.1517).

**3-((2,4-bis((4-methoxybenzyl)oxy)benzyl)amino)benzoic acid (2.26):** Compound **2.26** was prepared following general procedure B with compound **2.25**. The product was purified by flash

column chromatography (SiO<sub>2</sub>, CH<sub>2</sub>Cl<sub>2</sub>/CH<sub>3</sub>OH, 99.5:0.5). <sup>1</sup>H NMR (300 MHz, DMSO-*d*<sub>6</sub>) δ 12.64 (s, 1H), 7.38 (dd, *J* = 15.7, 8.6 Hz, 4H), 7.19 – 7.07 (m, 4H), 6.93 (d, *J* = 7.4 Hz, 4H), 6.74 (d, *J* = 7.4 Hz, 2H), 6.53 (d, *J* = 8.5 Hz, 1H), 6.28 (s, 1H), 5.09 (s, 2H), 4.96 (s, 2H), 4.18 (s, 2H), 3.75 (s, 3H), 3.74 (s, 3H) ppm; <sup>13</sup>C NMR (75 MHz, DMSO-*d*<sub>6</sub>) δ 167.9, 158.9, 158.5, 156.8, 148.8, 131.3, 129.6, 129.1, 129.0, 128.9, 128.5, 119.6, 116.5, 116.2, 113.8, 113.8, 112.7, 105.6, 100.5, 69.1, 55.1, 55.0, 40.8 ppm. HRESI m/z: 500.2063 (C<sub>30</sub>H<sub>29</sub>NO<sub>6</sub> + H<sup>+</sup> requires 500.2068)..

**2-(3-((2,4-Bis((4-methoxybenzyl)oxy)benzyl)amino)phenoxy)-2-methylpropanoic acid (2.28):**

Compound **2.28** was prepared following general procedure C from compound **2.27** (100 mg, 0.17 mmol). The product was purified by flash column chromatography (SiO<sub>2</sub>, CH<sub>2</sub>Cl<sub>2</sub>/CH<sub>3</sub>OH, 100:1) to give a white amorphous solid (62 mg, 75% yield). <sup>1</sup>H NMR (500 MHz, Methanol-*d*<sub>4</sub>) δ 7.35 (d, *J* = 8.7 Hz, 2H), 7.31 (d, *J* = 8.7 Hz, 2H), 7.15 (d, *J* = 8.3 Hz, 1H), 6.93 (dd, *J* = 8.0 Hz, 1H), 6.91 (d, *J* = 1.5 Hz, 2H), 6.89 (d, *J* = 1.5 Hz, 2H), 6.65 (d, *J* = 2.3 Hz, 1H), 6.50 (dd, *J* = 8.3, 2.4 Hz, 1H), 6.28 (ddd, *J* = 8.2, 2.2, 0.8 Hz, 1H), 6.20 (dd, *J* = 2.2 Hz, 1H), 6.18 (ddd, *J* = 8.1, 2.3, 0.8 Hz, 1H), 5.02 (s, 2H), 4.94 (s, 2H), 4.18 (s, 2H), 3.78 (s, 6H), 1.47 (s, 6H) ppm. <sup>13</sup>C NMR (101 MHz, Methanol-*d*<sub>4</sub>) δ 178.2, 160.9, 160.9, 160.5, 158.7, 157.7, 150.9, 130.6, 130.6, 130.5, 130.2, 130.2, 130.1, 121.4, 114.9, 114.8, 109.5, 109.4, 107.1, 106.2, 101.8, 80.0, 71.0, 70.9, 55.7, 55.6, 43.9, 25.7 ppm. HRESI m/z: 580.2304 (C<sub>30</sub>H<sub>29</sub>NO<sub>6</sub> + Na<sup>+</sup> requires 580.2306).

***In vitro* PPAR $\alpha$  functional reporter gene assay:** Agonist activity of test compounds against human PPAR $\alpha$  were analyzed using commercial kits (Human PPAR $\alpha$  Reporter Assay System, #IB00111, Indigo Biosciences). Protocols provided with the kit were followed for experimental execution. A suspension of reporter cells was prepared in Cell Recovery Medium (CRM: containing 10% charcoal stripped FBS). 200  $\mu$ L of the reporter cell suspension were dispensed into wells of white 96-well assay plates provided within the kit for a 4-6 h pre-incubation period

at 37 °C and 5% CO<sub>2</sub>. At the end of the pre-incubation period, the culture media was discarded and 200 µL of Compound Screening Medium (CSM: containing 10% charcoal stripped FBS) containing the requisite concentration of derivative to be evaluated was added to representative wells. Following a 22-24 h incubation at 37 °C and 5% CO<sub>2</sub>, the treatment media was discarded and 100 µL of the provided Luciferase Detection Reagent was added to each well. Luminescence was quantified using a GloMax Explorer (Promega). Dose-response analyses of reference compounds were performed via non-linear curve-fitting of signal to noise ratio (S/B) vs. Log[compound] using GraphPad Prism software.

***In vitro* PPAR $\gamma$  and PPAR $\delta$  functional reporter gene assay:** The PPAR $\gamma$  and PPAR $\delta$  dose-response of select compounds was evaluated using commercial kits (Human PPAR $\delta$  and PPAR $\gamma$  Reporter Assay Systems, Product #IB00101 and #IB00121, Indigo Biosciences). Protocols provided with the kit were followed for experimental execution. A suspension of Reporter Cells was prepared in Cell Recovery Medium (CRM: containing 10% charcoal stripped FBS). 100 µL of the Reporter Cell suspension was dispensed into wells of white 96-well assay plates provided within the kits. Immediately prior to assay setup, 100 µL of Compound Screening Medium (CSM: containing 10% charcoal stripped FBS) containing the 2x concentration of derivative to be evaluated was added to each well. Following a 22-24 h incubation at 37 °C and 5% CO<sub>2</sub>, the treatment media was discarded and 100 µL of the provided Luciferase Detection Reagent was dispensed to each well. Luminescence was quantified using a GloMax Explorer (Promega). Dose-response analyses of compounds were performed via non-linear curve-fitting of S/B vs. Log[compound] using GraphPad Prism software.

**Cell Culture:** 661W cells were cultured in 5.5mM glucose DMEM (Gibco, Waltham, MA) supplemented with 10% fetal bovine serum (Mediatech, Inc., Manassas, VA), 100U/ml penicillin

sodium, 100µg/ml streptomycin sulphate, and 0.25µg/ml amphotericin B (Mediatech, Inc., Manassas, VA). HRCECs were cultured in EGM-2MV-SingleQuots media (Lonza, Walkersville, MD). All cells were incubated in a humidified incubator at 37°C under 5% CO<sub>2</sub>.

**LDH Cytotoxicity Assay:** 661W cells were seeded in 96-well culture plate at a density of 6,700 cells per well. Following 24Hr of incubation with media containing various concentrations of ASD091, LDH assay was performed with the Thermo Scientific Pierce LDH Cytotoxicity Assay Kit as per manufacturer's protocol (ThermoFisher, Waltham, MA).

**Western blot analysis:** Cells in 24-well plates at 30-40% of confluence were incubate with various concentrations of ASD091 in culture media for 24 hours. DMSO was used as a control. Following the 24 hours of incubation, cells were harvested and 40µg of cell lysates were ran on 10% SDS-PAGE gel. Densitometry quantification was performed using ImageJ software (NIH, Bethesda). Antibodies used: PPAR- $\alpha$  (1:1000, ab126285, Abcam) and  $\beta$ -actin-HRP (1:2000, sc-1616HRP, Santa Cruz).

**RT-PCR analysis:** Total RNA were isolated with Trizol (ThermoFisher, Waltham, MA) from 661W cells incubated with ASD091 or DMSO for 24 hours. 1µg of RNA was used to synthesize cDNA with Multiscribe Reverse Transcriptase (ThermoFischer, Waltham, MA). Real-Time PCR was performed on Bio-RAD CFX96-Real-Time System (Bio-RAD, Hercules, CA) to detect *Acadm*, *Cpt1a*, *Fabp3* and *Slc25a20*. The primer sequences are as follows: *Acadm* (Fwd: 5'-AGTACCCGTTCCCTCTCATCA -3'; Rev: 5'-TACACCCATACGCCAACTCTT-3'), *Cpt1a* (Fwd: 5'-TGGCATCATCACTGGTGTGTT-3'; Rev: 5'-GTCTAGGGTCCGATTGATCTTTG -3'), *Fabp3* (Fwd: 5'-GTGACAGCAGATGACCGGAA -3'; Rev: 5'-TGCCATGAGTGAGAGTCAGGA-3'), and *Slc25a20* (Fwd: 5'-CTATGTTCCGCGTGTGCTTC -3'; Rev: 5'-GAAGCCTGAATCTGCAGTAAGC-3').

**Scratch-wound assay:** Cells were seeded on a collagen coated 6-well plates at a density of 600,000 per well. Once the cells have reached 100% confluency, a sterilized 1000- $\mu$ L tip was used to inflict a linear wound. Cell debris was removed by a gentle PBS wash, followed by replacement of media supplemented with varying concentrations of ASD091. Images were taken with Olympus CKX41 microscope, at 0Hr, 10Hr and 24Hr following the infliction of the wound. The wound closure was determined by the area of the remaining wound over time, using the ImageJ software (NIH, Bethesda) and the MRI Wound Healing Tool plug-in ([http://dev.mri.cnrs.fr/projects/imagej-macros/wiki/Wound\\_Healing\\_Tool](http://dev.mri.cnrs.fr/projects/imagej-macros/wiki/Wound_Healing_Tool)).

**Statistical analysis:** Experiments were performed three times in triplicate and representative data were shown. All values shown are expressed as mean  $\pm$  S.D. Differences between the groups were tested for statistical significance using Student's *t*-test. \* $P < 0.05$ , \*\* $P < 0.01$ , and \*\*\* $P < 0.001$ .

**Computational Methods:** Molecular modelling and docking procedures were executed using the standard protocol implemented in Maestro Molecule Builder of Schrödinger,<sup>5,16</sup> version 11.1. File preparation and docking protocol was completed as follows:

- 1. Protein Preparation:** The desired crystal structure was obtained from the Protein Data Bank and prepared with Schrödinger's *Protein Preparation Wizard* software. Proteins were preprocessed by assigning bond orders using the ccd database, adding hydrogens, creating zero-bond order to metals, creating disulfide bonds, filling missing side chains and loops using *Prime*, deleting water molecules beyond 5 Å, and generating Het state using *Epik* pH  $7 \pm 2$ . Het -COOH was modified to COO<sup>-</sup>. Structural refinement was done employing H-bond assignment by sampling water orientations, minimizing hydrogens of altered species at pH 7.0, and restraining minimization based on the OPLS3 force field. All remaining parameters were kept as default settings.

2. **Ligand Preparation:** SMILES files of each ligand were loaded into Schrödinger's *LigPrep* software. Ligand preparation employed the OPLS3 force field. Ionization states for pH  $7.0 \pm 2$  were generated with *Epik*. Ligands were desalted and tautomers were generated. Chirality specified in the ligand input file was retained.
3. **Receptor Grid Generation:** i) Receptor tab: select the native ligand and show markers, set the Van der Waals scaling factor to 1.0 with a partial charge cut off of 0.25. In advanced settings, select read from the input structure file and Force field OPLS3. ii) Site tab: Select centroid of workspace ligand, and dock ligand with length  $< 10 \text{ \AA}$ . In advanced settings set the box length =  $10 \text{ \AA}$ . iv) Constraints tab: H-Bond Tyr 464, His-440, Tyr-314 and Ser-280; v) Rotatable Groups tab: select all in the grid box.
4. **Ligand Docking:** Docking studies of compounds were performed using Schrödinger's *Glide* docking module from suite 2017-4. Docking was executed with the following parameters: Using partial charge input, scaling of Van der Waal radii with a scaling factor of 0.8 and partial charge cut off of 0.15, with XP precision, sample nitrogen inversion, sample ring conformation, bias sampling of torsion for amide group only, add *Epik* state penalties to docking score, OPLS3 force field with no constraints selected.

## 2.6 References

1. Deng, G.; Moran, E. P.; Cheng, R.; Matlock, G.; Zhou, K.; Moran, D.; Chen, D.; Yu, Q.; Ma, J. X., Therapeutic Effects of a Novel Agonist of Peroxisome Proliferator-Activated Receptor Alpha for the Treatment of Diabetic Retinopathy. *Invest. Ophthalmol. Vis. Sci.* **2017**, *58*, 5030-5042.
2. Xu, H. E.; Lambert, M. H.; Montana, V. G.; Plunket, K. D.; Moore, L. B.; Collins, J. L.; Oplinger, J. A.; Kliewer, S. A.; Gampe, R. T., Jr.; McKee, D. D.; Moore, J. T.; Willson, T. M., Structural



Determinants of Ligand Binding Selectivity between the Peroxisome Proliferator-Activated Receptors. *Proc. Natl. Acad. Sci. U.S.A.* **2001**, *98*, 13919-13924.

3. Li, J.; Kennedy, L. J.; Shi, Y.; Tao, S.; Ye, X.-Y.; Chen, S. Y.; Wang, Y.; Hernández, A. S.; Wang, W.; Devasthale, P. V.; Chen, S.; Lai, Z.; Zhang, H.; Wu, S.; Smirk, R. A.; Bolton, S. A.; Ryono, D. E.; Zhang, H.; Lim, N.-K.; Chen, B.-C.; Locke, K. T.; O'Malley, K. M.; Zhang, L.; Srivastava, R. A.; Miao, B.; Meyers, D. S.; Monshizadegan, H.; Search, D.; Grimm, D.; Zhang, R.; Harrity, T.; Kunselman, L. K.; Cap, M.; Kadiyala, P.; Hosagrahara, V.; Zhang, L.; Xu, C.; Li, Y.-X.; Muckelbauer, J. K.; Chang, C.; An, Y.; Krystek, S. R.; Blannar, M. A.; Zahler, R.; Mukherjee, R.; Cheng, P. T. W.; Tino, J. A., Discovery of an Oxybenzylglycine Based Peroxisome Proliferator Activated Receptor A Selective Agonist 2-((3-((2-(4-Chlorophenyl)-5-Methyloxazol-4-Yl)Methoxy)Benzyl)(Methoxycarbonyl)Amino)Acetic Acid (Bms-687453). *Journal of Medicinal Chemistry* **2010**, *53*, 2854-2864.

4. Bernardes, A.; Souza, P. C.; Muniz, J. R.; Ricci, C. G.; Ayers, S. D.; Parekh, N. M.; Godoy, A. S.; Trivella, D. B.; Reinach, P.; Webb, P.; Skaf, M. S.; Polikarpov, I., Molecular Mechanism of Peroxisome Proliferator-Activated Receptor Alpha Activation by Wy14643: A New Mode of Ligand Recognition and Receptor Stabilization. *J. Mol. Biol.* **2013**, *425*, 2878-2893.

5. Capelli, D.; Cerchia, C.; Montanari, R.; Loiodice, F.; Tortorella, P.; Laghezza, A.; Cervoni, L.; Pochetti, G.; Lavecchia, A., Structural Basis for Ppar Partial or Full Activation Revealed by a Novel Ligand Binding Mode. *Sci. Rep.* **2016**, *6*, 34792.

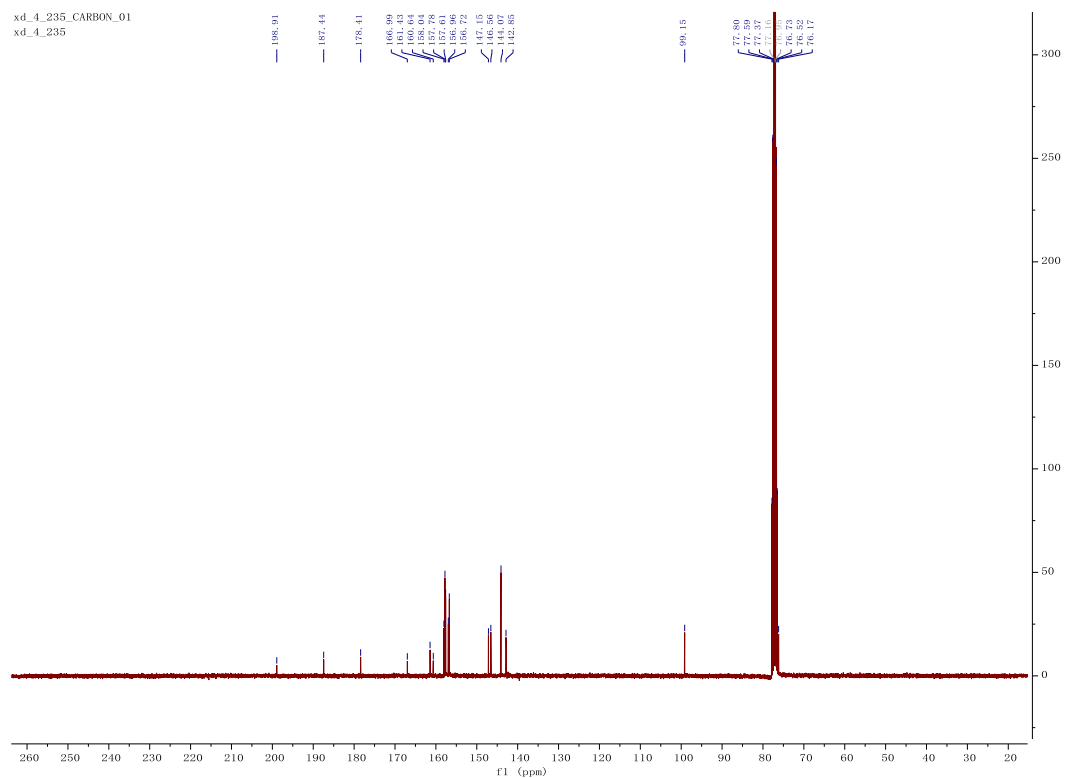
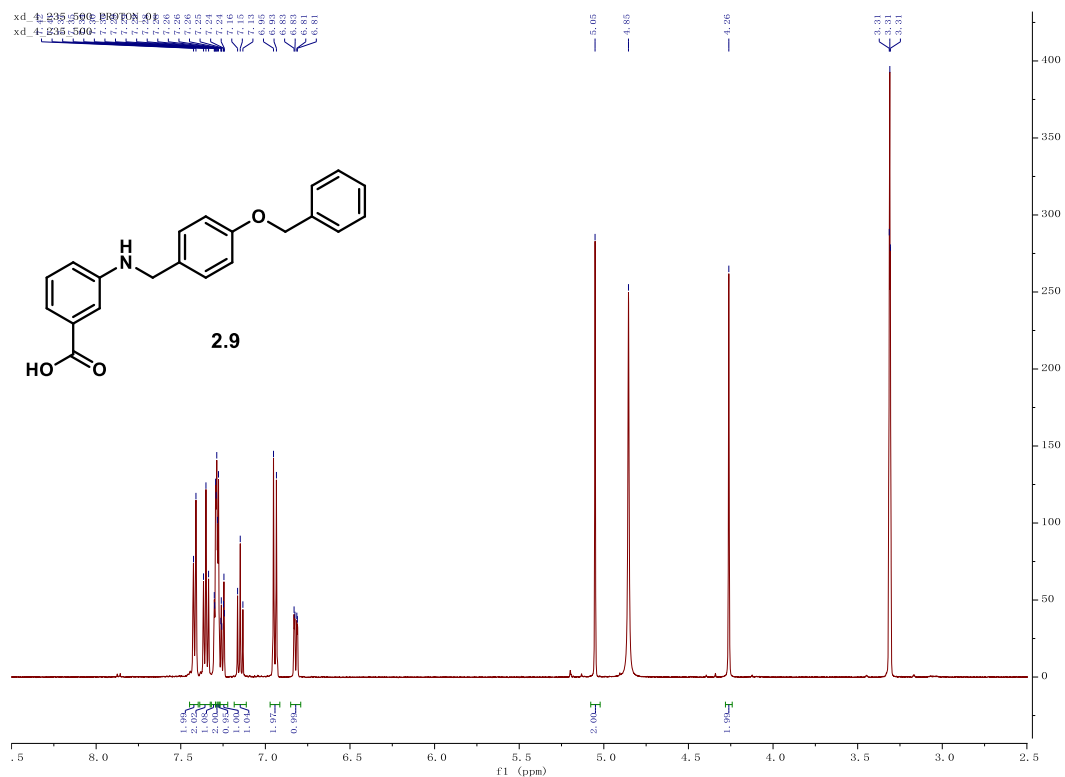
6. Gangwal, R. P.; Damre, M. V.; Das, N. R.; Sharma, S. S.; Sangamwar, A. T., Biological Evaluation and Structural Insights for Design of Subtype-Selective Peroxisome Proliferator Activated Receptor-Alpha (Ppar-Alpha) Agonists. *Bioorg Med Chem Lett* **2015**, *25*, 270-275.

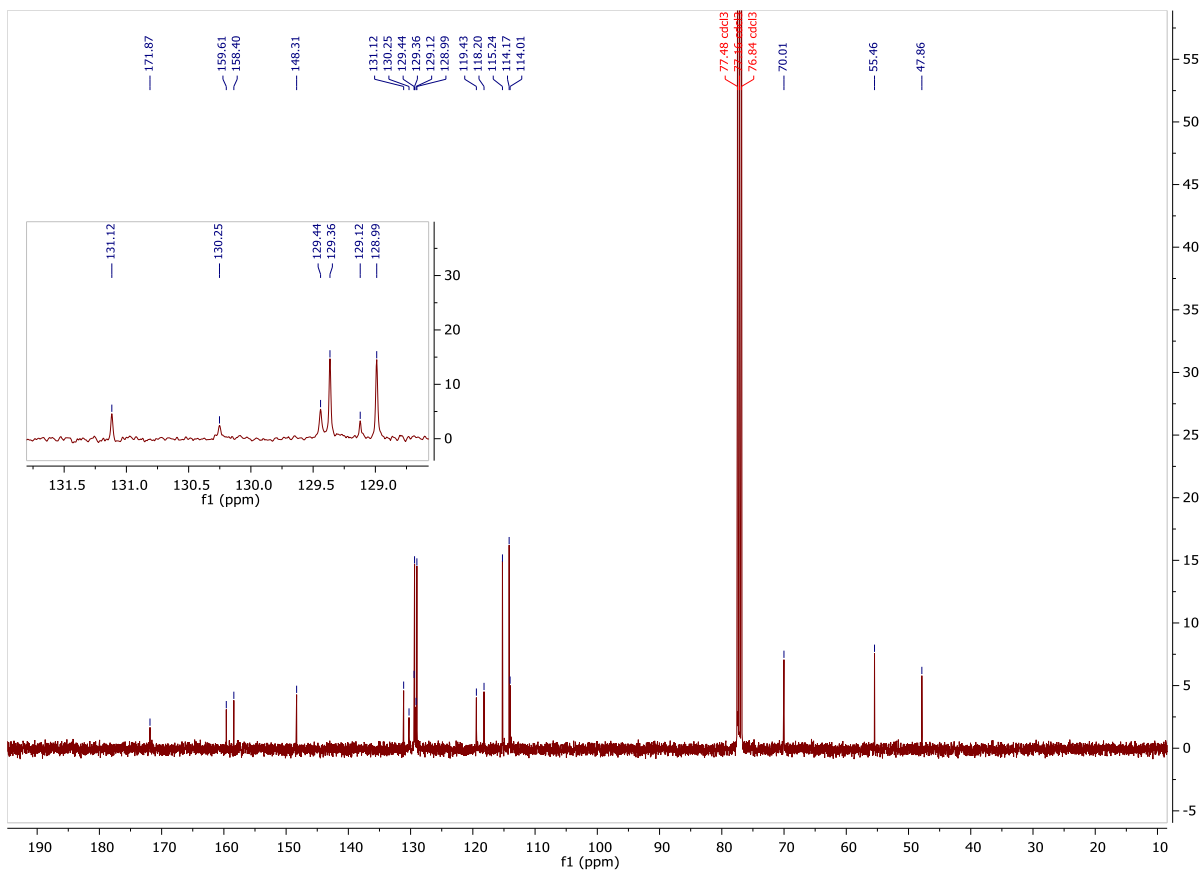
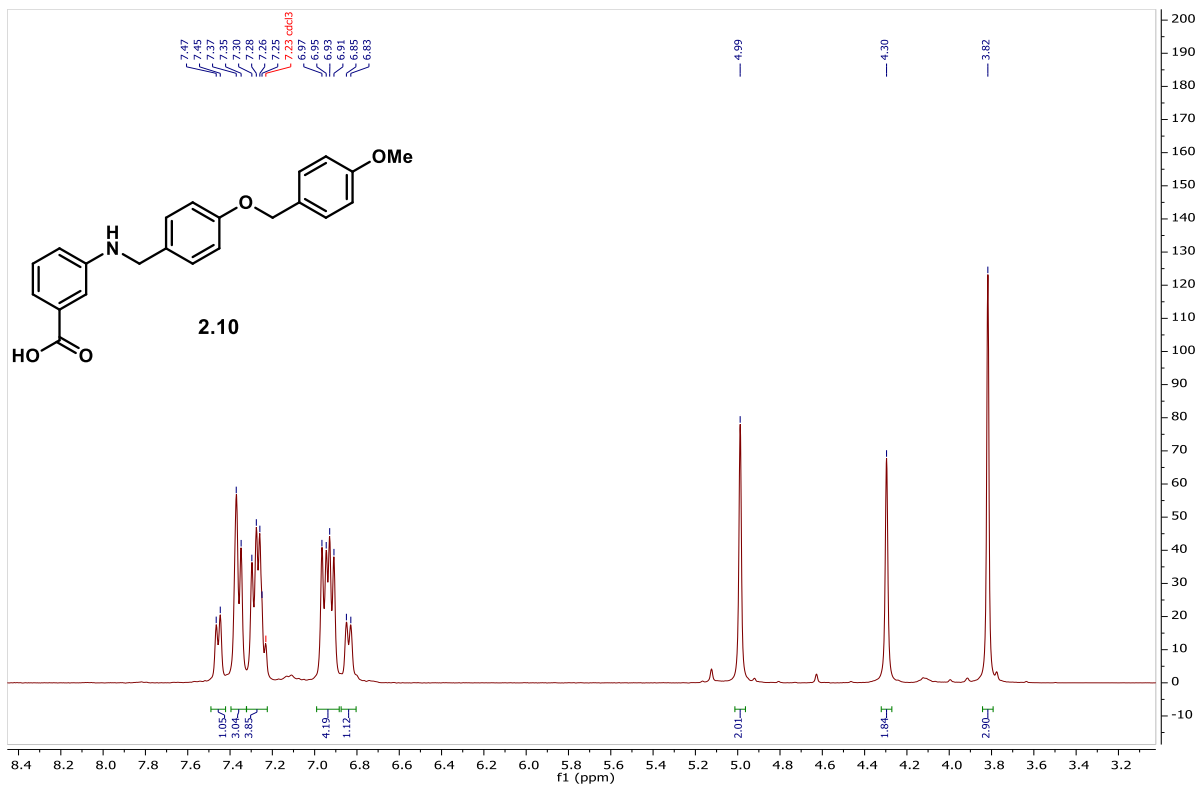
7. Mizuno, C. S.; Ma, G.; Khan, S.; Patny, A.; Avery, M. A.; Rimando, A. M., Design, Synthesis, Biological Evaluation and Docking Studies of Pterostilbene Analogs inside Pparalpha. *Bioorg. Med. Chem.* **2008**, *16*, 3800-3808.
8. Nomura, M.; Tanase, T.; Ide, T.; Tsunoda, M.; Suzuki, M.; Uchiki, H.; Murakami, K.; Miyachi, H., Design, Synthesis, and Evaluation of Substituted Phenylpropanoic Acid Derivatives as Human Peroxisome Proliferator Activated Receptor Activators. Discovery of Potent and Human Peroxisome Proliferator Activated Receptor A Subtype-Selective Activators. *Journal of Medicinal Chemistry* **2003**, *46*, 3581-3599.
9. Sierra, M. L.; Beneton, V.; Boullay, A. B.; Boyer, T.; Brewster, A. G.; Donche, F.; Forest, M. C.; Fouchet, M. H.; Gellibert, F. J.; Grillot, D. A.; Lambert, M. H.; Laroze, A.; Le Grumelec, C.; Linget, J. M.; Montana, V. G.; Nguyen, V. L.; Nicodeme, E.; Patel, V.; Penfornis, A.; Pineau, O.; Pohin, D.; Potvain, F.; Poulain, G.; Ruault, C. B.; Saunders, M.; Toum, J.; Xu, H. E.; Xu, R. X.; Pianetti, P. M., Substituted 2-[(4-Aminomethyl)Phenoxy]-2-Methylpropionic Acid Pparalpha Agonists. 1. Discovery of a Novel Series of Potent Hdlc Raising Agents. *J. Med. Chem.* **2007**, *50*, 685-695.
10. McMullen, P. D.; Bhattacharya, S.; Woods, C. G.; Sun, B.; Yarborough, K.; Ross, S. M.; Miller, M. E.; McBride, M. T.; LeCluyse, E. L.; Clewell, R. A.; Andersen, M. E., A Map of the Ppara Transcription Regulatory Network for Primary Human Hepatocytes. *Chem. Biol. Interact.* **2014**, *209*, 14-24.
11. Capelli, D.; Cerchia, C.; Montanari, R.; Liodice, F.; Tortorella, P.; Laghezza, A.; Cervoni, L.; Pochetti, G.; Lavecchia, A., Structural Basis for Ppar Partial or Full Activation Revealed by a Novel Ligand Binding Mode. *Sci. Rep.* **2016**, *6*, No. 34792.

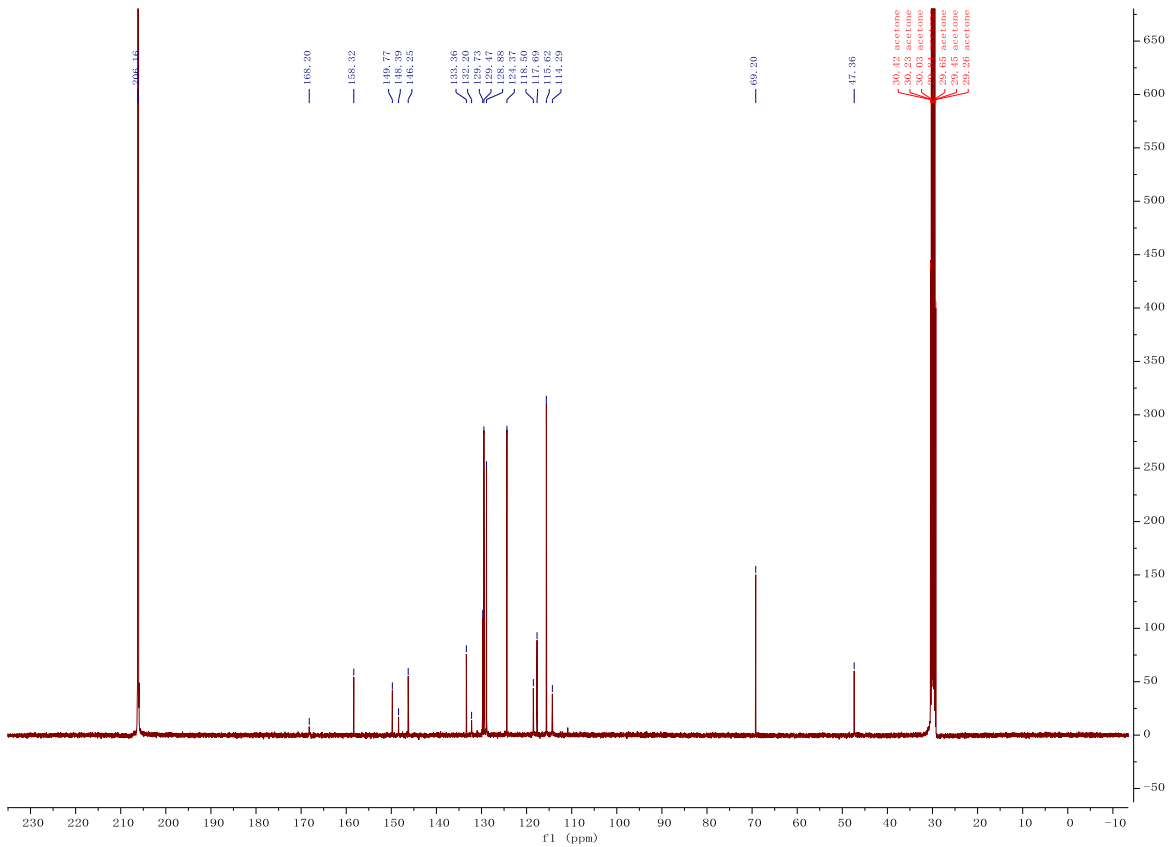
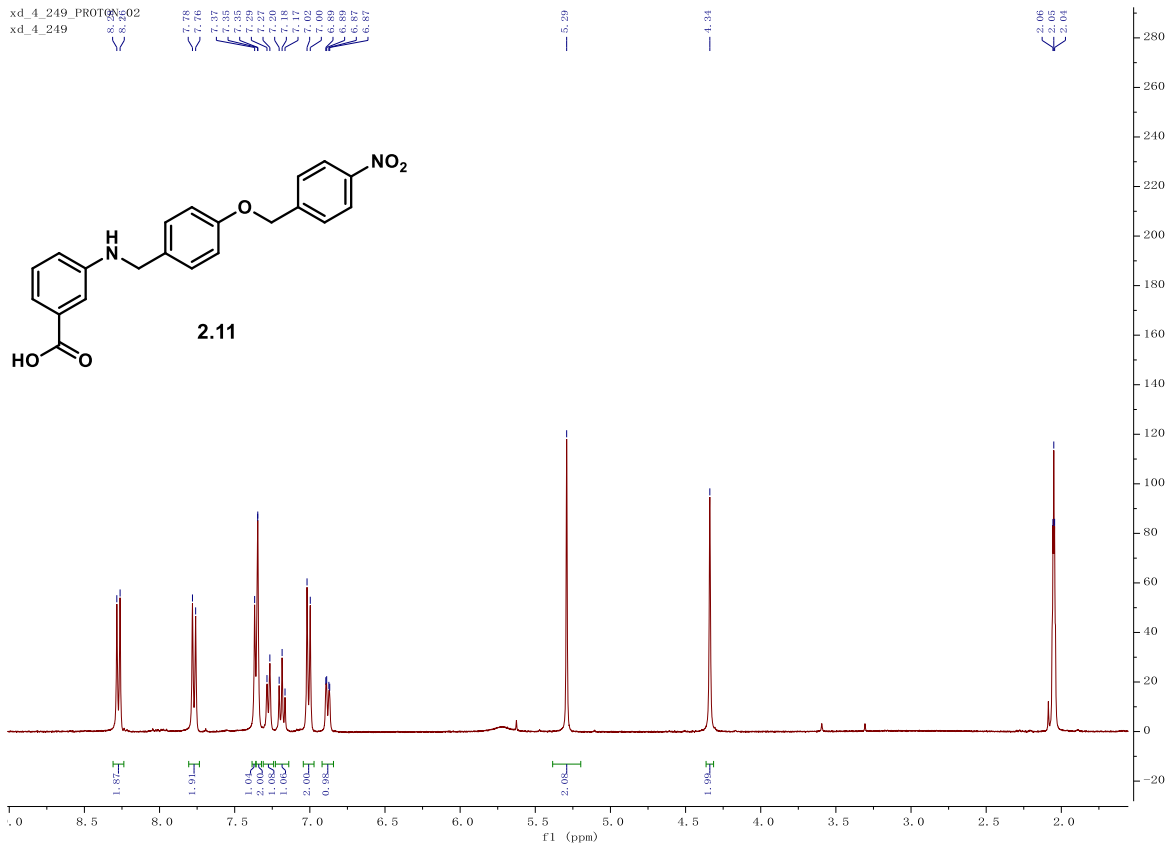
12. Pirat, C.; Farce, A.; Lebegue, N.; Renault, N.; Furman, C.; Millet, R.; Yous, S.; Speca, S.; Berthelot, P.; Desreumaux, P.; Chavatte, P., Targeting Peroxisome Proliferator-Activated Receptors (Ppars): Development of Modulators. *J. Med. Chem.* **2012**, *55*, 4027-4061.
13. Sasaki, Y.; Raza-Iqbal, S.; Tanaka, T.; Murakami, K.; Anai, M.; Osawa, T.; Matsumura, Y.; Sakai, J.; Kodama, T., Gene Expression Profiles Induced by a Novel Selective Peroxisome Proliferator-Activated Receptor Alpha Modulator (Spparmalpha) Pemafibrate. *Int J Mol Sci* **2019**, *20*, No. 5682.
14. Heimburg, T.; Chakrabarti, A.; Lancelot, J.; Marek, M.; Melesina, J.; Hauser, A. T.; Shaik, T. B.; Duclaud, S.; Robaa, D.; Erdmann, F.; Schmidt, M.; Romier, C.; Pierce, R. J.; Jung, M.; Sippl, W., Structure-Based Design and Synthesis of Novel Inhibitors Targeting Hdac8 from *Schistosoma Mansoni* for the Treatment of Schistosomiasis. *J. Med. Chem.* **2016**, *59*, 2423-2435.
15. Deshpande, A. M.; Bhuniya, D.; De, S.; Dave, B.; Vyavahare, V. P.; Kurhade, S. H.; Kandalkar, S. R.; Naik, K. P.; Kobal, B. S.; Kaduskar, R. D.; Basu, S.; Jain, V.; Patil, P.; Chaturvedi Joshi, S.; Bhat, G.; Raje, A. A.; Reddy, S.; Gundu, J.; Madgula, V.; Tambe, S.; Shitole, P.; Umrani, D.; Chugh, A.; Palle, V. P.; Mookhtiar, K. A., Discovery of Liver-Directed Glucokinase Activator Having Anti-Hyperglycemic Effect without Hypoglycemia. *Eur. J. Med. Chem.* **2017**, *133*, 268-286.
16. Friesner, R. A.; Murphy, R. B.; Repasky, M. P.; Frye, L. L.; Greenwood, J. R.; Halgren, T. A.; Sanschagrin, P. C.; Mainz, D. T., Extra Precision Glide: Docking and Scoring Incorporating a Model of Hydrophobic Enclosure for Protein-Ligand Complexes. *J. Med. Chem.* **2006**, *49*, 6177-6196.

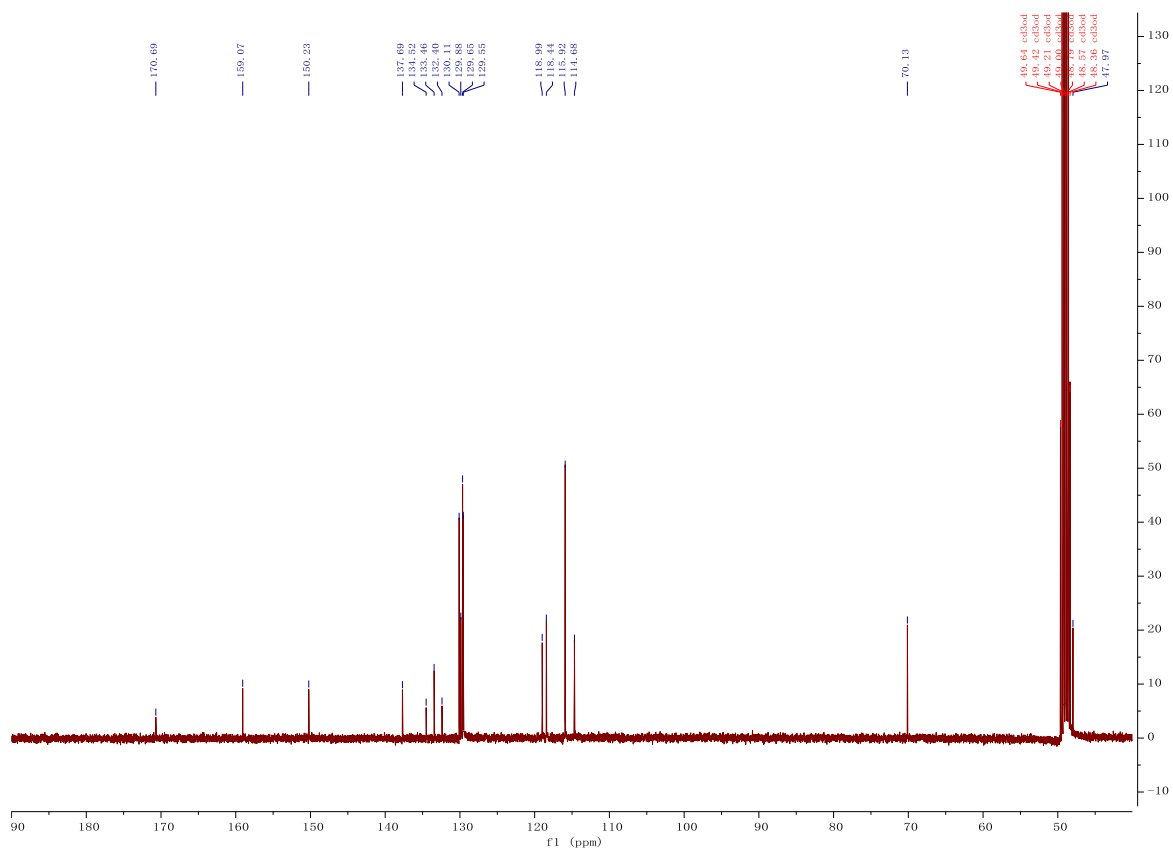
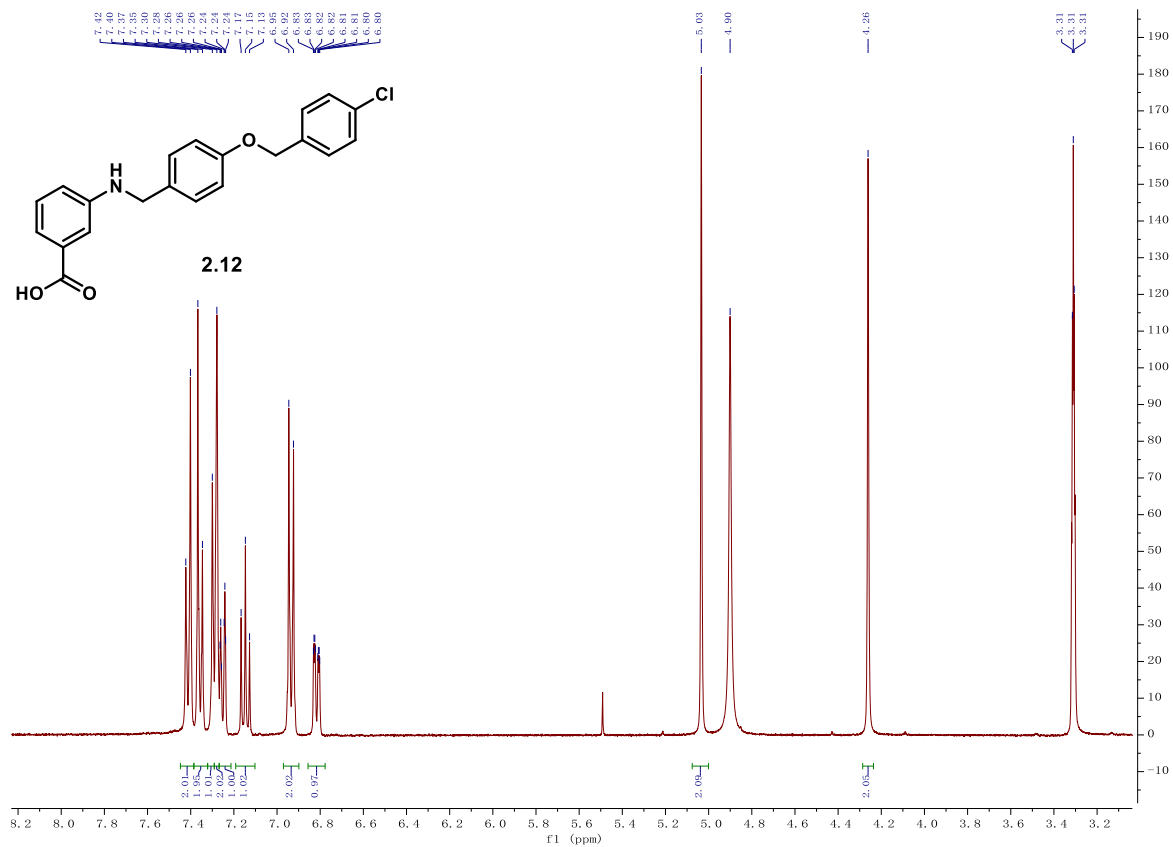
## Appendix 1 Supporting Information to Chapter 2

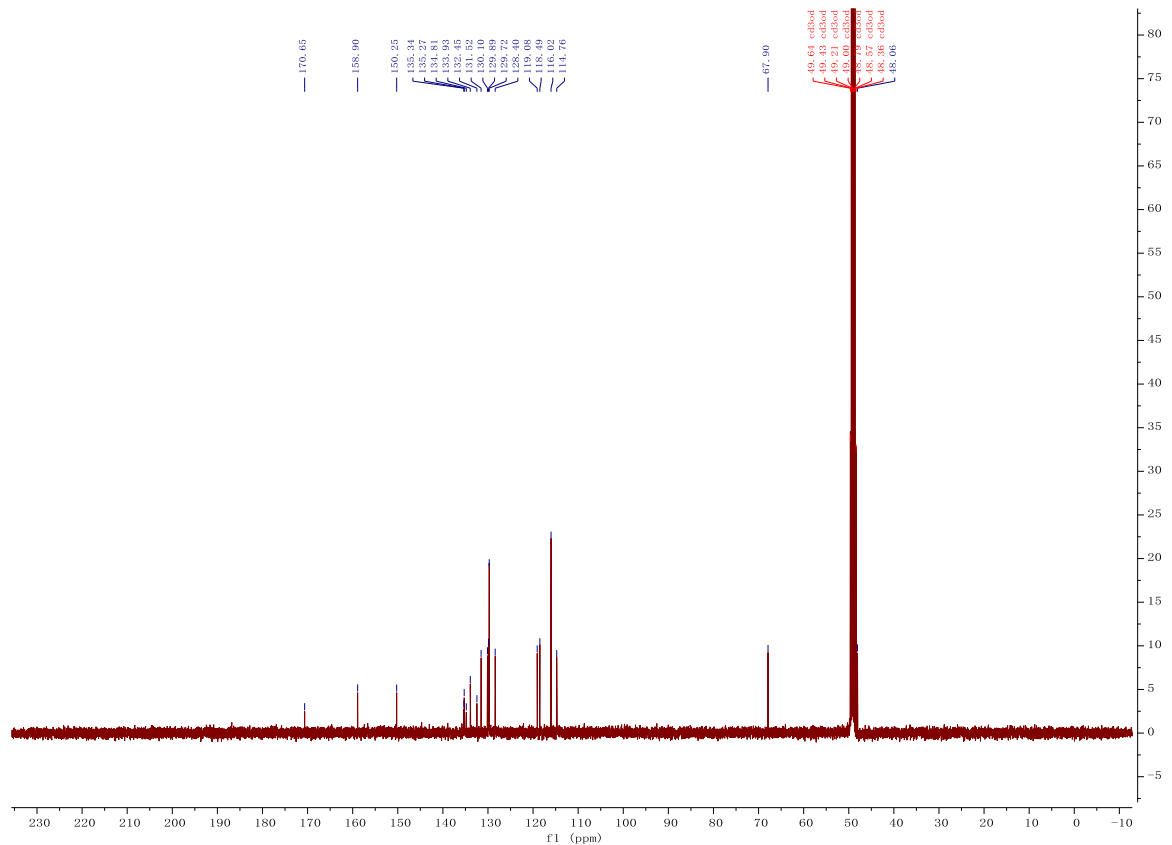
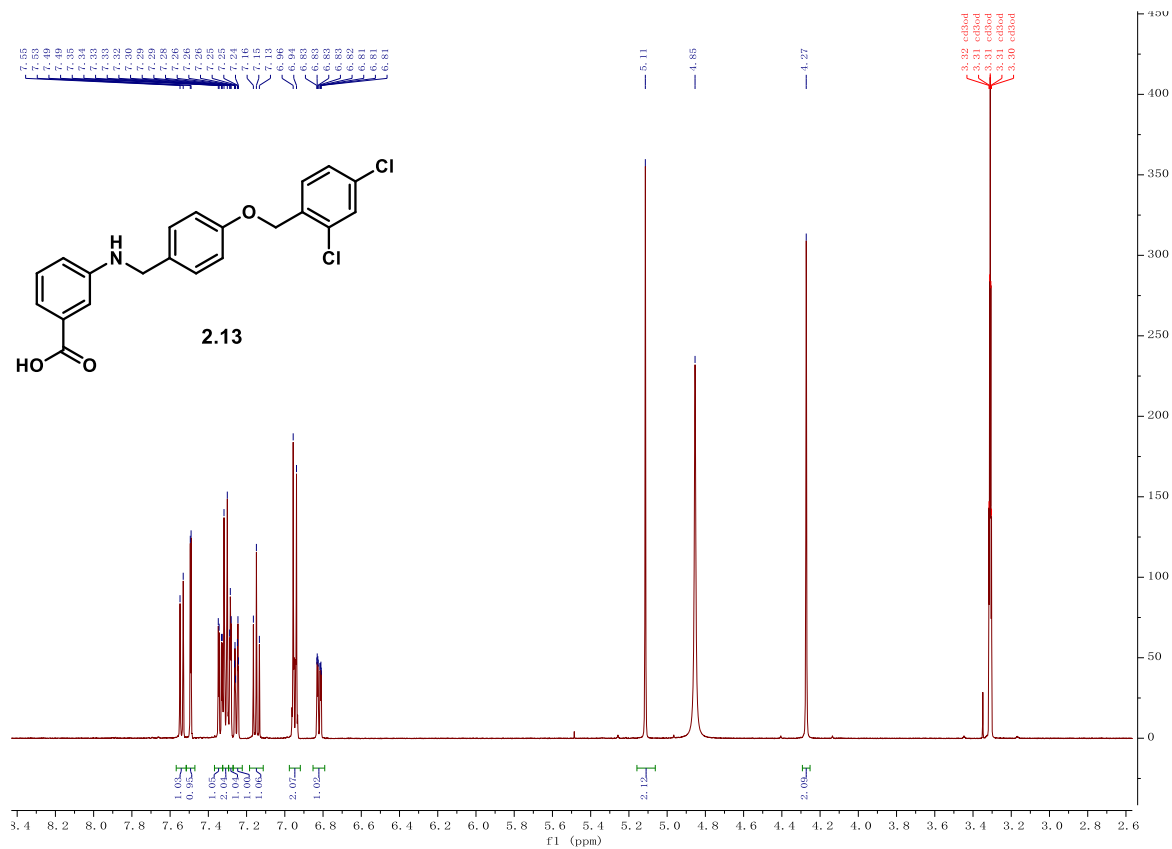
### Final compound <sup>1</sup>H and <sup>13</sup>C NMR spectra



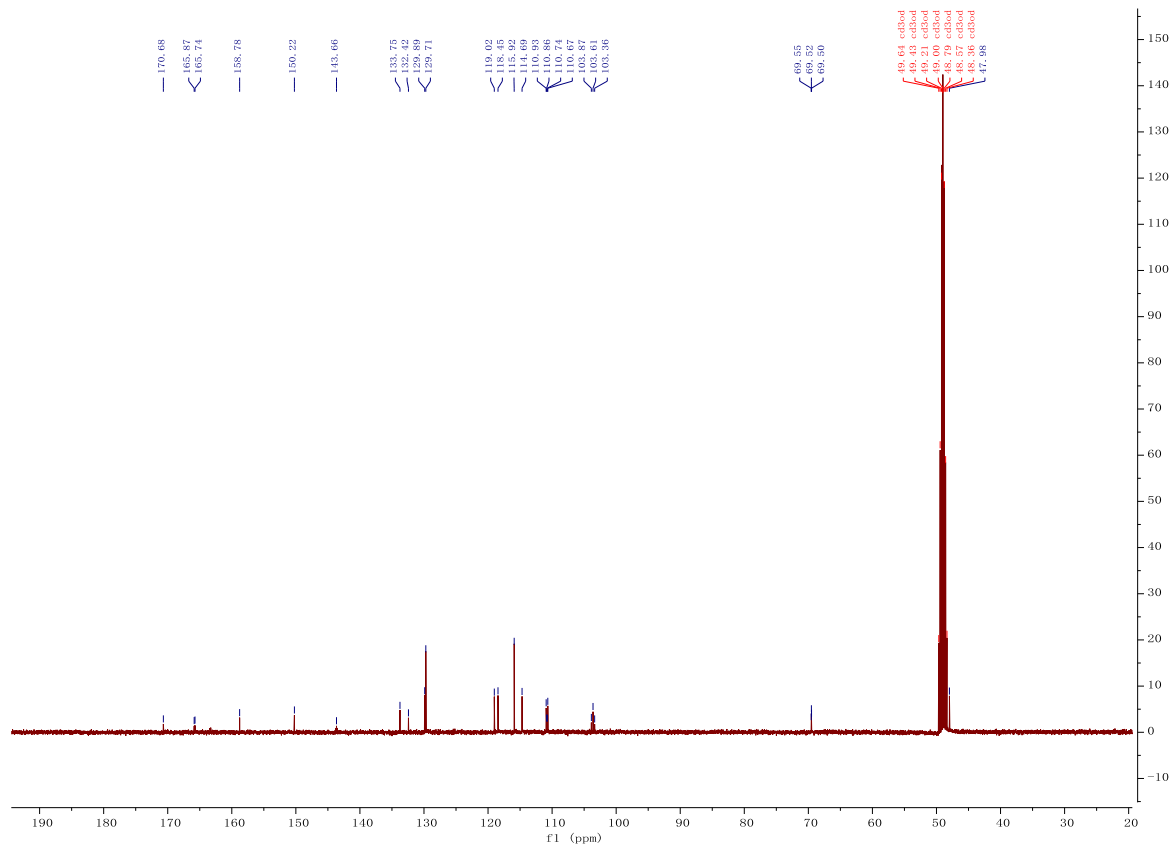
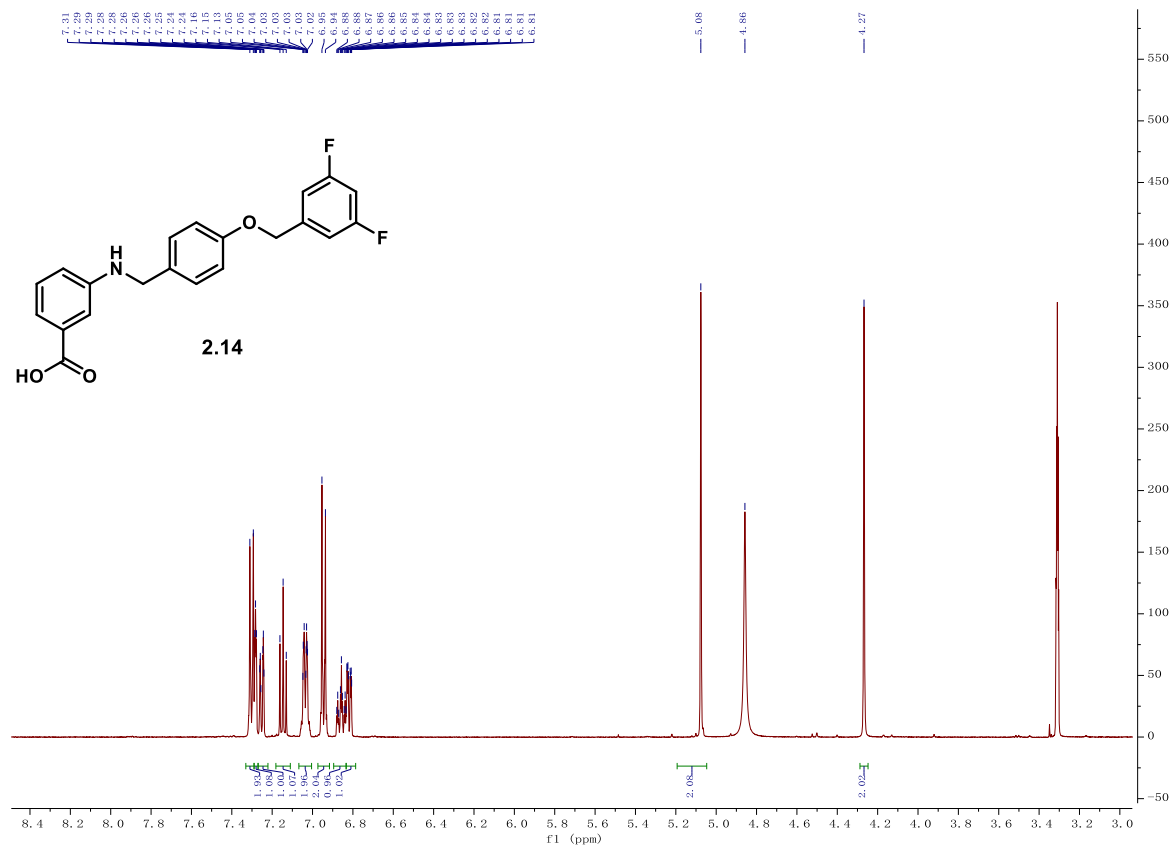


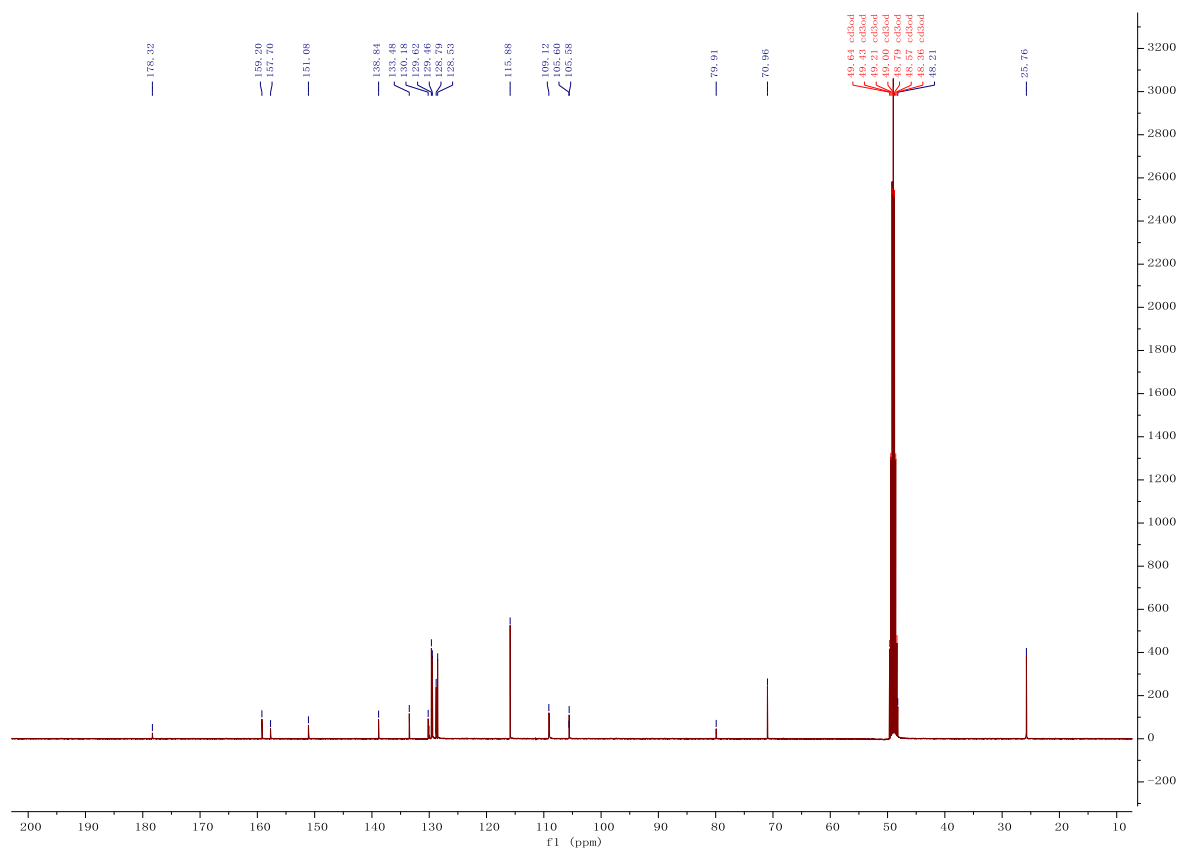
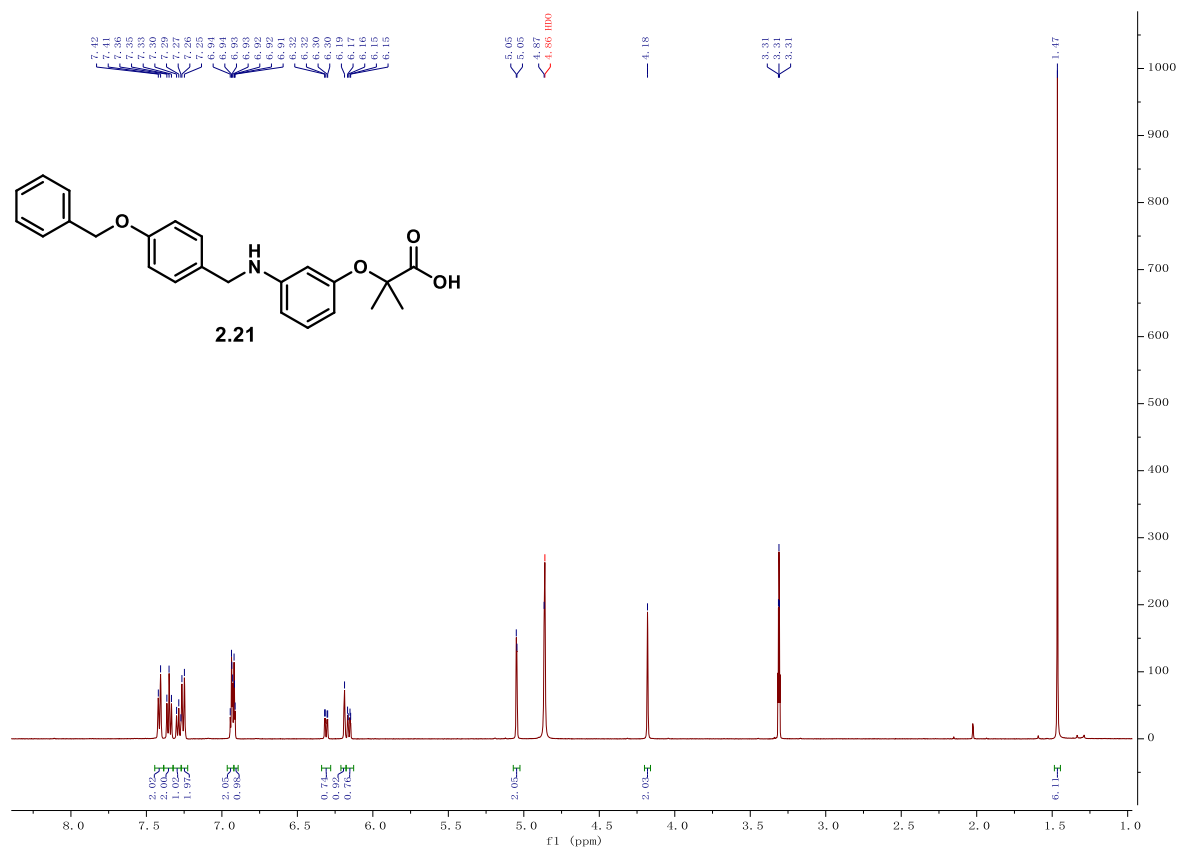


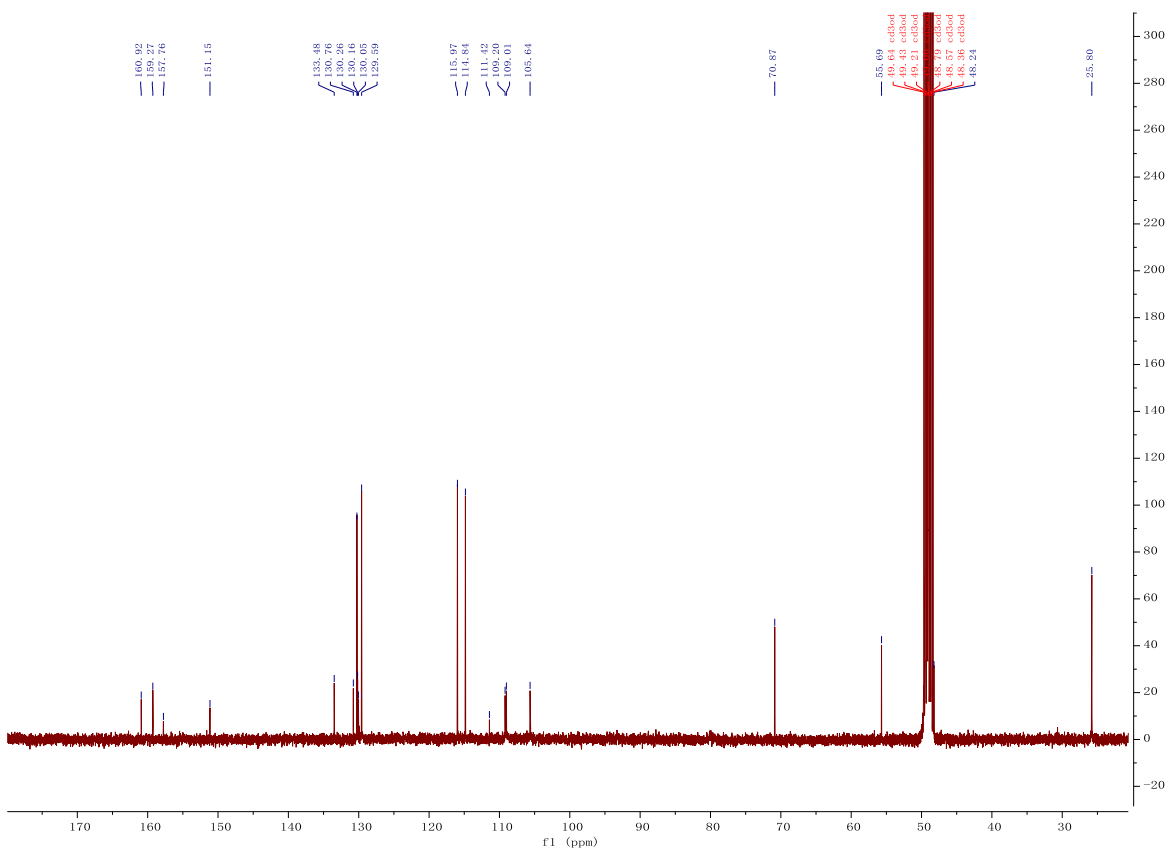
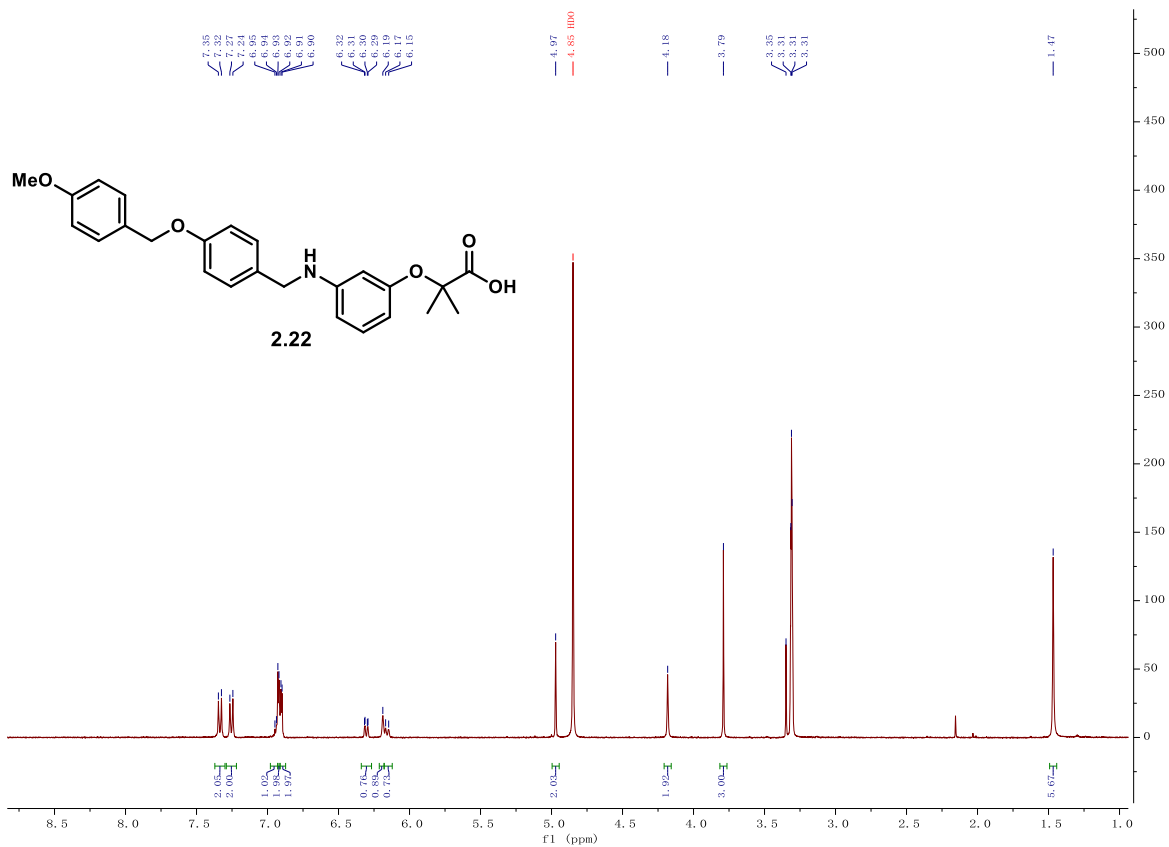


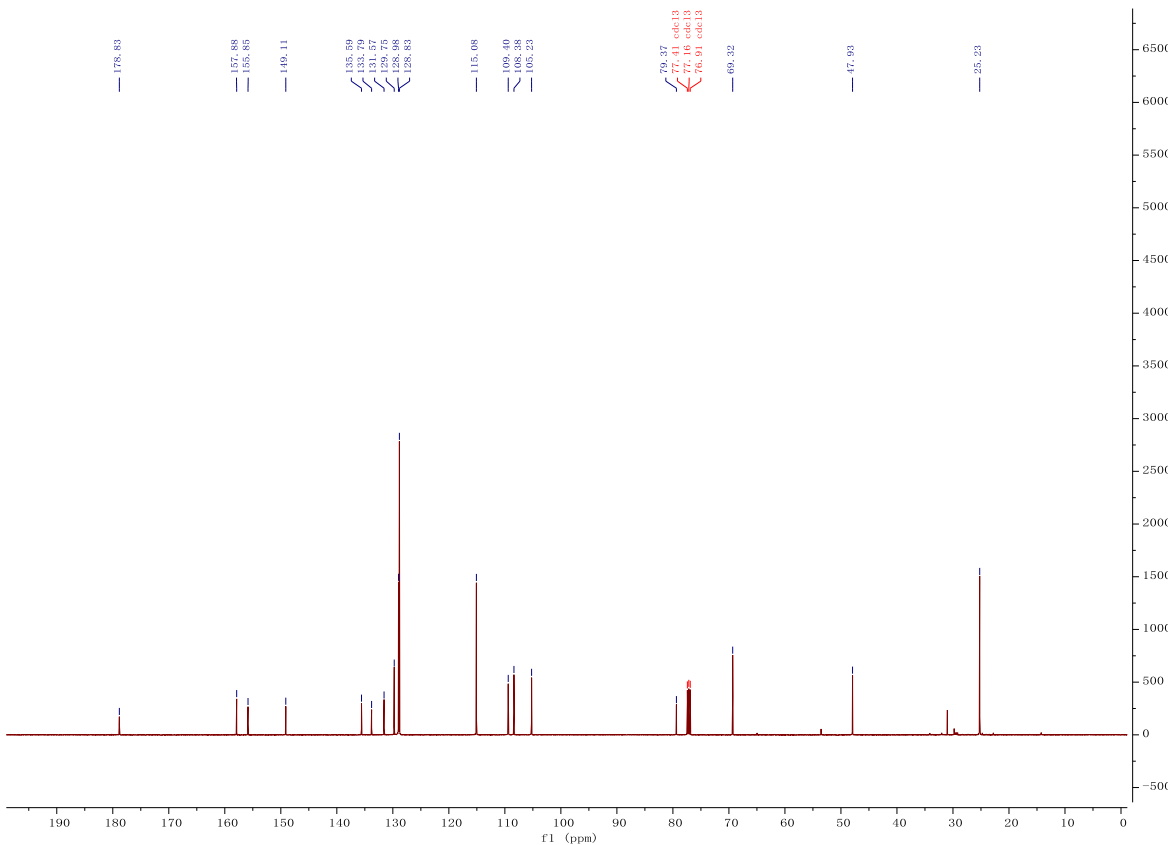
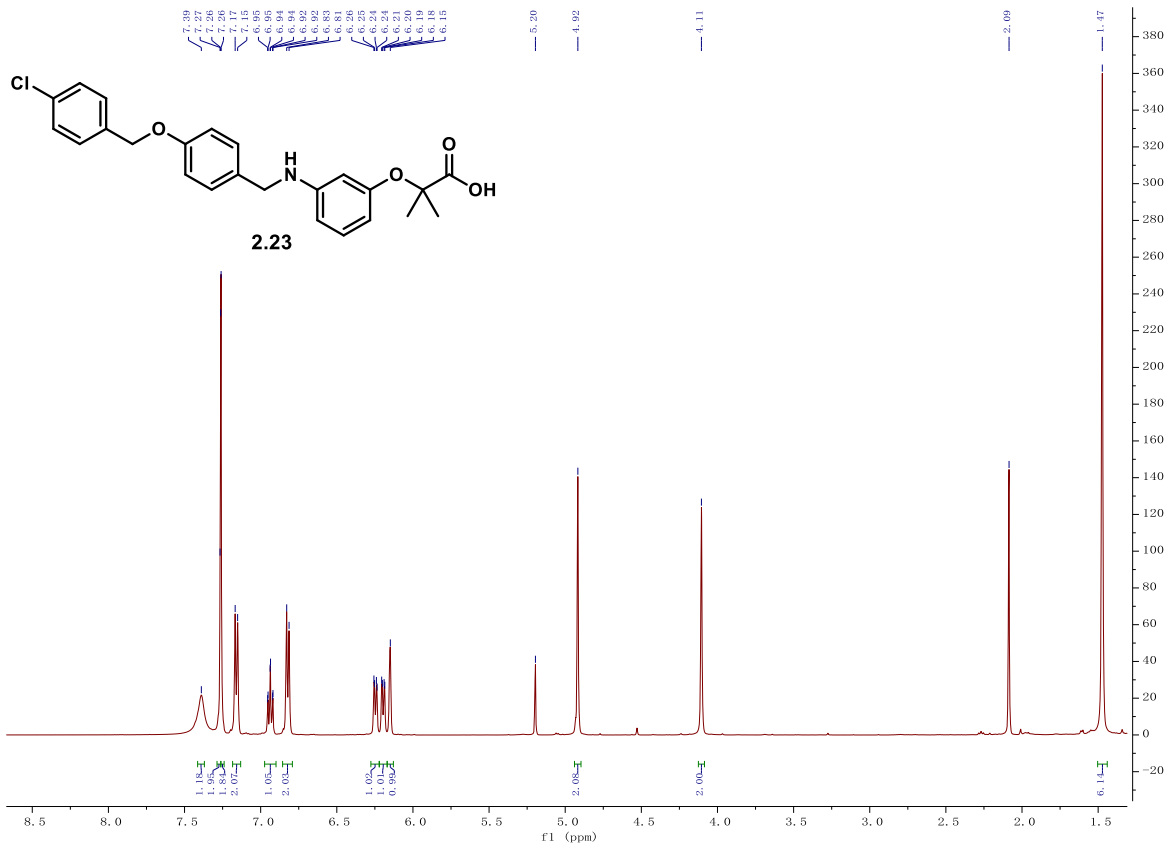


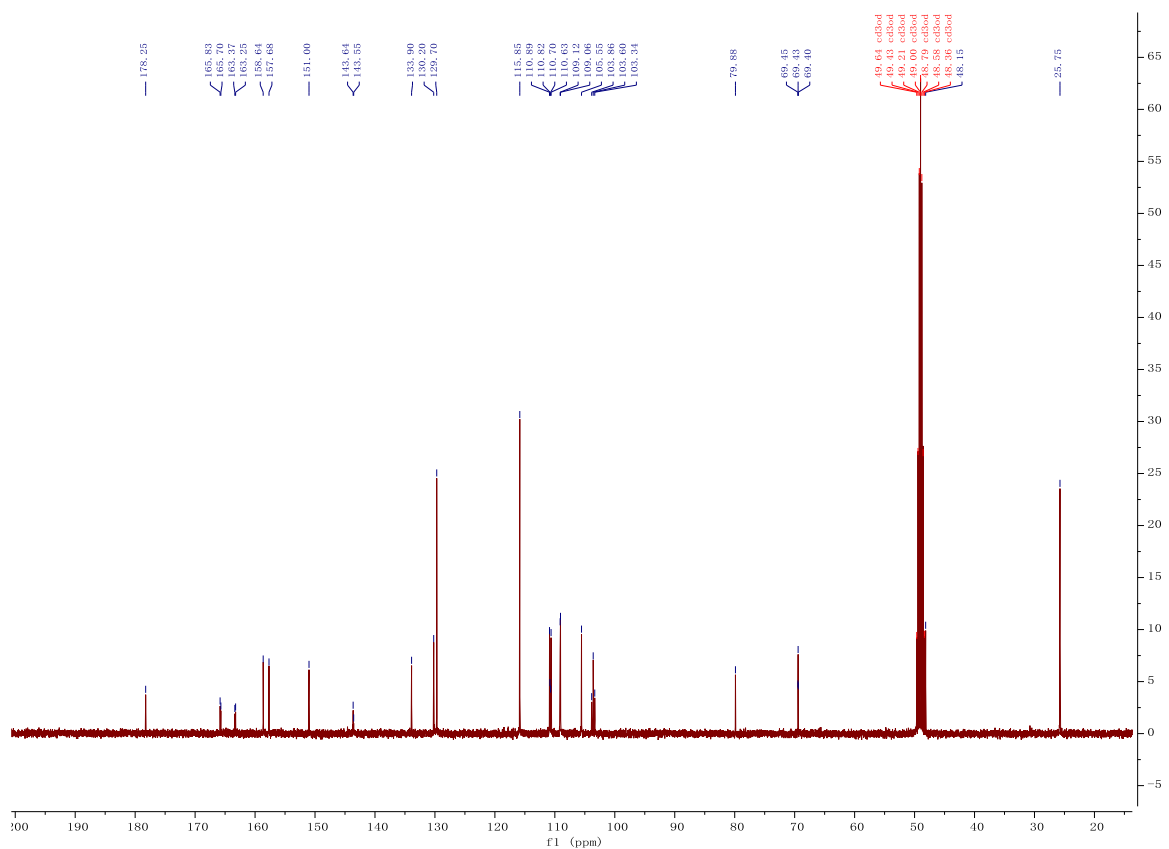
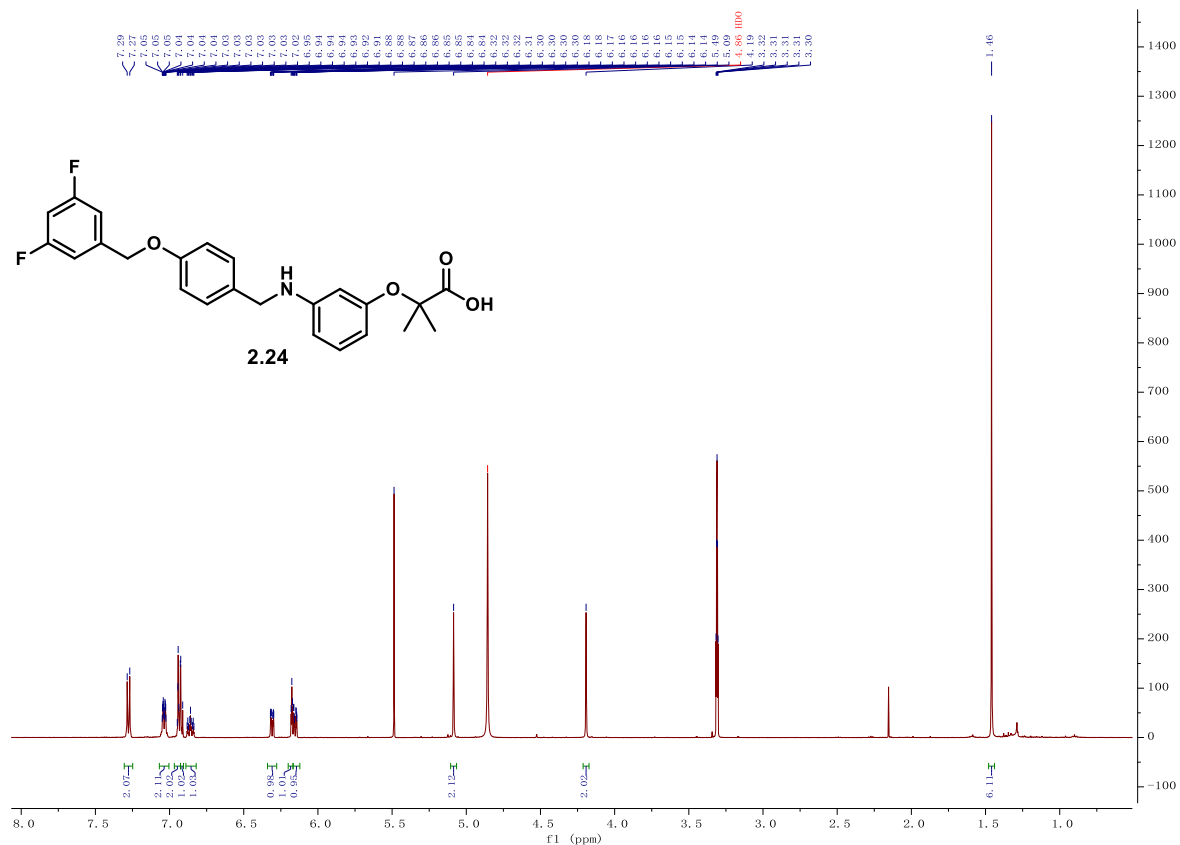


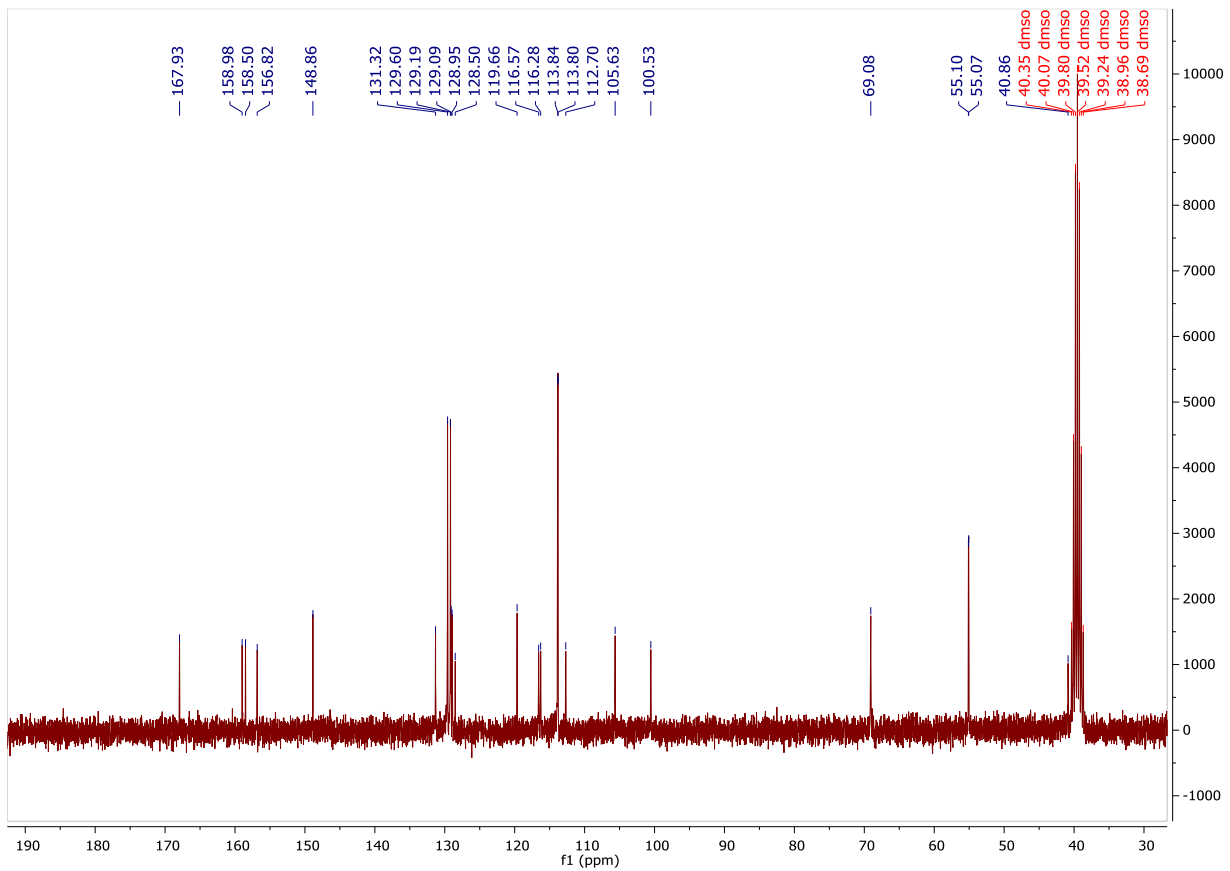
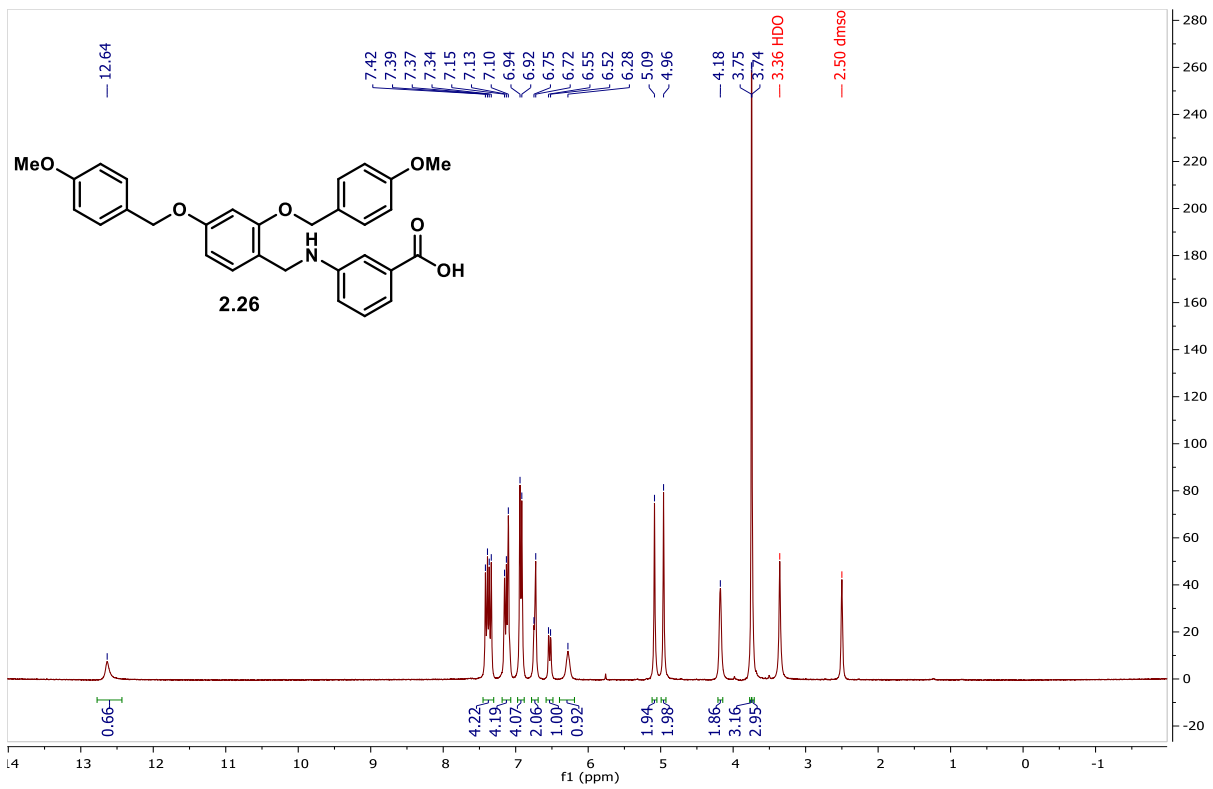






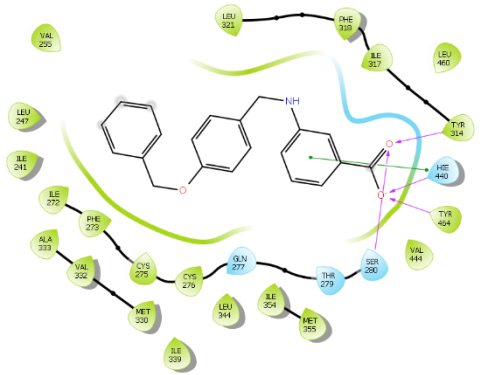
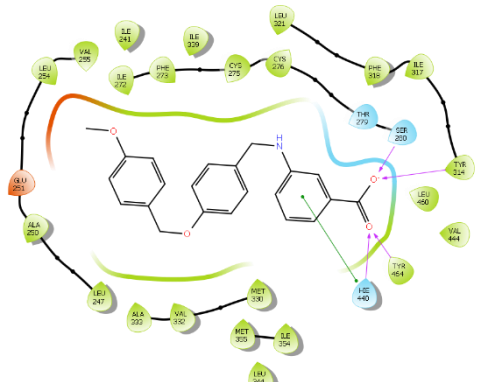
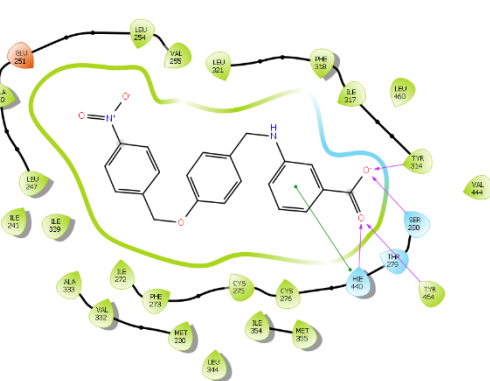








**GLIDE docking results for Ligands within the binding pocket of 2P54.**

ligand id	docking score (kcal/mol)	Interactions		Ligand Interaction Map
		H- bonds with carboxylate	Other significant interactions	
2.9	-9.468	Ser-280, Tyr-314, Tyr-464, His-440	His 440	
2.10	-10.193	Ser-280, Tyr-314, Tyr-464, His-440	His 440	
2.11	-9.894	Ser-280, Tyr-314, Tyr-464, His-440	His 440	

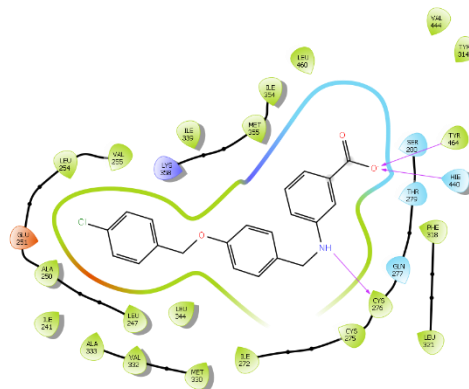


2.12

-9.553

Tyr-464,  
His-440,

Gln-277

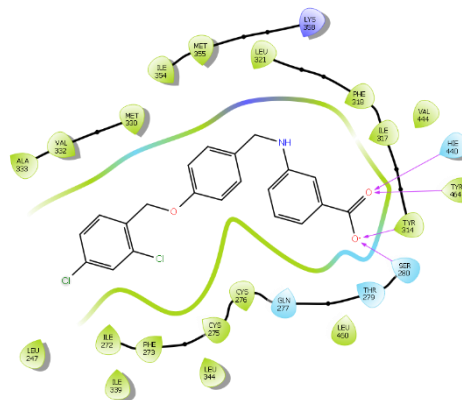


2.13

-10.954

Ser-280,  
Tyr-314,  
Tyr-464,  
His-440

-



## Chapter 3 Pharmacology and Second-generation SAR Studies of Selective PPAR $\alpha$

### Agonists

#### 3.1 Abstract

PPAR $\alpha$  is expressed in retinal Müller cells, endothelial cells, and in retinal pigment epithelium, and agonism of PPAR $\alpha$  with genetic or pharmacological tools ameliorates inflammation, vascular leakage, neurodegeneration, and neovascularization associated with retinal diseases in animal models. As such, PPAR $\alpha$  is a promising drug target for diabetic retinopathy and age-related macular degeneration. Herein, we report proof-of-concept *in vivo* efficacy in an STZ-induced vascular leakage model (rat) and preliminary pharmacokinetic assessment of a first-generation lead **3.4a** (A91). Additionally, we present the design, synthesis, and evaluation of second-generation analogs, which led to the discovery of **3.4u** and related compounds that reach cellular potencies <50 nM and exhibit >2,700-fold selectivity for PPAR $\alpha$  over other PPAR isoforms. These studies identify a pipeline of candidates positioned for detailed PK/PD and pre-clinical evaluation.

---

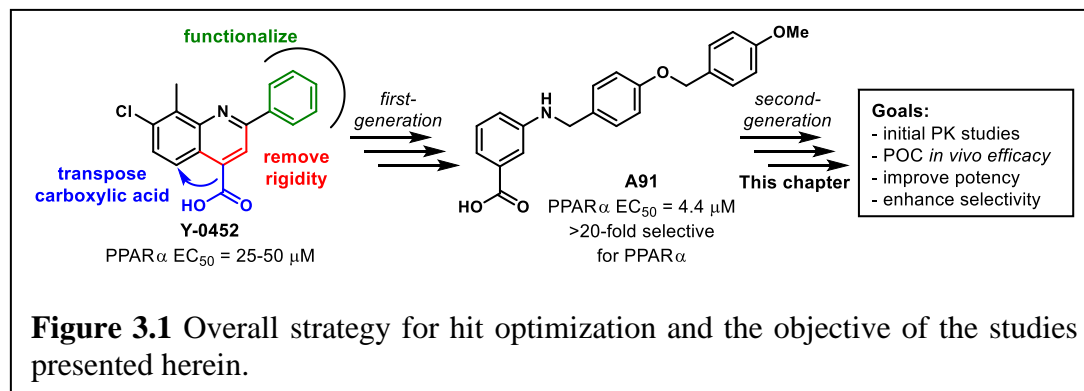
Reprinted with permission from: Xiaozheng Dou, Dinesh Nath, Younghwa Shin, Elmar Nurmammedov, Philip C. Bourne, Jian-Xing Ma, and Adam S. Duerfeldt, “Evolution of a 4-Benzyloxy-benzylamino Chemotype to Provide Efficacious, Potent, and Isoform Selective PPAR $\alpha$  Agonists as Leads for Retinal Disorders” *Journal of Medicinal Chemistry* 2020, 63 (6), 2854-2876 DOI: 10.1021/acs.jmedchem.9b01189. Copyright © 2020 American Chemical Society. X.D. conducted all the experiments described herein except for the synthesis of compounds designed for metabolism blocking by D.N., animal studies conducted by Y.S., and pharmacokinetic analysis conducted by E. N., X.D., D.N., and A.S.D. designed the research studies, analyzed, and interpreted the data, wrote, and reviewed the manuscript. Y.S., E.N., P.C.B., and J.-X.M. provided critical insight, expertise, personnel, and facilities and reviewed the manuscript.

## 3.2 Introduction

As described in chapter 2, we utilized *in silico* studies to propose that deconstruction of the rigid quinoline of the Y-0452 (**Figure 3.1**) would provide a more synthetically tractable and flexible scaffold, expected to exhibit improved complementarity to the U-shaped ligand binding pocket. Based on this design strategy, we developed the 4-benzyloxy-benzylamino chemotype to assess our hypothesis. In general, this small molecule family exhibits improved potency and selectivity over both Y-0452 (initial hit) and FenoFA, thus validating our rationale for further development of this chemotype and pursuing proof of concept studies. Compound A91 (**Figure 3.1**), a representative analogue from this series was advanced through rigorous biochemical evaluation to demonstrate typical downstream responses of PPAR $\alpha$  agonism including PPAR $\alpha$  upregulation, induction of target genes (e.g., *Acadm*, *Cpt1a*, *Fabp3*, and *Slc25a20*) and attenuation of cell migration.<sup>1</sup> Having identified a new class of PPAR $\alpha$  agonists and demonstrating useful SAR, the purpose of the work presented herein was to assess the preliminary PK and *in vivo* protection against vascular leakage of A91 to establish proof-of-concept and develop second-generation derivatives aimed at improving potency and selectivity of this chemotype.

## 3.3 Results and Discussion

### 3.3.1 PK/PD Profile of First-generation Lead



To  
gain  
insight  
about the  
metabolic  
stability

and rate of clearance, both of which influence bioavailability, A91 was assessed for intrinsic clearance in human and rat (Sprague-Dawley) liver microsomes. As shown in **Figure 3.2A**, compound A91 proved to be rather stable, with the mean half-life ( $t_{1/2}$ ) exceeding 60 minutes in both human and rat microsomes. These results indicate that this chemotype is likely to exhibit low clearance and that phase-I hepatic metabolism is unlikely to limit bioavailability.

In parallel, A91 was assessed for evidence of time-dependent inhibition against the major drug metabolizing cytochrome P450 isoforms (i.e., 1A, 2C9, 2C19, 2D6, and 3A). In this assay, peak areas corresponding to the metabolite of control substrates were recorded in the presence or absence of A91. This analysis was completed in the presence and absence of NADPH, to reveal time-dependence of inhibition. Test compounds which exhibit higher inhibition of metabolite formation in the absence of NADPH are deemed time-dependent inhibitors. As shown in **Figure 3.2B**, A91 exhibits no evidence of time-dependent inhibition for any of the CYP450s evaluated. This observation is especially important for CYP3A, as this family is responsible for the metabolism of statins, a drug class required for a majority of diabetics. These results indicate that CYP drug-drug interactions due to irreversible or tight binding are unlikely with this chemotype.

Lastly, A91 was evaluated for inhibition of the human ether-á-go-go (hERG) potassium channel. Inhibition of this channel is a flagship sign of cardiac toxicity. For this experiment, the automated whole cell patch-clamp (Qpatch 48) technique was used to record outward potassium currents from a single cell in the presence and absence of the compound of interest. As shown in **Figure 3.2C**, compound A91 exhibits low potency for the hERG channel (compounds that exhibit  $\geq 50\%$  inhibition at 10  $\mu\text{M}$  are flagged as toxic), indicating that this chemotype is unlikely to exhibit hERG-related cardiotoxicity, especially if potency for PPAR $\alpha$  is improved. It is also worth noting

that A91 exhibits no measurable cytotoxicity in the retinal pigment epithelium photoreceptor cell-line 661W at concentrations as high as 200  $\mu\text{M}$  as measured in a colorimetric enzyme coupled LDH detection cytotoxicity assay (appendix).

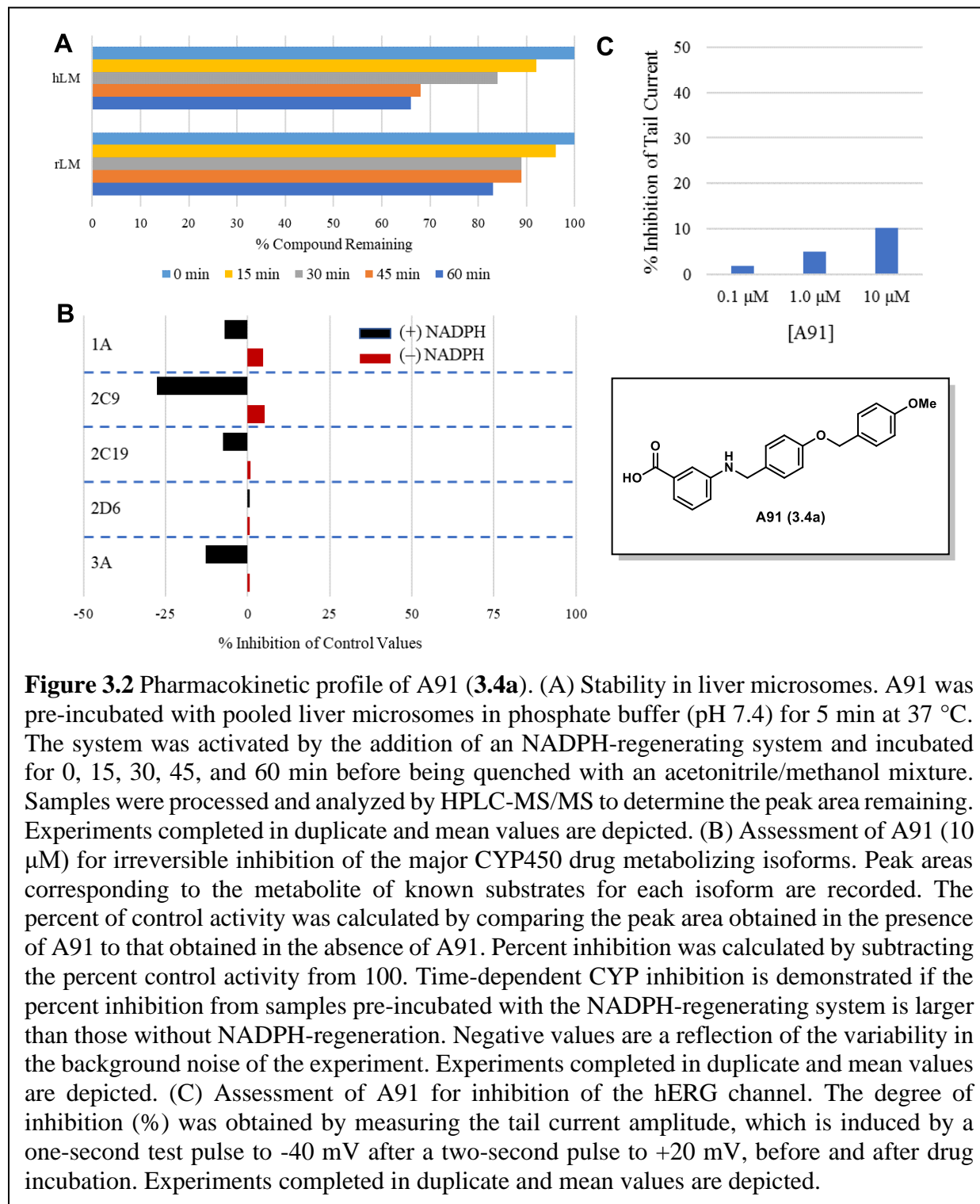


**Figure 3.2** Pharmacokinetic profile of A91 (**3.4a**). (A) Stability in liver microsomes. A91 was pre-incubated with pooled liver microsomes in phosphate buffer (pH 7.4) for 5 min at 37 °C. The system was activated by the addition of an NADPH-regenerating system and incubated for 0, 15, 30, 45, and 60 min before being quenched with an acetonitrile/methanol mixture. Samples were processed and analyzed by HPLC-MS/MS to determine the peak area remaining. Experiments completed in duplicate and mean values are depicted. (B) Assessment of A91 (10  $\mu\text{M}$ ) for irreversible inhibition of the major CYP450 drug metabolizing isoforms. Peak areas corresponding to the metabolite of known substrates for each isoform are recorded. The percent of control activity was calculated by comparing the peak area obtained in the presence of A91 to that obtained in the absence of A91. Percent inhibition was calculated by subtracting the percent control activity from 100. Time-dependent CYP inhibition is demonstrated if the percent inhibition from samples pre-incubated with the NADPH-regenerating system is larger than those without NADPH-regeneration. Negative values are a reflection of the variability in the background noise of the experiment. Experiments completed in duplicate and mean values are depicted. (C) Assessment of A91 for inhibition of the hERG channel. The degree of inhibition (%) was obtained by measuring the tail current amplitude, which is induced by a one-second test pulse to -40 mV after a two-second pulse to +20 mV, before and after drug incubation. Experiments completed in duplicate and mean values are depicted.

### 3.3.2 *In vivo* Efficacy of First-generation Lead

With a promising initial PK profile, and cellular potency and selectivity surpassing Fenofibrate (FenoFA), we advanced A91 to proof-of-concept *in vivo* efficacy studies in a well-established STZ-induced rat model of DR, which assesses the ability of a compound of interest to attenuate retinal vascular leakage—a major culprit behind diabetic macular edema and consequential vision loss. As shown in **Figure 3.3A**, systemic administration (i.p.) of compound A91 reduces retinal vascular leakage in diabetic rats to the range of the non-diabetic cohort at relatively the same dose as

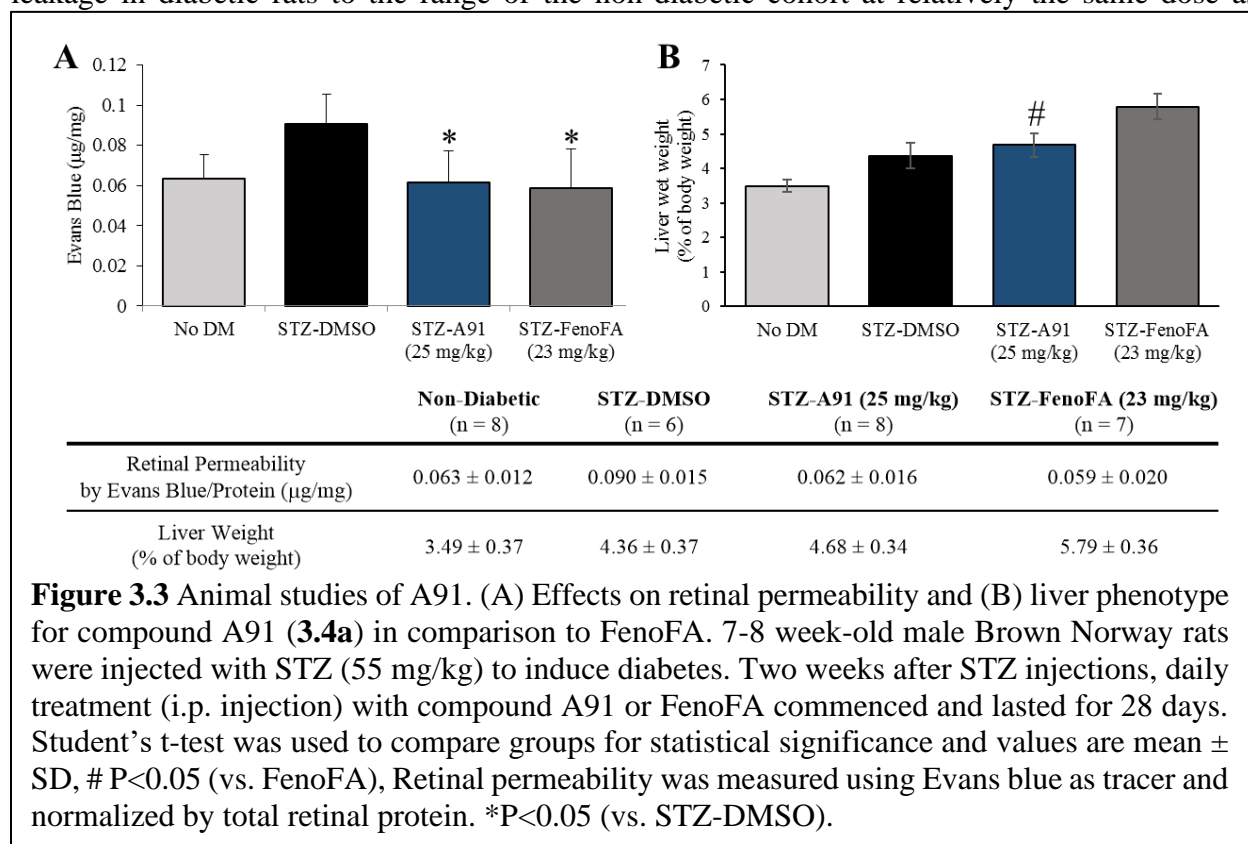
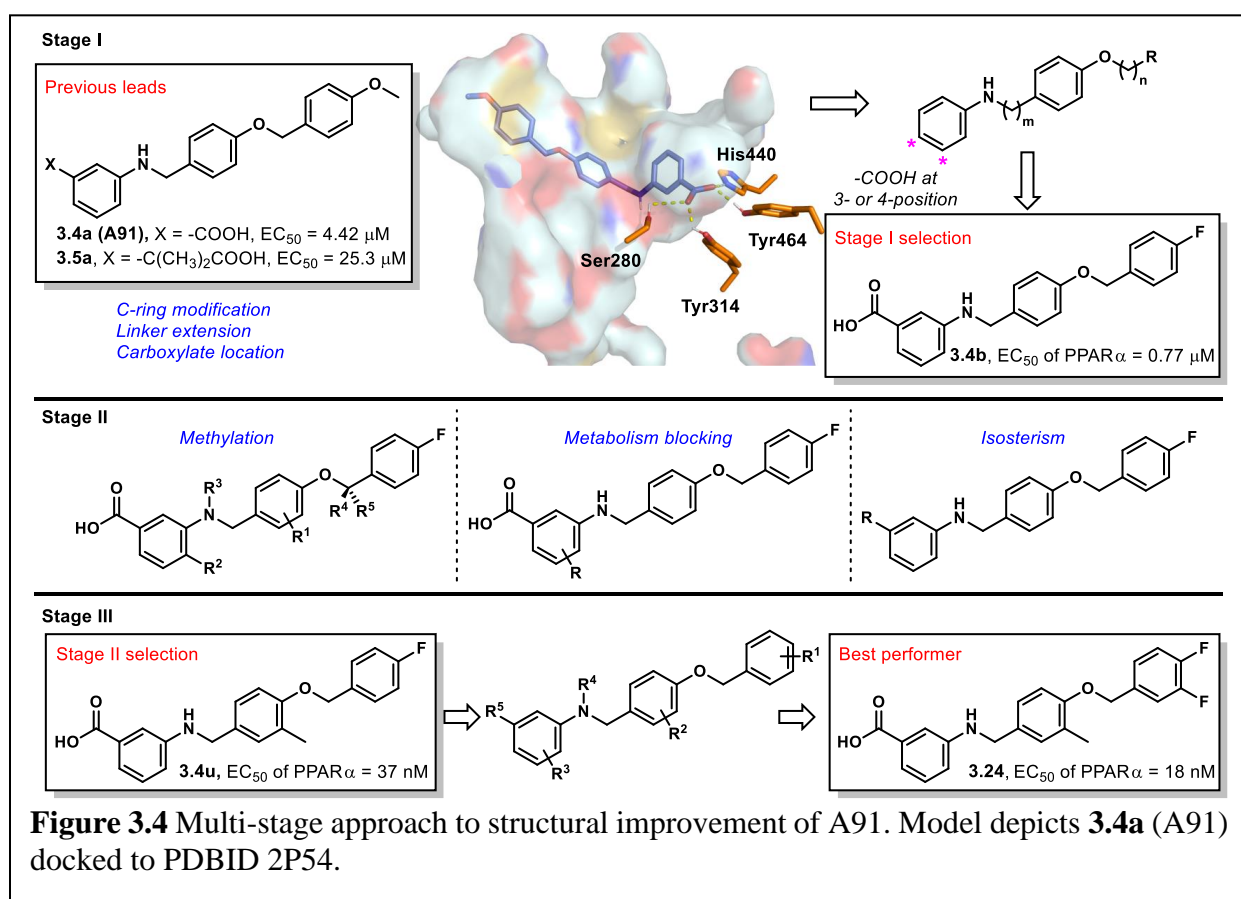


**Figure 3.3** Animal studies of A91. (A) Effects on retinal permeability and (B) liver phenotype for compound A91 (**3.4a**) in comparison to Fenofibrate. 7-8 week-old male Brown Norway rats were injected with STZ (55 mg/kg) to induce diabetes. Two weeks after STZ injections, daily treatment (i.p. injection) with compound A91 or Fenofibrate commenced and lasted for 28 days. Student's t-test was used to compare groups for statistical significance and values are mean ± SD, # P<0.05 (vs. Fenofibrate), Retinal permeability was measured using Evans blue as tracer and normalized by total retinal protein. \*P<0.05 (vs. STZ-DMSO).

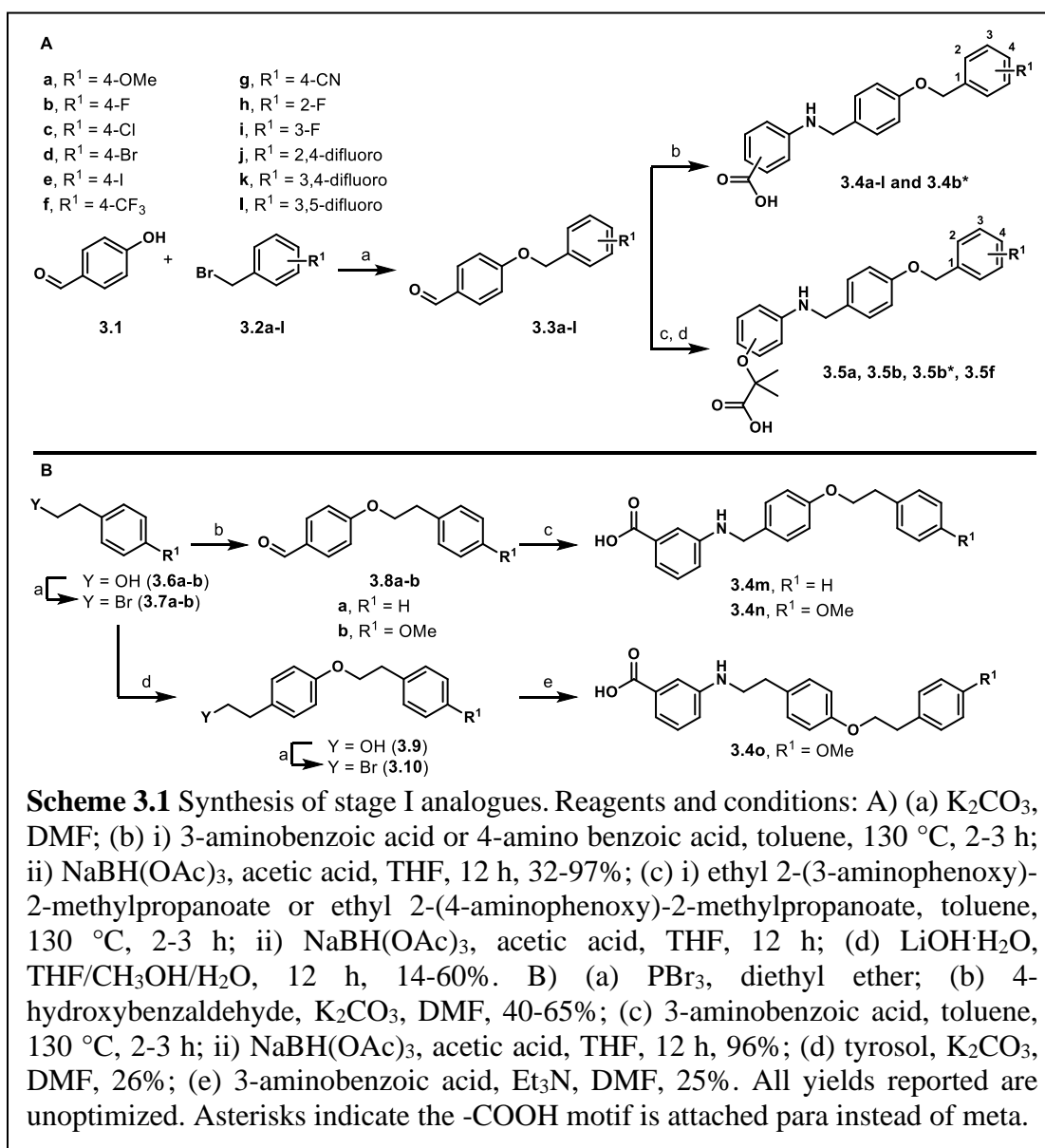
Fenofibrate. Of interesting note, A91 seems to lack signs of hepatomegaly (**Figure 3.3B**), a common side-effect of Fenofibrate/Fenofibrate observed in rodent models but not in humans. These *in vivo* results paired with the initial PK assessment, demonstrate that A91 1) exhibits *in vivo* efficacy in a relevant DR model following systemic administration, 2) is bioavailable, 3) survives first-pass metabolism and clearance mechanisms well enough to maintain efficacy, and 4) demonstrates a relatively safe profile (no observable toxicity) after daily i.p. injection for one-month.

Inspired by promising PK and *in vivo* results for A91, we commenced second-generation SAR studies with an aim of enhancing potency and isoform selectivity of this chemotype for PPAR $\alpha$ . Since no co-crystal structure of A91 existed at the onset of this work, we developed an *in-silico* model using the Schrodinger Drug Discovery Suite to gain insight into the putative binding mode and guide our evolution of this chemotype. For these studies we selected PDB 2P54, a co-crystal structure of a known PPAR $\alpha$  selective agonist GW590735 bound to human PPAR $\alpha$  (hPPAR $\alpha$ ). To validate our docking approach, constraints, and parameters, GW590735 was extracted, exposed to MM2 energy-minimization, and re-docked into the hPPAR $\alpha$  ligand binding domain to ensure that the results reproduced the bound conformation of the ligand. The overlay of co-crystallized and docked GW590735 showed excellent congruence (RMSD = 0.155 Å). Maintaining the same constraints and parameters, A91 was docked into hPPAR $\alpha$  and the results



were visually inspected for strategies to improve or introduce key interactions. Since our gatekeeper assay is a cell-based assessment and thus not based on direct binding affinity, scores were not used to prioritize ligands at this stage. Instead, visual inspection and structural modification hypotheses dictated the prioritization of derivatives selected for synthesis and assessment.

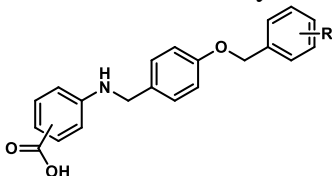
Our approach focused on three key principles. First, maintain a suitably positioned carboxylate (or isostere) to capture key hydrogen bonding interactions. Previous studies





demonstrate the significance of hydrogen bond interactions between hPPAR $\alpha$  Ser280, Tyr314, His440, and Tyr464 on the AF-2 helix and the carboxylate of known PPAR $\alpha$  ligands.<sup>2-9</sup> The ability to interact with all four of these residues is believed to be responsible for triggering full agonism of hPPAR $\alpha$ .<sup>3</sup> Poorer agonists tend to only interact with some of these hydrogen-bonding partners. It is worth noting that while historical PPAR $\alpha$  literature suggests a carboxylic acid is required for activity (a pharmacophore), examples of PPAR $\alpha$  agonists lacking this functionality have been reported,<sup>10,11</sup> demonstrating the -COOH motif can be altered. Secondly, we wanted to maintain the N-benzyl linkage to provide a complementary geometry for the U-shaped architecture of the

**Table 3.1** *In vitro* activity of **3.4a-l**<sup>a</sup>



	R	Ratio (5/50) <sup>b</sup>	Fold-Signal <sup>c</sup>	EC <sub>50</sub> hPPAR $\alpha$ ( $\mu$ M) <sup>d</sup>	EC <sub>50</sub> hPPAR $\gamma$ ( $\mu$ M)	EC <sub>50</sub> hPPAR $\delta$ ( $\mu$ M)	SI <sup>e</sup>
<b>3.4a (A91)</b>	4-OMe	0.5	1.4	4.43 $\pm$ 0.01	>100	>100	>20
<b>3.4b</b>	4-F	0.8	1.3	0.77 $\pm$ 0.03	>100	>100	>125
<b>3.4b*</b>	4-F	0.3	0.4				
<b>3.4c</b>	4-Cl	0.6	1.5	0.83 $\pm$ 0.04			
<b>3.4d</b>	4-Br	0.8	1.3	0.97 $\pm$ 0.14			
<b>3.4e</b>	4-I	0.7	1.1	1.45 $\pm$ 0.02			
<b>3.4f</b>	4-CF <sub>3</sub>	0.9	0.9	0.96 $\pm$ 0.11			
<b>3.4g</b>	4-CN	0.6	1.0				
<b>3.4h</b>	2-F	0.8	1.0				
<b>3.4i</b>	3-F	0.9	1.2	1.18 $\pm$ 0.05			
<b>3.4j</b>	2,4-difluoro	1.2	1.2	0.54 $\pm$ 0.09	>100	>100	>175
<b>3.4k</b>	3,4-difluoro	1.1	1.2	0.36 $\pm$ 0.01			
<b>3.4l</b>	3,5-difluoro	1.1	1.1				

GW590735  
Rosiglitazone  
GW0742

1.0

1.0

0.015

0.28

0.0019

<sup>a</sup>All analogues contain the carboxylate head-group at the *meta*-position of the A-ring unless otherwise indicated. \* indicates a *para*-carboxylate. <sup>b</sup>Ratio of relative light unit (RLU) signal at 5  $\mu$ M and 50  $\mu$ M compound concentrations. <sup>c</sup>Ratio of maximal signal (RLU) strength observed for the compound of interest to that obtained with GW590735. <sup>d</sup>EC<sub>50</sub> values represent the mean  $\pm$  SEM of at least two separate experiments performed in triplicate. <sup>e</sup>SI = EC<sub>50</sub> (PPAR $\gamma$  or PPAR $\delta$ ) / EC<sub>50</sub> (PPAR $\alpha$ ). Blank cells indicate compound was not selected for testing in the corresponding assay.

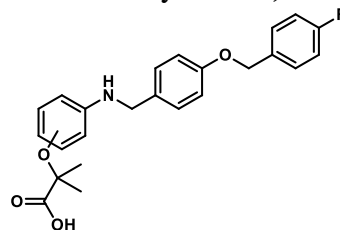
ligand-binding domain. Third, our *in-silico* studies consistently predicted the aryl tail (C-ring) to bind a hydrophobic pocket comprised of helices 6 and 7 and defined by Ile241, Leu247, Ala250, Leu254, and Ala333. Literature precedence demonstrates that improvement of this interaction with other PPAR $\alpha$  chemotypes has proven beneficial to enhancing ligand potency and selectivity.<sup>7-9</sup>

### 3.3.3 Stage I SAR: Linker Extension, C-ring Modification, Carboxylate Location

The first stage of our SAR (**Figure 3.4**) focused on assessing various hydrophobic substituents on the C-ring, probing the effects of linker extension, and determining optimal location for the carboxylate motif (or isostere). To generate stage I analogues, 4-

hydroxybenzaldehyde (**3.1**) was coupled with various benzyl bromides (**3.2a-3.2l**) to yield the corresponding 4-benzyloxybenzaldehydes **3.3a-3.2l** (**Scheme 3.1A**). These precursors were then coupled with 3-aminobenzoic acid (or 4-aminobenzoic acid in the case of **3.4b\***) via reductive amination to obtain **3.4a-3.4l** and

**Table 3.2** *In vitro* activity of **3.5a**, **3.5b**, **3.5b\***, **3.5f**<sup>a</sup>



Compound	R	Ratio (5/50) <sup>b</sup>	Fold-Signal <sup>c</sup>
<b>3.5a</b>	OMe	0.1	1.8
<b>3.5b</b>	F	0.2	2.0
<b>3.5b*</b>	F	0.6	1.8
<b>3.5f</b>	CF <sub>3</sub>	0.2	1.2

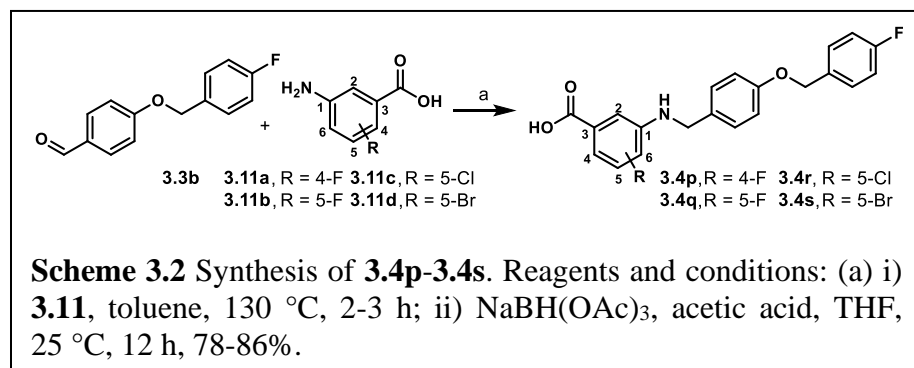
<sup>a</sup>All analogues contain the carboxylate head-group at the *meta*-position of the A-ring unless otherwise indicated. \* indicates a *para*-carboxylate. <sup>b</sup>Ratio of relative light unit (RLU) signal at 5  $\mu$ M and 50  $\mu$ M compound concentrations. <sup>c</sup>Ratio of maximal signal (RLU) strength observed for the compound of interest to that obtained with GW590735.

**3.4b\***. Following a similar synthetic approach, **3.5a**, **3.5b**, **3.5b\***, and **3.5f** that include the typical fibrate head-group were synthesized (**Scheme 3.1A**). The only difference in the generation of **3.5a**, **3.5b**, **3.5b\*** and **3.5f** was that the carboxylate remained protected as the ethyl ester until being revealed in the final step following saponification. Our previous studies indicated that the 4-

benzyloxy-benzylamino chemotype deviates from the fibrates in that incorporation of the classical  $\alpha$ -gem-dimethyl carboxylate “head-group” leads to *pan*-agonism and decreases potency. While these affects are obviously opposite to our goals, these analogues were generated to determine

if this trend continued to propagate through this series.

To generate derivatives with extended linkers the synthesis began with the transformation of primary alcohols **3.6a-3.6b** into the corresponding alkyl bromides **3.7a-3.6b** (Scheme 3.1B). These precursors were then utilized to *O*-alkylate 4-hydroxybenzaldehyde to generate **3.8a-3.8b**, which were coupled with 3-aminobenzoic acid through reductive amination to provide **3.4m** and



**3.4n** that included an extra -CH<sub>2</sub>- between the B and C-rings (Scheme 3.1B).

Analogue **3.4o** with an

additional -CH<sub>2</sub>- between the A and B rings and the B and C rings was also generated. Chemoselective alkylation of tyrosol with **3.7b** afforded **3.9**, which was converted to the corresponding alkyl bromide **3.10** that was used to *N*-alkylate 3-aminobenzoic acid (Scheme 3.1B).

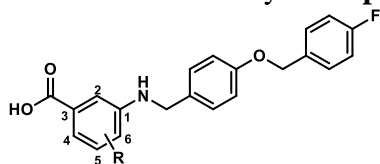
**Table 3.3** *In vitro* activity of **3.4m-3.4o**

Compound	m	n	R	Ratio (5/50) <sup>a</sup>	Fold-Signal <sup>b</sup>
<b>3.4m</b>	1	2	H	0.1	0.9
<b>3.4n</b>	1	2	OMe	0.1	0.9
<b>3.4o</b>	2	2	OMe	1.1	0.1

<sup>a</sup>Ratio of relative light unit (RLU) signal at 5  $\mu$ M and 50  $\mu$ M compound concentrations. <sup>b</sup>Ratio of maximal signal (RLU) strength observed for the compound of interest to that obtained with GW590735.

Stage I derivatives were evaluated for *in vitro* hPPAR $\alpha$  agonism in a commercially available luciferase cell reporter assay (Indigo Biosciences). This assay utilizes non-human mammalian cells engineered to express hPPAR $\alpha$  with the luciferase reporter gene functionally linked to a PPAR $\alpha$ -response promoter. Thus, quantifying changes in luciferase expression in compound treated reporter cells provides a sensitive method to quantify changes in PPAR $\alpha$  activity. As an initial first-pass assessment, all compounds were evaluated at two concentrations, 5  $\mu$ M and 50  $\mu$ M. This two-concentration approach is a cost-effective means to provide insight into 1) rough estimates of potency, 2) therapeutic window, and 3) relative levels of agonism. A 5:50 ratio  $\ll$ 1.0 indicates the compound is much more active at 50  $\mu$ M than 5  $\mu$ M, meaning the compound has poor potency. A 5:50 ratio  $\sim$ 1.0 indicates equal activity at both concentrations, meaning the EC<sub>50</sub> is  $<$ 5  $\mu$ M and is non-cytotoxic to the cells at a 10-fold higher concentration, as cell death results in a decrease in luminescence production. As one would presume, a 5:50 ratio of  $>$ 1.0 indicates a potency  $<$ 5  $\mu$ M, but also demonstrates toxicity at 50  $\mu$ M. Therefore, 5:50 ratios of  $\sim$ 1.0 are desirable. GW590735, a highly selective ( $\geq$ 500-fold over PPAR $\gamma$  and PPAR $\delta$ ) PPAR $\alpha$  partial

**Table 3.4** *In vitro* activity of **3.4p-3.4s**



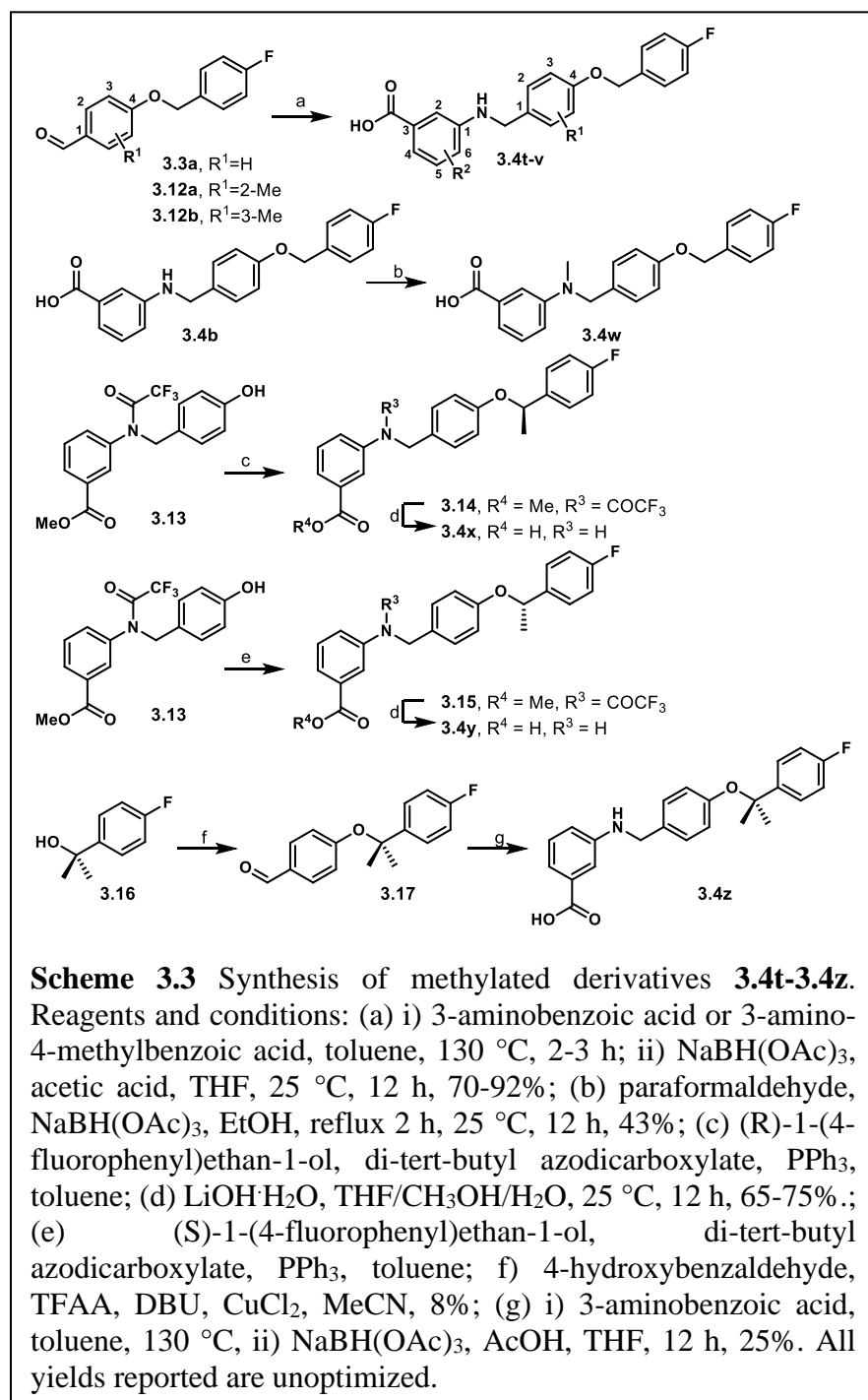
R	Ratio (5/50) <sup>a</sup>	Fold-Signal <sup>b</sup>	EC <sub>50</sub> hPPAR $\alpha$ ( $\mu$ M) <sup>c</sup>	EC <sub>50</sub> hPPAR $\gamma$ ( $\mu$ M)	EC <sub>50</sub> hPPAR $\delta$ ( $\mu$ M)	SI <sup>d</sup>
<b>3.4p</b>	4-F	0.8	1.2	1.61 $\pm$ 0.06		
<b>3.4q</b>	5-F	1.1	1.1	0.58 $\pm$ 0.04	$>$ 100	$>$ 100
<b>3.4r</b>	5-Cl	0.1	1.1			
<b>3.4s</b>	5-Br	1.3	1.4	1.12 $\pm$ 0.08	$>$ 100	$>$ 100

<sup>a</sup>Ratio of relative light unit (RLU) signal at 5  $\mu$ M and 50  $\mu$ M compound concentrations.

<sup>b</sup>Ratio of signal maximal signal (RLU) strength observed for the compound of interest to that obtained with GW590735. <sup>c</sup>EC<sub>50</sub> values represent the mean  $\pm$  SEM of at least two separate experiments performed in triplicate. <sup>d</sup>EC<sub>50</sub> (PPAR $\gamma$  or PPAR $\delta$ ) / EC<sub>50</sub> (PPAR $\alpha$ ). Blank cells indicate compound was not selected for testing in the corresponding assay.

agonist  
was  
employed  
as a  
positive  
control.<sup>8</sup>  
In  
line with  
our

hypothesis, the incorporation of lipophilic or electron withdrawing substituents on the C-ring of the benzoic acid chemotype (**3.4b-l**) provides an improvement in cellular activity in comparison to A91 (**3.4a**). Most analogues in the **3.4b-l** series exhibit 5:50 ratios >0.5, indicating EC<sub>50</sub> values <5 μM (**Table 3.1**). Comparison of **3.4b** and **3.4b\*** demonstrates that the 3-carboxylate is favored

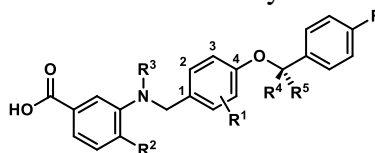


over the 4-carboxylate. Within this class, we advanced 8 derivatives to multi-point dose-response analysis in the same luciferase assay. Compounds were chosen based on a combination of interest, 5:50 ratio, and level of agonism. As shown in **Table 3.1**, the 4-F (**3.4b**), 4-Br (**3.4d**), 2,4-difluoro (**3.4j**), and 3,4-difluoro (**3.4k**) analogues all exhibit submicromolar activity and are ~2-3 fold more active than the 4-I (**3.4e**) and 4-CF<sub>3</sub> (**3.4f**). This result was somewhat

forecasted by our *in-silico* results, which predicted that substituents larger than a bromine at the 4-position would be problematic. Even though the 3-F (**3.4i**) is less active than the 4-F (**3.4b**), it was still more active than A91 (**3.4a**). Thus, it is not surprising that inclusion of fluorine at both the 3- and 4-positions (**3.4k**) of this scaffold results in additive properties and is the most potent compound of this series. Inclusion of the typical fibrate head-group (**3.5a**, **3.5b**, **3.5b\***, and **3.5f**) once again leads to decreased potency (**Table 3.2**) but often higher levels of agonism than the benzoic acid relatives (**3.5a** vs **A91**, **3.5b** vs **3.4b**, and **3.5f** vs **3.4f**). As shown in **Table 3.3**, analogs containing extended linkers **3.4m–3.4o** exhibited poor potency (**3.4m** and **3.4n**) or poor activation (**3.4o**) in comparison to related non-homologated derivatives.

From the stage I cohort, analogues **3.4b** and **3.4j** were selected to move forward to selectivity assessment, wherein equivalent luciferase assays were conducted on isogenic cell-lines engineered to overexpress either hPPAR $\gamma$  or hPPAR $\delta$ . Neither compound produced significant

**Table 3.5** *In vitro* activity of **3.4t–3.4z**



Compound	R <sup>1</sup>	R <sup>2</sup>	R <sup>3</sup>	R <sup>4</sup>	R <sup>5</sup>	Ratio (5/50) <sup>a</sup>	Fold-Signal <sup>b</sup>	EC <sub>50</sub> hPPAR $\alpha$ ( $\mu$ M) <sup>c</sup>	SI <sup>d</sup>
<b>3.4t</b>	2-OMe	H	H	H	H	0.8	1.2	1.45 $\pm$ 0.06	
<b>3.4u</b>	3-Me	H	H	H	H	1.4	1.2	0.037 $\pm$ 0.01	>2700
<b>3.4v</b>	H	Me	H	H	H	0.2	0.3		
<b>3.4w</b>	H	H	Me	H	H	0.8	1.7	0.90 $\pm$ 0.08	
<b>3.4x</b>	H	H	H	Me	H	0.1	0.6	25.6 $\pm$ 3.5	
<b>3.4y</b>	H	H	H	H	Me	0.2	1.6		
<b>3.4z</b>	H	H	H	Me	Me	0.2	0.8	8.52 $\pm$ 1.83	
<b>3.4a (A91)</b>						0.8	1.3	0.77 $\pm$ 0.03	>20
<b>3.4b</b>						0.5	1.4	4.43 $\pm$ 0.01	>125
GW590735						1.0	1.0	0.015 $\pm$ 0.002	

<sup>a</sup>Ratio of relative light unit (RLU) signal at 5  $\mu$ M and 50  $\mu$ M compound concentrations. <sup>b</sup>Ratio of signal maximal signal (RLU) strength observed for the compound of interest to that obtained with GW590735.

<sup>c</sup>EC<sub>50</sub> values represent the mean  $\pm$  SEM of at least two separate experiments performed in triplicate.

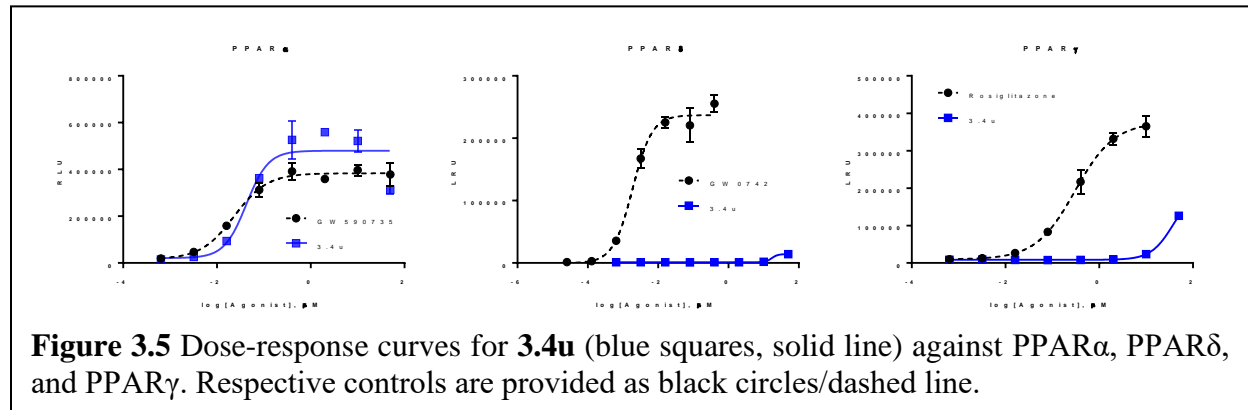
<sup>d</sup>EC<sub>50</sub> (PPAR $\gamma$  or PPAR $\delta$ ) / EC<sub>50</sub> (PPAR $\alpha$ ). Blank cells indicate compound was not selected for testing in the corresponding assay.

levels of hPPAR $\gamma$  or hPPAR $\delta$  agonism up to 100  $\mu$ M compound concentration, indicating a selectivity of >125-fold (**3.4b**) and >175-fold (**3.4j**) for hPPAR $\alpha$ . Rosiglitazone, a known selective PPAR $\gamma$  agonist, and GW0742, a known selective PPAR $\delta$  agonist, were employed as positive controls in these isogenic cell-lines.

### 3.3.4 Stage II SAR: Strategic Methylation, Metabolism Blocking, Carboxylate Isosteric Replacement

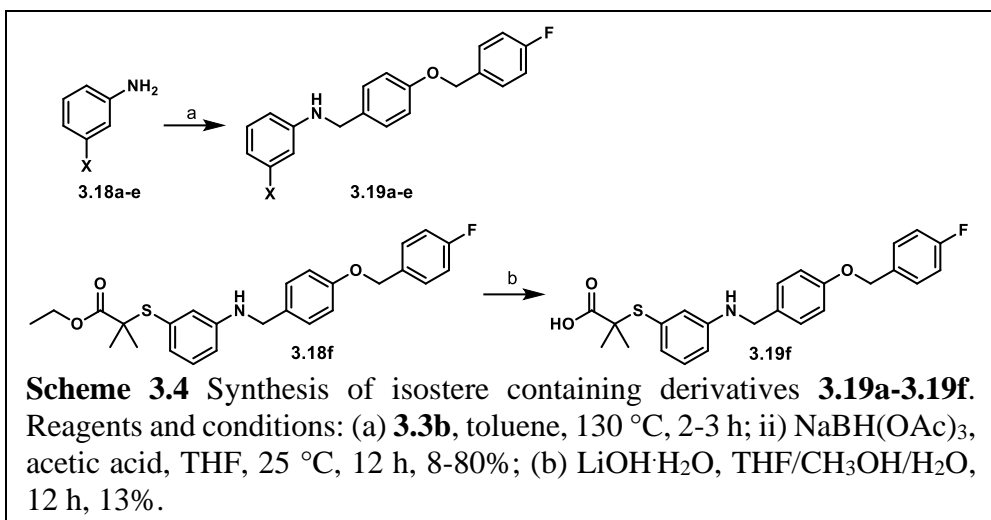
From the stage I results, compound **3.4b** was selected as the base structure from this family for advancement. Three strategies were leveraged to advance the SAR in stage II 1) methylation at strategic positions within the scaffold that were expected to enhance complementarity with the shape and hydrophobicity of the PPAR $\alpha$  ligand binding pocket; 2) blockage of predicted sites of metabolism; and 3) isosteric replacement of the carboxylate.

*In silico* prediction of major sites of metabolism for A91 with Schrodinger's P450 Site of



Metabolism software identified the A-ring as a potential liability for CYP450 oxidation (see appendix 2). As such, we synthesized **3.4p** and **3.4q** (Scheme 3.2) to interrogate the effects of fluorine blockage on activity. These two analogues were generated by coupling **3.3b** to 5-amino-2-fluorobenzoic acid (**3.11a**) or 5-amino-3-fluorobenzoic acid (**3.11b**) to produce **3.4p** and **3.4q**, respectively. The 5-fluoro variant (**3.4q**) exhibits a ~3-fold improvement in activity over the 4-fluoro derivative (**3.4p**) and is nearly equipotent to **3.4b** (Table 3.4). Interestingly, incorporation

of a chlorine at the 5-position of the A-ring (**3.4r**) greatly decreases potency (5:50 ratio = 0.11), while incorporation of a



bromine at the 5-position (**3.4s**) maintains potency in comparison to **3.4b** but introduces apparent cytotoxicity at elevated concentrations (5:50 ratio = 1.3). These results suggest that fluorine incorporation should be a viable strategy to block sites on the A-ring if proven to be problematic as this series progresses through development.

Inspired by frequently reported methyl effects in drug discovery,<sup>12</sup> analogues containing one or two methyl groups at different positions were synthesized (**Scheme 3.3**) using variations of chemistry discussed in **Schemes 3.1** and **3.2** and evaluated in the luciferase assay (**3.4t-3.4z**, **Table**

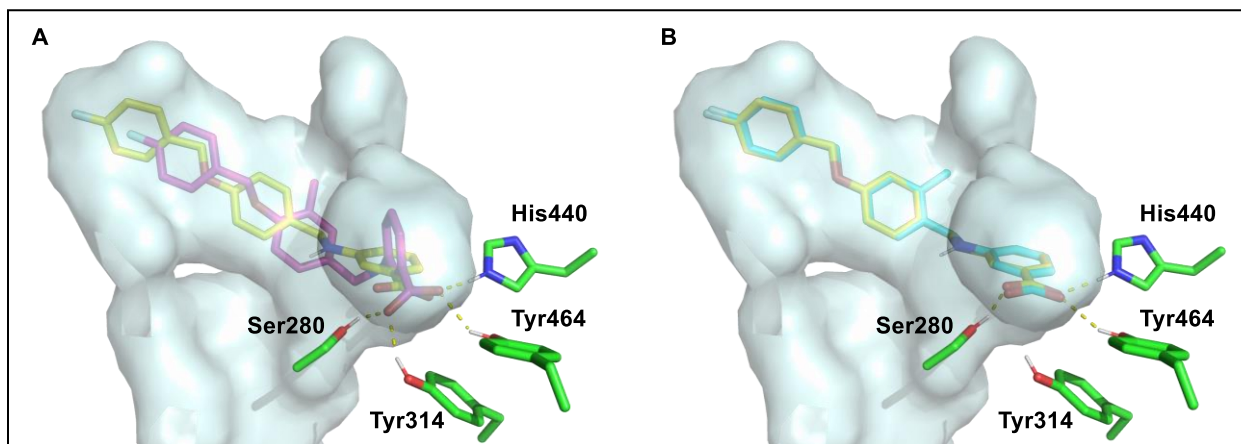


**Figure 3.6** Predicted binding modes of **3.4b**, **3.4t**, and **3.4u**, demonstrating the possible effects of methyl installation on the 2- or 3-position of the B ring. (A) Overlay of the predicted binding poses for **3.4b** (yellow) and **3.4u** (magenta). (B) Overlay of the predicted binding poses for **3.4b** (yellow) and **3.4t** (cyan). PDBID: 2P54. The pdb file of the docking model is included in the Experimental section.



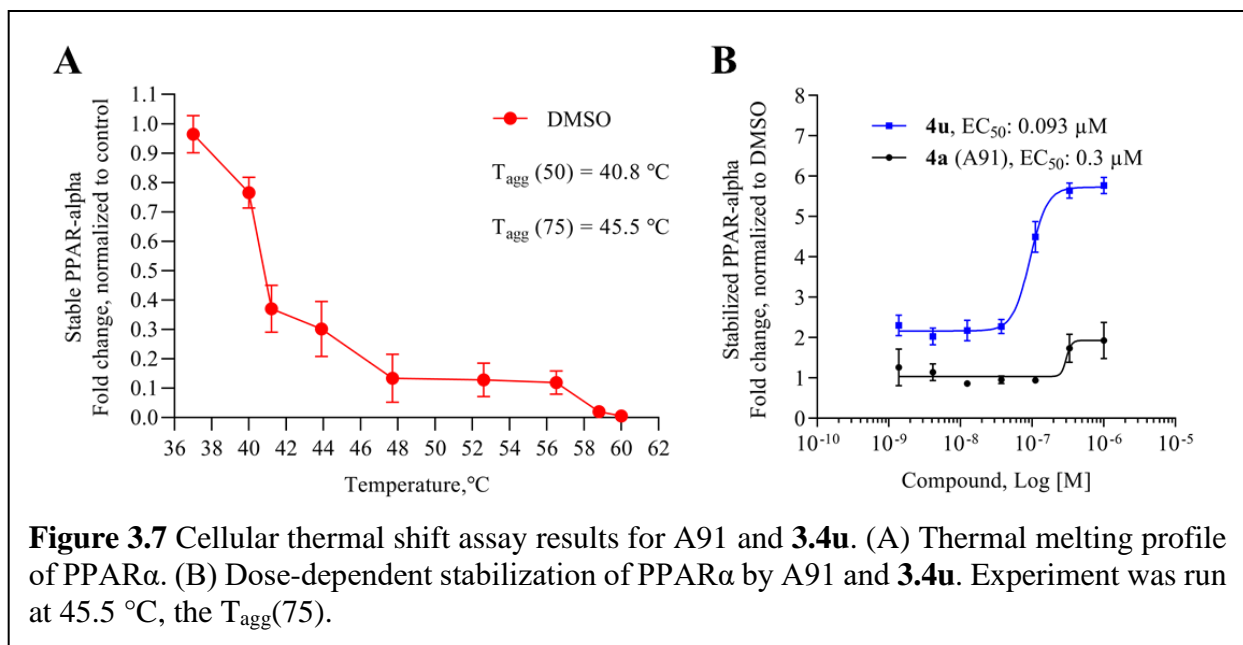
**3.5**). Specifically, we interrogated the effects of methylation on the 2- and 3-position of the B-ring, the 4-position of the A-ring, the nitrogen linker, and all possible variations on the benzylic position of the linker between the B- and C-rings (another predicted site of metabolic liability). Interestingly, installation of a methyl group at the 3-position of B-ring (**3.4u**) resulted in a drastic improvement in cellular activity, dropping the EC<sub>50</sub> to ~40 nM, a ~21-fold improvement from the *des*-methyl relative, **3.4b**, and improving the selectivity for the PPAR $\alpha$  isoform to >2,700-fold (**Figure 3.5**). However, methylation at alternate sites (**3.4t** and **3.4v-3.4z**) failed to induce similar effects on the activity, indicating that the improvement observed with **3.4u** is not likely to arise from an increase in general hydrophobicity but rather from improving aspects of target engagement.

While the reason for the drastic improvement in activity arising from incorporation of the methyl group at the 3-position of the B-ring is not obvious, we have interrogated this phenomenon briefly by *in silico* methods. Results from these studies suggest that methylation at the 3-position (**3.4u**) results in a binding shift that allows for improved hydrogen bonding with the Ser280, Tyr314, His440, and Tyr464 tetrad (**Figure 3.6A**). Additionally, **3.4u** is predicted to bind with the aromatic ring of the benzoic acid perpendicular to His440 thus allowing for T-shaped edge-to-face pi-interactions (**Figure 3.6A**). Methylation at the 2-position (**3.4t**), however, produces no such shift and **3.4t**

**Table 3.6** *In vitro* activity of carboxylate isosteres **3.19a-3.19f**

Compound	X	Ratio (5/50) <sup>a</sup>	Fold-Signal <sup>b</sup>
<b>3.19a</b>		1.0	0.1
<b>3.19b</b>		0.5	0.6
<b>3.19c</b>		1.2	0.1
<b>3.19d</b>		0.4	1.6
<b>3.19e</b>		0.9	0.1
<b>3.19f</b>		0.2	1.1
<b>3.4b</b>		0.8	1.3

**GW590735** 1.0 1.0  
<sup>a</sup>Ratio of relative light unit (RLU) signal at 5  $\mu$ M and 50  $\mu$ M compound concentrations. <sup>b</sup>Ratio of signal maximal signal (RLU) strength observed for the compound of interest to that obtained with GW590735.



overlays very well with the *des*-methyl analogue **3.4b** (Figure 3.6B). As such, it is not surprising that the activity of **3.4t** and **3.4b** are relatively similar.

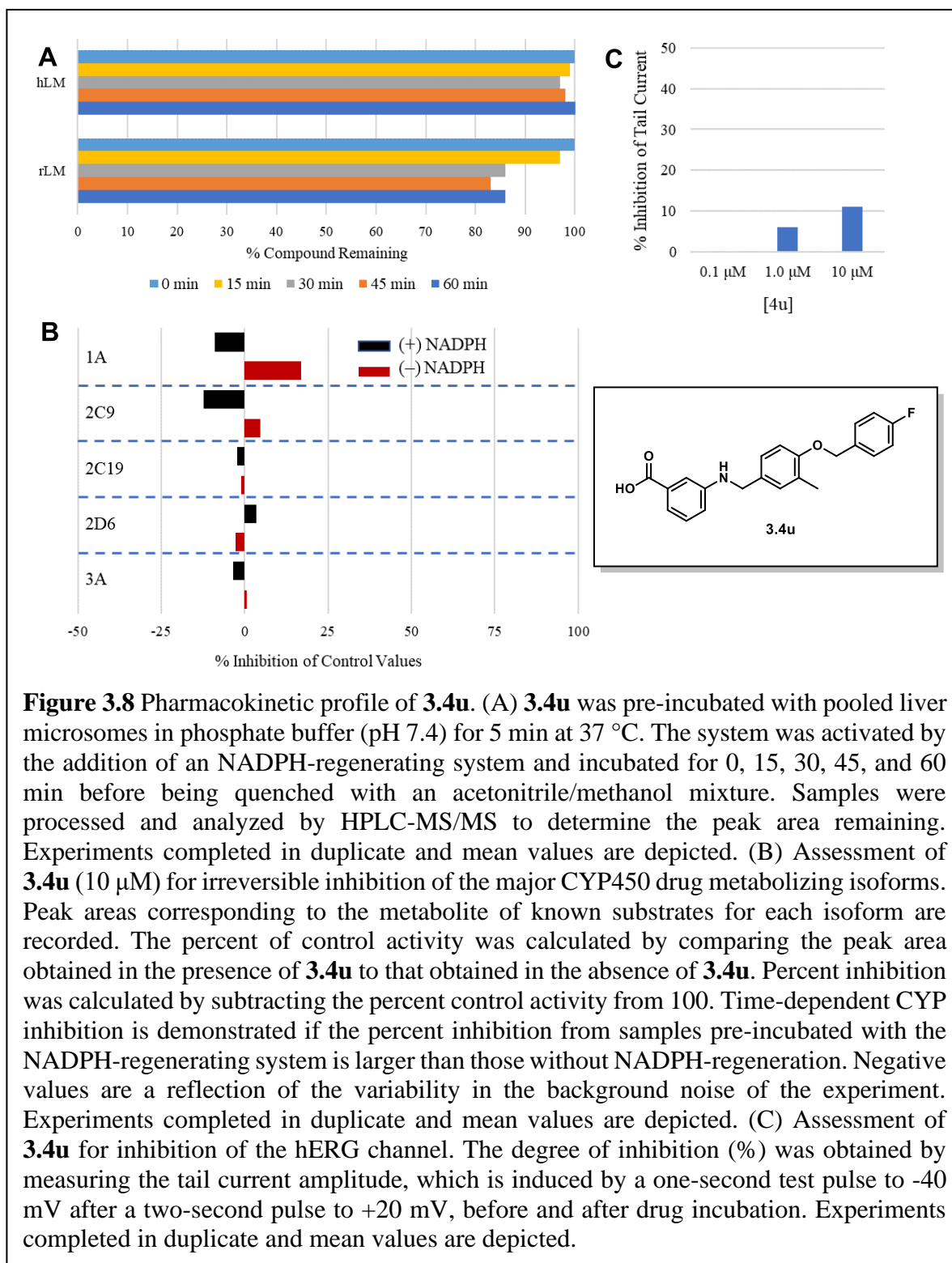
Coupling **3.3b** to a variety of anilines containing carboxylic acid surrogates (**3.18a-3.18e**) allowed us to assess the effect of isosteric replacement on PPAR $\alpha$  agonistic activity (**3.19a-3.19e**, Scheme 3.4). As seen in Table 3.6, replacement of the carboxylate with any of the isosteres resulted in dramatic decreases in activity, as noted by either a low 5:50 ratio or low overall signal. The exception being the tetrazole (**3.19d**), which exhibits decreased potency but comparable activation levels to the original carboxylate. This result confirms that the carboxylic acid is a key contributor to triggering PPAR $\alpha$  agonism but can indeed be modified. As part of this series, the thio-variant of the fibrate head-group was also synthesized and assessed (**3.19f**). Interestingly, this derivative exhibits an attenuated level of agonism compared to the parent analogue, **3.5b**. Differences in agonism levels now observed between the benzoic acid, fibrate head-group, and the thio- fibrate head-group strongly suggest that manipulation of this motif may provide a useful means to tune the level of agonism induced by a chemotype. This could be important as it is still

unknown what level of stimulation (partial or full-agonism) is optimal for PPAR $\alpha$  to have a therapeutic effect in the retina.

### 3.3.5 Additional Assessment of **3.4u**

As the most potent analogue identified in stages I and II, **3.4u** was selected for additional assessment. To confirm target engagement, evaluate binding potency, and provide some insight into selectivity in a relevant human retinal cell line (MIO-M1, Müller cells) we subjected **3.4u** to a CETSA (cellular thermal shift assay).<sup>13,14</sup> Unlike the luciferase assay, MIO-M1 cells are not engineered to specifically report engagement with PPAR $\alpha$  and thus provide a more realistic picture of compound behavior in a disease related cell setting. In an initial heat gradient, non-ligand associated PPAR $\alpha$  displayed a temperature-dependent decay, with T<sub>agg</sub>(50) and T<sub>agg</sub>(75) at 40.8 °C and 45.5 °C, respectively (**Figure 3.7A**). In a subsequent test, dose-dependent potency of the PPAR $\alpha$  agonists, A91 and **3.4u** were tested at 45.5 °C, the temperature point at which 75% of free PPAR $\alpha$  protein melted. As shown in **Figure 3.7B**, A91 improved PPAR $\alpha$  stability incrementally with an EC<sub>50</sub> of 0.3  $\mu$ M. On the other hand, **3.4u** rescued PPAR $\alpha$  stability by 3-fold with an EC<sub>50</sub> of 93 nM. The results for **3.4u** correlate well with the EC<sub>50</sub> value obtained from the luciferase assay (EC<sub>50</sub> = 37 nM), demonstrating consistency of this compound within different contexts and eluding to excellent intracellular selectivity.

Compound **3.4u** was assessed in the same PK studies as **3.4a** (A91). As seen in **Figure 3.8**, this analogue exhibits significantly improved stability in human and rat liver microsomes (**Figure**



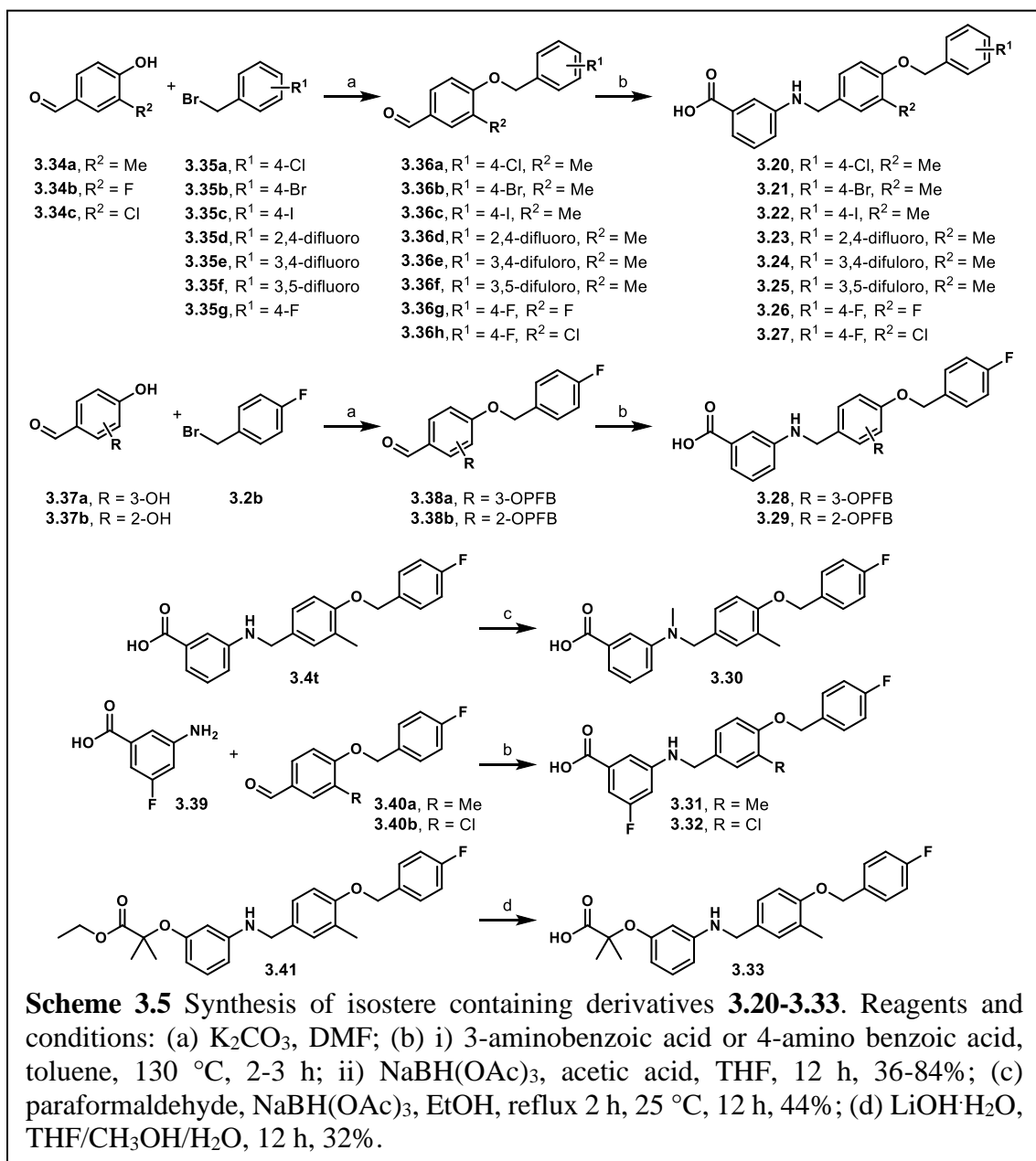
**3.8A**), shows no signs of irreversible inhibition of the major drug metabolizing CYP450s (**Figure 3.8B**) and is not considered a hERG liability (**Figure 3.8C**). It is important to note that while this compound exhibits 10% inhibition of hERG at 10  $\mu$ M (the same as A91), this analogue is ~20-fold more potent than A91.

### 3.3.6 Stage III SAR: Combining Lessons Learned.

Due to information gained from the stage I and II cohorts we designed and synthesized a

series

that



combined beneficial features from each stage. Utilizing established synthetic routes, compounds **3.20-3.33** were synthesized and evaluated in similar fashion to stage I and II derivatives (**Scheme 3.5**). As shown in **Table 3.4**, all stage III analogues exhibit submicromolar activity in the cell luciferase assay, with many derivatives revealing EC<sub>50</sub> values under 50 nM. Comparison of **3.24-3.29** to the corresponding *des*-methyl relatives demonstrates that the methyl effect is ~10-20-fold more potent for each derivative and thus exhibits exquisite consistency. Most notably, **3.22**, which contains an iodine at the 4-position on the C-ring, exhibits a 50-fold improvement in activity in comparison to the *des*-methyl B-ring relative. Based on the predicted shift in the binding pocket

**Table 3.7** *In vitro* activity of phase III analogues

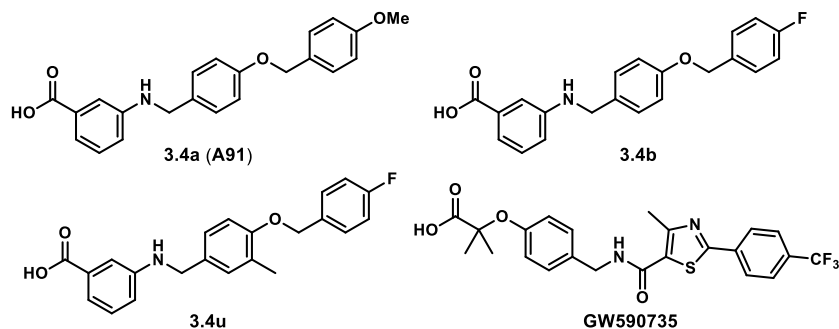
Compound	X	R <sup>1</sup>	R <sup>2</sup>	R <sup>3</sup>	R <sup>4</sup>	Ratio (5/50) <sup>a</sup>	Fold-Signal <sup>b</sup>	EC <sub>50</sub> hPPAR $\alpha$ ( $\mu$ M) <sup>c</sup>
<b>3.20</b>	COOH	4-Cl	3-Me	H	H	1.2	1.2	0.029
<b>3.21</b>	COOH	4-Br	3-Me	H	H	1.2	1.3	0.031
<b>3.22</b>	COOH	4-I	3-Me	H	H	1.8	1.5	0.027
<b>3.23</b>	COOH	2,4-difluoro	3-Me	H	H	1.2	1.4	0.056
<b>3.24</b>	COOH	3,4-difluoro	3-Me	H	H	1.4	1.6	0.018
<b>3.25</b>	COOH	3,5-difluoro	3-Me	H	H	1.1	1.6	
<b>3.26</b>	COOH	4-F	3-F	H	H	0.7	1.7	
<b>3.27</b>	COOH	4-F	3-Cl	H	H	1.1	1.5	
<b>3.28</b>	COOH	4-OPFB	3-OPFB	H	H	1.0	1.4	0.81
<b>3.29</b>	COOH	4-OPFB	2-OPFB	H	H	0.9	1.2	0.93
<b>3.30</b>	COOH	4-F	3-Me	H	Me	0.8	2.1	0.067
<b>3.31</b>	COOH	4-F	3-Me	F	H	0.9	1.5	0.040
<b>3.32</b>	COOH	4-F	3-Cl	F	H	1.1	1.8	0.052
<b>3.33</b>	OC(CH <sub>3</sub> ) <sub>2</sub> COOH	4-F	3-Me	H	H	1.0	1.6	0.74
<b>3.4b</b>						0.8	1.3	0.77
<b>3.4a (A91)</b>						0.5	1.4	4.43
GW590735						1.0	1.0	0.015

<sup>a</sup>Ratio of relative light unit (RLU) signal at 5  $\mu$ M and 50  $\mu$ M compound concentrations. <sup>b</sup>Ratio of signal maximal signal (RLU) strength observed for the compound of interest to that obtained with GW590735. <sup>c</sup>EC<sub>50</sub> values represent the mean  $\pm$  SEM of at least two separate experiments performed in triplicate. OPFB = *para*-fluorobenzyl. Numbering shown is based on the name of the resulting products. Blank cells indicate compound was not selected for testing in the corresponding assay.

(Figure 3.6) we suspect that room in the C-ring pocket is subsequently freed, allowing space for the larger iodine substituent that is not as easily accommodated with the *des*-methyl compound, **3.4e**. Consistent with the effect observed between **3.4w** and **3.4b**, N-methylation of the linker results in ~2-fold decrease in potency (**3.4u** vs. **3.30**). Furthermore, comparison of **3.4u** and **3.31** reveals that incorporation of the 3-F on the A-ring results in a maintenance in potency, a phenomenon first observed between **3.4b** and **3.4q**. Overall, the results from stage III analogues confirm trends seen in stages I and II, corroborate *in silico* docking predictions, and provide compelling evidence that the SAR for this chemotype is consistent, a desirable yet often elusive property in lead optimization.

### 3.3.7 Thermodynamic Binding Profiles

**Table 3.8** Thermodynamic Binding Profiles of Selected Ligands with the Ligand Binding Domain of PPAR $\alpha$ <sup>a</sup>

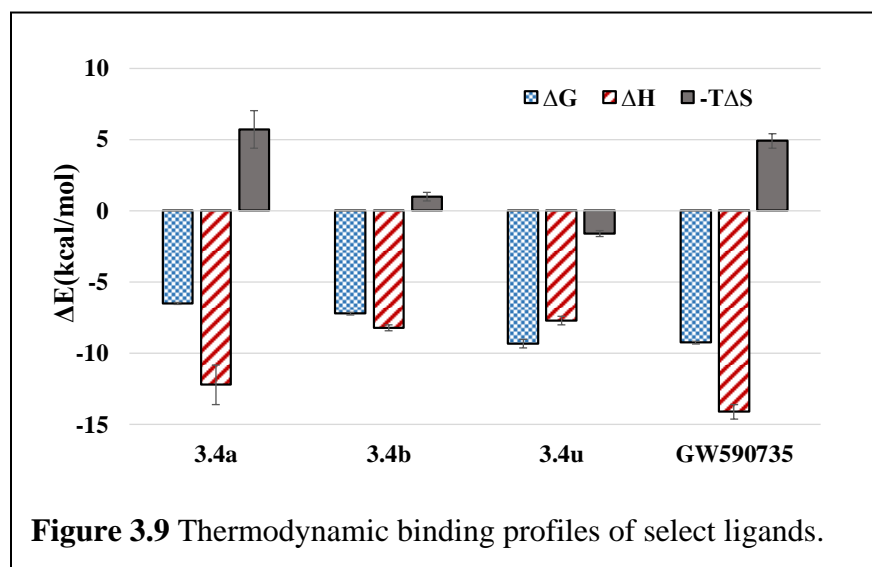


Compound	EC <sub>50</sub> (μM)	K <sub>d</sub> (μM)	ΔG (kcal/mol)	ΔH (kcal/mol)	-TΔS (kcal/mol)
<b>3.4a (A91)</b>	4.43 ± 0.01	16.90 ± 1.50	-6.50 ± 0.05	-12.20 ± 1.40	5.71 ± 1.31
<b>3.4b</b>	0.77 ± 0.03	5.32 ± 0.78	-7.20 ± 0.09	-8.18 ± 0.20	0.98 ± 0.27
<b>3.4u</b>	0.037 ± 0.005	0.14 ± 0.05	-9.39 ± 0.17	-7.75 ± 0.26	-1.65 ± 0.37
GW590735	0.015 ± 0.002	0.17 ± 0.03	-9.24 ± 0.09	-14.10 ± 0.50	4.90 ± 0.50

<sup>a</sup>Buffer: 20 mM HEPES, 150 mM NaCl, pH 7.4. Ligand solution: 200-1000 μM ligand in buffer with 0.8-10% DMSO. Protein solution: 30-85 μM PPAR $\alpha$  LBD in buffer with same concentration of DMSO as corresponding ligand solution. Thermodynamic parameters reported as mean ± S.D. of at least three separate experiments. All experiments were performed at 25 °C. N.D. = not determined.

To determine thermodynamic parameters relating to the formation of PPAR $\alpha$ /ligand complexes, we subjected structurally related **3.4a**, **3.4b**, and **3.4u** along with GW590735 (as a known agonist) to isothermal titration calorimetry (ITC). These analogues were selected, as they

only differ in single functionalities that produce significant changes in cellular activity and thus allowed for the correlation of binding thermodynamics to specific molecular features. Replacement of the C-ring 4-OMe (**3.4a**) with a 4-F (**3.4b**) produces a ~3-fold improvement in binding affinity, an observation consistent with cellular activity. Based on the thermodynamic profile (**Figure 3.9**, **Table 3.5**), the observed improvement in binding affinity is likely due to a 4.73 kcal/mol lower entropic penalty of binding for **3.4b**. Introduction of a methyl group on the B-ring (**3.4u**) dramatically improves (~38-fold) the binding affinity, also consistent with cellular results. As depicted in **Figure 3.9**, the incorporation of the methyl group at the 3-position of the B-ring produces a favorable  $-\Delta S$  term while also maintaining a favorable enthalpic contribution. The full thermodynamic binding profile of **3.4u** reveals enthalpically driven binding to PPAR $\alpha$ , helping to explain the significant jump in affinity.



Combined, these results suggest that the observed improvements in the cellular luciferase assay are likely due to improved binding profiles and not alterations in cellular permeability, solubility, or

other physicochemical properties that may affect activity. Likewise, the proximities of  $K_d$  and  $EC_{50}$  values provides compelling evidence that this chemotype exhibits high specificity for PPAR $\alpha$ . Attempts to obtain a  $K_d$  and thermodynamic binding profile for the fibrate headgroup containing



member of this series (**3.5b**) failed to produce reproducible data due to solubility issues under assay conditions.

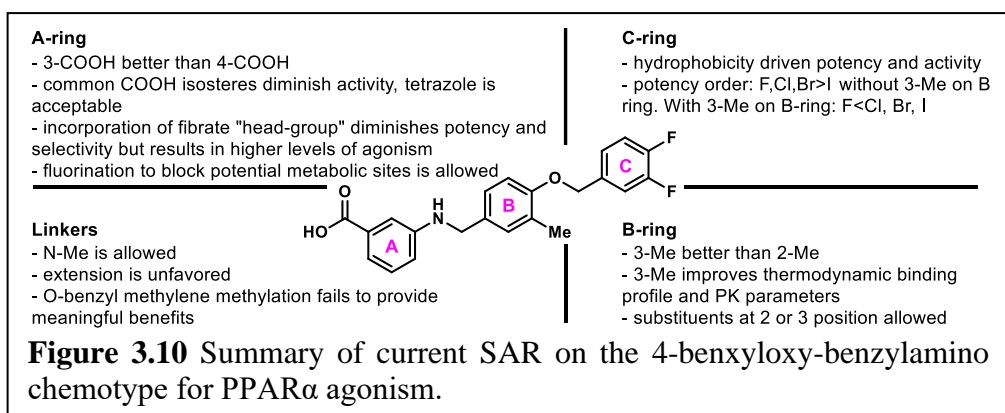
### 3.4 Conclusion

In conclusion, we have advanced our initial studies on the 4-benzyloxy-benzylamino chemotype as a novel PPAR $\alpha$  agonistic scaffold by providing proof-of-concept *in vivo* efficacy, preliminary pharmacokinetic assessment and the design, synthesis, and evaluation of second-generation analogues that provide highly potent and isoform selective leads. The data demonstrate that systemic A91 (**3.4a**) treatment (i.p. injection) reduces retinal vascular leakage in diabetic rats to the level of non-diabetic controls at relatively the same dose as Fenofibrate, without signs of hepatomegaly. A full PK profile of this chemotype has yet to be determined (due to resource limitations), limiting PK/PD correlations for the *in vivo* data in comparison to Fenofibrate. However, embedded in these results is confirmation that A91 1) exhibits *in vivo* efficacy in a relevant DR model following systemic administration, 2) is bioavailable, 3) survives first-pass metabolism and clearance mechanisms well enough to reach the site of disease and maintain efficacy, and 4) demonstrates a relatively safe profile (no observable toxicity) after daily intraperitoneal injection for one-month.

Utilizing A91 as a template we leveraged structure-guided design to develop second generation derivatives focused on improving the potency, affinity, and selectivity for PPAR $\alpha$ .

#### (Figure 3.10).

These efforts led to the discovery of **3.4u** and related



compounds that reach cellular potencies <50 nM and exhibit >2,700-fold selectivity for PPAR $\alpha$  over other PPAR isoforms. Importantly, we discovered that incorporation of a methyl at the 3-position of the B-ring leads to dramatic improvements in target engagement, selectivity, and cellular activity. Cellular thermal shift analysis confirms tight binding of the top candidates to hPPAR $\alpha$  and isothermal titration calorimetry further confirms a much-improved binding affinity and thermodynamic profile for **3.4u** in comparison to A91 (**3.4a**). Initial pharmacokinetic assessment of **3.4u** reveals microsomal stability in both human and rat microsomes, no evidence of irreversible inhibition of major drug metabolizing CYP450 enzymes, and a low risk for hERG interactions at relevant concentrations.

Detailed determination of a full PK/PD profile of this chemotype and advanced *in vivo* studies are ongoing and will be communicated in due time. Priority studies moving forward will focus on determining drug exposure in the retina after systemic administration and determining a more comprehensive metabolic profile, including phase-II conjugations. The data reported within, however, emphasize the promise of the 4-benzyloxy-benzylamino chemotype as a PPAR $\alpha$  agonistic family with efficacy in the retina after systemic administration and identify a pipeline of candidates positioned for detailed PK/PD and pre-clinical evaluation.

## **3.5 Experimental Section**

### **3.5.1 General Synthetic Information**

Starting materials, ACS grade DCM, methanol, ethyl acetate, toluene, anhydrous DMF, THF were purchased from TCI Chemicals, Oakwood, Alfa Aesar, Boron Molecular, Fisher Scientific or Sigma-Aldrich. All reactions requiring anhydrous conditions were run under a nitrogen atmosphere. NMR were collected on a 400, 500, and 600 MHz (specified below) Varian VNMRS Direct Drive spectrometer equipped with an indirect detection probe. NMR data were

collected at 25 °C unless otherwise indicated. Pulse sequences were used as supplied by Varian VNMRJ 4.2 software. All NMR data was processed in MestReNova v11.0. High resolution mass spectrometry was obtained from and analyzed by the Mass Spectrometry Facility at the University of Oklahoma. All analogues evaluated in biological assays were >95% purity based on HPLC and NMR analyses.

**Purity Analysis of Final Analogues.** Ultra-high-pressure liquid chromatography (UPLC) separation of samples (25 uM) was performed using an Agilent 1290 UPLC system equipped with an Agilent Zorbax Eclipse Plus reverse-phase column (ODS-18; 50 mm x 2.1 mm, 1.8- μm particle size). Mobile phase A consisted of 100% Optima<sup>®</sup> LC/MS submicron filtered water (Fisher Scientific). Mobile phase B consisted of 100% Optima<sup>®</sup> LC/MS acetonitrile. A binary gradient at 0.65 mL/min flow rate was applied as follows: 100% solvent A from 0 to 1 min linear gradient to 20% solvent B, linear gradient to 80% solvent B from 1 to 8 min, linear gradient to 100% solvent B from 8 to 9.1 min, 100% solvent B from 9.1 to 10.3 min, and linear gradient to return the mobile phase to 100% solvent A from 10.3 to 10.4 min, which was maintained for an additional 3 min before the next sample was injected. The UPLC column eluent was introduced into an Agilent 1290 Infinity Diode Array Detector. Absorbance was scanned from 190 to 400 nm. Absorbance intensity at 154 nm was quantitated by area integration. For accurate mass confirmation the eluent traveled in series from the DAD to an Agilent 6545 UHD Accurate Mass QTOF device equipped with an electrospray ionization source operated in negative ion mode. Nitrogen was used as a nebulizing gas (40 pounds/inch<sup>2</sup>) and a drying gas (325 °C and 10 L/min flow rate). Fragmentor, skimmer, and capillary voltages were 180, 45, and 2500 V, respectively. Data was collected with Mass Hunter Acquisition (B.08.00) and analyzed with Mass Hunter Qualitative (B.07.00).

**General Procedure A (Reductive amination).** Requisite aniline (1.0 eq.) was dissolved in toluene (30 mL), and the requisite aldehyde (1.02 eq.) was added. The reaction mixture was heated for 2 h under reflux using a Dean–Stark trap. Subsequently, the solvent was evaporated under reduced pressure. The crude product was dissolved in THF (0.1 M) and cooled to 0 °C prior to the addition of neat sodium triacetoxyborohydride (2.0 eq.). The resulting reaction mixture was stirred for 15 min, after which acetic acid (0.01 eq.) was added to the reaction. The mixture was then allowed to stir for 12 h at 25 °C while monitoring by TLC. Upon complete consumption of the aniline, the reaction was quenched through slow addition of water. The mixture was extracted three times with EtOAc, the organic layers were combined and washed with brine. The organic layer was dried over anhydrous sodium sulfate, filtered, and evaporated under vacuum. The product was purified by column chromatography (SiO<sub>2</sub>) using dichloromethane/methanol (99.5:0.5) as the eluent.

**General Procedure B (Ester saponification).** To a stirred solution of the requisite ethyl ester (1.0 eq.) in THF/MeOH/H<sub>2</sub>O mixture (0.1 M, 3:1:1) was added lithium hydroxide monohydrate (5.0 eq.) and the reaction mixture was stirred for 12 h at 25 °C. The reaction mixture was concentrated to remove organic solvents. The aqueous layer was acidified to pH 2.0 with 1 N aq. HCl and then extracted with EtOAc. The organic layer was washed with water and brine. The resulting organic layer was dried over anhydrous Na<sub>2</sub>SO<sub>4</sub>, filtered, and evaporated under vacuum. The product was purified by column chromatography (SiO<sub>2</sub>) using dichloromethane/methanol (99:1) as the eluent.

3-(((4-((4-methoxybenzyl)oxy)benzyl)amino)benzoic acid (**3.4a**): Reaction scale: 100 mg (0.73 mmol) of 3-amino benzoic acid. Compound **3.4a** was prepared following General Procedure A with aldehyde **3.3a** (0.74 mmol). The product was purified by flash column chromatography (SiO<sub>2</sub>,

CH<sub>2</sub>Cl<sub>2</sub>/CH<sub>3</sub>OH, 99.5:0.5) to give a white amorphous solid (210 mg, 80% yield). <sup>1</sup>H NMR (400 MHz, Chloroform-*d*) δ 7.46 (d, *J* = 7.7 Hz, 1H), 7.36 (d, *J* = 9.2 Hz, 3H), 7.27 (q, *J* = 6.3, 4.1 Hz, 4H), 6.94 (dd, *J* = 14.6, 8.1 Hz, 4H), 6.84 (d, *J* = 8.3 Hz, 1H), 4.99 (s, 2H), 4.30 (s, 2H), 3.82 (s, 3H) ppm; <sup>13</sup>C NMR (101 MHz, Chloroform-*d*) δ 171.8, 159.6, 158.4, 148.3, 131.1, 130.2, 129.4, 129.3 (2C), 129.1, 128.9 (2C), 119.4, 118.2, 115.2 (2C), 114.2 (2C), 114.0, 70.0, 55.4, 47.8 ppm. HRESI m/z: 364.1449 (C<sub>22</sub>H<sub>21</sub>NO<sub>4</sub> + H<sup>+</sup> requires 364.1543).

3-((4-((4-fluorobenzyl)oxy)benzyl)amino)benzoic acid (**3.4b**): Reaction scale: 50 mg (0.36 mmol) of 3-amino benzoic acid. Compound **3.4b** was prepared following General Procedure A with aldehyde **3.3b** (0.37 mmol). The product was purified by flash column chromatography (SiO<sub>2</sub>, CH<sub>2</sub>Cl<sub>2</sub>/CH<sub>3</sub>OH, 99.5:0.5) to give a white amorphous solid (40 mg, 32% yield). <sup>1</sup>H NMR (600 MHz, DMSO-*d*<sub>6</sub>) δ 7.48 (dd, *J* = 8.3, 5.5 Hz, 2H), 7.27 (d, *J* = 8.2 Hz, 2H), 7.21 (dd, *J* = 9.3, 8.9 Hz, 2H), 7.16 (dd, *J* = 1.9 Hz, 1H), 7.13 (dd, *J* = 7.7 Hz, 1H), 7.09 (d, *J* = 7.6 Hz, 1H), 6.96 (d, *J* = 8.7 Hz, 2H), 6.82 – 6.60 (m, 1H), 6.44 (t, *J* = 6.0 Hz, 1H), 5.04 (s, 2H), 4.21 (d, *J* = 5.8 Hz, 2H). <sup>13</sup>C NMR (151 MHz, DMSO-*d*<sub>6</sub>) δ 167.8, 161.7 (d, *J* = 243.5 Hz), 157.1, 148.7, 133.4 (d, *J* = 3.1 Hz), 131.9, 131.4, 129.8 (d, *J* = 8.4 Hz, 2C), 128.8, 128.3 (2C), 116.6, 116.3, 115.2 (d, *J* = 21.3 Hz, 2C), 114.6 (2C), 112.9, 68.4, 45.7. TOFMSESI m/z: 352.1357 (C<sub>21</sub>H<sub>18</sub>FNO<sub>3</sub> + H<sup>+</sup> requires 352.1304).

4-((4-((4-fluorobenzyl)oxy)benzyl)amino)benzoic acid (**3.4b\***): Reaction scale: 50 mg (0.36 mmol) of 4-amino benzoic acid. Compound **3.4b\*** was prepared following General Procedure A with aldehyde **3.3b** (0.37 mmol). The product was purified by flash column chromatography (SiO<sub>2</sub>, CH<sub>2</sub>Cl<sub>2</sub>/CH<sub>3</sub>OH, 99.5:0.5) to give a white amorphous solid (60 mg, 52% yield). <sup>1</sup>H NMR (400 MHz, Methanol-*d*<sub>4</sub>) δ 7.75 (d, *J* = 8.8 Hz, 2H), 7.45 (dd, *J* = 8.5, 5.5 Hz, 2H), 7.27 (d, *J* = 8.5 Hz, 2H), 7.13 – 7.04 (m, 2H), 6.95 (d, *J* = 8.6 Hz, 2H), 6.59 (d, *J* = 8.8 Hz, 2H), 5.04 (s, 2H), 4.30 (s,

2H).  $^{13}\text{C}$  NMR (101 MHz, Methanol- $d_4$ )  $\delta$  170.8, 168.3 (d,  $J = 244.5$  Hz), 168.1, 166.5, 162.6, 159.3, 154.4, 133.0 (d,  $J = 3.2$  Hz), 132.6 (2C), 130.7, 130.6 (2C), 129.6 (d,  $J = 8.6$  Hz, 2C), 118.5, 116.3 (d,  $J = 21.6$  Hz, 2C), 116.0 (2C), 112.5 (2C), 70.3, 47.3. TOFMSESI  $m/z$ : 352.1357 ( $\text{C}_{21}\text{H}_{18}\text{FNO}_3 + \text{H}^+$  requires 352.1304).

3-((4-((4-chlorobenzyl)oxy)benzyl)amino)benzoic acid (**3.4c**): Reaction scale: 100 mg (0.73 mmol) of 3-amino benzoic acid. Compound **3.4c** was prepared following General Procedure A with aldehyde **3.3c** (0.74 mmol). The product was purified by flash column chromatography ( $\text{SiO}_2$ ,  $\text{CH}_2\text{Cl}_2/\text{CH}_3\text{OH}$ , 99.5:0.5) to give a white amorphous solid (203.3 mg, 76% yield).  $^1\text{H}$  NMR (400 MHz, Methanol- $d_4$ )  $\delta$  7.41 (d,  $J = 8.5$  Hz, 2H), 7.36 (d,  $J = 8.5$  Hz, 2H), 7.29 (d,  $J = 6.3$  Hz, 2H), 7.28 (s, 1H), 7.25 (dt,  $J = 7.6, 1.3$  Hz, 1H), 7.15 (t,  $J = 7.8$  Hz, 2H), 6.93 (d,  $J = 8.6$  Hz, 1H), 6.82 (ddd,  $J = 8.0, 2.5, 1.1$  Hz, 1H), 5.03 (s, 2H), 4.26 (s, 2H).  $^{13}\text{C}$  NMR (101 MHz, Methanol- $d_4$ )  $\delta$  169.3, 157.6, 148.8, 136.3, 133.1, 132.0, 131.0, 128.7 (2C), 128.5, 128.2 (2C), 128.1 (2C), 117.6, 117.0, 114.5 (2C), 113.2, 68.7, 46.5. TOFMSESI  $m/z$ : 366.0897 ( $\text{C}_{21}\text{H}_{18}\text{ClNO}_3 - \text{H}^+$  requires 366.0902).

3-((4-((4-bromobenzyl)oxy)benzyl)amino)benzoic acid (**3.4d**): Reaction scale: 50 mg (0.36 mmol) of 3-amino benzoic acid. Compound **3.4d** was prepared following General Procedure A with aldehyde **3.3d** (0.37 mmol). The product was purified by flash column chromatography ( $\text{SiO}_2$ ,  $\text{CH}_2\text{Cl}_2/\text{CH}_3\text{OH}$ , 99.5:0.5) to give a white amorphous solid (96 mg, 65% yield).  $^1\text{H}$  NMR (600 MHz, DMSO- $d_6$ )  $\delta$  12.68 (s, 1H), 7.57 (d,  $J = 8.5$  Hz, 2H), 7.39 (d,  $J = 8.0$  Hz, 2H), 7.27 (d,  $J = 8.2$  Hz, 2H), 7.18 (dd,  $J = 2.0$  Hz, 1H), 7.13 (dd,  $J = 7.6$  Hz, 1H), 7.10 (ddd,  $J = 7.5, 1.5$  Hz, 1H), 6.95 (d,  $J = 8.8$  Hz, 2H), 6.78 (ddd,  $J = 8.0, 1.8$  Hz, 1H), 6.44 (s, 1H), 5.05 (s, 2H), 4.21 (s, 2H).  $^{13}\text{C}$  NMR (151 MHz, DMSO- $d_6$ )  $\delta$  168.3, 157.4, 149.1, 137.1, 132.5, 131.9, 131.8 (2C), 130.2

(2C), 129.3, 128.8 (2C), 121.3, 117.1, 116.7, 115.1 (2C), 113.4, 68.8, 46.2. TOFMSESI m/z: 412.0512 (C<sub>21</sub>H<sub>18</sub>BrNO<sub>3</sub> + H<sup>+</sup> requires 412.0543).

3-((4-((4-iodobenzyl)oxy)benzyl)amino)benzoic acid (**3.4e**): Reaction scale: 100 mg (0.73 mmol) of 3-amino benzoic acid. Compound **3.4e** was prepared following General Procedure A with aldehyde **3.3e** (0.74 mmol). The product was purified by flash column chromatography (SiO<sub>2</sub>, CH<sub>2</sub>Cl<sub>2</sub>/CH<sub>3</sub>OH, 99.5:0.5) to give a white amorphous solid (210 mg, 80% yield). <sup>1</sup>H NMR (600 MHz, DMSO-*d*<sub>6</sub>) δ 7.74 (d, *J* = 8.3 Hz, 2H), 7.27 (d, *J* = 8.4 Hz, 2H), 7.24 (d, *J* = 8.0 Hz, 2H), 7.17 (dd, *J* = 1.9 Hz, 1H), 7.14 (dd, *J* = 7.7 Hz, 1H), 7.13 – 7.07 (m, 1H), 6.94 (d, *J* = 8.6 Hz, 2H), 6.78 (ddd, *J* = 8.3, 1.7 Hz, 1H), 5.03 (s, 2H), 4.20 (s, 2H). <sup>13</sup>C NMR (151 MHz, DMSO-*d*<sub>6</sub>) δ 167.7, 157.0, 148.6, 137.2 (2C), 137.0, 132.0, 131.2, 129.8 (2C), 128.8, 128.3 (2C), 116.7, 116.4, 114.6 (2C), 112.9, 93.7, 68.4, 45.7. TOFMSESI m/z: 460.0424 (C<sub>21</sub>H<sub>18</sub>INO<sub>3</sub> + H<sup>+</sup> requires 460.0404).

3-((4-((4-(trifluoromethyl)benzyl)oxy)benzyl)amino)benzoic acid (**3.4f**): Reaction scale: 100 mg (0.73 mmol) of 3-amino benzoic acid. Compound **3.4f** was prepared following General Procedure A with aldehyde **3.3f** (0.74 mmol). The product was purified by flash column chromatography (SiO<sub>2</sub>, CH<sub>2</sub>Cl<sub>2</sub>/CH<sub>3</sub>OH, 99.5:0.5) to give a white amorphous solid (170 mg, 58% yield). <sup>1</sup>H NMR (600 MHz, DMSO-*d*<sub>6</sub>) δ 12.60 (s, 1H), 7.75 (d, *J* = 8.1 Hz, 2H), 7.65 (d, *J* = 8.1 Hz, 2H), 7.28 (d, *J* = 8.7 Hz, 2H), 7.16 (dd, *J* = 2.6, 1.9 Hz, 1H), 7.13 (dd, *J* = 8.5, 7.7 Hz, 1H), 7.09 (ddd, *J* = 7.6, 1.6 Hz, 1H), 6.98 (d, *J* = 8.7 Hz, 2H), 6.78 (ddd, *J* = 8.1, 2.6, 1.2 Hz, 1H), 6.45 (t, *J* = 6.0 Hz, 1H), 5.20 (s, 2H), 4.21 (d, *J* = 5.8 Hz, 2H). <sup>13</sup>C NMR (151 MHz, DMSO-*d*<sub>6</sub>) δ 167.8, 156.9, 148.7, 142.1, 132.1, 131.3, 128.8, 128.4 (2C), 128.2 (q, *J* = 29.2, 30.8, 33.0 Hz), 127.9 (2C), 125.3 (q, *J* = 3.6 Hz, 2C), 124.2 (q, *J* = 271.2, 271.8, 272.3 Hz), 116.6, 116.3, 114.6 (2C), 112.8, 68.2, 45.7. TOFMSESI m/z: 400.1139 (C<sub>22</sub>H<sub>18</sub>F<sub>3</sub>NO<sub>3</sub> - H<sup>+</sup> requires 400.1166).

3-((4-((4-cyanobenzyl)oxy)benzyl)amino)benzoic acid (**3.4g**): Reaction scale: 100 mg (0.73 mmol) of 3-amino benzoic acid. Compound **3.4g** was prepared following General Procedure A with aldehyde **3.3g** (0.74 mmol). The product was purified by flash column chromatography (SiO<sub>2</sub>, CH<sub>2</sub>Cl<sub>2</sub>/CH<sub>3</sub>OH, 99.5:0.5) to give a white amorphous solid (110 mg, 42% yield). <sup>1</sup>H NMR (600 MHz, DMSO-*d*<sub>6</sub>) δ 12.63 (s, 1H), 7.84 (d, *J* = 8.2 Hz, 2H), 7.62 (d, *J* = 7.9 Hz, 2H), 7.28 (d, *J* = 8.3 Hz, 2H), 7.19 (dd, *J* = 2.0 Hz, 1H), 7.14 (dd, *J* = 7.7 Hz, 1H), 7.12 (d, *J* = 8.7 Hz, 1H), 7.00 – 6.90 (m, 2H), 6.79 (dt, *J* = 7.8, 2.0 Hz, 1H), 6.45 (s, 1H), 5.18 (s, 2H), 4.22 (s, 2H). <sup>13</sup>C NMR (151 MHz, DMSO-*d*<sub>6</sub>) δ 167.9, 156.8, 148.7, 143.0, 132.4 (2C), 132.2, 131.3, 128.9, 128.4 (2C), 128.0 (2C), 118.8, 116.7, 116.4, 114.7 (2C), 112.9, 110.4, 68.2, 45.8. TOFMSESI *m/z*: 359.1406 (C<sub>22</sub>H<sub>18</sub>N<sub>2</sub>O<sub>3</sub> + H<sup>+</sup> requires 359.1390).

3-((4-((2-fluorobenzyl)oxy)benzyl)amino)benzoic acid (**3.4h**): Reaction scale: 50 mg (0.36 mmol) of 3-amino benzoic acid. Compound **3.4h** was prepared following General Procedure A with aldehyde **3.3h** (0.37 mmol). The product was purified by flash column chromatography (SiO<sub>2</sub>, CH<sub>2</sub>Cl<sub>2</sub>/CH<sub>3</sub>OH, 99.5:0.5) to give a white amorphous solid (122 mg, 97% yield). <sup>1</sup>H NMR (600 MHz, DMSO-*d*<sub>6</sub>) δ 12.60 (s, 1H), 7.54 (t, *J* = 7.4 Hz, 1H), 7.41 (q, *J* = 6.4 Hz, 1H), 7.29 (d, *J* = 8.2 Hz, 2H), 7.24 (d, *J* = 10.1 Hz, 1H), 7.22 (d, *J* = 7.4 Hz, 1H), 7.18 (s, 1H), 7.14 (t, *J* = 7.7 Hz, 1H), 7.10 (d, *J* = 7.6 Hz, 1H), 6.98 (d, *J* = 8.5 Hz, 2H), 6.79 (d, *J* = 7.8 Hz, 1H), 6.44 (s, 1H), 5.10 (s, 2H), 4.22 (d, *J* = 4.4 Hz, 2H). <sup>13</sup>C NMR (151 MHz, DMSO-*d*<sub>6</sub>) δ 167.8, 160.4 (d, *J* = 245.9 Hz), 157.1, 148.7, 132.1, 131.3, 130.6 (d, *J* = 4.1 Hz), 130.3 (d, *J* = 8.3 Hz), 128.9, 128.4 (2C), 124.5 (d, *J* = 3.5 Hz), 123.9 (d, *J* = 14.7 Hz), 116.7, 116.3, 115.4 (d, *J* = 21.1 Hz), 114.6 (2C), 112.9, 63.5 (d, *J* = 3.4 Hz), 45.8. TOFMSESI *m/z*: 374.1169 (C<sub>21</sub>H<sub>18</sub>FNO<sub>3</sub> + Na<sup>+</sup> requires 374.1163).

3-((4-((3-fluorobenzyl)oxy)benzyl)amino)benzoic acid (**3.4i**): Reaction scale: 50 mg (0.36 mmol) of 3-amino benzoic acid. Compound **3.4i** was prepared following General Procedure A with



aldehyde **3.3i** (0.37 mmol). The product was purified by flash column chromatography (SiO<sub>2</sub>, CH<sub>2</sub>Cl<sub>2</sub>/CH<sub>3</sub>OH, 99.5:0.5) to give a white amorphous solid (96 mg, 65% yield). <sup>1</sup>H NMR (600 MHz, DMSO-*d*<sub>6</sub>) δ 12.61 (s, 1H), 7.46 – 7.38 (m, 1H), 7.29 – 7.28 (m, 2H), 7.28 – 7.27 (m, 1H), 7.26 – 7.24 (m, 1H), 7.20 – 7.17 (m, 1H), 7.16 – 7.14 (m, 1H), 7.14 – 7.12 (m, 1H), 7.13 – 7.08 (m, 1H), 6.99 – 6.95 (m, 2H), 6.81 – 6.75 (m, 1H), 6.44 (t, *J* = 5.8 Hz, 1H), 5.10 (s, 2H), 4.21 (d, *J* = 4.4 Hz, 2H). <sup>13</sup>C NMR (101 MHz, DMSO-*d*<sub>6</sub>) δ 167.8, 162.2 (d, *J* = 243.5 Hz), 157.0, 148.7, 140.2 (d, *J* = 7.3 Hz), 132.0, 131.3, 130.4 (d, *J* = 8.3 Hz), 128.9, 128.4 (2C), 123.4 (d, *J* = 2.8 Hz), 116.7, 116.4, 114.7 (2C), 114.5 (d, *J* = 20.9 Hz), 114.1 (d, *J* = 21.9 Hz), 112.9, 68.3, 45.8. TOFMSESI *m/z*: 352.1360 (C<sub>21</sub>H<sub>18</sub>FNO<sub>3</sub> + H<sup>+</sup> requires 352.1343).

3-(((4-((2,4-difluorobenzyl)oxy)benzyl)amino)benzoic acid (**3.4j**): Reaction scale: 50 mg (0.36 mmol) of 3-amino benzoic acid. Compound **4j** was prepared following General Procedure A with aldehyde **3j** (0.37 mmol). The product was purified by flash column chromatography (SiO<sub>2</sub>, CH<sub>2</sub>Cl<sub>2</sub>/CH<sub>3</sub>OH, 99.5:0.5) to give a white amorphous solid (100 mg, 70% yield). <sup>1</sup>H NMR (600 MHz, DMSO-*d*<sub>6</sub>) δ 12.62 (s, 1H), 7.60 (ddd, *J* = 8.6, 6.7 Hz, 1H), 7.32 – 7.27 (m, 1H), 7.29 – 7.26 (m, 2H), 7.17 (dd, *J* = 1.9 Hz, 1H), 7.14 (d, *J* = 7.7 Hz, 1H), 7.13 – 7.11 (m, 1H), 7.10 – 7.09 (m, 1H), 6.98 (d, *J* = 8.6 Hz, 2H), 6.83 – 6.73 (m, 1H), 6.46 (t, *J* = 6.3 Hz, 1H), 5.07 (s, 2H), 4.22 (d, *J* = 4.7 Hz, 2H). <sup>13</sup>C NMR (151 MHz, DMSO-*d*<sub>6</sub>) δ 167.8, 161.4 (dd, *J* = 4.0, 12.6 Hz), 161.4 (dd, *J* = 12.1, 499.9 Hz), 157.0, 148.7, 132.2, 132.1 (dd, *J* = 5.7, 10.1 Hz), 131.3, 128.8, 128.4 (2C), 120.4 (dd, *J* = 3.4, 14.4 Hz), 116.7, 116.3, 114.6 (2C), 112.9, 111.5 (dd, *J* = 3.8, 21.3 Hz), 104.0 (t, *J* = 25.8 Hz), 63.1 (d, *J* = 2.9 Hz), 45.7. TOFMSESI *m/z*: 392.1085 (C<sub>21</sub>H<sub>17</sub>F<sub>2</sub>NO<sub>3</sub> + Na<sup>+</sup> requires 392.1069).

3-(((4-((3,4-difluorobenzyl)oxy)benzyl)amino)benzoic acid (**3.4k**): Reaction scale: 50 mg (0.36 mmol) of 3-amino benzoic acid. Compound **3.4k** was prepared following General Procedure A

with aldehyde **3.3k** (0.37 mmol). The product was purified by flash column chromatography (SiO<sub>2</sub>, CH<sub>2</sub>Cl<sub>2</sub>/CH<sub>3</sub>OH, 99.5:0.5) to give a white amorphous solid (106 mg, 79% yield). <sup>1</sup>H NMR (600 MHz, DMSO-*d*<sub>6</sub>) δ 12.61 (s, 1H), 7.51 (ddd, *J* = 11.6, 7.8, 2.0 Hz, 1H), 7.44 (ddd, *J* = 10.8, 8.4 Hz, 1H), 7.30 (d, *J* = 4.0 Hz, 1H), 7.27 (d, *J* = 8.4 Hz, 2H), 7.16 (dd, *J* = 1.9 Hz, 1H), 7.13 (dd, *J* = 7.7 Hz, 1H), 7.09 (ddd, *J* = 7.6, 1.3 Hz, 1H), 6.96 (d, *J* = 8.7 Hz, 2H), 6.77 (ddd, *J* = 8.0, 2.6, 1.2 Hz, 1H), 6.45 (t, *J* = 6.1 Hz, 1H), 5.06 (s, 2H), 4.21 (d, *J* = 5.7 Hz, 2H). <sup>13</sup>C NMR (151 MHz, DMSO-*d*<sub>6</sub>) δ 167.8, 156.9, 149.3 (dd, *J* = 12.7, 245.6 Hz), 148.9 (dd, *J* = 12.4, 245.3 Hz), 148.7, 135.0 (dd, *J* = 3.6, 5.8 Hz), 132.1, 131.3, 128.8, 128.3 (2C), 124.4 (dd, *J* = 3.5, 6.5 Hz), 117.5 (d, *J* = 17.1 Hz), 116.7 (d, *J* = 17.5 Hz), 116.6, 116.3, 114.6 (2C), 112.9, 67.8, 45.7. TOFMSESI *m/z*: 370.1238 (C<sub>21</sub>H<sub>17</sub>F<sub>2</sub>NO<sub>3</sub> + H<sup>+</sup> requires 370.1249).

3-((4-((3,5-difluorobenzyl)oxy)benzyl)amino)benzoic acid (**3.4l**): Reaction scale: 100 mg (0.73 mmol) of 3-amino benzoic acid. Compound **3.4l** was prepared following General Procedure A with aldehyde **3.3l** (0.74 mmol). The product was purified by flash column chromatography (SiO<sub>2</sub>, CH<sub>2</sub>Cl<sub>2</sub>/CH<sub>3</sub>OH, 99.5:0.5) to give a white amorphous solid (196 mg, 73% yield). <sup>1</sup>H NMR (600 MHz, DMSO-*d*<sub>6</sub>) δ 12.61 (s, 1H), 7.28 (d, *J* = 8.3 Hz, 2H), 7.19 (dd, *J* = 2.4, 9.1 Hz, 1H), 7.17 (dd, *J* = 1.8 Hz, 2H), 7.15 (d, *J* = 3.7 Hz, 1H), 7.13 (d, *J* = 7.7 Hz, 1H), 7.10 (ddd, *J* = 1.4, 7.6 Hz, 1H), 6.97 (d, *J* = 8.6 Hz, 2H), 6.78 (ddd, *J* = 1.2, 2.5, 8.0 Hz, 1H), 6.45 (t, *J* = 5.8 Hz, 1H), 5.11 (s, 2H), 4.22 (d, *J* = 5.1 Hz, 2H). <sup>13</sup>C NMR (151 MHz, DMSO-*d*<sub>6</sub>) δ 167.8, 162.4 (dd, *J* = 13.0, 246.5 Hz, 2C), 156.7, 148.7, 141.9 (t, *J* = 9.2 Hz), 132.2, 131.3, 128.8, 128.4 (2C), 116.7, 116.3, 114.7 (2C), 112.9, 110.3 (dd, *J* = 5.2, 20.3 Hz, 2C), 103.0 (t, *J* = 25.8 Hz), 67.8, 45.7. TOFMSESI *m/z*: 368.1120 (C<sub>21</sub>H<sub>17</sub>F<sub>2</sub>NO<sub>3</sub> - H<sup>+</sup> requires 368.1104).

3-((4-phenethoxybenzyl)amino)benzoic acid (**3.4m**): Reaction scale: 50 mg (0.36 mmol) of 3-amino benzoic acid. Compound **3.4m** was prepared following General Procedure A with aldehyde

**3.8a** (0.37 mmol). The product was purified by flash column chromatography (SiO<sub>2</sub>, CH<sub>2</sub>Cl<sub>2</sub>/CH<sub>3</sub>OH, 99.5:0.5) to give a white amorphous solid (121 mg, 96% yield). <sup>1</sup>H NMR (600 MHz, Methanol-*d*<sub>4</sub>) δ 7.39 (s, 1H), 7.28 (t, *J* = 2.0 Hz, 1H), 7.27 (s, 2H), 7.26 (d, *J* = 3.5 Hz, 2H), 7.24 (s, 2H), 7.19 (h, *J* = 4.1 Hz, 1H), 7.14 (t, *J* = 7.8 Hz, 1H), 6.84 (d, *J* = 8.6 Hz, 2H), 6.81 (dd, *J* = 1.9, 8.4 Hz, 1H), 4.23 (s, 2H), 4.13 (t, *J* = 6.9 Hz, 2H), 3.02 (t, *J* = 6.9 Hz, 2H). <sup>13</sup>C NMR (151 MHz, Methanol-*d*<sub>4</sub>) δ 169.3, 157.9, 148.8, 138.5, 131.6, 131.1, 128.6 (2C), 128.5, 128.2 (2C), 128.0 (2C), 125.9 (2C), 117.6, 117.0, 114.2, 113.3, 68.5, 46.7, 35.3. TOFMSESI *m/z*: 346.1443 (C<sub>22</sub>H<sub>21</sub>NO<sub>3</sub> - H<sup>+</sup> requires 346.1449).

3-((4-(4-methoxyphenoxy)benzyl)amino)benzoic acid (**3.4n**): Reaction scale: 50 mg (0.36 mmol) of 3-amino benzoic acid. Compound **3.4n** was prepared following General Procedure A with aldehyde **3.8b** (0.37 mmol). The product was purified by flash column chromatography (SiO<sub>2</sub>, CH<sub>2</sub>Cl<sub>2</sub>/CH<sub>3</sub>OH, 99.5:0.5) to give a white amorphous solid (130 mg, 96% yield). <sup>1</sup>H NMR (600 MHz, Methanol-*d*<sub>4</sub>) δ 7.28 (d, *J* = 2.2 Hz, 1H), 7.25 (d, *J* = 8.1 Hz, 2H), 7.25 (s, 1H), 7.18 (d, *J* = 8.2 Hz, 2H), 7.14 (t, *J* = 7.8 Hz, 1H), 6.84 (d, *J* = 8.8 Hz, 2H), 6.83 (d, *J* = 8.7 Hz, 2H), 6.83 – 6.78 (m, 1H), 4.24 (s, 2H), 4.09 (t, *J* = 6.9 Hz, 2H), 3.75 (s, 3H), 2.96 (t, *J* = 6.9 Hz, 2H). <sup>13</sup>C NMR (151 MHz, Methanol-*d*<sub>4</sub>) δ 170.7, 159.8, 159.4, 150.3, 133.0, 132.5, 131.8, 130.9 (2C), 129.9, 129.6 (2C), 119.0, 118.4, 115.7 (2C), 114.9 (2C), 114.8, 70.1, 55.7, 48.1, 35.9. TOFMSESI *m/z*: 378.1709 (C<sub>23</sub>H<sub>23</sub>NO<sub>4</sub> + H<sup>+</sup> requires 378.1700).

3-((4-(4-methoxyphenoxy)phenethyl)amino)benzoic acid (**3.4o**): 3-amino benzoic acid (50 mg, 0.36 mmol) and compound **3.10** (113 mg, 0.37 mmol) were dissolved in DMF. Triethylamine (102 μL, 0.72 mmol) was added at 25 °C and the reaction was stirred for 12 h upon which the reaction was deemed complete by TLC. The reaction was quenched with aq. 1N HCl (3 mL). The solution was diluted with EtOAc (30 mL). The organic layer was washed with water (3 × 20 mL) and brine

(3 × 20 mL). The organic layer was dried over Na<sub>2</sub>SO<sub>4</sub>, filtered, and concentrated under vacuum. The product was purified by flash column chromatography (SiO<sub>2</sub>, CH<sub>2</sub>Cl<sub>2</sub>/CH<sub>3</sub>OH, 99.5:0.5) to give a white amorphous solid (36 mg, 25% yield). <sup>1</sup>H NMR (500 MHz, Methanol-*d*<sub>4</sub>) δ 7.36 – 7.29 (m, 1H), 7.27 (ddd, *J* = 7.7, 1.6, 1.1 Hz, 1H), 7.19 (d, *J* = 6.6 Hz, 2H), 7.17 (d, *J* = 6.7 Hz, 2H), 7.14 (d, *J* = 7.7 Hz, 1H), 6.90 (ddd, *J* = 8.0, 2.4, 1.1 Hz, 1H), 6.84 (t, *J* = 2.0 Hz, 2H), 6.83 (t, *J* = 2.1 Hz, 2H), 4.41 (t, *J* = 6.9 Hz, 2H), 4.09 (t, *J* = 6.9 Hz, 2H), 3.75 (s, 3H), 2.97 (t, *J* = 7.0 Hz, 2H), 2.96 (t, *J* = 6.9 Hz, 2H). <sup>13</sup>C NMR (126 MHz, Methanol-*d*<sub>4</sub>) δ 168.5, 159.8, 159.1, 149.3, 132.2, 131.8, 131.4, 131.0 (2C), 130.9 (2C), 130.1, 120.8, 119.8, 116.7, 115.7 (2C), 114.8 (2C), 70.1, 66.8, 55.6, 35.9, 35.3. TOFMSESI *m/z*: 392.1870 (C<sub>24</sub>H<sub>25</sub>NO<sub>4</sub> + H<sup>+</sup> requires 392.1856).

2-fluoro-5-((4-((4-fluorobenzyl)oxy)benzyl)amino)benzoic acid (**3.4p**): Reaction scale: 50 mg (0.32 mmol) of 5-amino-2-fluorobenzoic acid (**3.11a**). Compound **3.4p** was prepared following the General Procedure A with aldehyde **3.3b** (0.33 mmol). The product was purified by flash column chromatography (SiO<sub>2</sub>, CH<sub>2</sub>Cl<sub>2</sub>/CH<sub>3</sub>OH, 99.5:0.5) to give a white amorphous solid (98 mg, 82% yield). <sup>1</sup>H NMR (600 MHz, DMSO-*d*<sub>6</sub>) δ 7.48 (dd, *J* = 8.5, 5.7 Hz, 2H), 7.26 (d, *J* = 8.4 Hz, 2H), 7.21 (t, *J* = 8.9 Hz, 1H), 7.01 – 6.97 (m, 1H), 7.00 – 6.93 (m, 3H), 6.75 (dt, *J* = 8.8, 3.5 Hz, 1H), 6.31 (s, 1H), 5.05 (s, 2H), 4.17 (s, 2H). <sup>13</sup>C NMR (151 MHz, DMSO-*d*<sub>6</sub>) δ 165.6, 161.7 (d, *J* = 243.5 Hz), 157.1, 152.9 (d, *J* = 244.7 Hz), 144.9, 133.4, 131.8, 129.9 (d, *J* = 8.2 Hz, 2C), 128.4 (2C), 117.3 (d, *J* = 7.4 Hz), 116.9 (d, *J* = 23.3 Hz, 2C), 115.3, 115.1, 114.7 (2C), 113.7, 68.4, 46.2. TOFMSESI *m/z*: 368.1093 (C<sub>21</sub>H<sub>17</sub>F<sub>2</sub>NO<sub>3</sub> - H<sup>+</sup> requires 368.1104).

3-fluoro-5-((4-((4-fluorobenzyl)oxy)benzyl)amino)benzoic acid (**3.4q**): Reaction scale: 50 mg (0.32 mmol) of 3-amino-5-fluorobenzoic acid (**3.11b**). Compound **3.4q** was prepared following the General Procedure A with aldehyde **3.3b** (0.33 mmol). The product was purified by flash column chromatography (SiO<sub>2</sub>, CH<sub>2</sub>Cl<sub>2</sub>/CH<sub>3</sub>OH, 99.5:0.5) to give a white amorphous solid (102

mg, 86% yield).  $^1\text{H}$  NMR (400 MHz, Methanol- $d_4$ )  $\delta$  7.45 – 7.37 (m, 2H), 7.26 (d,  $J = 8.4$  Hz, 2H), 7.11 (t,  $J = 1.8$  Hz, 1H), 7.10 – 7.00 (m, 2H), 6.96 – 6.89 (m, 2H), 6.87 (dt,  $J = 9.1, 1.9$  Hz, 1H), 6.47 (dt,  $J = 11.4, 2.3$  Hz, 1H), 4.98 (s, 2H), 4.22 (s, 2H).  $^{13}\text{C}$  NMR (101 MHz, Methanol- $d_4$ )  $\delta$  169.4 (d,  $J = 3.3$  Hz), 165.1 (d,  $J = 241.1$  Hz), 163.8 (d,  $J = 244.7$  Hz), 159.2, 152.0 (d,  $J = 11.1$  Hz), 134.8 (d,  $J = 3.2$  Hz), 134.1 (d,  $J = 9.9$  Hz), 132.8, 130.6 (d,  $J = 8.1$  Hz, 2C), 129.6 (2C), 116.2, 116.0 (2C), 111.1 (d,  $J = 2.0$  Hz), 104.5 (d,  $J = 24.0$  Hz, 2C), 103.9 (d,  $J = 26.0$  Hz), 70.3, 47.8. TOFMSESI  $m/z$ : 368.1096 ( $\text{C}_{21}\text{H}_{17}\text{F}_2\text{NO}_3 - \text{H}^+$  requires 368.1104).

3-chloro-5-((4-((4-fluorobenzyl)oxy)benzyl)amino)benzoic acid (**3.4r**): Reaction scale: 50 mg (0.29 mmol) of 3-amino-5-chlorobenzoic acid (**3.11c**). Compound **3.4r** was prepared following the General Procedure A with aldehyde **3.3b** (0.30 mmol). The product was purified by flash column chromatography ( $\text{SiO}_2$ ,  $\text{CH}_2\text{Cl}_2/\text{CH}_3\text{OH}$ , 99.5:0.5) to give a white amorphous solid (88 mg, 78% yield).  $^1\text{H}$  NMR (500 MHz, Methanol- $d_4$ )  $\delta$  7.42 (dd,  $J = 8.4, 5.4$  Hz, 2H), 7.26 (d,  $J = 8.3$  Hz, 2H), 7.17 (dt,  $J = 16.7, 1.7$  Hz, 2H), 7.07 (t,  $J = 8.8$  Hz, 2H), 6.93 (d,  $J = 8.5$  Hz, 2H), 6.75 (t,  $J = 2.1$  Hz, 1H), 5.00 (s, 2H), 4.23 (s, 2H).  $^{13}\text{C}$  NMR (101 MHz, DMSO- $d_6$ )  $\delta$  166.6, 161.7 (d,  $J = 243.5$  Hz), 157.2, 150.1, 133.7, 133.3 (d,  $J = 3.0$  Hz), 133.0, 131.3, 129.9, 129.8, 128.4 (2C), 115.5, 115.3, 115.1, 114.8, 114.7 (2C), 112.0, 68.5, 45.6. TOFMSESI  $m/z$ : 384.0812 ( $\text{C}_{21}\text{H}_{17}\text{ClFNO}_3 - \text{H}^+$  requires 384.0808).

3-bromo-5-((4-((4-fluorobenzyl)oxy)benzyl)amino)benzoic acid (**3.4s**): Reaction scale: 50 mg (0.23 mmol) of 3-amino-5-bromobenzoic acid (**3.11d**). Compound **3.4s** was prepared following the General Procedure A with aldehyde **3.3b** (0.23 mmol). The product was purified by flash column chromatography ( $\text{SiO}_2$ ,  $\text{CH}_2\text{Cl}_2/\text{CH}_3\text{OH}$ , 99.5:0.5) to give a pale amorphous solid (85 mg, 86% yield).  $^1\text{H}$  NMR (400 MHz, Methanol- $d_4$ )  $\delta$  7.42 (dd,  $J = 8.5, 5.4$  Hz, 2H), 7.29 (d,  $J = 1.7$  Hz, 1H), 7.26 (d,  $J = 8.3$  Hz, 2H), 7.21 (t,  $J = 1.8$  Hz, 1H), 7.07 (t,  $J = 8.8$  Hz, 2H), 6.93 (d,  $J =$

8.4 Hz, 2H), 6.91 (t,  $J = 2.1$  Hz, 1H), 5.00 (s, 2H), 4.23 (s, 2H).  $^{13}\text{C}$  NMR (101 MHz, Methanol- $d_4$ )  $\delta$  169.1, 165.0, 161.9 (d,  $J = 146.3$  Hz), 159.3, 151.5, 134.8, 134.2, 132.7, 130.6 (d,  $J = 8.2$  Hz), 129.6 (2C), 123.7, 120.9, 119.9, 116.2, 116.04, 116.01 (2C), 113.6, 70.29, 47.67. TOFMSESI  $m/z$ : 428.0295 ( $\text{C}_{21}\text{H}_{17}\text{BrFNO}_3 - \text{H}^+$  requires 428.0303).

3-((4-((4-fluorobenzyl)oxy)-2-methylbenzyl)amino)benzoic acid (**3.4t**): Reaction scale: 50 mg (0.36 mmol) of 3-amino benzoic acid. Compound **3.4t** was prepared following General Procedure A with aldehyde **3.12a** (0.37 mmol). The product was purified by flash column chromatography ( $\text{SiO}_2$ ,  $\text{CH}_2\text{Cl}_2/\text{CH}_3\text{OH}$ , 99.5:0.5) to give a white amorphous solid (100 mg, 70% yield).  $^1\text{H}$  NMR (400 MHz,  $\text{DMSO}-d_6$ )  $\delta$  12.53 (s, 1H), 7.48 (dd,  $J = 8.5, 5.7$  Hz, 2H), 7.25 – 7.16 (m, 2H), 7.18 (s, 1H), 7.17 (d,  $J = 4.0$  Hz, 1H), 7.14 (d,  $J = 7.6$  Hz, 1H), 7.11 (dt,  $J = 7.6, 1.5$  Hz, 1H), 6.86 (d,  $J = 2.6$  Hz, 1H), 6.79 (td,  $J = 8.6, 2.3$  Hz, 2H), 6.31 – 5.95 (m, 1H), 5.05 (s, 2H), 4.15 (d,  $J = 4.5$  Hz, 2H), 2.30 (s, 3H).  $^{13}\text{C}$  NMR (101 MHz,  $\text{DMSO}-d_6$ )  $\delta$  167.7, 157.1, 148.8, 148.1 (d,  $J = 330.2$  Hz), 137.3, 133.4 (d,  $J = 2.9$  Hz), 131.3, 129.7, 129.6, 129.4, 128.7 (d,  $J = 7.3$  Hz, 2C), 116.7, 116.5, 116.1, 115.1 (d,  $J = 21.4$  Hz, 2C), 112.5, 111.6, 68.3, 44.2, 18.7. TOFMSESI  $m/z$ : 364.1360 ( $\text{C}_{22}\text{H}_{20}\text{FNO}_3 - \text{H}^+$  requires 364.1354).

3-((4-((4-fluorobenzyl)oxy)-3-methylbenzyl)amino)benzoic acid (**4u**): Reaction scale: 100 mg (0.72 mmol) of 3-amino benzoic acid. Compound **4u** was prepared following General Procedure A with aldehyde **12b** (0.73 mmol). The product was purified by flash column chromatography ( $\text{SiO}_2$ ,  $\text{CH}_2\text{Cl}_2/\text{CH}_3\text{OH}$ , 99.5:0.5) to give a white amorphous solid (200 mg, 75% yield).  $^1\text{H}$  NMR (600 MHz,  $\text{DMSO}-d_6$ )  $\delta$  7.49 (dd,  $J = 8.5, 5.7$  Hz, 2H), 7.21 (dd,  $J = 8.9$  Hz, 2H), 7.17 (dd,  $J = 2.0$  Hz, 1H), 7.15 (d,  $J = 2.4$  Hz, 1H), 7.14 (s, 1H), 7.11 (s, 1H), 7.10 (ddd,  $J = 7.5, 1.4$  Hz, 1H), 6.95 (d,  $J = 8.3$  Hz, 1H), 6.82 – 6.67 (m, 1H), 5.06 (s, 2H), 4.17 (s, 2H), 2.16 (s, 3H).  $^{13}\text{C}$  NMR (151 MHz,  $\text{DMSO}-d_6$ )  $\delta$  167.7, 161.6 (d,  $J = 243.3$  Hz), 155.1, 148.7, 133.7 (d,  $J = 2.9$  Hz), 131.5,

131.2, 129.5, 129.4 (d,  $J = 8.2$  Hz, 2C), 128.8, 125.8, 125.6, 116.6, 116.3, 115.2 (d,  $J = 21.3$  Hz, 2C), 112.8, 111.6, 68.5, 45.8, 16.2. TOFMSESI  $m/z$ : 388.1328 ( $C_{22}H_{20}FNO_3 + Na^+$  requires 388.1319).

3-(((4-((4-fluorobenzyl)oxy)benzyl)amino)-4-methylbenzoic acid (**3.4v**): Reaction scale: 50 mg (0.33 mmol) of 3-amino-4-methylbenzoic acid. Compound **3.4v** was prepared following the General Procedure A with aldehyde **3.3b** (0.34 mmol). The product was purified by flash column chromatography ( $SiO_2$ ,  $CH_2Cl_2/CH_3OH$ , 99.5:0.5) to give a white amorphous solid (111 mg, 92% yield).  $^1H$  NMR (600 MHz, Methanol- $d_4$ )  $\delta$  7.44 (t,  $J = 6.7$  Hz, 2H), 7.31 (d,  $J = 8.1$  Hz, 2H), 7.26 (s, 1H), 7.21 (d,  $J = 7.8$  Hz, 1H), 7.08 (t,  $J = 8.6$  Hz, 2H), 7.01 (d,  $J = 7.7$  Hz, 1H), 6.95 – 6.91 (m, 2H), 5.02 (s, 2H), 4.36 (s, 2H), 2.18 (s, 3H).  $^{13}C$  NMR (101 MHz, DMSO- $d_6$ )  $\delta$  168.4, 161.7 (d,  $J = 243.6$  Hz), 157.0, 145.9, 133.4 (d,  $J = 3.0$  Hz), 132.2, 129.9, 129.8, 129.4, 128.0 (2C), 127.9, 126.2, 117.1, 115.3, 115.0, 114.6 (2C), 114.4, 110.0, 68.4, 45.7, 17.8. TOFMSESI  $m/z$ : 364.1342 ( $C_{22}H_{20}FNO_3 - H^+$  requires 364.1354).

3-(((4-((4-fluorobenzyl)oxy)benzyl)(methyl)amino)benzoic acid (**3.4w**): Paraformaldehyde (5 mg, 0.16 mmol), compound **3.4b** (30 mg, 0.08 mmol), sodium triacetoxyborohydride (6.2 mg, 0.096 mmol) and 2 mL of ethanol were combined in a 10 mL of round bottom flask with a reflux condenser. The mixture was heated for 2 h at 100 °C and subsequently cooled to 25 ° for 12 h. The solvent was removed under vacuum and the residue was dissolved in EtOAc (60 mL). The organic layer was washed with aq. 1N HCl (20 mL), water (20 mL), and brine (20 mL). The organic layer was dried over  $Na_2SO_4$ , filtered, and concentrated under vacuum. The compound was purified by flash column chromatography ( $SiO_2$ ,  $CH_2Cl_2/CH_3OH$ , 99.5:0.5) to give a white amorphous solid **3.4w** (13 mg, 43% yield).  $^1H$  NMR (400 MHz, Methanol- $d_4$ )  $\delta$  7.4 (d,  $J = 5.5$  Hz, 1H), 7.4 – 7.4 (m, 2H), 7.3 (dt,  $J = 1.3, 7.6$  Hz, 1H), 7.2 (t,  $J = 7.9$  Hz, 1H), 7.1 (d,  $J = 8.6$  Hz, 2H), 7.1 (t,  $J =$

8.8 Hz, 2H), 7.0 (ddd,  $J = 1.1, 2.8, 8.3$  Hz, 1H), 6.9 (d,  $J = 8.7$  Hz, 2H), 5.0 (s, 2H), 4.5 (s, 2H), 3.0 (s, 3H).  $^{13}\text{C}$  NMR (101 MHz, Methanol- $d_4$ )  $\delta$  170.7, 163.8 (d,  $J = 244.4$  Hz), 159.2, 151.1, 134.8 (d,  $J = 3.3$  Hz), 132.4, 132.3, 130.6 (d,  $J = 8.3$  Hz, 2C), 130.0, 129.2 (2C), 118.8, 118.2, 116.1 (d,  $J = 21.7$  Hz, 2C), 116.0 (2C), 114.5, 70.3, 56.8, 38.9. TOFMSESI  $m/z$ : 388.1328 ( $\text{C}_{25}\text{H}_{26}\text{FNO}_4 + \text{H}$  requires 388.1319). TOFMSESI  $m/z$ : 366.1509 ( $\text{C}_{22}\text{H}_{20}\text{FNO}_3 + \text{H}^+$  requires 366.1500).

(R)-3-(((4-(1-(4-fluorophenyl)ethoxy)benzyl)amino)benzoic acid (**3.4x**): Compound **3.13** (53 mg, 0.15 mmol), (*S*)-1-(4-fluorophenyl)ethan-1-ol (21 mg, 0.15 mmol), and  $\text{PPh}_3$  (39 mg, 0.15 mmol) were dissolved in toluene (2.5 mL) and cooled to 0 °C. A solution of *Dt*BAD (35 mg, 0.15 mmol) in toluene (5 mL) was added dropwise to the mixture. The reaction was warmed to 25 °C and stirred at for 12 h, at which time the reaction was deemed complete by TLC. The solvent was removed under reduced pressure. The residue was purified by flash column chromatography ( $\text{SiO}_2$ , hexanes/ethyl acetate = 2: 1) to provide the desired product **3.14** as colorless oil. The resulting product **3.14** (50 mg, 0.114 mmol) was dissolved in a THF/MeOH/ $\text{H}_2\text{O}$  (3:1:1) mixture and  $\text{LiOH}\cdot\text{H}_2\text{O}$  (24 mg, 0.57 mmol) was added. The reaction stirred at 25 °C for 12 h upon which the reaction was deemed complete by TLC. The reaction was quenched with aq. 1N HCl (3 mL) and extracted with EtOAc ( $3 \times 10$  mL). The organic layers were combined dried over  $\text{Na}_2\text{SO}_4$ , filtered and concentrated by vacuum. The product **3.4x** was purified by flash column chromatography ( $\text{SiO}_2$ ,  $\text{CH}_2\text{Cl}_2/\text{CH}_3\text{OH}$ , 99.5:0.5) to give a white amorphous solid (25 mg, 65% yield).  $[\alpha]^{20}_{\text{D}} = +22.0$  ( $c = 9.1$  mg/mL,  $l = 0.5$  dm, MeOH).  $^1\text{H}$  NMR (400 MHz, Methanol- $d_4$ )  $\delta$  7.35 (dd,  $J = 8.6, 5.4$  Hz, 2H), 7.29 – 7.24 (m, 1H), 7.26 – 7.23 (m, 1H), 7.19 – 7.15 (m, 2H), 7.15 – 7.09 (m, 1H), 7.01 (t,  $J = 8.8$  Hz, 2H), 6.80 (d,  $J = 6.6$  Hz, 2H), 6.79 – 6.75 (m, 1H), 5.33 (q,  $J = 6.4$  Hz, 1H), 4.17 (s, 2H), 1.54 (d,  $J = 6.4$  Hz, 3H).  $^{13}\text{C}$  NMR (101 MHz, Methanol- $d_4$ )  $\delta$  170.7, 163.5 (d,  $J =$



243.8 Hz), 158.2, 150.2, 140.7 (d,  $J = 3.1$  Hz), 133.1, 132.4, 129.9, 129.5 (2C), 128.7 (d,  $J = 8.3$  Hz, 2C), 119.0, 118.4, 117.1 (2C), 116.1 (d,  $J = 21.7$  Hz, 2C), 114.7, 76.4, 48.0, 24.7. TOFMSESI  $m/z$ : 364.1363 ( $C_{22}H_{20}FNO_3 - H^+$  requires 364.1354).

(S)-3-((4-(1-(4-fluorophenyl)ethoxy)benzyl)amino)benzoic acid (**3.4y**): Compound **3.13** (60 mg, 0.17 mmol), (*R*)-1-(4-fluorophenyl)ethan-1-ol (24 mg, 0.17 mmol), and  $PPh_3$  (45 mg, 0.17 mmol) were dissolved in toluene (2.5 mL) and cooled to 0 °C. A solution of *Dt*BAD (39 mg, 0.17 mmol) in toluene (5 mL) was added dropwise to the mixture. The reaction was warmed to 25 °C and stirred at for 12 h, at which time the reaction was deemed complete by TLC. The solvent was removed under reduced pressure. The residue was purified by flash column chromatography ( $SiO_2$ , hexanes/ethyl acetate = 2: 1) to provide the desired product **3.15** as colorless oil. The resulting product **3.15** (24 mg, 0.05mmol) (23 mg, 0.049 mmol) was dissolved in a THF/MeOH/H<sub>2</sub>O (3:1:1) mixture and LiOH·H<sub>2</sub>O (10 mg, 0.25 mmol) was added. The reaction stirred at 25 °C for 12 h upon which the reaction was deemed complete by TLC. The reaction was quenched with aq. 1N HCl (3 mL) and extracted with EtOAc (3 × 10 mL). The organic layers were combined, dried over  $Na_2SO_4$ , filtered, and concentrated by vacuum. The product **3.4y** was purified by flash column chromatography ( $SiO_2$ ,  $CH_2Cl_2/CH_3OH$ , 99.5:0.5) to give a white amorphous solid (14 mg, 75% yield).  $[\alpha]_D^{20} = -22.0$  ( $c = 9.1$  mg/mL,  $l = 0.5$  dm, MeOH). <sup>1</sup>H NMR (600 MHz, Methanol-*d*<sub>4</sub>)  $\delta$  7.40 – 7.34 (m, 2H), 7.28 – 7.24 (m, 1H), 7.27 – 7.22 (m, 1H), 7.21 – 7.16 (m, 2H), 7.13 (t,  $J = 7.8$  Hz, 1H), 7.02 (t,  $J = 8.8$  Hz, 2H), 6.82 – 6.80 (m, 2H), 6.79 (ddd,  $J = 8.1, 2.5, 1.0$  Hz, 1H), 5.36 (q,  $J = 6.4$  Hz, 1H), 4.19 (s, 2H), 1.55 (d,  $J = 6.4$  Hz, 3H). <sup>13</sup>C NMR (151 MHz, Methanol-*d*<sub>4</sub>)  $\delta$  170.8, 163.7 (d,  $J = 243.9$  Hz), 158.3, 150.4, 140.9 (d,  $J = 2.9$  Hz), 133.3, 132.5, 130.0, 129.7 (2C), 128.8 (d,  $J = 8.4$  Hz, 2C), 119.2, 118.6, 117.3 (2C), 116.3 (d,  $J = 21.6$  Hz, 2C), 114.8, 76.5, 48.2, 24.8. TOFMSESI  $m/z$ : 364.1365 ( $C_{22}H_{20}FNO_3 - H^+$  requires 364.1354).

*4-((2-(4-fluorophenyl)propan-2-yl)oxy)benzaldehyde (3.17)*: To a solution of compound **3.16** (1.5 g, 8.2 mmol) in MeCN (10 mL) at 0 °C was added DBU (3.7 g, 24.6 mmol). TFAA (1.14 mL, 8.2 mmol) was added dropwise and the solution was stirred for 30 min. Then the mixture was added dropwise to a solution of compound **3.1** (1 g, 8.2 mmol) and CuCl<sub>2</sub>·H<sub>2</sub>O (1.4 mg, 0.0082 mmol) in MeCN (10 mL) over a period of 5 min at 0 °C. The mixture was allowed to warm to 25 °C and stir for 12 h. The solvent was removed under reduced pressure and the residue was diluted in DCM (40 mL). The organic layer was washed sequentially with aq. 1N HCl (2 × 20 mL), aq. 1N NaOH (2 × 20 mL), sat. aq. NaHCO<sub>3</sub> (2 × 20 mL), and brine (20 mL). The organic layer was dried over Na<sub>2</sub>SO<sub>4</sub>, filtered, and concentrated in vacuo. Compound **3.17** was purified by silica gel chromatography (SiO<sub>2</sub>, hexanes/ethyl acetate = 20:1) to provide the desired product as colorless oil. Yield: 8%. <sup>1</sup>H NMR (500 MHz, Chloroform-*d*) δ 9.81 (s, 1H), 7.68 – 7.62 (m, 2H), 7.44 – 7.36 (m, 2H), 7.10 – 7.01 (m, 2H), 6.78 – 6.69 (m, 2H), 1.78 (s, 6H). <sup>13</sup>C NMR (126 MHz, Chloroform-*d*) δ 190.9, 162.1 (d, *J* = 246.5 Hz), 161.6, 141.3 (d, *J* = 3.4 Hz), 131.4, 129.8, 126.9 (d, *J* = 8.0 Hz), 119.1, 115.7 (d, *J* = 21.4 Hz), 81.1, 29.8.

*3-(((4-((2-(4-fluorophenyl)propan-2-yl)oxy)benzyl)amino)benzoic acid (3.4z)*: Compound **3.4z** was prepared following the General Procedure A with aldehyde **3.17** (0.62 mmol). The desired product was purified by flash column chromatography (SiO<sub>2</sub>, CH<sub>2</sub>Cl<sub>2</sub>/CH<sub>3</sub>OH, 99.5:0.5) to give a white amorphous solid (60 mg, 25% yield). <sup>1</sup>H NMR (500 MHz, DMSO-*d*<sub>6</sub>) δ 8.4 (s, 1H) 7.53 – 7.45 (m, 2H), 7.22 – 7.13 (m, 2H), 7.14 (d, *J* = 2.3 Hz, 1H), 7.16 – 7.08 (m, 2H), 7.12 – 7.05 (m, 1H), 7.07 (s, 1H), 6.70 (dt, *J* = 6.2, 2.9 Hz, 1H), 6.62 – 6.55 (m, 2H), 6.26 (t, *J* = 5.9 Hz, 1H), 4.13 (d, *J* = 5.4 Hz, 2H), 1.63 (s, 6H). <sup>13</sup>C NMR (101 MHz, DMSO-*d*<sub>6</sub>) δ 168.4, 161.1 (d, *J* = 243.0 Hz), 154.1, 148.6, 142.3 (d, *J* = 3.1 Hz), 132.8, 128.5, 127.9 (2C), 127.3 (d, *J* = 8.0 Hz, 2C), 119.9 (2C),

116.8, 115.5, 115.0 (d,  $J = 21.0$  Hz, 2C), 112.9, 102.2, 79.4, 45.8, 29.1 (2C). TOFMSESI  $m/z$ : 402.1482 ( $C_{23}H_{22}FNO_3 + Na^+$  requires 402.1476).

2-(3-((4-((4-Methoxybenzyl)oxy)benzyl)amino)phenoxy)-2-methylpropanoic acid (**3.5a**):

Reaction scale: 99 mg (0.22 mmol) of ethyl 2-(3-((4-((4-methoxybenzyl)oxy)benzyl)amino)phenoxy)-2-methylpropanoate. Compound **3.5a** was prepared following General Procedure B. The product was purified by flash column chromatography ( $SiO_2$ ,  $CH_2Cl_2/CH_3OH$ , 100:1) to give a white amorphous solid (13 mg, 14% yield).  $^1H$  NMR (400 MHz, Methanol- $d_4$ )  $\delta$  7.34 (d,  $J = 8.6$  Hz, 2H), 7.25 (d,  $J = 8.5$  Hz, 2H), 6.93 (d,  $J = 2.8$  Hz, 1H), 6.92 (d,  $J = 3.1$  Hz, 2H), 6.90 (d,  $J = 3.1$  Hz, 2H), 6.34 – 6.26 (m, 1H), 6.19 (s, 1H), 6.16 (d,  $J = 8.6$  Hz, 1H), 4.97 (s, 2H), 4.18 (s, 2H), 3.79 (s, 3H), 1.47 (s, 6H).  $^{13}C$  NMR (101 MHz, Methanol- $d_4$ )  $\delta$  160.9, 159.3, 157.8, 151.1, 133.5, 130.8, 130.3 (2C), 130.2, 130.0, 129.6 (2C), 116.0 (2C), 114.8 (2C), 111.4, 109.2, 109.0, 105.6, 70.9, 55.7, 48.2, 25.8 (2C). HRESI  $m/z$ : 444.1771 ( $C_{25}H_{27}NO_5 + Na^+$  requires 444.1781).

2-(3-((4-((4-fluorobenzyl)oxy)benzyl)amino)phenoxy)-2-methylpropanoic acid (**3.5b**):

Reaction scale: 96 mg (0.22 mmol) of ethyl 2-(3-((4-((4-fluorobenzyl)oxy)benzyl)amino)phenoxy)-2-methylpropanoate. Compound **3.5b** was prepared following General Procedure B. The product was purified by flash column chromatography ( $SiO_2$ ,  $CH_2Cl_2/CH_3OH$ , 100:1) to give a white amorphous solid (19 mg, 21% yield).  $^1H$  NMR (600 MHz, Methanol- $d_4$ )  $\delta$  7.58 – 7.39 (m, 2H), 7.26 (d,  $J = 8.4$  Hz, 2H), 7.16 – 7.02 (m, 2H), 6.94 (d,  $J = 4.2$  Hz, 1H), 6.92 (dd,  $J = 8.4, 1.5$  Hz, 2H), 6.39 – 6.26 (m, 1H), 6.18 (t,  $J = 2.0$  Hz, 1H), 6.16 (dd,  $J = 8.0, 2.0$  Hz, 1H), 5.02 (s, 2H), 4.18 (s, 2H), 1.47 (s, 6H).  $^{13}C$  NMR (151 MHz, Methanol- $d_4$ )  $\delta$  168.9, 154.3 (d,  $J = 244.4$  Hz), 149.6, 148.3, 141.6, 125.4 (d,  $J = 3.4$  Hz), 124.2, 121.1 (d,  $J = 8.4$  Hz, 2C), 120.7, 120.1 (2C), 106.6 (d,

$J = 21.8$  Hz, 2C), 106.5 (2C), 99.8, 99.6, 96.2, 70.5, 60.8, 38.7, 16.3 (2C). TOFMSESI  $m/z$ : 410.1761 ( $C_{24}H_{24}FNO_4 + H^+$  requires 410.1762).

2-(4-((4-((4-fluorobenzyl)oxy)benzyl)amino)phenoxy)-2-methylpropanoic acid (**3.5b\***): Reaction scale: 96 mg (0.22 mmol) of ethyl 2-(4-((4-((4-fluorobenzyl)oxy)benzyl)amino)phenoxy)-2-methylpropanoate. Compound **3.5b\*** was prepared following General Procedure B. The product was purified by flash column chromatography ( $SiO_2$ ,  $CH_2Cl_2/CH_3OH$ , 100:1) to give a white amorphous solid (62 mg, 60% yield).  $^1H$  NMR (400 MHz,  $DMSO-d_6$ )  $\delta$  7.48 (dd,  $J = 8.3, 5.5$  Hz, 2H), 7.27 (d,  $J = 8.1$  Hz, 2H), 7.20 (t,  $J = 8.7$  Hz, 2H), 6.95 (d,  $J = 8.1$  Hz, 2H), 6.65 (d,  $J = 8.3$  Hz, 2H), 6.46 (d,  $J = 8.3$  Hz, 2H), 5.04 (s, 2H), 4.10 (s, 2H), 1.36 (s, 6H).  $^{13}C$  NMR (101 MHz,  $DMSO-d_6$ )  $\delta$  175.3, 161.7 (d,  $J = 243.5$  Hz), 157.1, 145.4, 144.5, 133.5 (d,  $J = 3.1$  Hz), 132.5, 129.9 (d,  $J = 8.3$  Hz, 2C), 128.6, 121.5, 115.3 (d,  $J = 21.3$  Hz, 2C), 114.6, 112.6, 78.8, 68.4, 46.5, 25.0 (2C). TOFMSESI  $m/z$ : 460.1732 ( $C_{24}H_{24}FNO_4 + H^+$  requires 410.1762).

2-methyl-2-(3-((4-((4-(trifluoromethyl)benzyl)oxy)benzyl)amino)phenoxy)propanoic acid (**3.5f**): Reaction scale: 107 mg (0.22 mmol) of ethyl 2-methyl-2-(3-((4-((4-(trifluoromethyl)benzyl)oxy)benzyl)amino)phenoxy)propanoate. Compound **3.5f** was prepared following General Procedure B. The product was purified by flash column chromatography ( $SiO_2$ ,  $CH_2Cl_2/CH_3OH$ , 100:1) to give a white amorphous solid (30 mg, 30% yield).  $^1H$  NMR (400 MHz,  $Methanol-d_4$ )  $\delta$  7.67 (d,  $J = 8.3$  Hz, 2H), 7.62 (d,  $J = 8.2$  Hz, 2H), 7.27 (d,  $J = 8.6$  Hz, 2H), 6.98 – 6.90 (m, 2H), 6.92 (d,  $J = 8.0$  Hz, 1H), 6.30 (ddd,  $J = 8.0, 2.2, 0.9$  Hz, 1H), 6.17 (t,  $J = 2.2$  Hz, 1H), 6.16 – 6.13 (m, 1H), 5.15 (s, 2H), 4.19 (s, 2H), 1.46 (s, 6H).  $^{13}C$  NMR (151 MHz,  $Methanol-d_4$ )  $\delta$  168.8, 149.4, 148.2, 141.6, 134.0, 124.4 (d,  $J = 2.3$  Hz), 121.3 (q,  $J = 32.1$  Hz), 120.7, 120.2 (2C), 119.2 (2C), 116.8 (q,  $J = 3.9$  Hz, 2C), 116.3 (q,  $J = 271.2$  Hz), 106.4 (d,  $J = 2.2$  Hz, 2C),

99.7 (d,  $J = 3.8$  Hz), 99.6 (d,  $J = 1.8$  Hz), 96.2 (d,  $J = 3.6$  Hz), 70.5, 60.5 (d,  $J = 2.8$  Hz), 38.7, 16.3 (2C). TOFMSESI  $m/z$ : 460.1732 ( $C_{25}H_{24}F_3NO_4 + H^+$  requires 460.1730).

N-(3-((4-((4-fluorobenzyl)oxy)benzyl)amino)phenyl)methanesulfonamide (**3.19a**): Reaction scale: 50 mg (0.27 mmol) of N-(3-aminophenyl)methanesulfonamide (**3.18a**). Compound **3.19a** was prepared following General Procedure A with aldehyde **3.3b** (0.28 mmol). The product was purified by flash column chromatography ( $SiO_2$ ,  $CH_2Cl_2/CH_3OH$ , 99.5:0.5) to give a white amorphous solid (27 mg, 25% yield).  $^1H$  NMR (500 MHz,  $DMSO-d_6$ )  $\delta$  9.39 (s, 1H), 7.48 (dd,  $J = 8.4, 5.7$  Hz, 2H), 7.26 (d,  $J = 8.5$  Hz, 2H), 7.20 (t,  $J = 8.8$  Hz, 2H), 6.95 (d,  $J = 4.7$  Hz, 2H), 6.94 (d,  $J = 4.1$  Hz, 1H), 6.47 (d,  $J = 2.1$  Hz, 1H), 6.38 – 6.32 (m, 1H), 6.31 (s, 1H), 6.33 – 6.26 (m, 1H), 5.05 (s, 2H), 4.13 (d,  $J = 5.9$  Hz, 2H), 2.87 (s, 3H).  $^{13}C$  NMR (101 MHz,  $DMSO-d_6$ )  $\delta$  161.7 (d,  $J = 243.6$  Hz), 157.0, 149.4, 139.0, 133.4 (d,  $J = 3.1$  Hz), 132.1, 129.8 (d,  $J = 8.2$  Hz, 2C), 129.4, 128.5 (2C), 115.2 (d,  $J = 21.4$  Hz, 2C), 114.6 (2C), 108.0, 107.2, 103.5, 68.4, 45.8, 38.8. TOFMSESI  $m/z$ : 423.1160 ( $C_{21}H_{21}FN_2O_3S + H^+$  requires 423.1149).

3-((4-((4-fluorobenzyl)oxy)benzyl)amino)-N-hydroxybenzamide (**3.19b**): Reaction scale: 50 mg (0.33 mmol) of 3-amino-N-hydroxybenzamide (**3.18b**). Compound **3.19b** was prepared following General Procedure A with aldehyde **3.3b** (0.34 mmol). The product was purified by flash column chromatography ( $SiO_2$ ,  $CH_2Cl_2/CH_3OH$ , 99.5:0.5) to give a white amorphous solid (96 mg, 80% yield).  $^1H$  NMR (400 MHz,  $Methanol-d_4$ )  $\delta$  7.44 (dd,  $J = 8.5, 5.5$  Hz, 2H), 7.29 (d,  $J = 8.6$  Hz, 2H), 7.15 (d,  $J = 7.8$  Hz, 1H), 7.12 – 7.08 (m, 2H), 7.08 – 7.07 (m, 1H), 7.05 (d,  $J = 2.6$  Hz, 1H), 6.93 (d,  $J = 8.6$  Hz, 2H), 6.77 (dd,  $J = 7.8, 2.0$  Hz, 1H), 5.02 (s, 2H), 4.27 (s, 2H).  $^{13}C$  NMR (101 MHz,  $Methanol-d_4$ )  $\delta$  201.5, 192.0 (d,  $J = 244.5$  Hz), 187.3, 178.5, 163.8, 163.0 (d,  $J = 3.2$  Hz), 161.6, 158.8 (d,  $J = 8.3$  Hz, 2C), 158.2, 157.8 (2C), 145.5, 144.8, 144.3 (d,  $J = 21.8$  Hz, 2C), 144.1 (2C), 141.0, 98.5, 76.1. TOFMSESI  $m/z$ : 351.1291 ( $C_{21}H_{19}FN_2O_3 - OH^- + 2H^+$  requires 351.1503).

3-((4-((4-fluorobenzyl)oxy)benzyl)amino)benzenesulfonamide (**3.19c**): Reaction scale: 100 mg (0.58 mmol) of 3-aminobenzenesulfonamide (**3.18c**). Compound **3.19c** was prepared following General Procedure A with aldehyde **3.3b** (0.59 mmol). The product was purified by flash column chromatography (SiO<sub>2</sub>, CH<sub>2</sub>Cl<sub>2</sub>/CH<sub>3</sub>OH, 99.5:0.5) to give a white amorphous solid (17 mg, 8% yield). <sup>1</sup>H NMR (600 MHz, Methanol-*d*<sub>4</sub>) δ 7.44 (dd, *J* = 8.6, 5.5 Hz, 2H), 7.31 – 7.26 (m, 2H), 7.20 (t, *J* = 7.9 Hz, 1H), 7.14 (t, *J* = 2.0 Hz, 1H), 7.12 – 7.09 (m, 2H), 7.07 (s, 1H), 6.97 – 6.91 (m, 2H), 6.78 (ddd, *J* = 8.2, 2.4, 1.0 Hz, 1H), 5.02 (s, 2H), 4.27 (s, 2H). <sup>13</sup>C NMR (151 MHz, Methanol-*d*<sub>4</sub>) δ 163.8 (d, *J* = 244.4 Hz), 159.2, 150.5, 145.4, 134.8 (d, *J* = 2.9 Hz), 133.0, 130.6 (d, *J* = 8.1 Hz, 2C), 130.5, 129.7 (2C), 117.2, 116.1 (d, *J* = 21.8 Hz, 2C), 116.0 (2C), 114.6, 110.5, 70.3, 47.8. TOFMSESI *m/z*: 421.0645 (C<sub>20</sub>H<sub>19</sub>FN<sub>2</sub>O<sub>3</sub>S + Cl<sup>-</sup> requires 421.0794).

N-(4-((4-fluorobenzyl)oxy)benzyl)-3-(1H-tetrazol-5-yl)aniline (**3.19d**): Reaction scale: 100 mg (0.62 mmol) of 3-(1H-tetrazol-5-yl)aniline (**3.18d**). Compound **3.19d** was prepared following General Procedure A with compound **3.3b** (0.63 mmol). The product was purified by flash column chromatography (SiO<sub>2</sub>, CH<sub>2</sub>Cl<sub>2</sub>/CH<sub>3</sub>OH, 99.5:0.5) to give a white amorphous solid (100 mg, 43% yield). <sup>1</sup>H NMR (400 MHz, Methanol-*d*<sub>4</sub>) δ 7.45 (dd, *J* = 8.5, 5.6 Hz, 2H), 7.37 – 7.30 (m, 2H), 7.30 – 7.24 (m, 2H), 7.20 (dt, *J* = 7.5, 1.3 Hz, 1H), 7.14 – 7.04 (m, 2H), 7.00 – 6.92 (m, 2H), 6.83 (ddd, *J* = 8.1, 2.5, 1.1 Hz, 1H), 5.03 (s, 2H), 4.32 (s, 2H). <sup>13</sup>C NMR (101 MHz, Methanol-*d*<sub>4</sub>) δ 163.8 (d, *J* = 244.6 Hz), 159.2, 157.7, 151.0, 134.8 (d, *J* = 3.4 Hz), 133.2, 131.0, 130.6 (d, *J* = 8.1 Hz, 2C), 129.7 (2C), 125.6, 117.1, 116.1 (d, *J* = 18.6 Hz, 2C), 116.01, 115.99 (2C), 111.7, 70.3, 47.8. TOFMSESI *m/z*: 376.1575 (C<sub>21</sub>H<sub>18</sub>FN<sub>5</sub>O + H<sup>+</sup> requires 376.1568).

(3-((4-((4-fluorobenzyl)oxy)benzyl)amino)phenyl)boronic acid (**3.19e**): Reaction scale: 100 mg (0.58 mmol) of (3-aminophenyl)boronic acid (**3.18e**). Compound **3.19e** was prepared following General Procedure A with aldehyde **3.3b** (0.59 mmol). The product was purified by flash column

chromatography (SiO<sub>2</sub>, CH<sub>2</sub>Cl<sub>2</sub>/CH<sub>3</sub>OH, 99.5:0.5) to give a white amorphous solid (109 mg, 42% yield). <sup>1</sup>H NMR (400 MHz, Methanol-*d*<sub>4</sub>) δ 7.43 (dd, *J* = 8.6, 5.5 Hz, 2H), 7.28 (d, *J* = 8.6 Hz, 2H), 7.11 – 7.08 (m, 1H), 7.07 (d, *J* = 8.8 Hz, 2H), 6.98 – 6.89 (m, 2H), 6.84 (s, 1H), 6.84 – 6.79 (m, 1H), 6.67 (ddd, *J* = 8.1, 2.5, 1.2 Hz, 1H), 5.01 (s, 2H), 4.23 (s, 2H). <sup>13</sup>C NMR (101 MHz, Methanol-*d*<sub>4</sub>) δ 165.0, 162.6, 159.1, 149.3, 134.9 (d, *J* = 3.3 Hz), 133.8 (2C), 130.6 (dd, *J* = 8.5, 23.6 Hz), 129.6 (d, *J* = 21.7 Hz), 129.3 (d, *J* = 6.9 Hz), 123.0 (2C), 119.1 (2C), 116.7 – 116.0 (m), 115.9 (2C), 115.6 (d, *J* = 11.9 Hz), 70.3, 48.3. TOFMSESI *m/z*: 352.1537 (C<sub>20</sub>H<sub>19</sub>BFNO<sub>3</sub> + H<sup>+</sup> requires 352.1515).

2-((3-((4-((4-fluorobenzyl)oxy)benzyl)amino)phenyl)thio)-2-methylpropanoic acid (**3.19f**): Reaction scale: 190 mg (0.56 mmol) of ethyl 2-((3-aminophenyl)thio)-2-methylpropanoate (**3.18f**).

Compound **3.19f** was prepared following General Procedure B with compound **3.3b** (0.57 mmol).

The product was purified by flash column chromatography (SiO<sub>2</sub>, CH<sub>2</sub>Cl<sub>2</sub>/CH<sub>3</sub>OH, 100:1) to give a white amorphous solid (30 mg, 13% yield). <sup>1</sup>H NMR (400 MHz, Methanol-*d*<sub>4</sub>) δ 7.47 – 7.38 (m, 2H), 7.30 – 7.23 (m, 2H), 7.13 – 6.97 (m, 2H), 7.01 (t, *J* = 7.8 Hz, 1H), 6.96 – 6.88 (m, 2H), 6.76 (dd, *J* = 2.4, 1.6 Hz, 1H), 6.72 (ddd, *J* = 7.5, 1.7, 1.0 Hz, 1H), 6.63 (ddd, *J* = 8.2, 2.4, 1.0 Hz, 1H), 5.01 (s, 2H), 4.21 (s, 2H), 1.37 (s, 6H). <sup>13</sup>C NMR (101 MHz, Methanol-*d*<sub>4</sub>) δ 178.3, 163.8 (d, *J* = 244.5 Hz), 159.1, 150.3, 134.8 (d, *J* = 3.1 Hz), 133.5, 133.3, 130.6 (d, *J* = 8.1 Hz, 2C), 130.0, 129.7 (2C), 125.7, 121.6, 116.1 (d, *J* = 21.7 Hz, 2C), 115.9 (2C), 115.1, 70.2, 52.0, 48.0, 26.6 (2C). TOFMSESI *m/z*: 448.1358 (C<sub>24</sub>H<sub>24</sub>FNO<sub>3</sub>S + Na<sup>+</sup> requires 448.1359).

3-((4-((4-chlorobenzyl)oxy)-3-methylbenzyl)amino)benzoic acid (**3.20**): Reaction scale: 50 mg (0.36 mmol) of 3-amino benzoic acid. Compound **3.20** was prepared following General Procedure A with 4-((4-chlorobenzyl)oxy)-3-methylbenzaldehyde (0.37 mmol). The product was purified by flash column chromatography (SiO<sub>2</sub>, CH<sub>2</sub>Cl<sub>2</sub>/CH<sub>3</sub>OH, 99.5:0.5) to give a white amorphous solid

(50 mg, 36% yield).  $^1\text{H}$  NMR (600 MHz,  $\text{DMSO-}d_6$ )  $\delta$  12.61 (s, 1H), 7.45 (d,  $J = 8.6$  Hz, 2H), 7.43 (d,  $J = 8.6$  Hz, 2H), 7.14 (d,  $J = 1.9$  Hz, 1H), 7.13 (d,  $J = 2.5$  Hz, 1H), 7.13 – 7.10 (m, 1H), 7.09 (d,  $J = 6.7$  Hz, 1H), 7.08 – 7.04 (m, 1H), 6.91 (d,  $J = 8.4$  Hz, 1H), 6.75 (ddd,  $J = 8.0, 2.5, 1.2$  Hz, 1H), 6.41 (t,  $J = 6.0$  Hz, 1H), 5.06 (s, 2H), 4.15 (d,  $J = 5.6$  Hz, 2H), 2.15 (s, 3H).  $^{13}\text{C}$  NMR (151 MHz,  $\text{DMSO-}d_6$ )  $\delta$  177.3, 164.5, 158.2, 146.0, 141.7, 141.0, 140.8, 139.0, 138.6 (2C), 138.3, 137.9 (2C), 135.3, 135.1, 126.1, 125.8, 122.3, 121.1, 77.8, 55.3, 25.7. TOFMSESI  $m/z$ : 404.1006 ( $\text{C}_{22}\text{H}_{20}\text{ClNO}_3 + \text{Na}^+$  requires 404.1024).

3-(((4-((4-bromobenzyl)oxy)-3-methylbenzyl)amino)benzoic acid (**3.21**): Reaction scale: 50 mg (0.36 mmol) of 3-amino benzoic acid. Compound **3.21** was prepared following General Procedure A with 4-(((4-bromobenzyl)oxy)-3-methylbenzaldehyde (0.37 mmol). The product was purified by flash column chromatography ( $\text{SiO}_2$ ,  $\text{CH}_2\text{Cl}_2/\text{CH}_3\text{OH}$ , 99.5:0.5) to give a white amorphous solid (70 mg, 45% yield).  $^1\text{H}$  NMR (600 MHz,  $\text{DMSO-}d_6$ )  $\delta$  12.62 (s, 1H), 7.58 (d,  $J = 8.4$  Hz, 2H), 7.41 (d,  $J = 8.3$  Hz, 2H), 7.16 (d,  $J = 2.1$  Hz, 1H), 7.17 – 7.14 (m, 1H), 7.16 – 7.12 (m, 1H), 7.13 – 7.09 (m, 1H), 7.12 – 7.07 (m, 1H), 6.93 (d,  $J = 8.3$  Hz, 1H), 6.77 (dd,  $J = 8.0, 1.1$  Hz, 1H), 6.42 (t,  $J = 6.0$  Hz, 1H), 5.07 (s, 2H), 4.17 (d,  $J = 5.4$  Hz, 2H), 2.17 (s, 3H).  $^{13}\text{C}$  NMR (151 MHz,  $\text{DMSO-}d_6$ )  $\delta$  167.8, 155.0, 148.8, 137.0, 131.5, 131.3 (2C), 131.2, 129.5, 129.4 (2C), 128.8, 125.8, 125.6, 120.7, 116.6, 116.3, 112.9, 111.6, 68.3, 45.9, 16.2. TOFMSESI  $m/z$ : 426.0648 ( $\text{C}_{22}\text{H}_{20}\text{BrNO}_3 + \text{H}^+$  requires 426.0699).

3-(((4-((4-iodobenzyl)oxy)-3-methylbenzyl)amino)benzoic acid (**3.22**): Reaction scale: 50 mg (0.36 mmol) of 3-amino benzoic acid. Compound **3.22** was prepared following General Procedure A with 4-(((4-bromobenzyl)oxy)-3-methylbenzaldehyde (0.37 mmol). The product was purified by flash column chromatography ( $\text{SiO}_2$ ,  $\text{CH}_2\text{Cl}_2/\text{CH}_3\text{OH}$ , 99.5:0.5) to give a white amorphous solid (90 mg, 52% yield).  $^1\text{H}$  NMR (600 MHz,  $\text{DMSO-}d_6$ )  $\delta$  12.62 (s, 1H), 7.75 (d,  $J = 8.2$  Hz, 2H),



7.25 (d,  $J = 7.9$  Hz, 2H), 7.16 (s, 1H), 7.15 (s, 1H), 7.14 (d,  $J = 7.9$  Hz, 1H), 7.11 (d,  $J = 8.1$  Hz, 1H), 7.09 (d,  $J = 7.8$  Hz, 1H), 6.92 (d,  $J = 8.3$  Hz, 1H), 6.77 (d,  $J = 8.0$  Hz, 1H), 6.40 (t,  $J = 6.1$  Hz, 1H), 5.05 (s, 2H), 4.17 (d,  $J = 5.5$  Hz, 2H), 2.17 (s, 3H).  $^{13}\text{C}$  NMR (151 MHz, DMSO- $d_6$ )  $\delta$  167.8, 155.0, 148.7, 137.3, 137.2 (2C), 131.5, 131.3, 129.5 (2C), 129.4, 128.8, 125.8, 125.6, 116.6, 116.2, 112.9, 111.6, 93.6, 68.5, 45.9, 16.2. TOFMSESI  $m/z$ : 472.0399 ( $\text{C}_{22}\text{H}_{20}\text{INO}_3 - \text{H}^+$  requires 472.0415).

3-((4-((2,4-difluorobenzyl)oxy)-3-methylbenzyl)amino)benzoic acid (**3.23**): Reaction scale: 40 mg (0.29 mmol) of 3-amino benzoic acid. Compound **3.23** was prepared following General Procedure A with 4-((2,4-difluorobenzyl)oxy)-3-methylbenzaldehyde (0.30 mmol). The product was purified by flash column chromatography ( $\text{SiO}_2$ ,  $\text{CH}_2\text{Cl}_2/\text{CH}_3\text{OH}$ , 99.5:0.5) to give a white amorphous solid (87 mg, 78% yield).  $^1\text{H}$  NMR (600 MHz, DMSO- $d_6$ )  $\delta$  12.61 (s, 1H), 7.61 (ddd,  $J = 8.5, 6.6$  Hz, 1H), 7.30 (ddd,  $J = 10.5, 2.6$  Hz, 1H), 7.16 (dd,  $J = 1.9$  Hz, 1H), 7.15 (s, 1H), 7.14 (s, 1H), 7.14 – 7.13 (m, 1H), 7.11 (d,  $J = 8.1$  Hz, 1H), 7.09 (d,  $J = 7.5$  Hz, 1H), 7.01 (d,  $J = 8.2$  Hz, 1H), 6.80 – 6.72 (m, 1H), 6.43 (t,  $J = 6.0$  Hz, 1H), 5.08 (s, 2H), 4.18 (d,  $J = 5.5$  Hz, 2H), 2.12 (s, 3H).  $^{13}\text{C}$  NMR (151 MHz, DMSO- $d_6$ )  $\delta$  167.8, 161.5 – 160.8 (m), 159.6, 155.0, 148.7, 131.7 (d,  $J = 13.3$  Hz), 131.7 – 131.5 (m), 131.3, 129.5, 128.8, 125.9, 125.7, 120.7, 116.6, 116.3, 112.9, 111.8, 111.5, 104.0 (t,  $J = 25.8$  Hz), 63.3, 45.8, 16.1. TOFMSESI  $m/z$ : 406.1243 ( $\text{C}_{22}\text{H}_{19}\text{F}_2\text{NO}_3 + \text{Na}^+$  requires 406.1225).

3-((4-((3,4-difluorobenzyl)oxy)-3-methylbenzyl)amino)benzoic acid (**3.24**): Reaction scale: 100 mg (0.73 mmol) of 3-amino benzoic acid. Compound **3.24** was prepared following General Procedure A with 4-((3,4-difluorobenzyl)oxy)-3-methylbenzaldehyde (0.74 mmol). The product was purified by flash column chromatography ( $\text{SiO}_2$ ,  $\text{CH}_2\text{Cl}_2/\text{CH}_3\text{OH}$ , 99.5:0.5) to give a white amorphous solid (170 mg, 61% yield).  $^1\text{H}$  NMR (600 MHz, DMSO- $d_6$ )  $\delta$  12.60 (s, 1H), 7.51 (tt,  $J$

= 8.0, 4.0 Hz, 1H), 7.45 (ddd,  $J = 10.7, 9.9, 8.4$  Hz, 1H), 7.31 (dd,  $J = 6.4$  Hz, 1H), 7.16 (d,  $J = 1.8$  Hz, 1H), 7.16 (s, 1H), 7.15 – 7.13 (m, 1H), 7.13 – 7.10 (m, 1H), 7.09 (d,  $J = 7.5$  Hz, 1H), 6.93 (d,  $J = 8.4$  Hz, 1H), 6.80 – 6.75 (m, 1H), 6.42 (t,  $J = 6.0$  Hz, 1H), 5.07 (s, 2H), 4.17 (d,  $J = 5.4$  Hz, 2H), 2.18 (s, 3H).  $^{13}\text{C}$  NMR (151 MHz, DMSO- $d_6$ )  $\delta$  167.8, 154.9, 149.9 (dd,  $J = 12.5, 73.4$  Hz), 148.7, 148.3 (dd,  $J = 12.6, 73.0$  Hz), 135.3 (dd,  $J = 3.7, 5.8$  Hz), 131.7, 131.3, 129.5, 128.8, 125.8, 125.6, 124.1 (dd,  $J = 3.4, 6.7$  Hz), 117.5 (d,  $J = 17.2$  Hz), 116.6, 116.34 (d,  $J = 10.7$  Hz), 116.26, 112.9, 111.6, 67.9, 45.8, 16.2. TOFMSESI  $m/z$ : 406.1243 ( $\text{C}_{22}\text{H}_{19}\text{F}_2\text{NO}_3 + \text{Na}^+$  requires 406.1225).

3-((4-((3,5-difluorobenzyl)oxy)-3-methylbenzyl)amino)benzoic acid (**3.25**): Reaction scale: 40 mg (0.29 mmol) of 3-amino benzoic acid. Compound **3.25** was prepared following General Procedure A with 4-((3,5-difluorobenzyl)oxy)-3-methylbenzaldehyde (0.30 mmol). The product was purified by flash column chromatography ( $\text{SiO}_2$ ,  $\text{CH}_2\text{Cl}_2/\text{CH}_3\text{OH}$ , 99.5:0.5) to give a white amorphous solid (83 mg, 74% yield).  $^1\text{H}$  NMR (600 MHz, Methanol- $d_4$ )  $\delta$  7.28 (d,  $J = 2.3$  Hz, 1H), 7.25 (d,  $J = 7.7$  Hz, 1H), 7.19 (s, 1H), 7.15 (d,  $J = 7.9$  Hz, 1H), 7.13 (s, 1H), 7.08 – 7.02 (m, 2H), 6.89 – 6.87 (m, 1H), 6.86 (d,  $J = 8.5$  Hz, 1H), 6.81 (dd,  $J = 7.9, 2.3$  Hz, 1H), 5.10 (s, 2H), 4.24 (s, 2H), 2.26 (s, 3H).  $^{13}\text{C}$  NMR (151 MHz, Methanol- $d_4$ )  $\delta$  164.6 (dd,  $J = 13.0, 247.4$  Hz, 2C), 156.7, 150.3, 143.9 (t,  $J = 9.2$  Hz), 133.4, 131.0 (2C), 129.8, 127.9, 127.0 (2C), 119.0, 118.2, 114.8, 112.6 (dd,  $J = 2.4, 4.2$  Hz), 110.6 (dd,  $J = 5.3, 20.7$  Hz, 2C), 103.6 (t,  $J = 25.8$  Hz), 69.6, 48.1, 16.5. TOFMSESI  $m/z$ : 382.1268 ( $\text{C}_{22}\text{H}_{19}\text{F}_2\text{NO}_3 - \text{H}^+$  requires 382.1260).

3-((3-fluoro-4-((4-fluorobenzyl)oxy)benzyl)amino)benzoic acid (**3.26**): Reaction scale: 50 mg (0.36 mmol) of 3-amino benzoic acid. Compound **3.26** was prepared following General Procedure A with 3-fluoro-4-((4-fluorobenzyl)oxy)benzaldehyde (0.37 mmol). The product was purified by flash column chromatography ( $\text{SiO}_2$ ,  $\text{CH}_2\text{Cl}_2/\text{CH}_3\text{OH}$ , 99.5:0.5) to give a white amorphous solid (100 mg, 75% yield).  $^1\text{H}$  NMR (600 MHz, DMSO- $d_6$ )  $\delta$  12.64 (s, 1H), 7.49 (dd,  $J = 8.5, 5.7$  Hz,

2H), 7.23 – 7.20 (m, 2H), 7.20 – 7.19 (m, 1H), 7.18 (d,  $J = 1.9$  Hz, 1H), 7.16 – 7.15 (m, 1H), 7.14 (d,  $J = 7.8$  Hz, 1H), 7.11 (d,  $J = 1.4$  Hz, 1H), 7.10 (q,  $J = 1.6$  Hz, 1H), 6.77 (ddd,  $J = 7.9, 2.5, 1.2$  Hz, 1H), 6.50 (t,  $J = 6.1$  Hz, 1H), 5.12 (s, 2H), 4.23 (d,  $J = 5.9$  Hz, 2H).  $^{13}\text{C}$  NMR (151 MHz, DMSO- $d_6$ )  $\delta$  167.7, 161.9 (d,  $J = 243.9$  Hz), 151.7 (d,  $J = 243.9$  Hz), 148.5, 144.6 (d,  $J = 10.7$  Hz), 133.4 (d,  $J = 5.0$  Hz), 132.8 (d,  $J = 2.9$  Hz), 131.3, 130.0 (d,  $J = 8.5$  Hz, 2C), 128.9, 123.0 (d,  $J = 3.0$  Hz), 116.9, 116.4, 115.4, 115.3 (d,  $J = 21.3$  Hz, 2C), 114.7 (d,  $J = 18.3$  Hz), 112.9, 69.6, 45.3. TOFMSESI  $m/z$ : 368.1110 ( $\text{C}_{21}\text{H}_{17}\text{F}_2\text{NO}_3 - \text{H}^+$  requires 368.1104).

3-((3-chloro-4-((4-fluorobenzyl)oxy)benzyl)amino)benzoic acid (**3.27**): Reaction scale: 100 mg (0.72 mmol) of 3-amino benzoic acid. Compound **3.27** was prepared following General Procedure A with 3-chloro-4-((4-fluorobenzyl)oxy)benzaldehyde (0.73 mmol). The product was purified by flash column chromatography ( $\text{SiO}_2$ ,  $\text{CH}_2\text{Cl}_2/\text{CH}_3\text{OH}$ , 99.5:0.5) to give a white amorphous solid (120 mg, 43% yield).  $^1\text{H}$  NMR (600 MHz, DMSO- $d_6$ )  $\delta$  12.65 (s, 1H), 7.50 (dd,  $J = 8.3, 5.6$  Hz, 2H), 7.42 (d,  $J = 2.0$  Hz, 1H), 7.27 (d,  $J = 8.5$  Hz, 1H), 7.23 (t,  $J = 8.7$  Hz, 2H), 7.19 (d,  $J = 8.4$  Hz, 1H), 7.15 (d,  $J = 2.5$  Hz, 1H), 7.14 (d,  $J = 7.7$  Hz, 1H), 7.11 (d,  $J = 7.5$  Hz, 1H), 6.79 – 6.69 (m, 1H), 6.51 (s, 1H), 5.15 (s, 2H), 4.23 (d,  $J = 5.9$  Hz, 2H).  $^{13}\text{C}$  NMR (151 MHz, DMSO- $d_6$ )  $\delta$  167.8, 161.8 (d,  $J = 243.5$  Hz), 152.2, 148.4, 133.6, 132.8 (d,  $J = 3.1$  Hz), 131.4, 129.7 (d,  $J = 8.4$  Hz, 2C), 128.9, 128.5, 126.9, 121.4, 116.9, 116.3, 115.3 (d,  $J = 21.3$  Hz, 2C), 114.3, 112.9, 69.3, 45.2. TOFMSESI  $m/z$ : 384.0820 ( $\text{C}_{21}\text{H}_{17}\text{ClFNO}_3 - \text{H}$  requires 384.0808).

3-((3,4-bis((4-fluorobenzyl)oxy)benzyl)amino)benzoic acid (**3.28**): Reaction scale: 50 mg (0.36 mmol) of 3-amino benzoic acid. Compound **3.28** was prepared following General Procedure A with 3,4-bis((4-fluorobenzyl)oxy)benzaldehyde (0.37 mmol). The product was purified by flash column chromatography ( $\text{SiO}_2$ ,  $\text{CH}_2\text{Cl}_2/\text{CH}_3\text{OH}$ , 99.5:0.5) to give a white amorphous solid (95 mg, 58% yield).  $^1\text{H}$  NMR (400 MHz, DMSO- $d_6$ )  $\delta$  12.62 (s, 1H), 7.45 (dd,  $J = 2.1, 6.2$  Hz, 2H), 7.44

(dd,  $J = 2.4, 5.8$  Hz, 2H), 7.24 – 7.16 (m, 2H), 7.17 (d,  $J = 2.5$  Hz, 2H), 7.19 – 7.12 (m, 1H), 7.13 (d,  $J = 7.6$  Hz, 1H), 7.11 (s, 1H), 7.10 (d,  $J = 5.9$  Hz, 1H), 6.99 (d,  $J = 8.2$  Hz, 1H), 6.88 (dd,  $J = 1.9, 8.2$  Hz, 1H), 6.77 (dt,  $J = 2.0, 7.7$  Hz, 1H), 6.42 (t,  $J = 6.0$  Hz, 1H), 5.06 (s, 2H), 5.05 (s, 2H), 4.19 (d,  $J = 5.3$  Hz, 2H).  $^{13}\text{C}$  NMR (101 MHz, DMSO- $d_6$ )  $\delta$  167.8, 161.7 (d,  $J = 243.3$  Hz), 160.5 (d,  $J = 243.5$  Hz), 148.7, 148.1, 147.0, 133.6 (d,  $J = 3.2$  Hz), 133.4 (d,  $J = 3.1$  Hz), 132.9, 131.3, 129.8 (d,  $J = 8.3$  Hz, 2C), 129.7 (d,  $J = 8.2$  Hz, 2C), 128.8, 119.9, 116.7, 116.3, 115.3 (d,  $J = 21.3$  Hz, 2C), 115.1 (d,  $J = 21.3$  Hz, 2C), 114.6, 113.9, 113.0, 69.50, 69.47, 46.0. TOFMSESI  $m/z$ : 474.1525 ( $\text{C}_{28}\text{H}_{23}\text{F}_2\text{NO}_4 - \text{H}^+$  requires 474.1522).

3-((2,4-bis((4-fluorobenzyl)oxy)benzyl)amino)benzoic acid (**3.29**): Reaction scale: 50 mg (0.36 mmol) of 3-amino benzoic acid. Compound **3.29** was prepared following General Procedure A with 2,4-bis((4-fluorobenzyl)oxy)benzaldehyde (0.37 mmol). The product was purified by flash column chromatography ( $\text{SiO}_2$ ,  $\text{CH}_2\text{Cl}_2/\text{CH}_3\text{OH}$ , 99.5:0.5) to give a white amorphous solid (102 mg, 59% yield).  $^1\text{H}$  NMR (600 MHz, DMSO- $d_6$ )  $\delta$  12.61 (s, 1H), 7.52 (dd,  $J = 5.7, 8.4$  Hz, 2H), 7.47 (dd,  $J = 5.7, 8.5$  Hz, 2H), 7.24 – 7.19 (m, 2H), 7.21 – 7.16 (m, 2H), 7.15 (d,  $J = 2.0$  Hz, 1H), 7.13 (d,  $J = 8.1$  Hz, 1H), 7.12 (d,  $J = 7.7$  Hz, 1H), 7.09 (d,  $J = 7.6$  Hz, 1H), 6.75 (t,  $J = 1.7$  Hz, 1H), 6.74 (d,  $J = 2.3$  Hz, 1H), 6.56 (dd,  $J = 2.3, 8.4$  Hz, 1H), 6.29 (t,  $J = 6.1$  Hz, 1H), 5.16 (s, 2H), 5.03 (s, 2H), 4.20 (d,  $J = 5.3$  Hz, 2H).  $^{13}\text{C}$  NMR (151 MHz, DMSO- $d_6$ )  $\delta$  167.8, 161.7 (d,  $J = 243.9$  Hz), 161.6 (d,  $J = 243.5$  Hz), 158.3, 156.6, 148.8, 133.4 (d,  $J = 2.9$  Hz), 133.3 (d,  $J = 2.8$  Hz), 131.3, 129.9 (d,  $J = 8.2$  Hz, 2C), 129.5 (d,  $J = 8.2$  Hz, 2C), 128.8, 128.6, 119.9, 116.5, 116.3, 115.19 (d,  $J = 21.3$  Hz, 2C), 115.17 (d,  $J = 21.4$  Hz, 2C), 112.6, 105.8, 100.5, 68.6 (2C), 40.8. TOFMSESI  $m/z$ : 476.1663 ( $\text{C}_{28}\text{H}_{23}\text{F}_2\text{NO}_4 + \text{H}^+$  requires 476.1668).

3-(((4-((4-fluorobenzyl)oxy)-3-methylbenzyl)(methyl)amino)benzoic acid (**3.30**): Paraformaldehyde (5 mg, 0.16 mmol), compound **3.4u** (30 mg, 0.08 mmol), sodium

triacetoxyborohydride (6.2 mg, 0.096 mmol) and 2 mL of ethanol were combined in a 10 mL round bottom flask and refluxed for 2 hr at 100 °C. The reaction was then cooled to 25 °C for 12 h. The solvent was removed by vacuum and the residue was dissolved in EtOAc (60 mL). The organic layer was washed with aq. 1N HCl (20 mL), water (20 mL), and brine (20 mL). The organic layer was dried over Na<sub>2</sub>SO<sub>4</sub>, filtered, and concentrated by vacuum. The compound was purified by flash column chromatography (SiO<sub>2</sub>, CH<sub>2</sub>Cl<sub>2</sub>/CH<sub>3</sub>OH, 99.5:0.5) to give a white amorphous solid (13 mg, 44% yield). <sup>1</sup>H NMR (600 MHz, Methanol-*d*<sub>4</sub>) δ 7.47 – 7.42 (m, 2H), 7.42 (d, *J* = 1.7 Hz, 1H), 7.37 – 7.29 (m, 1H), 7.23 (t, *J* = 7.9 Hz, 1H), 7.08 (t, *J* = 8.8 Hz, 2H), 7.01 (d, *J* = 2.2 Hz, 1H), 6.98 – 6.96 (m, 1H), 6.96 – 6.94 (m, 1H), 6.85 (d, *J* = 8.3 Hz, 1H), 4.99 (s, 2H), 4.46 (s, 2H), 3.00 (s, 3H), 2.18 (s, 3H). <sup>13</sup>C NMR (151 MHz, Methanol-*d*<sub>4</sub>) δ 169.3, 162.3 (d, *J* = 244.4 Hz), 155.7, 149.7, 133.6 (d, *J* = 3.3 Hz), 131.0, 130.4, 128.9 (d, *J* = 8.3 Hz, 2C), 128.6, 126.7, 125.0, 117.3, 116.7, 114.7 (d, *J* = 21.8 Hz, 2C), 113.0, 111.39, 111.36, 68.9, 55.4, 37.4, 15.2. TOFMSESI *m/z*: 378.1509 (C<sub>23</sub>H<sub>22</sub>FNO<sub>3</sub>- H<sup>+</sup> requires 378.1511).

3-fluoro-5-((4-((4-fluorobenzyl)oxy)-3-methylbenzyl)amino)benzoic acid (**3.31**): Reaction scale: 50 mg (0.32 mmol) of 3-amino-5-fluorobenzoic acid. Compound **3.31** was prepared following General Procedure A with aldehyde **3.12b**. The product was purified by flash column chromatography (SiO<sub>2</sub>, CH<sub>2</sub>Cl<sub>2</sub>/CH<sub>3</sub>OH, 99.5:0.5) to give a white amorphous solid (104 mg, 84% yield). <sup>1</sup>H NMR (400 MHz, Methanol-*d*<sub>4</sub>) δ 7.47 (dd, *J* = 8.4, 5.2 Hz, 2H), 7.38 (d, *J* = 2.2 Hz, 1H), 7.22 (dd, *J* = 8.5, 2.2 Hz, 1H), 7.13 – 7.02 (m, 4H), 6.88 (d, *J* = 9.2 Hz, 1H), 6.48 (d, *J* = 11.3 Hz, 1H), 5.09 (s, 2H), 4.25 (s, 2H). <sup>13</sup>C NMR (101 MHz, Methanol-*d*<sub>4</sub>) δ 169.5, 165.1 (d, *J* = 241.1 Hz), 163.8 (d, *J* = 244.3 Hz), 157.2, 152.1, 135.1 (d, *J* = 2.3 Hz), 134.3 (d, *J* = 10.0 Hz), 132.5, 130.9, 130.4 (d, *J* = 8.2 Hz), 128.1, 126.9 (2C), 116.1 (d, *J* = 21.6 Hz), 112.8 (2C), 111.1, 104.4 (d, *J* =

24.0 Hz), 103.9 (d,  $J = 25.8$  Hz), 70.4, 47.9, 16.6. TOFMSESI  $m/z$ : 382.1254 ( $C_{22}H_{19}F_2NO_3 - H^+$  requires 382.1260).

3-((3-chloro-4-((4-fluorobenzyl)oxy)benzyl)amino)-5-fluorobenzoic acid (**3.32**): Reaction scale: 50 mg (0.32 mmol) of 3-amino-5-fluorobenzoic acid. Compound **3.32** was prepared following General Procedure A with 3-chloro-4-((4-fluorobenzyl)oxy)benzaldehyde. The product was purified by flash column chromatography ( $SiO_2$ ,  $CH_2Cl_2/CH_3OH$ , 99.5:0.5) to give a white amorphous solid (109 mg, 84% yield).  $^1H$  NMR (400 MHz, Methanol- $d_4$ )  $\delta$  7.51 – 7.43 (m, 2H), 7.38 (d,  $J = 2.2$  Hz, 1H), 7.22 (dd,  $J = 8.4, 2.2$  Hz, 1H), 7.09 (dt,  $J = 5.9, 2.1$  Hz, 2H), 6.92 – 6.84 (m, 1H), 6.48 (dt,  $J = 11.4, 2.3$  Hz, 1H), 5.09 (s, 2H), 4.25 (s, 2H).  $^{13}C$  NMR (101 MHz, Methanol- $d_4$ )  $\delta$  169.4 (d,  $J = 3.4$  Hz), 165.1 (d,  $J = 241.2$  Hz), 163.9 (d,  $J = 244.8$  Hz) 154.5, 151.8 (d,  $J = 11.0$  Hz), 134.5, 134.3 (d,  $J = 3.1$  Hz), 134.2 (d,  $J = 3.7$  Hz), 130.5, 130.4, 130.1, 127.8, 124.3, 116.3, 116.1, 115.6, 111.1, 104.7 (d,  $J = 24.1$  Hz), 103.9, 71.3, 47.3. TOFMSESI  $m/z$ : 402.1317 ( $C_{21}H_{16}ClF_2NO_3 - H^+$  requires 402.0714).

2-(3-((4-((4-fluorobenzyl)oxy)-3-methylbenzyl)amino)phenoxy)-2-methylpropanoic acid (**3.33**): Reaction scale: 99 mg (0.22 mmol) of ethyl 2-(3-((4-((4-fluorobenzyl)oxy)-3-methylbenzyl)amino)phenoxy)-2-methylpropanoate. Compound **3.33** was prepared following General Procedure B. The product was purified by flash column chromatography ( $SiO_2$ ,  $CH_2Cl_2/CH_3OH$ , 100:1) to give a white amorphous solid (30 mg, 32% yield).  $^1H$  NMR (400 MHz, Methanol- $d_4$ )  $\delta$  7.41 (dd,  $J = 8.5, 5.5$  Hz, 2H), 7.11 (d,  $J = 2.1$  Hz, 1H), 7.09 (d,  $J = 6.0$  Hz, 1H), 7.06 (t,  $J = 7.7$  Hz, 2H), 6.92 (t,  $J = 8.0$  Hz, 1H), 6.83 (d,  $J = 8.3$  Hz, 1H), 6.30 (dd,  $J = 8.1, 2.1$  Hz, 1H), 6.20 (t,  $J = 2.3$  Hz, 1H), 6.17 (dd,  $J = 8.0, 2.3$  Hz, 1H), 4.98 (s, 2H), 4.12 (s, 2H), 2.19 (s, 3H), 1.46 (s, 6H).  $^{13}C$  NMR (101 MHz, Methanol- $d_4$ )  $\delta$  178.2, 163.7 (d,  $J = 244.2$  Hz), 157.7, 157.0, 151.0, 135.1 (d,  $J = 3.3$  Hz), 133.1, 130.9, 130.3 (d,  $J = 8.1$  Hz, 2C), 130.2, 127.9, 126.9,

116.1 (d,  $J = 21.7$  Hz, 2C), 112.7, 109.2, 109.1, 105.7, 79.9, 70.3, 48.3, 25.8 (2C), 16.6. TOFMSESI m/z: 422.1784 ( $C_{25}H_{26}FNO_4 - H^+$  requires 422.1773).

### 3.5.2 Biological Assay Protocols

***In vitro* PPAR functional reporter gene assay.** Agonist activity of test compounds against human PPAR $\alpha$ , was analyzed using commercial kits from Indigo Biosciences (hPPAR $\alpha$ : IB00111, hPPAR $\gamma$ : IB00101; hPPAR $\delta$ : IB00121. Protocols provided with the kit were followed for experimental execution. Briefly, a suspension of reporter cells was prepared in Cell Recovery Medium (CRM: containing 10% charcoal stripped fetal bovine serum (FBS)). 200  $\mu$ L of the reporter cell suspension was dispensed into wells of white 96-well assay plates provided within the kit for a 4-6 h pre-incubation period at 37 °C and 5% CO $_2$ . At the end of the pre-incubation period, the culture media was discarded and 200  $\mu$ L of Compound Screening Medium (CSM: containing 10% charcoal stripped FBS) containing the requisite concentration of derivative to be evaluated was added to representative wells. Following a 22-24 h incubation at 37 °C and 5% CO $_2$ , the treatment media were discarded and 100  $\mu$ L of the provided Luciferase Detection Reagent was added to each well. Luminescence was quantified using a GloMax Explorer (Promega). Dose-response analyses of compounds were performed via non-linear curve-fitting with four parameters. Plots of relative light units vs. Log[compound, ( $\mu$ M)] were generated using GraphPad Prism software, which was also used to calculate EC $_{50}$  and SEM values. Unless otherwise noted, each compound evaluated was tested in three separate experiments in triplicate.

**Cellular thermal shift assay.** The cellular thermal shift assay (CETSA) was performed with MIO-M1 cells, a cell line derived from human retinal Müller glial cells, cultured in DMEM medium supplemented with 10% FBS. For an initial determination of the thermal melting profile of PPAR $\alpha$ , cells were dispensed into a 96-well PCR plate in the above medium (6000 cells/well/50

μl) and subjected to a temperature gradient (40-60 °C) for 10 min. Cold non-denaturing lysis buffer (PBS supplemented with 0.1% TritonX-100 and 1x protease inhibitors) was added to the wells, and the plate was rocked, and then incubated for 15 min on ice. Subsequently, centrifugation was performed at 14,000 rpm to sediment the unstable protein content. Supernatant was collected and loaded for SDS-PAGE, and immuno-detection was performed using an anti-PPAR $\alpha$  antibody. The PPAR $\alpha$  band was quantified on a LI-COR C-Digit Blot Scanner, and subsequently T<sub>agg</sub>(50) and T<sub>agg</sub>(75) values were calculated for PPAR $\alpha$ . In a subsequent run, cells were treated at various doses (1, 0.3, 0.1, 0.037, 0.012, 0.004 and 0.0014 μM) of FA, **4a** (A91) and **4u** together with DMSO controls, for 3 h. Cells were then subjected to heat shock at T<sub>agg</sub>(75) for 10 min, and unstable protein was removed by centrifugation. Following an immuno-blotting step, bands of stable PPAR $\alpha$  protein was quantified, normalized to loading control and plotted using GraphPad Prism software. EC<sub>50</sub> values of FA, **4a** (A91) and **4u** were calculated. Data obtained from a single experiment run in duplicate.

### 3.5.3 Pharmacokinetic Analyses

Studies were carried out by Eurofins Discovery Services. Experimental protocols presented below are pulled directly from company provided SOPs. All experiments were run in duplicate.

**Microsomal stability.** The following procedure is designed to determine the stability of a test compound in pooled liver microsomes from human or rat in a 96-well format. The test compound is quantified at five time points by HPLC-MS/MS analysis. The test compound was pre-incubated with pooled liver microsomes in phosphate buffer (pH 7.4) for 5 min in a 37 °C shaking water bath. The reaction was initiated by adding NADPH-generating system and incubated for 0, 15, 30, 45, and 60 min. The reaction is stopped by transferring the incubation mixture to acetonitrile/methanol. Samples are then mixed and centrifuged. Supernatants are used for HPLC-



MS/MS using selected reaction monitoring. The HPLC system consists of a binary LC pump with an autosampler, a C-18 column, and a gradient. Four reference compounds are tested in each assay. Propranolol and imipramine are relatively stable, whereas verapamil and terfenadine are readily metabolized. Peak areas corresponding to the test compound are recorded. The compound remaining is calculated by comparing the peak area at each time point to time zero. The half-life is calculated from the slope of the initial linear range of the logarithmic curve of compound remaining (%) vs. time, assuming first order kinetics. In addition, the intrinsic clearance ( $Cl_{int}$ ) is calculated from the half-life using the following equation:  $Cl_{int} = 0.693/(t_{1/2} \times [\text{protein}])$  and units are  $\mu\text{L}/\text{min}/\text{mg}$  protein. Human liver microsomes: mixed gender and pool of 50 donors; rat liver microsomes: male, Sprague-Dawley, pool of 100 or more.

**Time-dependent CYP inhibition.** The following procedure is designed to assess if a test compound displays time-dependent inhibition on cytochrome P450 activity in pooled human liver microsomes in a 96-well plate format. Test compounds were assessed at 10  $\mu\text{M}$  with 0.1% DMSO. The test compound was pre-incubated with human liver microsomes (mixed gender, pool of 50 donors, 1 mg/mL) in phosphate buffer (pH 7.4) for 30 min in a 37 °C shaking water bath. The pre-incubation is performed in two sets: in the presence and absence of NADPH-generating system, respectively. The reaction was then initiated by adding one volume of the pre-incubation mixture to nine volumes of a mixture of the substrate and the NADPH-generating system. The incubation was allowed for 10 min and stopped by transferring the reaction mixture to acetonitrile/methanol. Samples were mixed and centrifuged and supernatants used for HPLC-MS/MS analysis of the respective metabolite. Reference time dependent inhibitors were tested in each assay at multiple concentrations to obtain  $IC_{50}$  (concentration causing a half-maximal inhibition of the control value) values for both reaction conditions ( $\pm$ NADPH). Peak areas corresponding to the metabolite were

recorded. The percent of control activity was calculated by comparing the peak area in the presence of the test compound to the control samples containing the same solvent. Subsequently, the percent inhibition was calculated by subtracting the percent control activity from 100. The  $IC_{50}$  value was determined by non-linear regression analysis of the concentration-response curve using the Hill equation. Reference compounds: phenacetin (CYP1A), diclofenac (CYP2C9), omeprazole (CYP2C19), dextromethorphan (CYP2D6), and midazolam (CYP3A).

**hERG Automated Patch-Clamp.** The automated whole cell patch-clamp (Qpatch 48) technique was used to record outward potassium currents from a single cell. CHO-K1 (Chinese Hamster Ovary) cells stably transfected with human hERG cDNA were used. The cells were harvested by trypsinization and maintained in Serum Free Medium at room temperature before recording. The cells were washed and re-suspended in Extracellular Solution before being applied to the automated patch-clamp sites. The test solutions are prepared in the Extracellular Solution on the day of patch-clamp assay. The assay can tolerate up to 1% DMSO. Test compounds were assessed at three concentrations (0.1, 1 and 10  $\mu$ M). Intracellular Solution: 130 mM KCl, 10 mM NaCl, 1 mM  $MgCl_2$ , 10 mM EGTA, 5 mM MgATP, 10 mM HEPES (pH adjusted to 7.2 with KOH) Extracellular Solution: 137 mM NaCl, 4 mM KCl, 1.8 mM  $CaCl_2$ , 1 mM  $MgCl_2$ , 10 mM D(+)-Glucose, 10 mM HEPES (pH adjusted to 7.4 with NaOH) After whole cell configuration was achieved, the cell was held at -80 mV. A 50 ms pulse to -40 mV was delivered to measure the leaking current, which was subtracted from the tail current on-line. Then the cell was depolarized to +20 mV for 2 s, followed by a 1 s pulse to -40 mV to reveal the hERG tail current. This paradigm was delivered once every 5 s to monitor the current amplitude. The assay was conducted at room temperature. The Extracellular Solution (control) was applied first and the cell was stabilized in the solution for 5 min. Then the test compound was applied from low to high concentrations

sequentially on the same cell. The cells were incubated with each test concentration for 5 min. The reference compound E-4031 was tested concurrently at multiple concentrations to obtain an IC<sub>50</sub> value. The percent inhibition of hERG channel was calculated by comparing the tail current amplitude before and after application of the compound (the current difference was normalized to control).

***In vivo* retinal vascular permeability assay.** All *in vivo* experiments were performed in compliance with the NIH guidelines for the Care and Use of Animals and approved by the Institutional Animal Care and Use Committees at the University of Oklahoma Health Sciences Center. Brown Norway rats were purchased from Charles Rivers Laboratories (Wilmington, MA). Diabetes was induced in male Brown Norway rats (at the ages of 8 weeks) using an intraperitoneal injection of STZ (55 mg/kg of body weight). Diabetes was confirmed 3 days following STZ injection and rats with blood glucose levels higher than 350 mg/dl were used as diabetic rats. Two weeks following the STZ injection, the animals received daily injections of the compound for another 4 weeks, with the same volume vehicle as control. The rats were then used for retinal vascular permeability assay using Evan blue as tracer as described previously<sup>15</sup> and described as follows. At the study end-point, the animals were anesthetized by intraperitoneal injection of Ketamine (75 mg/kg, Zetamine™, MWI, Boise, ID) and Xylazine (10 mg/kg, AnaSed™, LA, MWI, Boise, ID). Evans blue (30 mg/ml) (Sigma-Aldrich, St. Louis, MO) was administered over 10 s through the femoral vein using 30G needle under microscopic inspection at the dosage of 1 µl/g body weight. The animals were placed on a warm pad for 2 hrs to ensure the complete circulation of Evans blue. The animals were perfused via the left ventricle with 1% paraformaldehyde in citrate buffer (pH 4.2), which was pre-warmed to 37°C to prevent vasoconstriction. Immediately after perfusion, the eyeball was enucleated, and the retina was

carefully dissected under an operating microscope. The retinal homogenate was incubated with formamide for 18 hrs at 70°C to extract the Evans blue. Then the extract was ultra-centrifuged (Optima TLX Ultracentrifuge, Beckman Coulter Inc., Brea, CA) at 80,000 rpm and 4°C for 30 minutes. The supernatant was used for measurement of absorbance at 620 nm with a spectrophotometer (DU-800 UV/Vis Spectrophotometer, the Lab World Group, Woburn, MA). Concentrations of Evans blue in the extracts were calculated based on a standard curve of Evans blue in formamide. The concentration of Evans blue was normalized by total protein concentration in the supernatant. The result of retinal vascular permeability was expressed in  $\mu\text{g}$  of Evans blue/mg of proteins. All values are expressed as mean  $\pm$  SD. Student's t-test was used to compare 2 groups, and P values less than 0.05 were considered statistically significant.

#### **3.5.4 Docking Protocols**

Molecular modelling and docking procedures were executed using the standard protocol implemented in Maestro Molecule Builder of Schrödinger,<sup>3,16</sup> version 11.9. File preparation and docking protocol was completed as follows:

**Protein Preparation.** The desired crystal structure (PDB: 2P54) was obtained from the Protein Data Bank and prepared with Schrödinger's *Protein Preparation Wizard* software. Proteins were preprocessed by assigning bond orders using the ccd database, adding hydrogens, creating zero-bond order to metals, creating disulfide bonds, filling missing side chains and loops using *Prime*, deleting water molecules beyond 5 Å, and generating Het state using *Epik* pH  $7 \pm 2$ . Het -COOH was modified to  $\text{COO}^-$ . Structural refinement was done employing H-bond assignment by sampling water orientations, minimizing hydrogens of altered species at pH 7.0, and restraining minimization based on the OPLS3 force field. All remaining parameters were kept as default settings.

**Ligand Preparation.** SMILES files of each ligand were loaded into Schrödinger's *LigPrep* software. Ligand preparation employed the OPLS3 force field. Ionization states for pH  $7.0 \pm 2$  were generated with *Epik*. Ligands were desalted and tautomers were generated. Chirality specified in the ligand input file was retained.

**Receptor Grid Generation.** i) Receptor tab: select the native ligand and show markers, set the Van der Waals scaling factor to 1.0 with a partial charge cut off of 0.25. In advanced settings, select read from the input structure file and Force field OPLS3. ii) Site tab: Select centroid of workspace ligand, and dock ligand with length  $< 10 \text{ \AA}$ . In advanced settings set the box length =  $10 \text{ \AA}$ . iv) Constraints tab: H-Bond Tyr 464, His-440, Tyr-314 and Ser-280; v) Rotatable Groups tab: select all in the grid box.

**Ligand Docking.** Docking studies of compounds were performed using Schrödinger's *Glide* docking module from suite 2017-4. Docking was executed with the following parameters: Using partial charge input, scaling of Van der Waal radii with a scaling factor of 0.8 and partial charge cut off of 0.15, with XP precision, sample nitrogen inversion, sample ring conformation, bias sampling of torsion for amide group only, add *Epik* state penalties to docking score, OPLS3 force field with no constraints selected.

**Metabolism Prediction.** Metabolism prediction studies were performed using Schrödinger's P450 Site of Metabolism module. After conducting *Ligand Preparation* (see above), compound **4b** was subjected to metabolism prediction studies with 2C9, 2D6, and 3A4. For these calculations, default parameters were held constant. The algorithm calculates reactivity of each ligand based on Hammett and Taft linear free energy schemes for these promiscuous P450 enzymes, which are believed to be the most independent on structural restrictions. The software then subjects the ligand of interest to induced-fit docking (2C9 and 2D6) to identify possible sites

of metabolism based on Fe-accessibility. Intrinsic reactivity and site of metabolism data is then output as 1) Fe-accessibility, 2) Intrinsic reactivity, 3) and overall SOM score (the linear combination of the accessibility and the intrinsic reactivity), which identifies the major predicted sites of P450 metabolism.

### 3.6 References

1. Dou, X. Z.; Nath, D.; Shin, Y.; Ma, J. X.; Duerfeldt, A. S., Structure-Guided Evolution of a 2-Phenyl-4-Carboxyquinoline Chemotype into Ppar-Alpha Selective Agonists: New Leads for Oculovascular Conditions. *Bioorg. Med. Chem. Lett.* **2018**, *28*, 2717-2722.
2. Bernardes, A.; Souza, P. C. T.; Muniz, J. R. C.; Ricci, C. G.; Ayers, S. D.; Parekh, N. M.; Godoy, A. S.; Trivella, D. B. B.; Reinach, P.; Webb, P.; Skai, M. S.; Polikarpov, I., Molecular Mechanism of Peroxisome Proliferator-Activated Receptor Alpha Activation by Wy14643: A New Mode of Ligand Recognition and Receptor Stabilization. *J. Mol. Biol.* **2013**, *425*, 2878-2983.
3. Capelli, D.; Cerchia, C.; Montanari, R.; Loiodice, F.; Tortorella, P.; Laghezza, A.; Cervoni, L.; Pochetti, G.; Lavecchia, A., Structural Basis for Ppar Partial or Full Activation Revealed by a Novel Ligand Binding Mode. *Sci. Rep.* **2016**, *6*, No. 34792.
4. Gangwal, R. P.; Damre, M. V.; Das, N. R.; Sharma, S. S.; Sangamwar, A. T., Biological Evaluation and Structural Insights for Design of Subtype-Selective Peroxisome Proliferator Activated Receptor-Alpha (Ppar-Alpha) Agonists. *Bioorg. Med. Chem. Lett.* **2015**, *25*, 270-275.
5. Li, J.; Kennedy, L. J.; Shi, Y.; Tao, S.; Ye, X. Y.; Chen, S. Y.; Wang, Y.; Hernandez, A. S.; Wang, W.; Devasthale, P. V.; Chen, S.; Lai, Z.; Zhang, H.; Wu, S.; Smirk, R. A.; Bolton, S. A.; Ryono, D. E.; Zhang, H.; Lim, N. K.; Chen, B. C.; Locke, K. T.; O'Malley, K. M.; Zhang, L.; Srivastava, R. A.; Miao, B.; Meyers, D. S.; Monshizadegan, H.; Search, D.; Grimm, D.; Zhang, R.; Harrity, T.; Kunselman, L. K.; Cap, M.; Kadiyala, P.; Hosagrahara, V.; Zhang, L.; Xu, C.; Li,

Y. X.; Muckelbauer, J. K.; Chang, C.; An, Y.; Krystek, S. R.; Blonar, M. A.; Zahler, R.; Mukherjee, R.; Cheng, P. T.; Tino, J. A., Discovery of an Oxybenzylglycine Based Peroxisome Proliferator Activated Receptor Alpha Selective Agonist 2-((3-((2-(4-Chlorophenyl)-5-Methyloxazol-4-Yl)Methoxy)Benzyl)(Methoxycarbonyl)Amino)Acetic Acid (Bms-687453). *J. Med. Chem.* **2010**, *53*, 2854-2864.

6. Mizuno, C. S.; Ma, G.; Khan, S.; Patny, A.; Avery, M. A.; Rimando, A. M., Design, Synthesis, Biological Evaluation and Docking Studies of Pterostilbene Analogs inside Pparalpha. *Bioorg. Med. Chem.* **2008**, *16*, 3800-3808.

7. Nomura, M.; Tanase, T.; Ide, T.; Tsunoda, M.; Suzuki, M.; Uchiki, H.; Murakami, K.; Miyachi, H., Design, Synthesis, and Evaluation of Substituted Phenylpropanoic Acid Derivatives as Human Peroxisome Proliferator Activated Receptor Activators. Discovery of Potent and Human Peroxisome Proliferator Activated Receptor Alpha Subtype-Selective Activators. *J. Med. Chem.* **2003**, *46*, 3581-3599.

8. Sierra, M. L.; Beneton, V.; Boullay, A. B.; Boyer, T.; Brewster, A. G.; Donche, F.; Forest, M. C.; Fouchet, M. H.; Gellibert, F. J.; Grillot, D. A.; Lambert, M. H.; Laroze, A.; Le Grumelec, C.; Linget, J. M.; Montana, V. G.; Nguyen, V. L.; Nicodeme, E.; Patel, V.; Penfornis, A.; Pineau, O.; Pohin, D.; Potvain, F.; Poulain, G.; Ruault, C. B.; Saunders, M.; Toum, J.; Xu, H. E.; Xu, R. X.; Pianetti, P. M., Substituted 2-[(4-Aminomethyl)Phenoxy]-2-Methylpropionic Acid Pparalpha Agonists. 1. Discovery of a Novel Series of Potent Hdlc Raising Agents. *J. Med. Chem.* **2007**, *50*, 685-695.

9. Xu, H. E.; Lambert, M. H.; Montana, V. G.; Plunket, K. D.; Moore, L. B.; Collins, J. L.; Oplinger, J. A.; Kliewer, S. A.; Gampe, R. T., Jr.; McKee, D. D.; Moore, J. T.; Willson, T. M., Structural

Determinants of Ligand Binding Selectivity between the Peroxisome Proliferator-Activated Receptors. *Proc. Natl. Acad. Sci. U.S.A.* **2001**, *98*, 13919-13924.

10. Zhao, S.; Kanno, Y.; Li, W.; Sasaki, T.; Zhang, X.; Wang, J.; Cheng, M.; Koike, K.; Nemoto, K.; Li, H., Identification of Picrasidine C as a Subtype-Selective Ppara Agonist. *J. Nat. Prod.* **2016**, *79*, 3127-3133.

11. Pirat, C.; Farce, A.; Lebegue, N.; Renault, N.; Furman, C.; Millet, R.; Yous, S.; Speca, S.; Berthelot, P.; Desreumaux, P.; Chavatte, P., Targeting Peroxisome Proliferator-Activated Receptors (Ppars): Development of Modulators. *J. Med. Chem.* **2012**, *55*, 4027-4061.

12. Schonherr, H.; Cernak, T., Profound Methyl Effects in Drug Discovery and a Call for New C-H Methylation Reactions. *Angew. Chem. Int. Ed.* **2013**, *52*, 12256-12267.

13. Molina, D. M.; Jafari, R.; Ignatushchenko, M.; Seki, T.; Larsson, E. A.; Dan, C.; Sreekumar, L.; Cao, Y.; Nordlund, P., Monitoring Drug Target Engagement in Cells and Tissues Using the Cellular Thermal Shift Assay. *Science* **2013**, *341*, 84-87.

14. Babic, I.; Kesari, S.; Nurmammedov, E., Cellular Target Engagement—a New Paradigm in Drug Discovery. *Future Med. Chem.* **2018**, *10*, 1641-1644.

15. Zhang, S. X.; Ma, J. X.; Sima, J.; Y., C.; Hu, M. S.; Otlecz, A.; Lambrou, G. N., Genetic Difference in Susceptibility to the Blood-Retina Barrier Breakdown in Diabetes and Oxygen-Induced Retinopathy. *Am J. Pathol.* **2005**, *166*, 313-321.

16. Friesner, R. A.; Murphy, R. B.; Repasky, M. P.; Frye, L. L.; Greenwood, J. R.; Halgren, T. A.; Sanschagrin, P. C.; Mainz, D. T., Extra Precision Glide: Docking and Scoring Incorporating a Model of Hydrophobic Enclosure for Protein-Ligand Complexes. *J. Med. Chem.* **2006**, *49*, 6177-6196.



## Appendix 2 Supporting Information to Chapter 3

### PPAR $\alpha$ luciferase two-concentration assessment

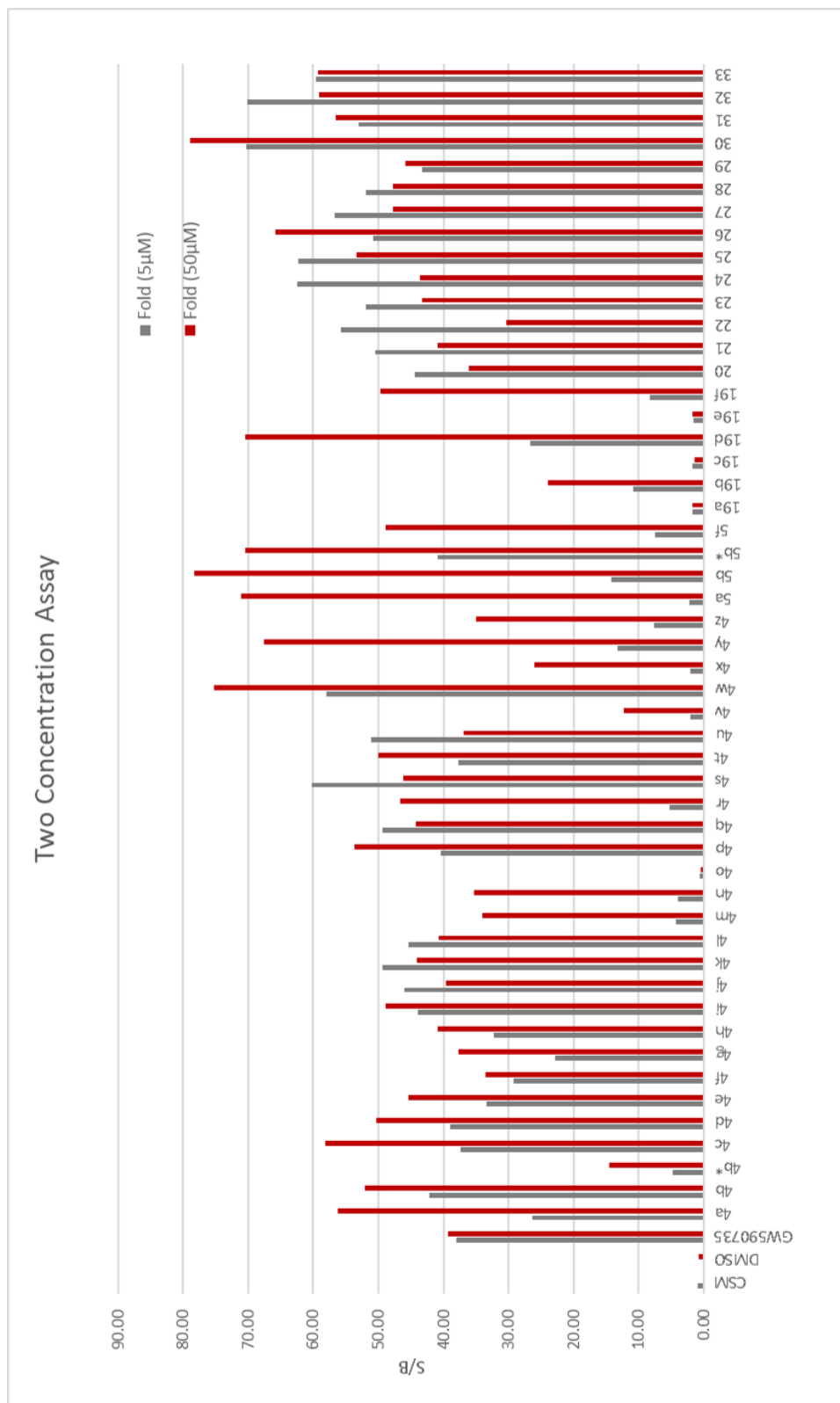


**Figure 1. Initial two-concentration assessment of 4a-4z, 5a, 5b, 5b\*, 5f, 20a-20f, and 21-34 for PPAR $\alpha$  agonism in a luciferase-based cellular assay (Indigo). Results presented from a single experiment as mean signal/mean background (S/B). GW590735 was evaluated at 5  $\mu$ M and 40  $\mu$ M due to observed cytotoxicity at higher concentrations.**

## Isothermal calorimetry

ITC experiments were performed using a MicroCal PEAQ ITC (MicroCal Inc., Northampton, MA, USA). PPAR $\alpha$  was concentrated down to a final concentration of 3.27 mg/mL using an Amicon Ultra-15 centrifugal concentrator (Millipore). Buffer (20 mM HEPES, 150 mM NaCl, pH 7.4) was used to dilute the ligand stock solution (10, 12.5, or 25 mM in DMSO). DMSO was added to the protein solution at the same percentage (0.8-10%) of the ligand solution. Samples were centrifuged before the experiment to eliminate possible aggregates. The protein solution (30-85  $\mu$ M) was placed in the sample cell, and the ligand solution (2.3-15 times more concentrated than the protein) was loaded into the syringe injector. The detailed experimental parameters are shown below. The titrations involved 19 injections of 2  $\mu$ L at 150 s intervals or 13 injections of 3  $\mu$ L at 150 s intervals. The experiment was set at 25  $^{\circ}$ C and the syringe stirring speed was set at 750 rpm. Titration of ligand at same concentration into buffer with same percentage DMSO were used as a reference control. The thermodynamic data were processed with MicroCal PEAQ-ITC Analysis Software provided by Malvern. The one-site binding model was selected to calculate the value of the dissociation constant ( $K_d$ ), the enthalpy ( $\Delta H$ ), the binding free energy ( $\Delta G$ ), and the entropy ( $-T\Delta S$ ).

Ligand	[PPAR $\alpha$ ] $\mu$ M	[Ligand] nM	DMSO% (v/v)
<b>3.4a (A91)</b>	85	0.2	0.8%
<b>3.4b</b>	60	0.5	2%
<b>3.4u</b>	30	0.25	2%
<b>GW590735</b>	80	0.5	2%

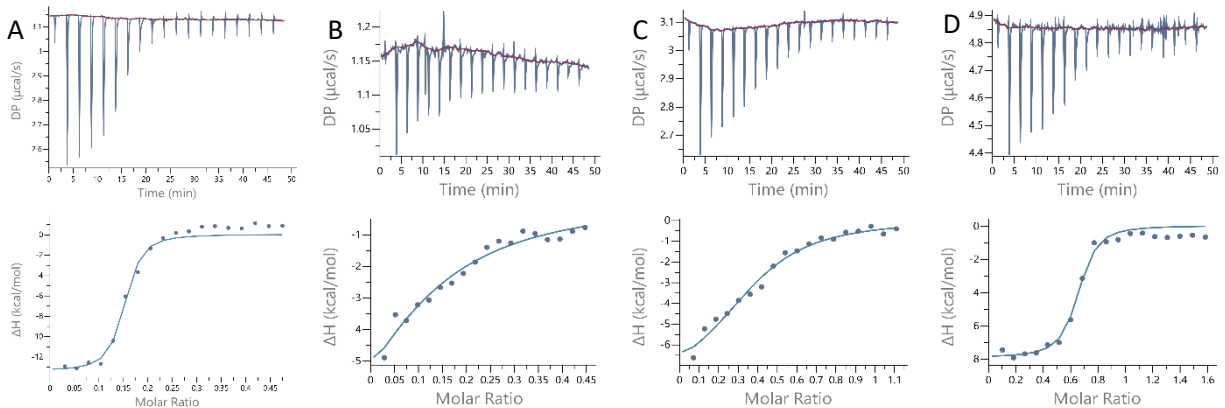


**Figure S2. Isothermal titration calorimetry thermograms of select ligands to PPAR $\alpha$ -LBD.** The upper panel shows the raw data of a representative ITC experiment. The lower panel shows the corresponding binding isotherm fit according to the “one binding site” model. A) GW590735; B) compound **3.4a**; C) compound **3.4b**; and D) compound **3.4u**.

### Protein expression and purification

Protein was expressed from the pET28c vector (Novagen) in *Escherichia coli* strain Rosetta<sup>TM</sup> (DE3) grown in LB media to an OD of 0.6 and then induced with 1 mM IPTG for 20 h at 18 °C. Cells were harvested and resuspended in Buffer A (20 mM Tris, 150 mM NaCl, 5% glycerol, 5 mM imidazole, pH 8.0) at 5 ml/g pellet weight. Cultures were lysed using an Emulsiflex C-3 homogenizer (Avestin), and the lysate clarified by centrifugation (22,000  $\times$  g, 40 min). The supernatant was loaded onto a 5ml HisTrap FF Crude column (GE Life Sciences) and eluted with a linear gradient of 5-500 mM imidazole over 20 column volumes. Fractions containing PPAR $\alpha$  were identified by sodium dodecyl sulfate–polyacrylamide gel electrophoresis analysis. The His-Tag was removed by thrombin cleavage (10 U thrombin/mg) dialyzed overnight at 4 °C against buffer B (20 mM Tris, 150 mM NaCl, 5% glycerol, pH 8.0). The uncleaved protein was removed by reloading the sample onto the 5 ml HisTrap FF Crude column (GE Life Sciences). The flow through was concentrated to a final volume of 5 ml using an Amicon Ultra-15 centrifugal concentrator (Millipore), and loaded on to a HiLoad Superdex 200PG size exclusion

chromatography column (GE Life Sciences) pre-equilibrated with Buffer C (20 mM HEPES, 150 mM NaCl, pH 7.4).

### CETSA data

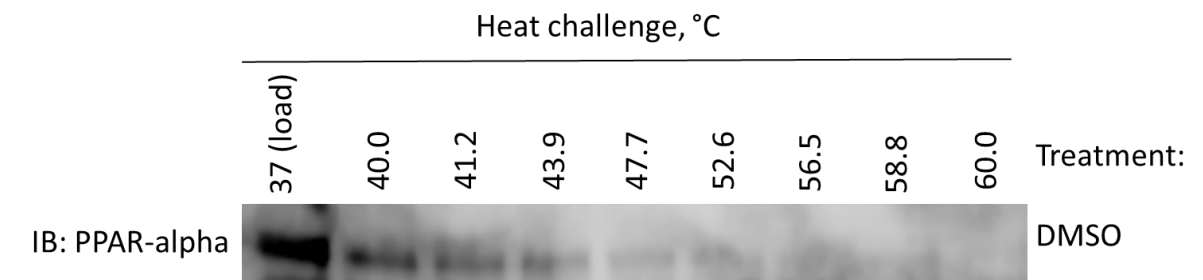


**Figure S3. Melting profile of hPPAR $\alpha$ .** MIO-M1 cells were subjected to a heat gradient to determine the thermal melting profile of hPPAR $\alpha$ . Band intensity of remaining stable protein at each temperature was quantified, and subsequently the temperature of aggregation ( $T_{agg50}$  and  $T_{agg75}$ ) was determined as 40.8 °C and 45.5 °C, respectively.

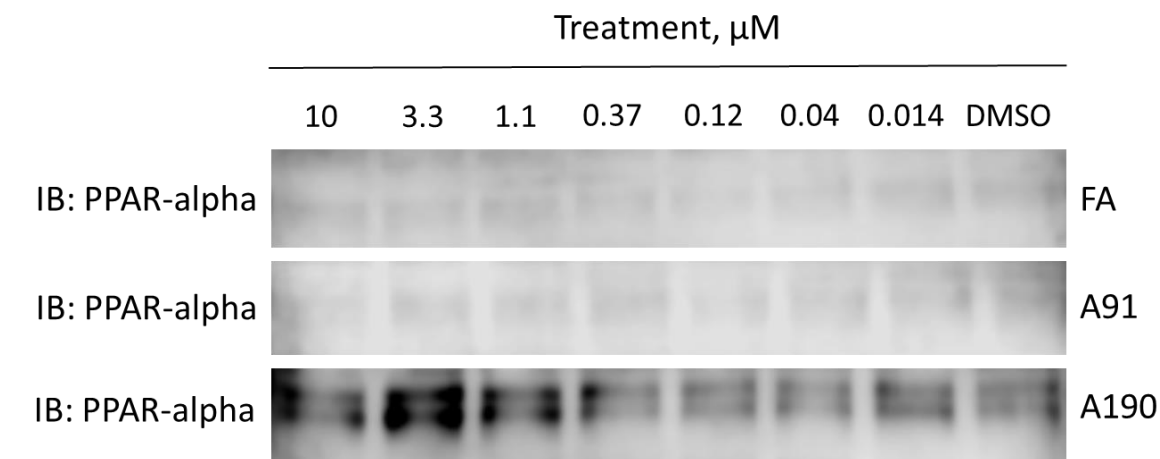


**Figure S4. Dose-response CETSA at 45.5 °C.** MIO-M1 cells treated with increasing doses of inhibitors were subjected to heat challenge at  $T_{agg75}$  of 45.5 °C. Band intensity of remaining stabilized protein at each dose was quantified, and subsequently the  $EC_{50}$  for each inhibitor was determined.

### LDH Cytotoxicity Data

661W mouse photoreceptor cells were cultured on 96-well plate (6700 cells per well) with varying concentrations of DMSO, GW7647, or A91 (0 to 200  $\mu$ M) to induce cytotoxicity. Following overnight incubation with the compounds, culture media from the 96-well plate was collected for the LDH quantification assay, which performed following the manufacturer's

instructions (Thermo Scientific, #88953). In short, 50  $\mu\text{L}$  of culture medium was mixed and incubated with 50  $\mu\text{L}$  of Reaction Mixture at 25  $^{\circ}\text{C}$  for 30 minutes. 50  $\mu\text{L}$  of Stop Solution was added and the absorbance was measured at 490 nm and 680 nm. Cell death (percentage of maximum LDH release control) was then determined following the manufacturer's protocols.

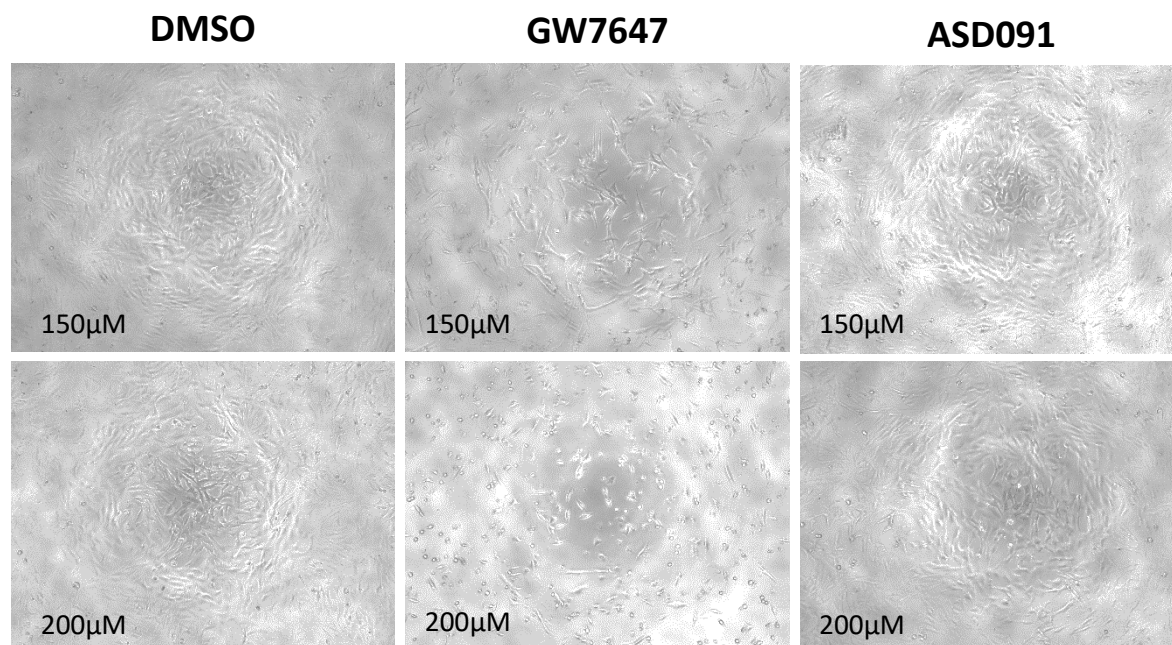


**Figure S5.** Cellular morphology after compound treatment under light microscopy. Unlike GW7647, ASD091-treated cells did not exhibit any obvious signs of cellular morphology changes at all concentrations tested.

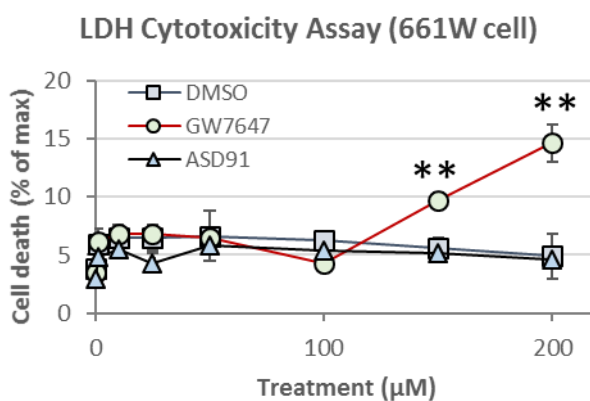


**Figure S6.** Cytotoxicity of A91 (3.4a) in a retinal epithelium photoreceptor cell-line 661W. LDH activities were measured to determine dose-dependent cytotoxicity of ASD091. No significant

LDH activities were detected in all concentrations of ASD091 tested, whereas GW7647 began to induce cell death 150  $\mu$ M (mean  $\pm$  SD;  $n=3$ ). \*\* $P<0.01$ .

### *In silico* Metabolic Predictions

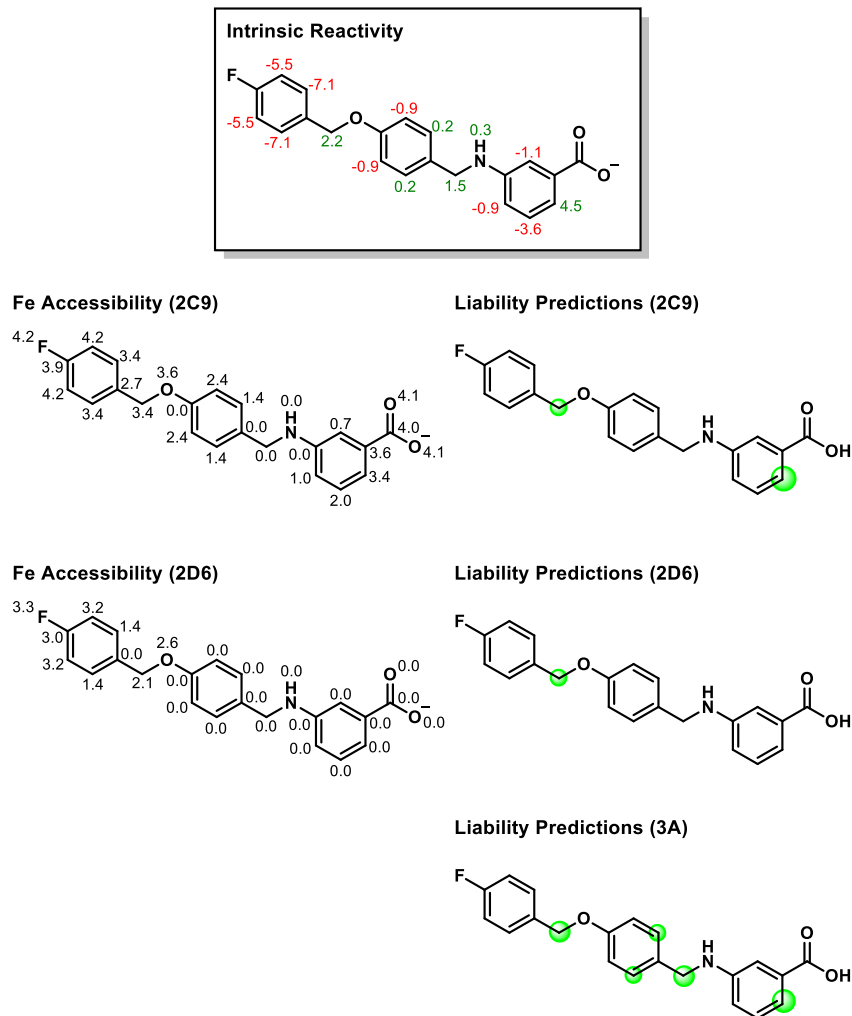
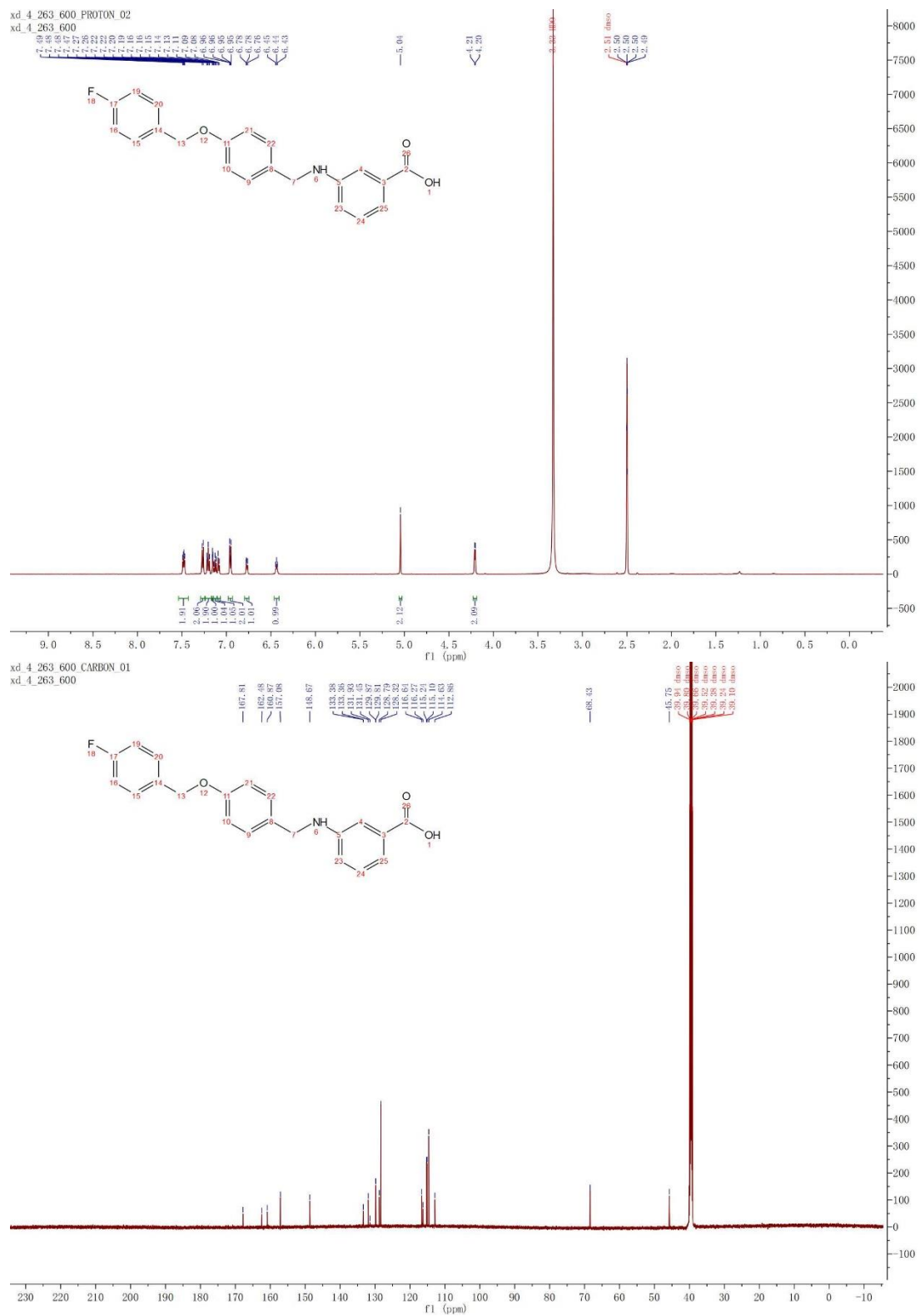


**Figure S7.** *In silico* metabolic predictions determined by Schrodinger's P450 Site of Metabolism Module. Predictions calculated for **3.4b** against 2C9, 2D6, and 3A4 CYPs. Components are described as transcribed directly from the manufacturer's manual. **Intrinsic Reactivity** = atoms are labeled with the intrinsic reactivity calculated with Hammett and Taft methodology. Positive values are predicted to be more reactive, negative values are predicted to be less reactive. **Fe Accessibility** = atoms are labeled with accessibility to the iron. This is defined as the natural logarithm of the number of poses for the atom in which the atom was within 5 Å of Fe. Larger values indicate greater accessibility. **Liability Predictions** = linear combination of the accessibility and the intrinsic reactivity. Results are displayed as green circles, in which the radius is proportional to the score. Larger circles mean higher reactivity.

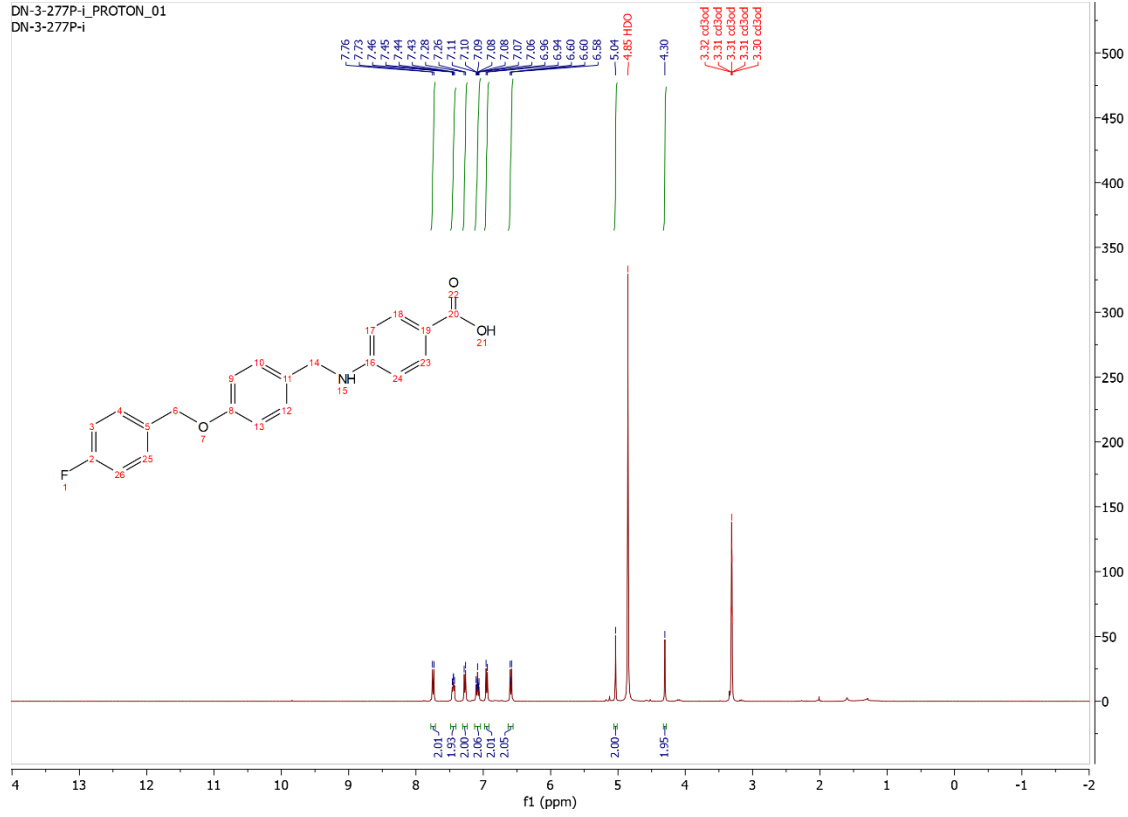
# Final compound <sup>1</sup>H and <sup>13</sup>C NMR spectra

## 3.4b

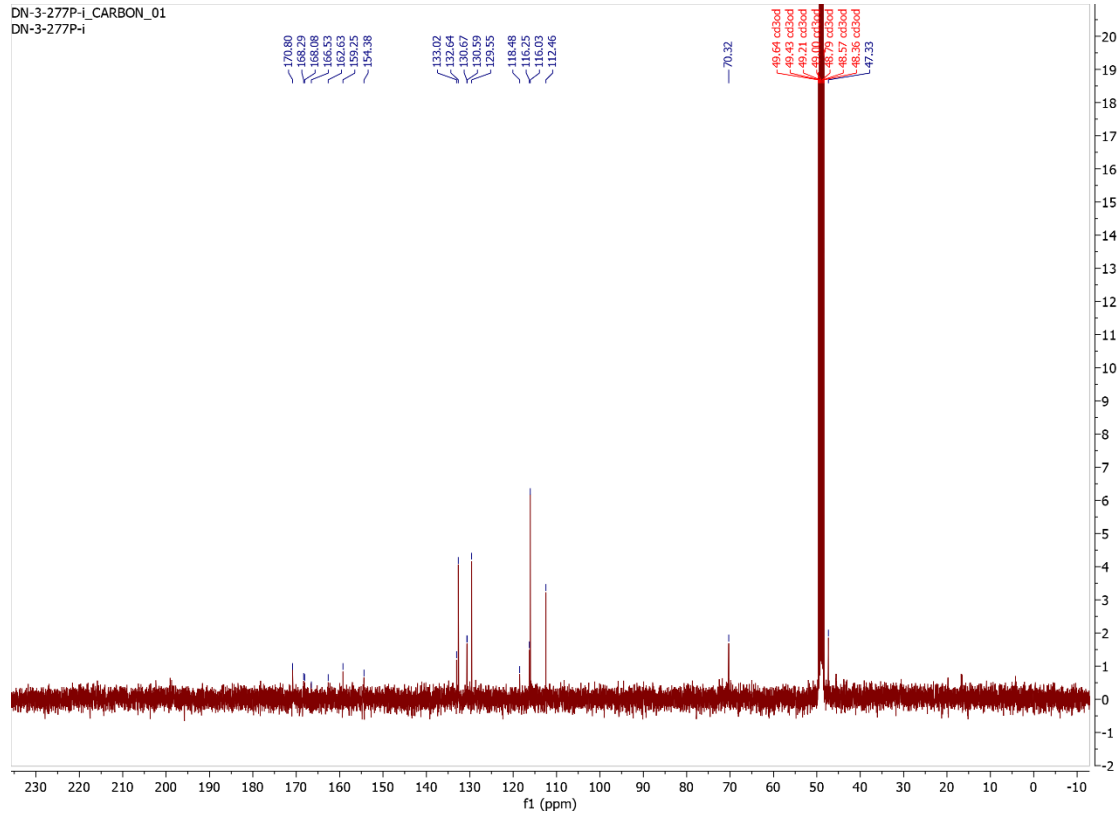


### 3.4b\*

DN-3-277P-i\_PROTON\_01  
DN-3-277P-i



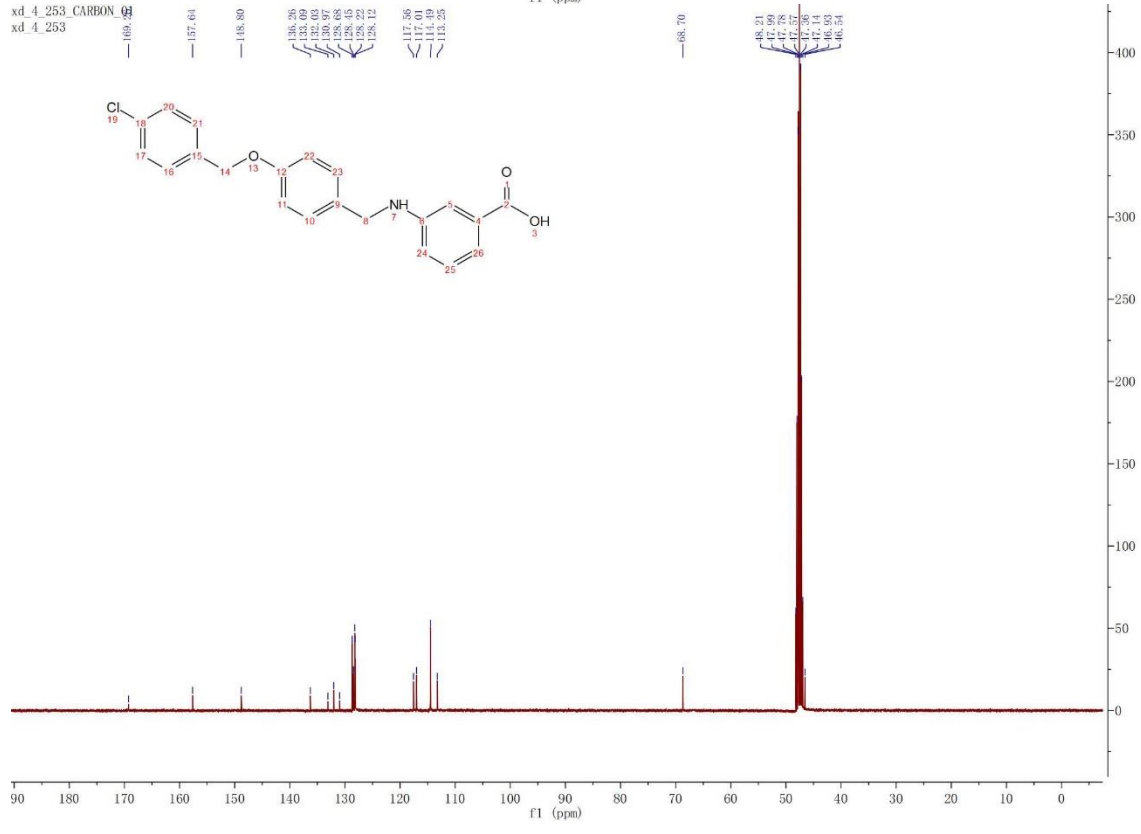
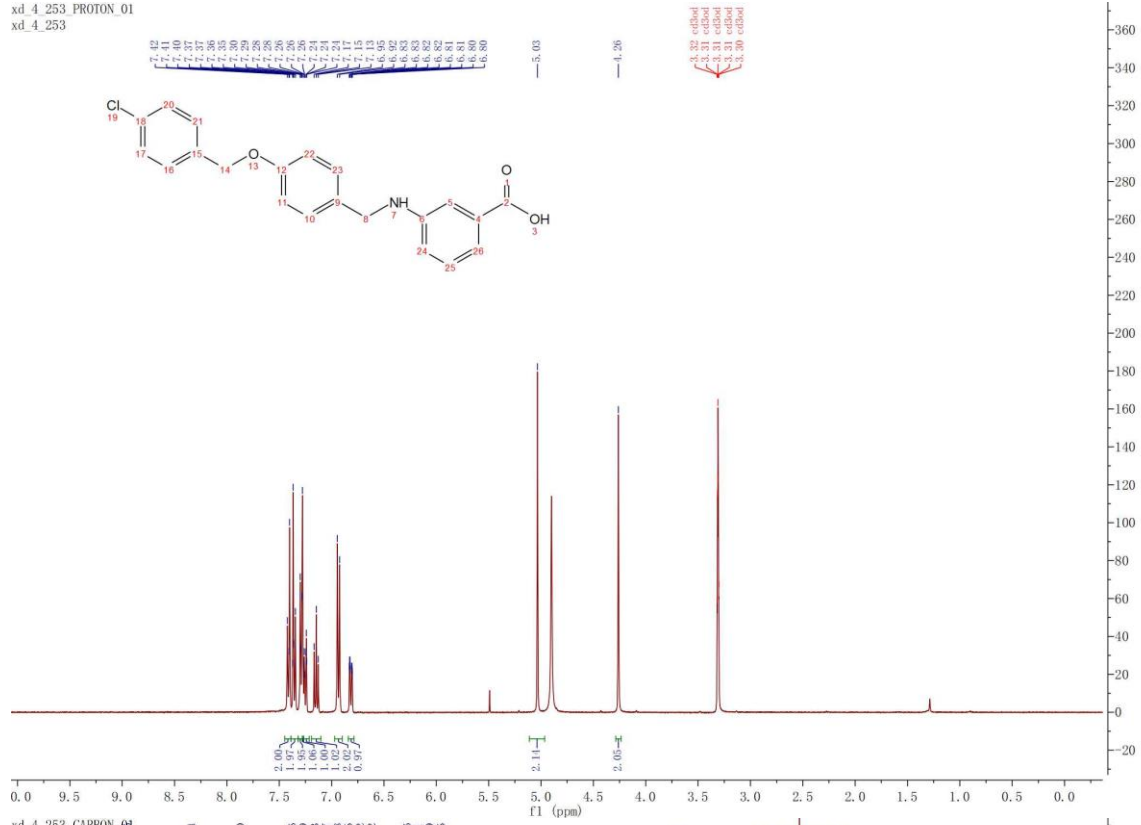
DN-3-277P-i CARBON\_01  
DN-3-277P-i





# 3.4c

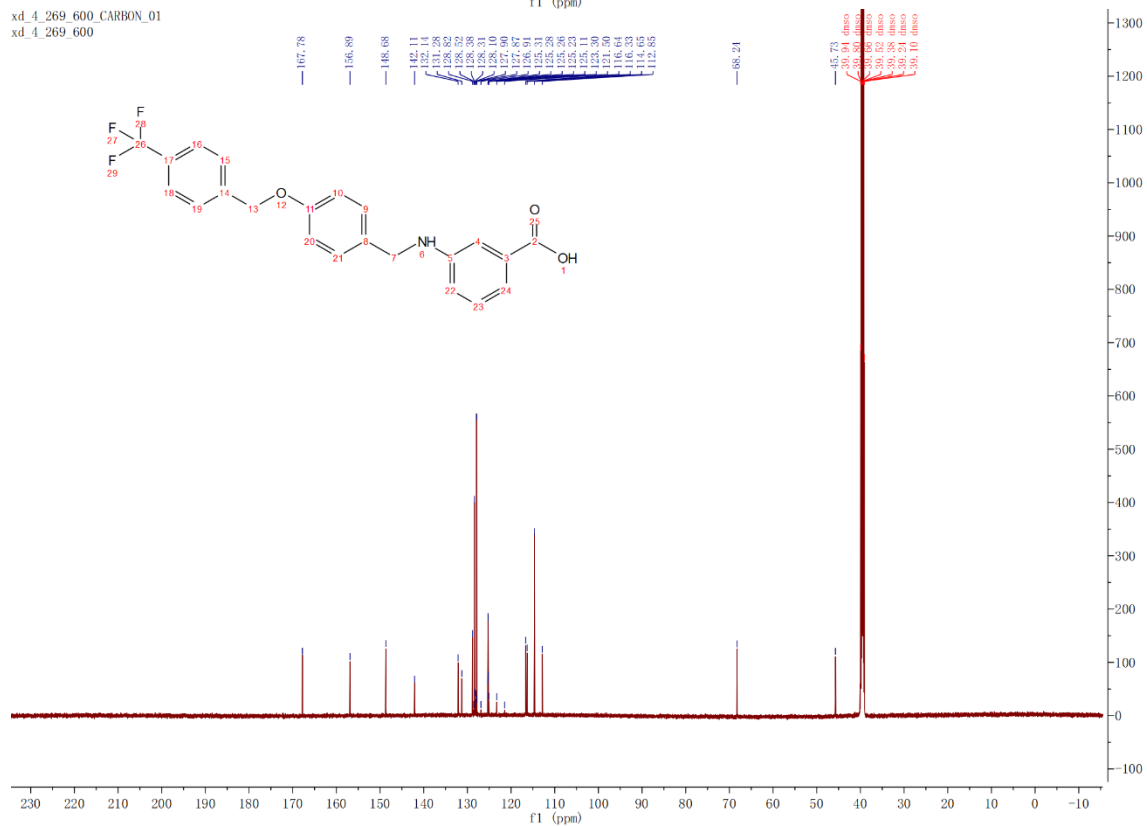
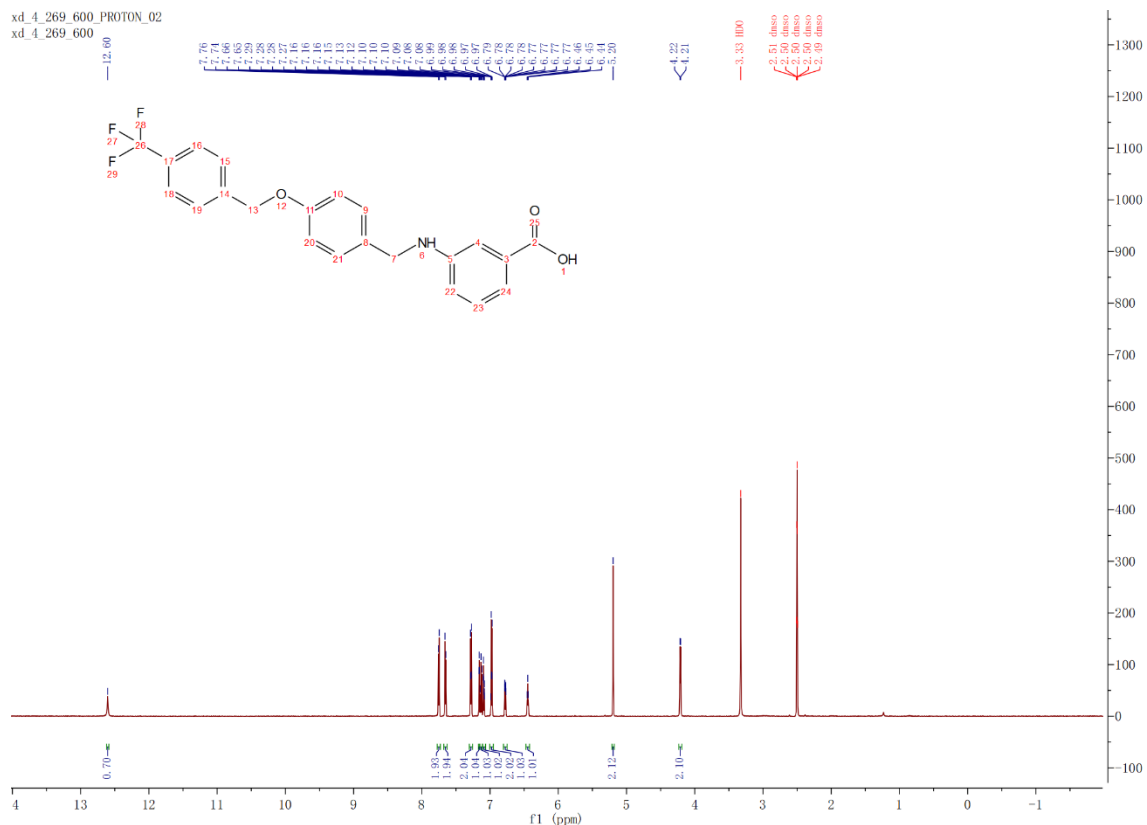
xd\_4\_253 PROTON\_01  
xd\_4\_253







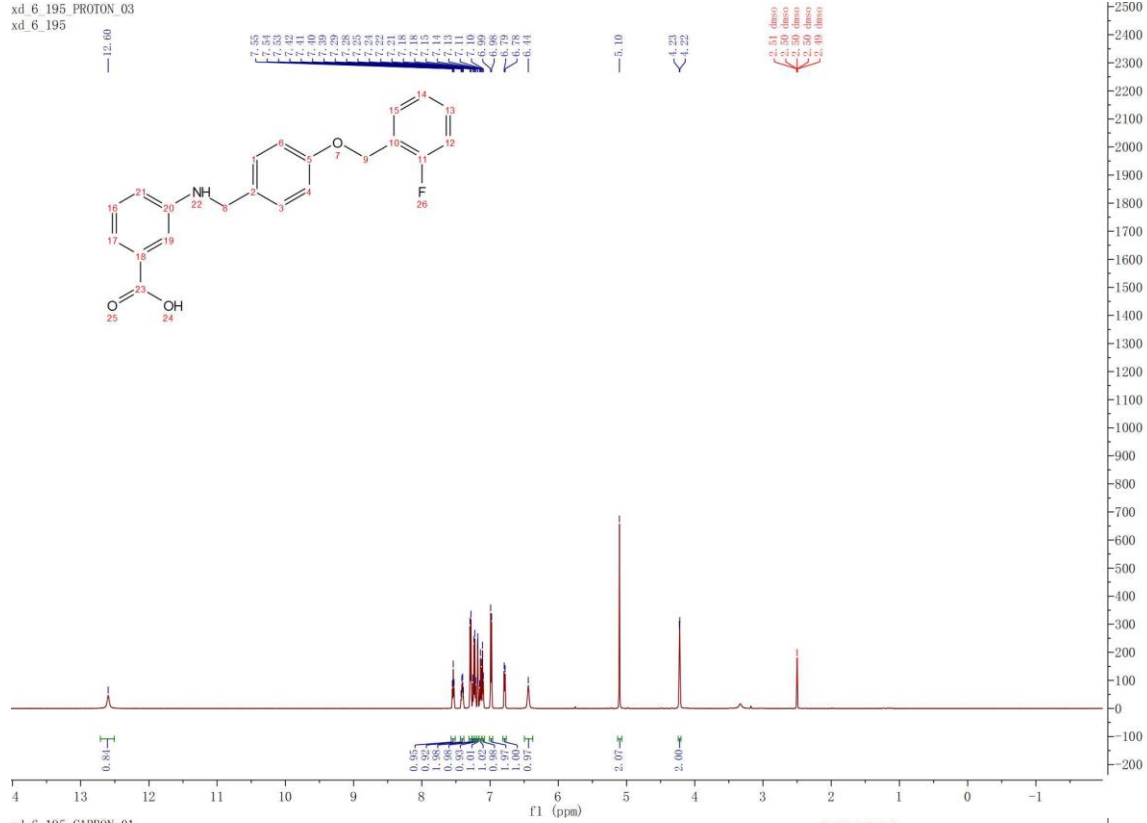
# 3.4f



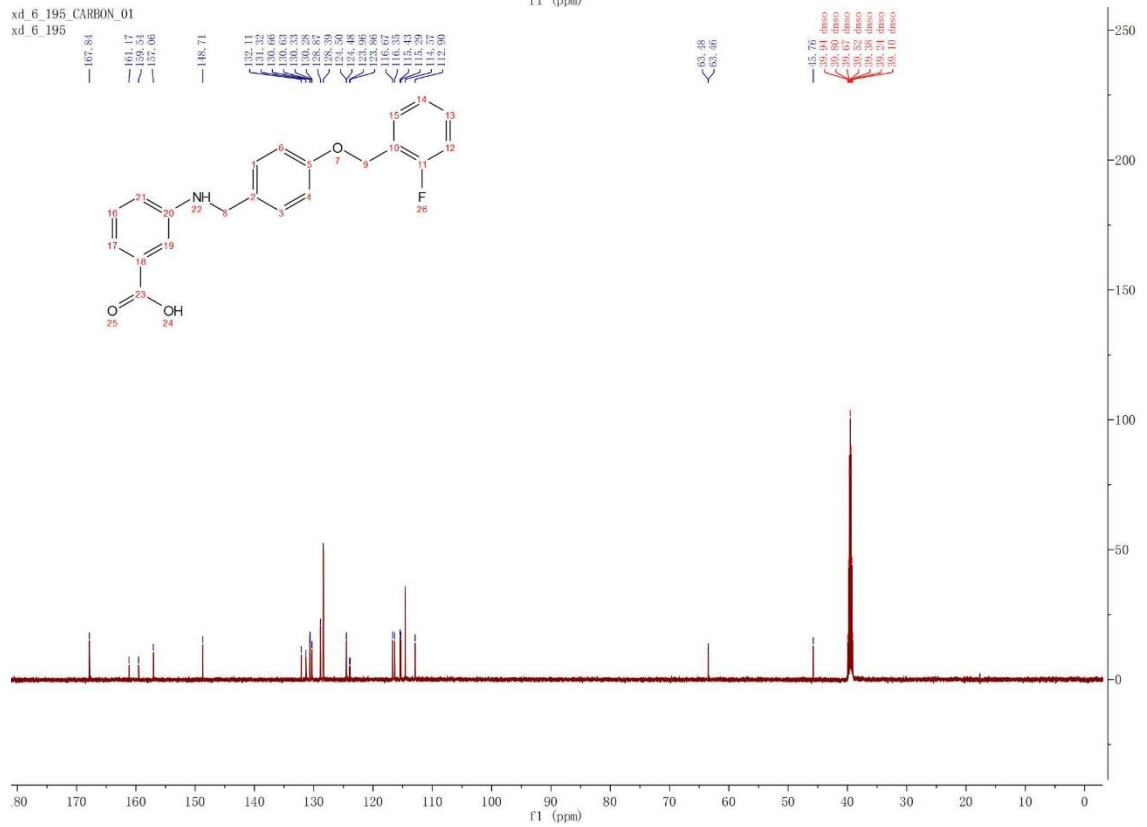


### 3.4h

xd\_6\_195 PROTON\_03  
 xd\_6\_195



xd\_6\_195 CARBON\_01  
 xd\_6\_195



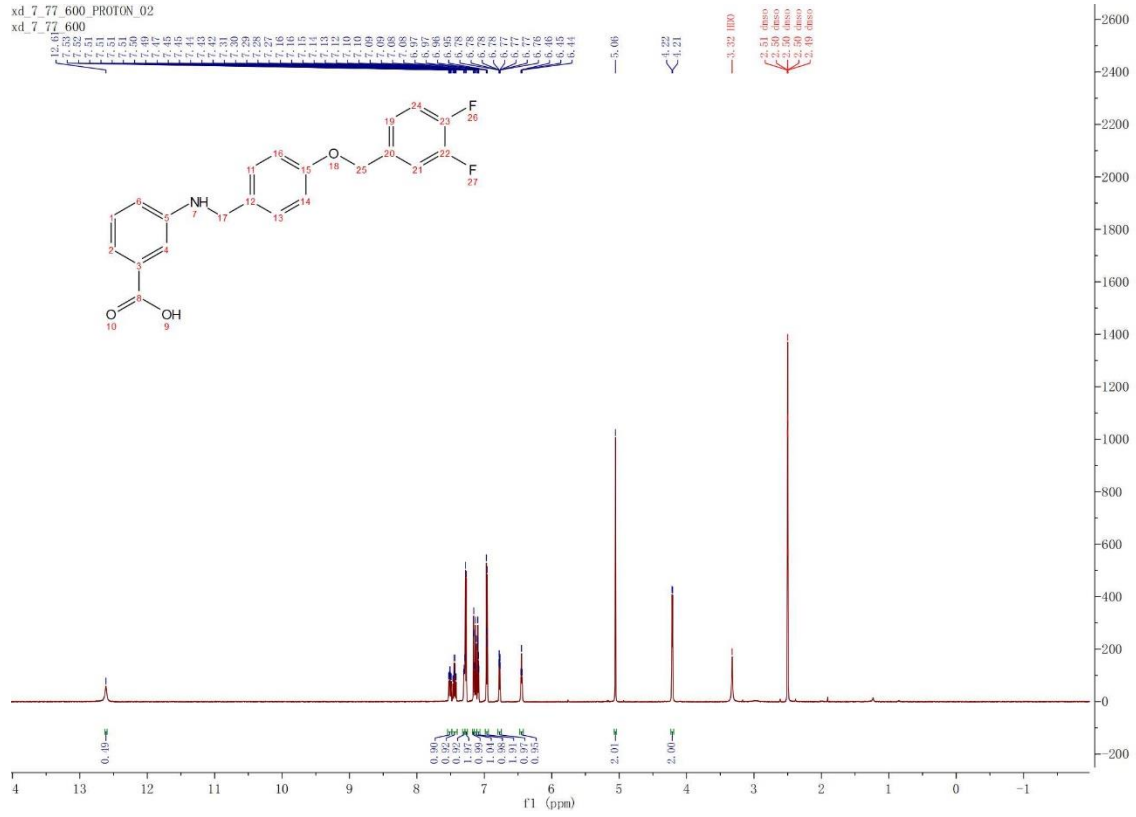




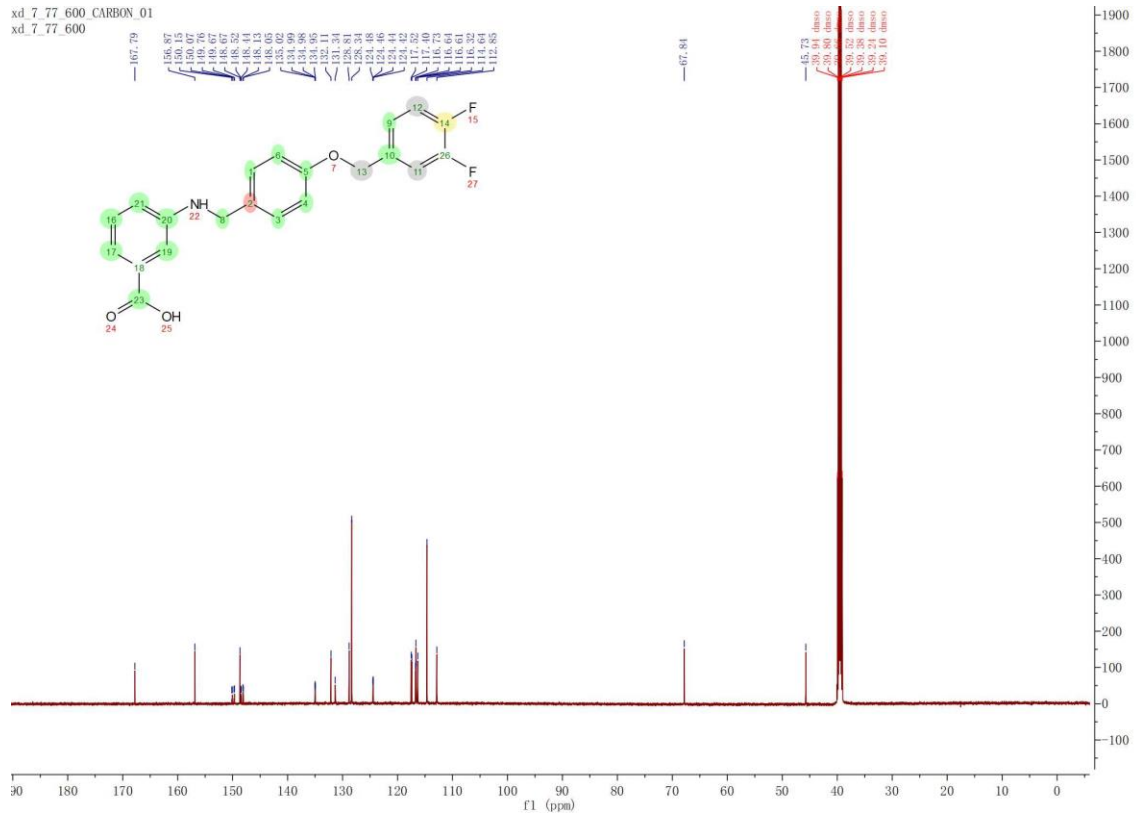


# 3.4k

xd\_7\_77\_600 PROTON\_02  
 xd\_7\_77\_600



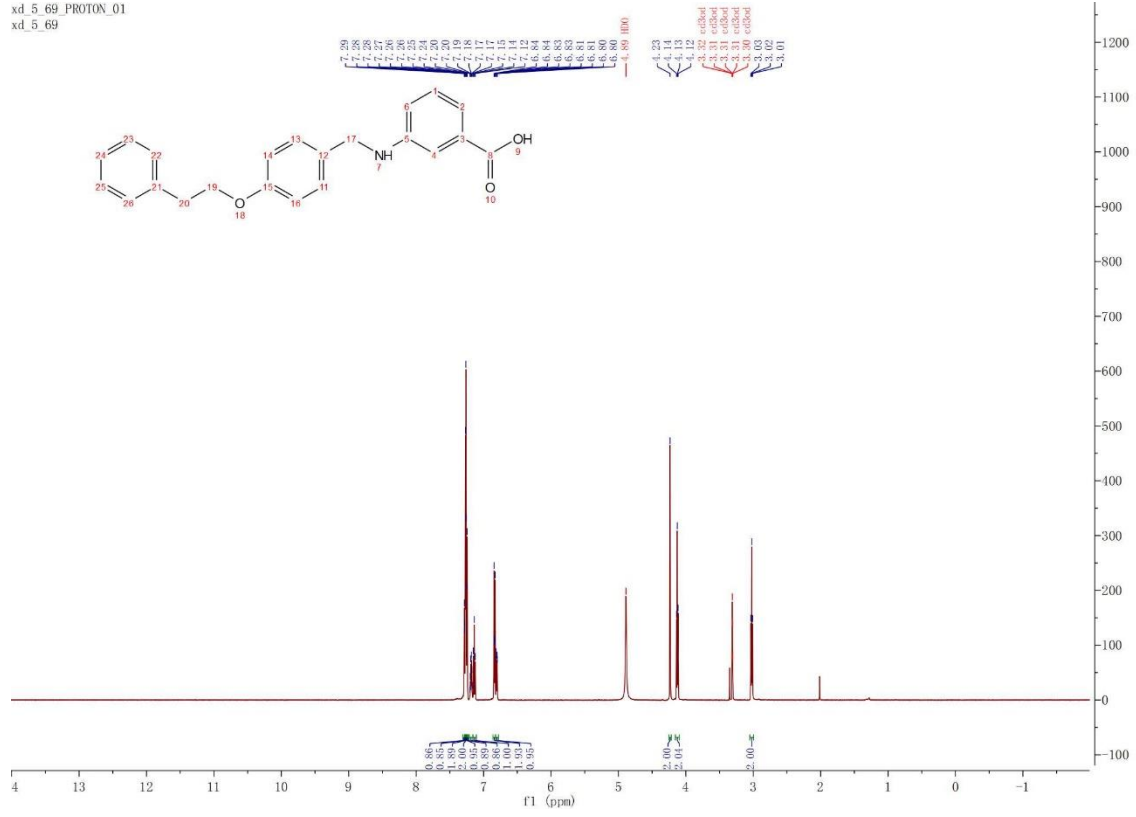
xd\_7\_77\_600 CARBON\_01  
 xd\_7\_77\_600



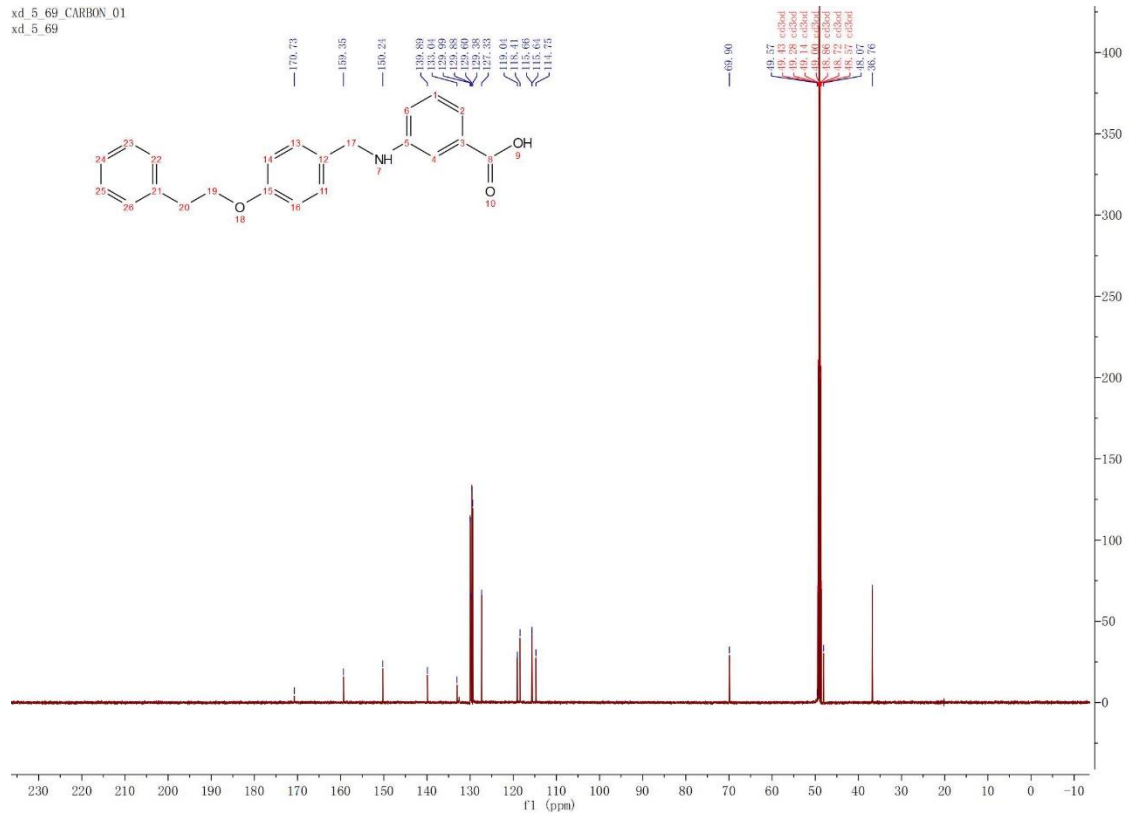


# 3.4m

xd\_5\_69\_PROTON\_01  
xd\_5\_69

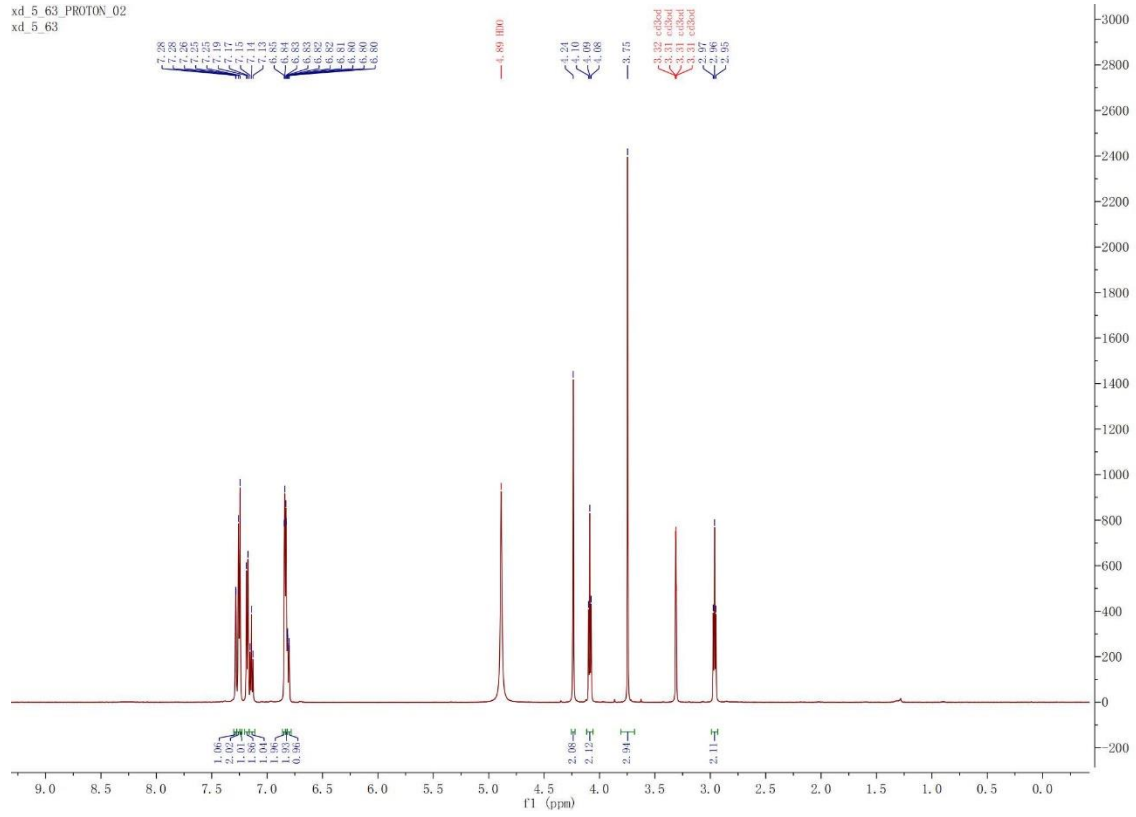


xd\_5\_69\_CARBON\_01  
xd\_5\_69

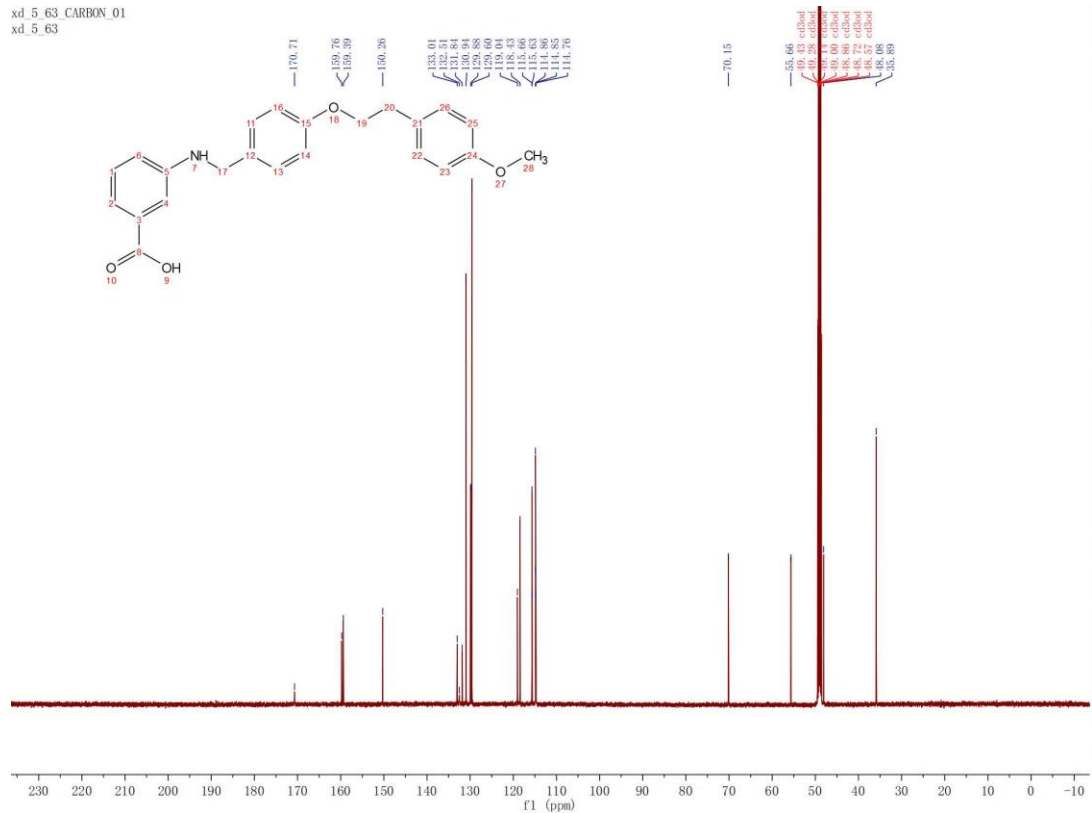


# 3.4n

xd\_5\_63\_PROTON\_02  
xd\_5\_63

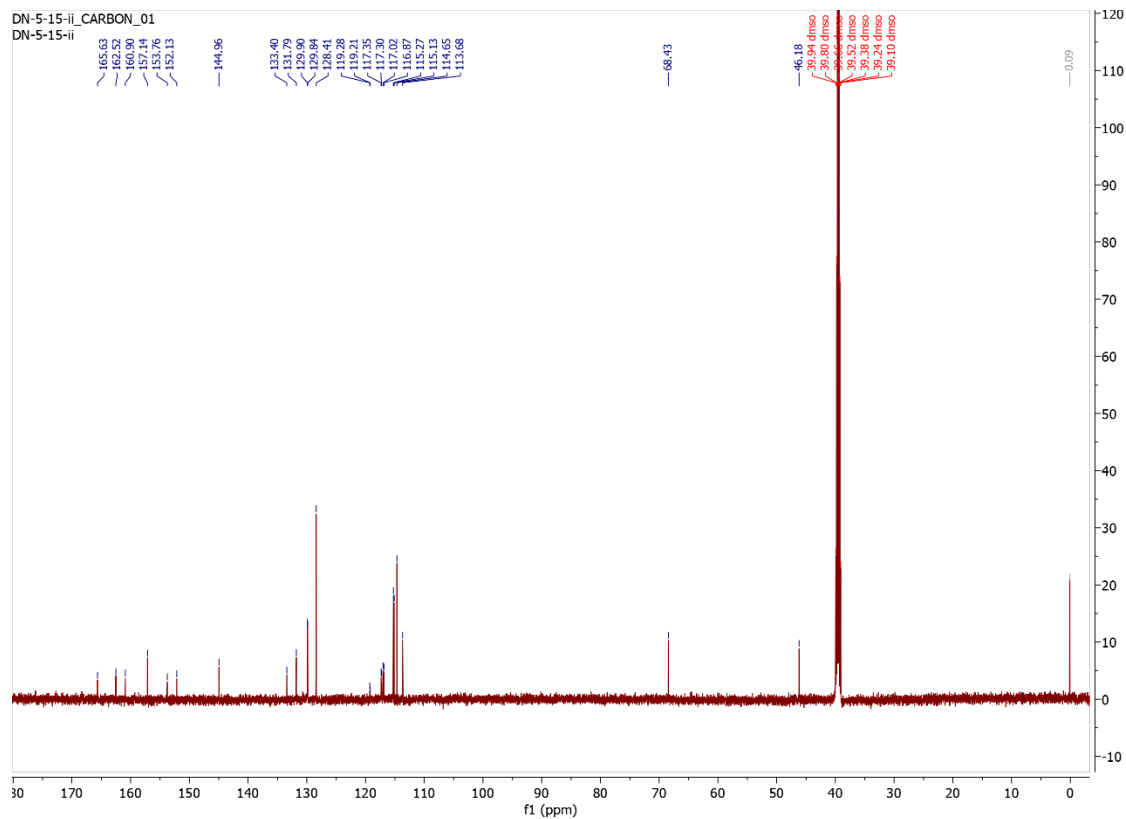
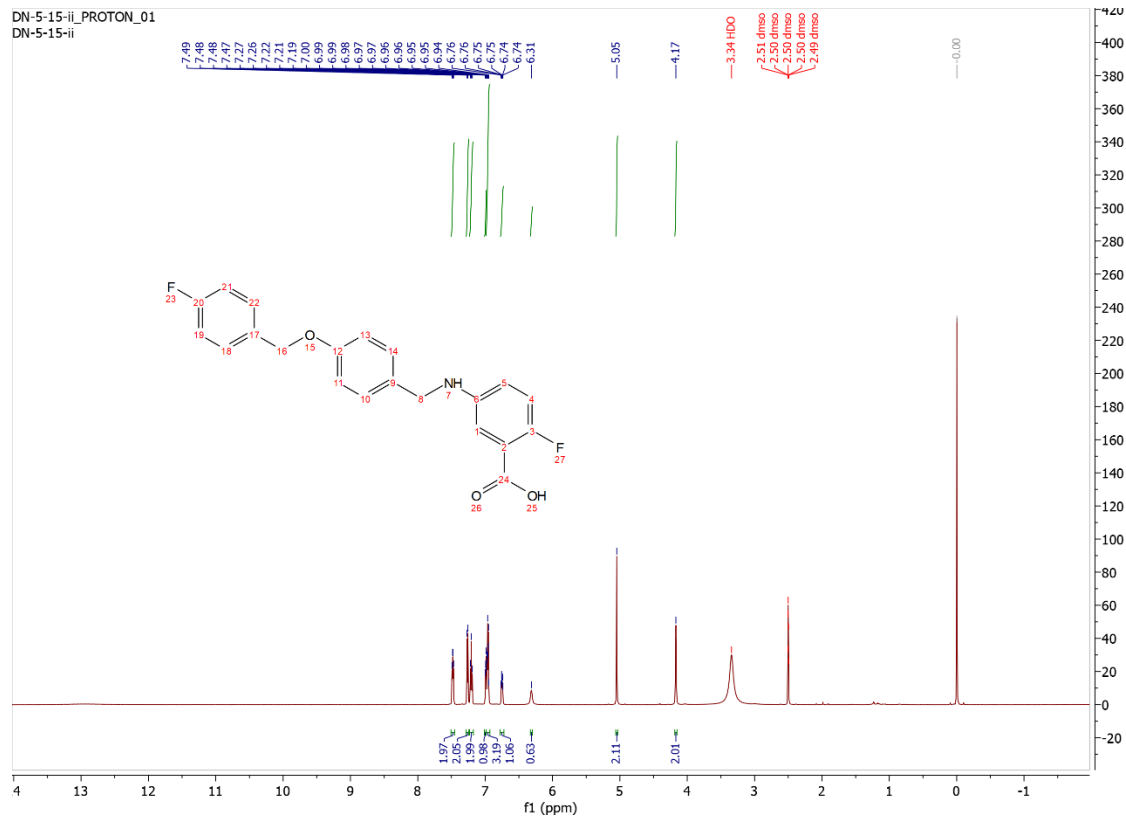


xd\_5\_63\_CARBON\_01  
xd\_5\_63

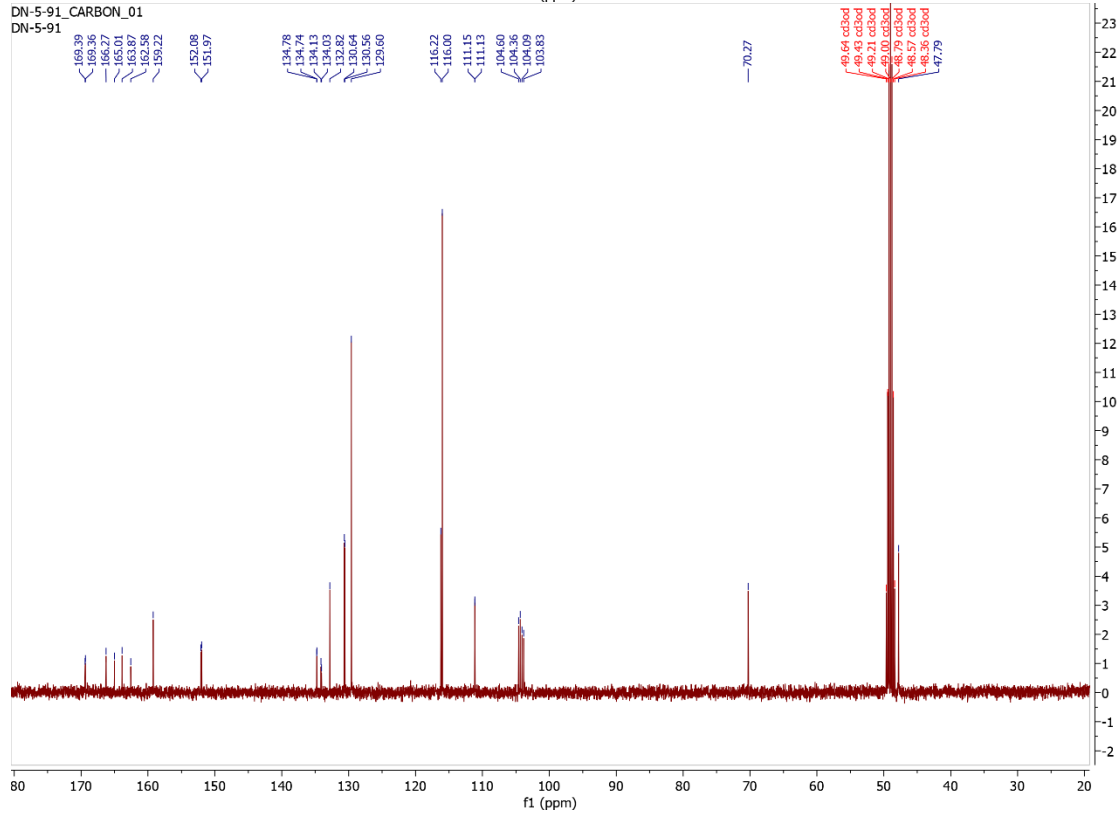
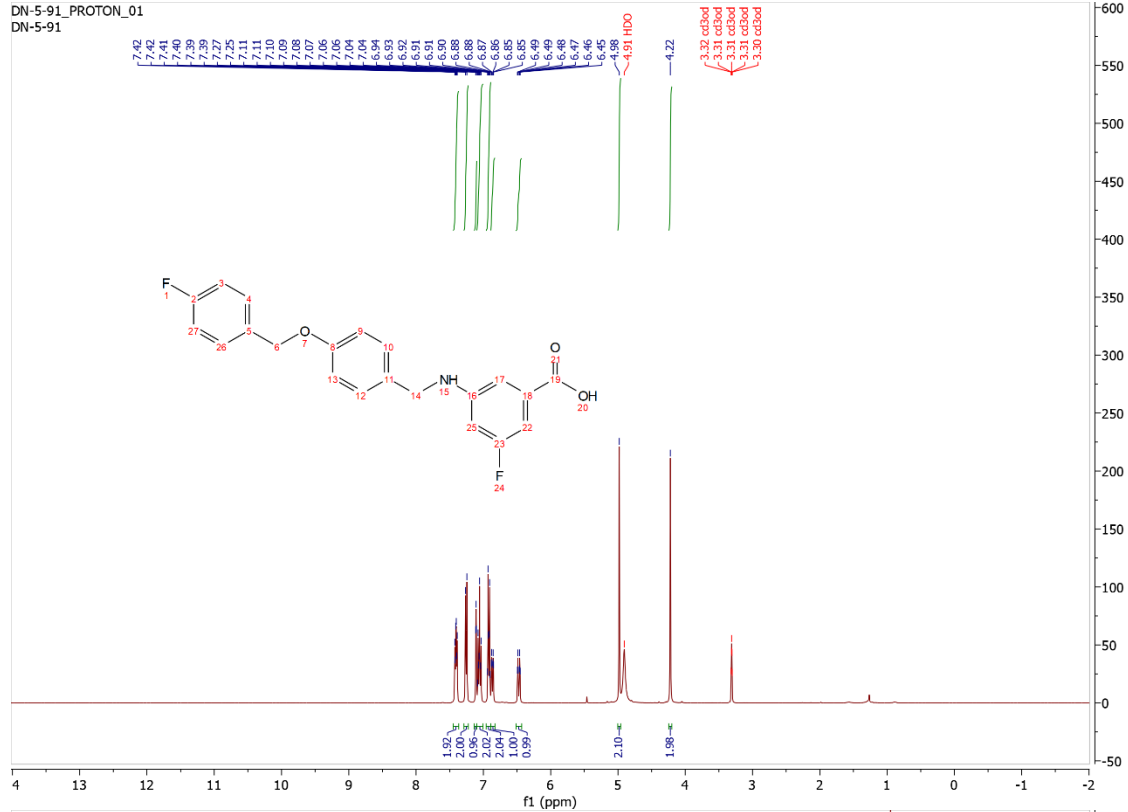




### 3.4p

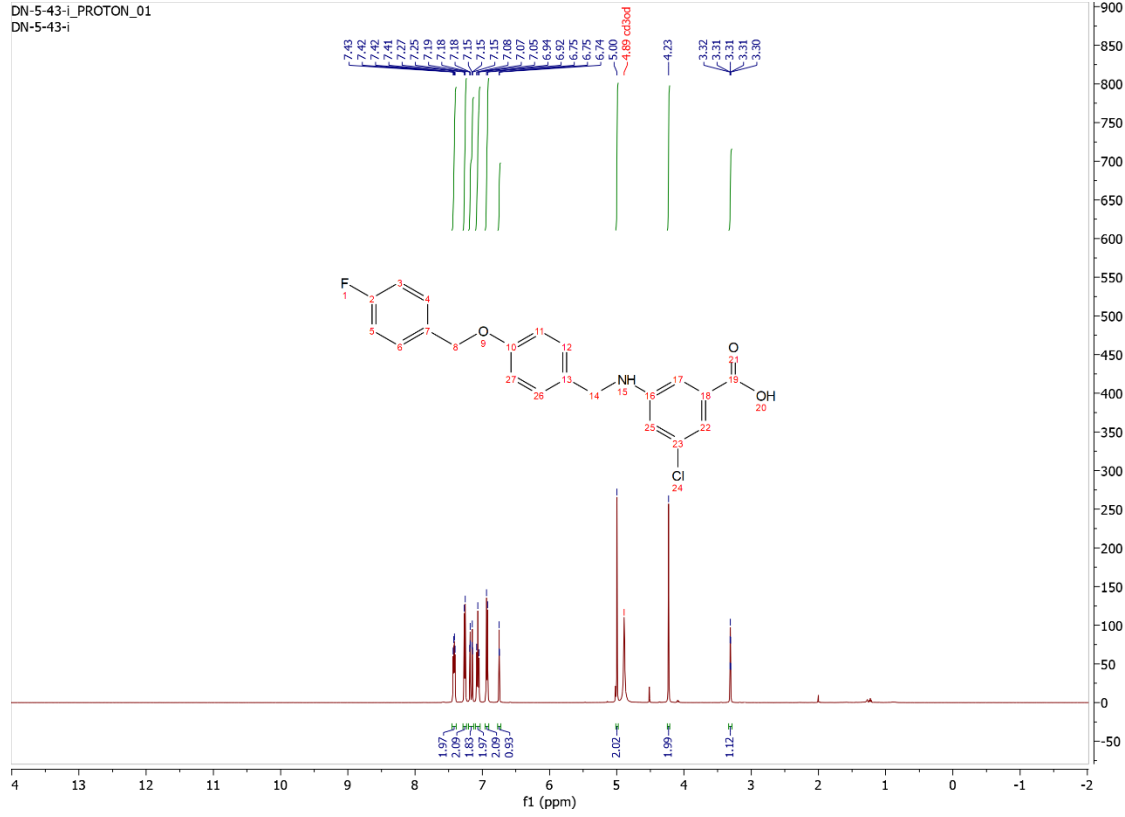


# 3.4q

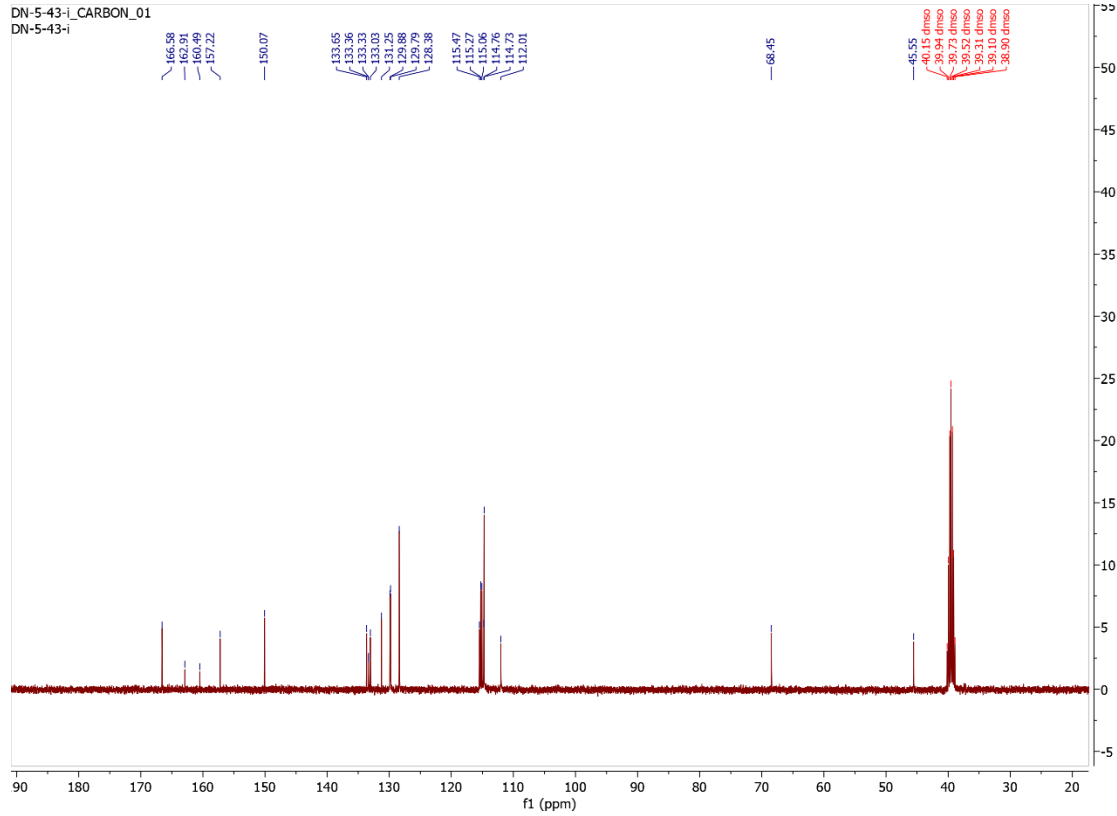


# 3.4r

DN-5-43-i\_PROTON\_01  
DN-5-43-i

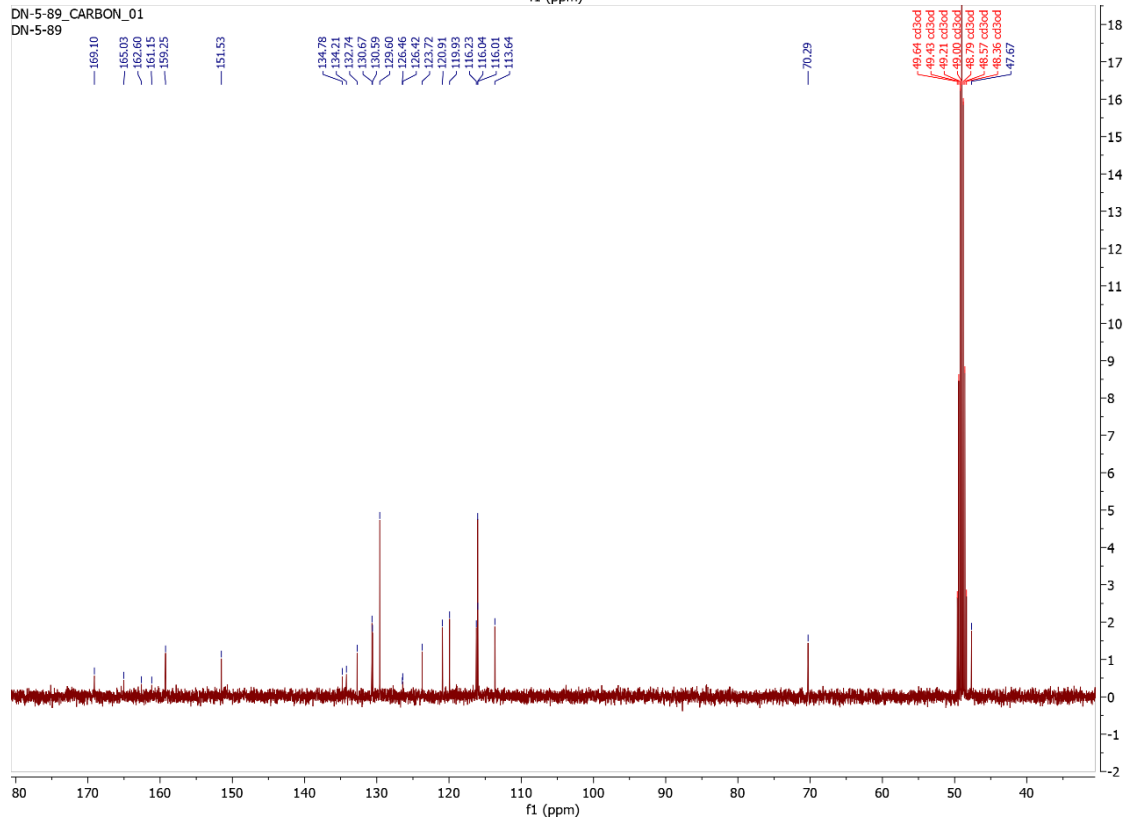
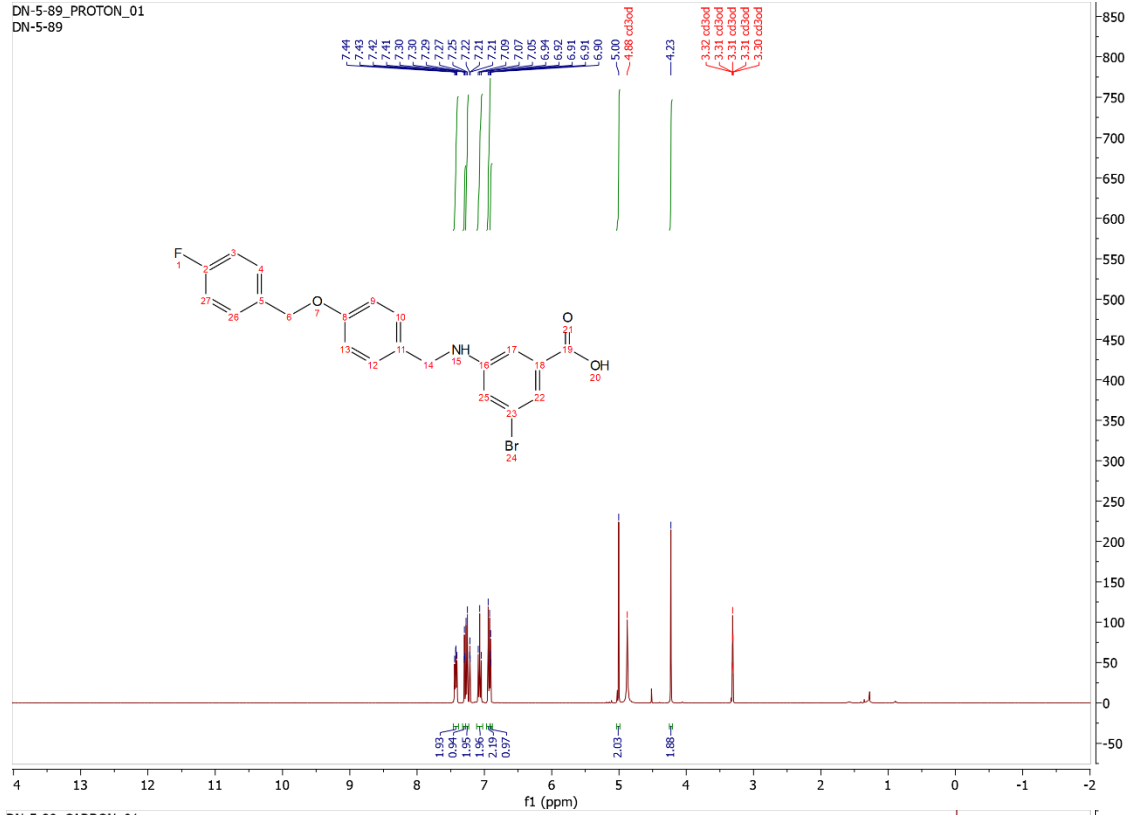


DN-5-43-i\_CARBON\_01  
DN-5-43-i



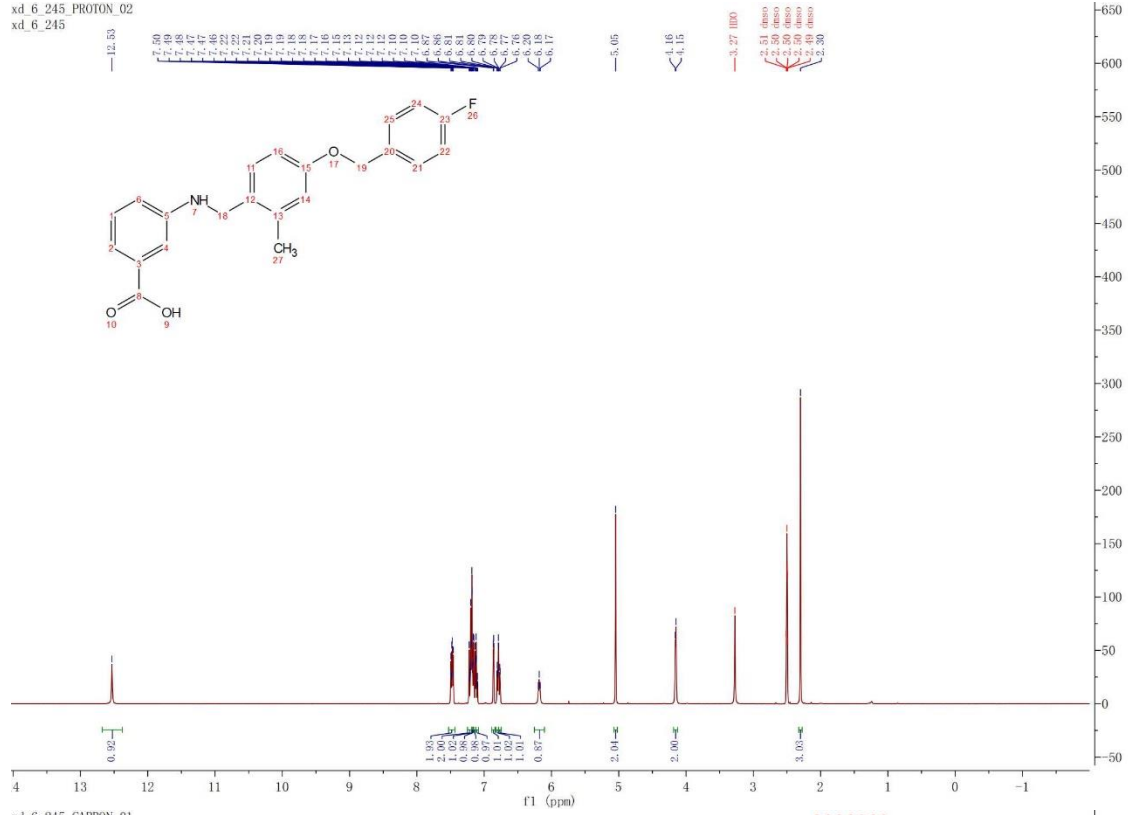


### 3.4s

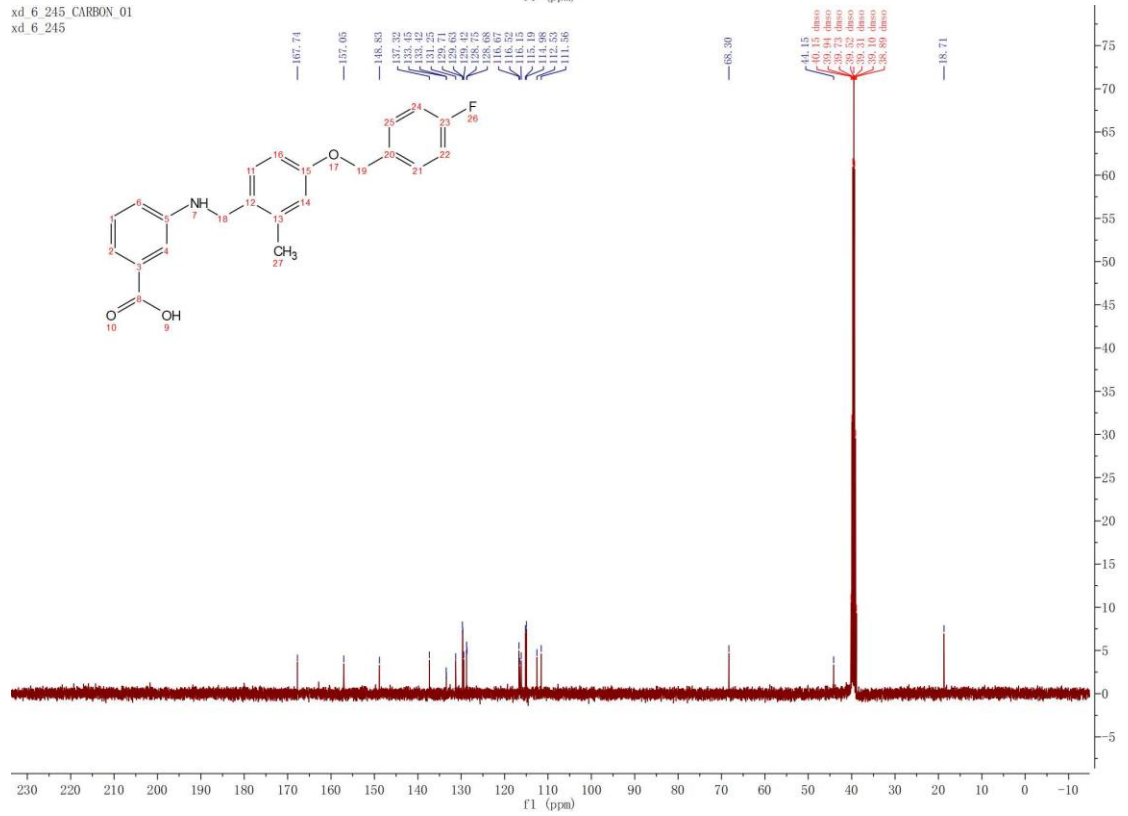


### 3.4t

xd\_6\_245\_PROTON\_Q2  
xd\_6\_245

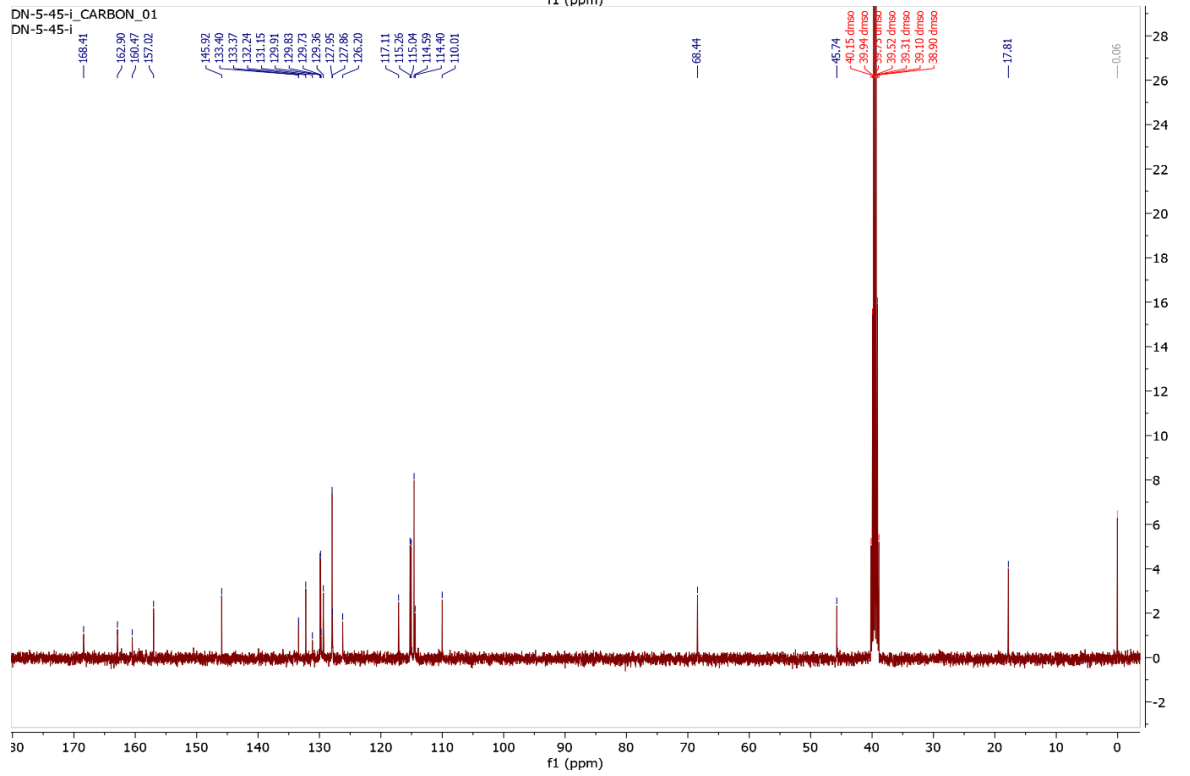
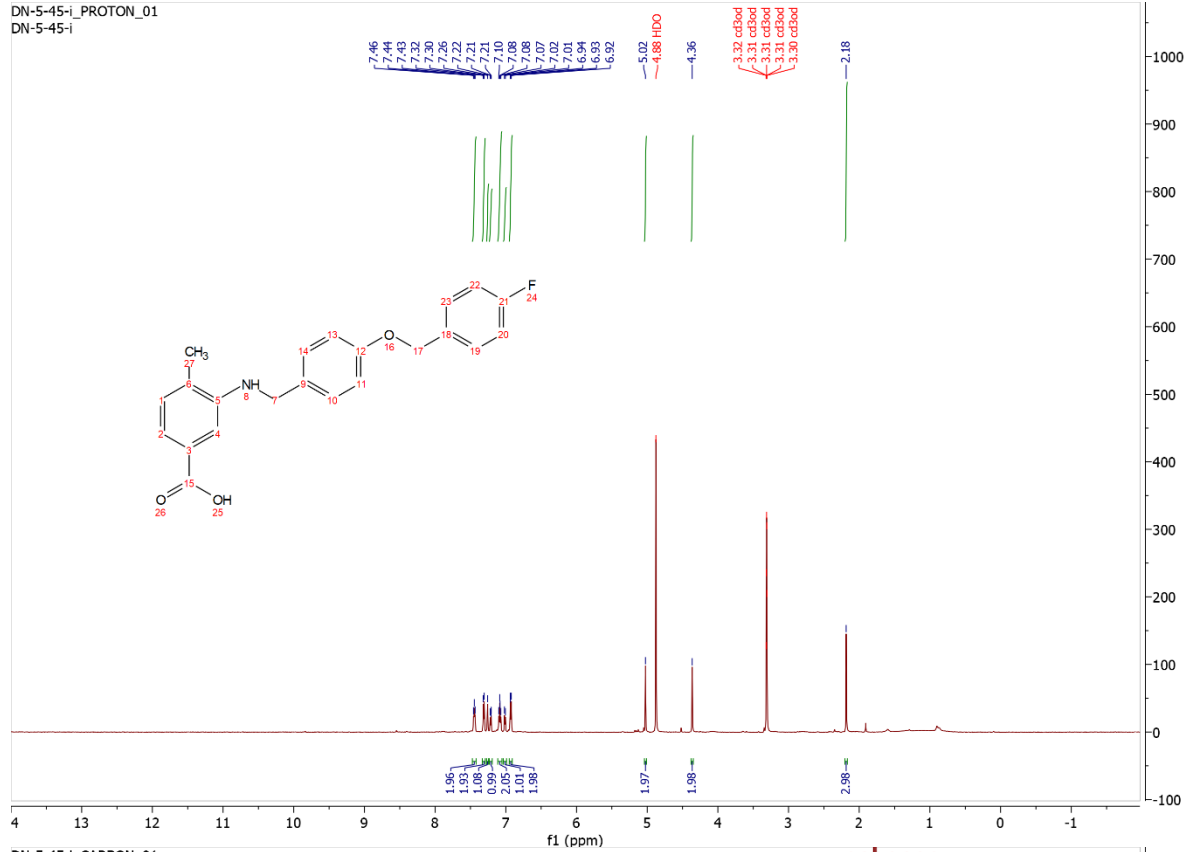


xd\_6\_245 CARBON\_Q1  
xd\_6\_245





### 3.4v



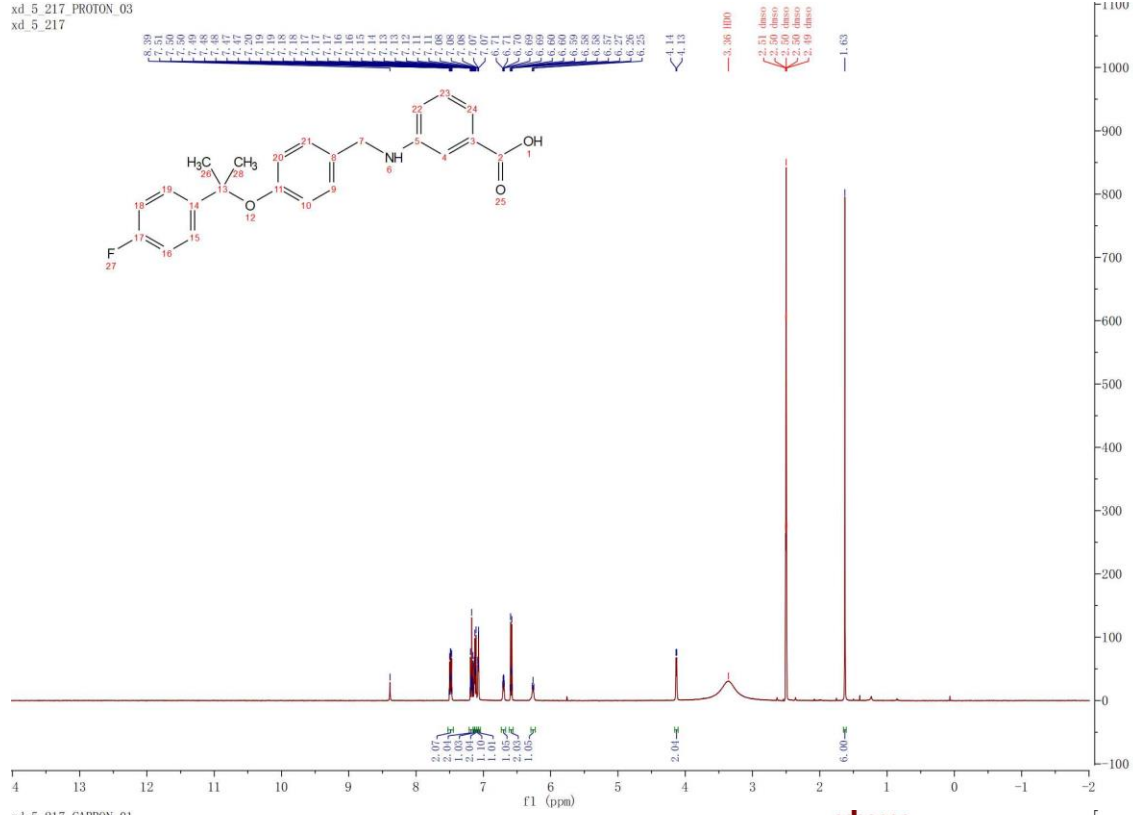




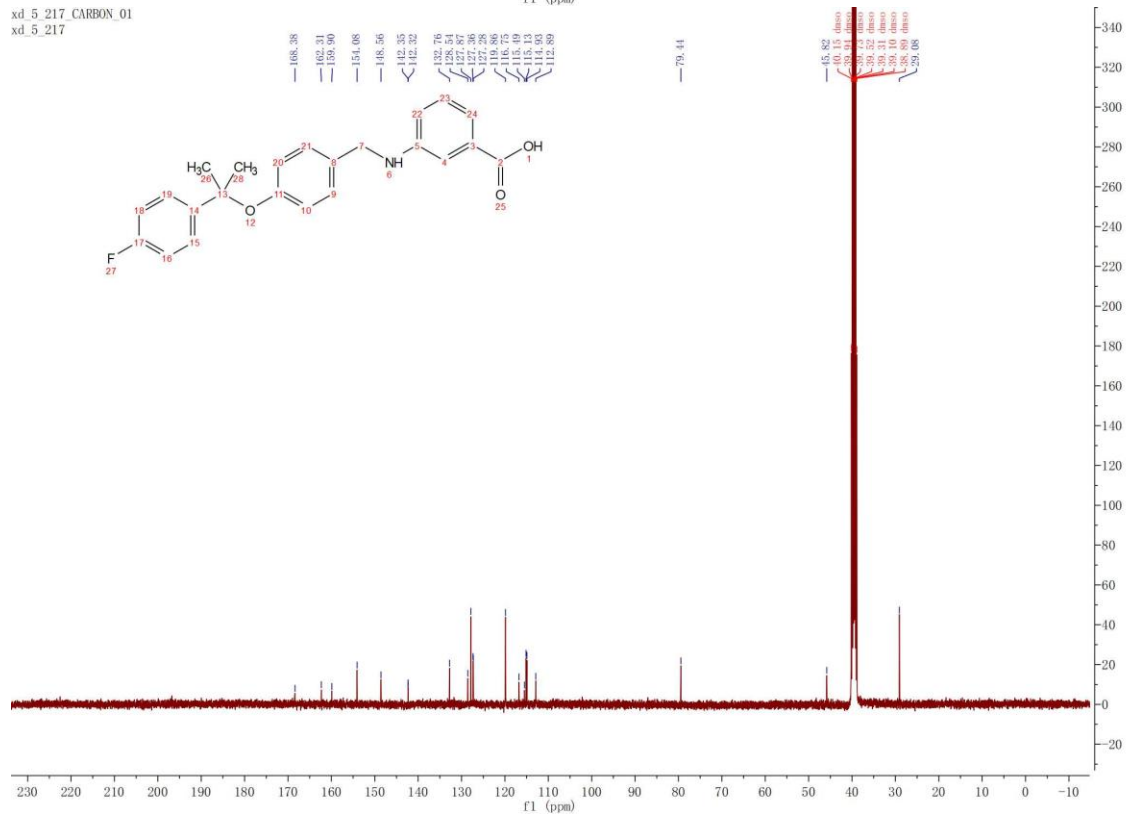


# 3.4z

xd\_5\_217\_PROTON\_03  
xd\_5\_217



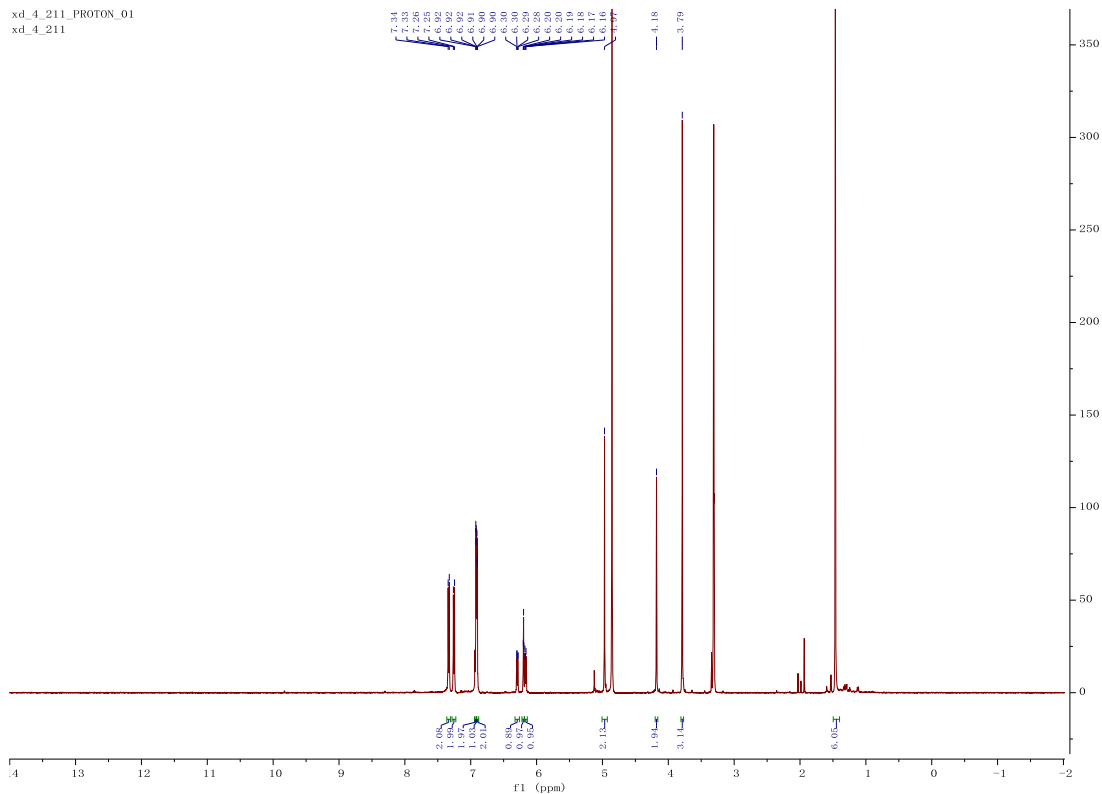
xd\_5\_217\_CARBON\_01  
xd\_5\_217



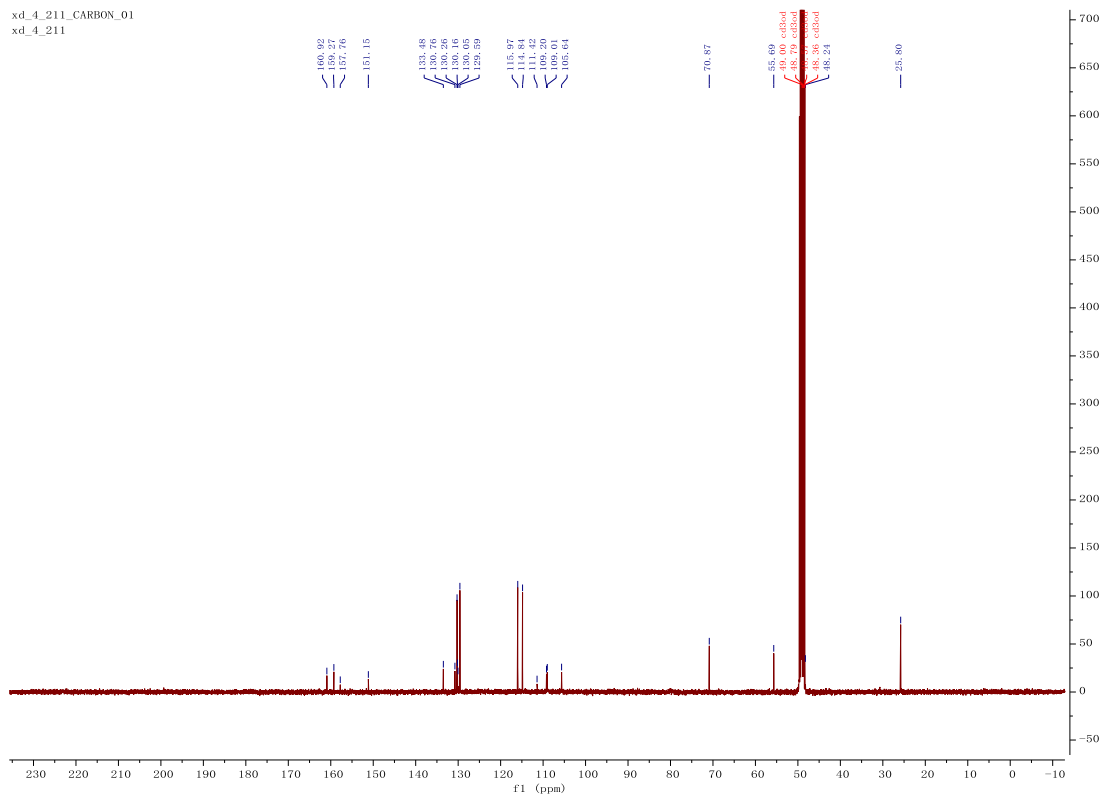


# 3.5a

xd\_4\_211\_PROTON\_01  
xd\_4\_211

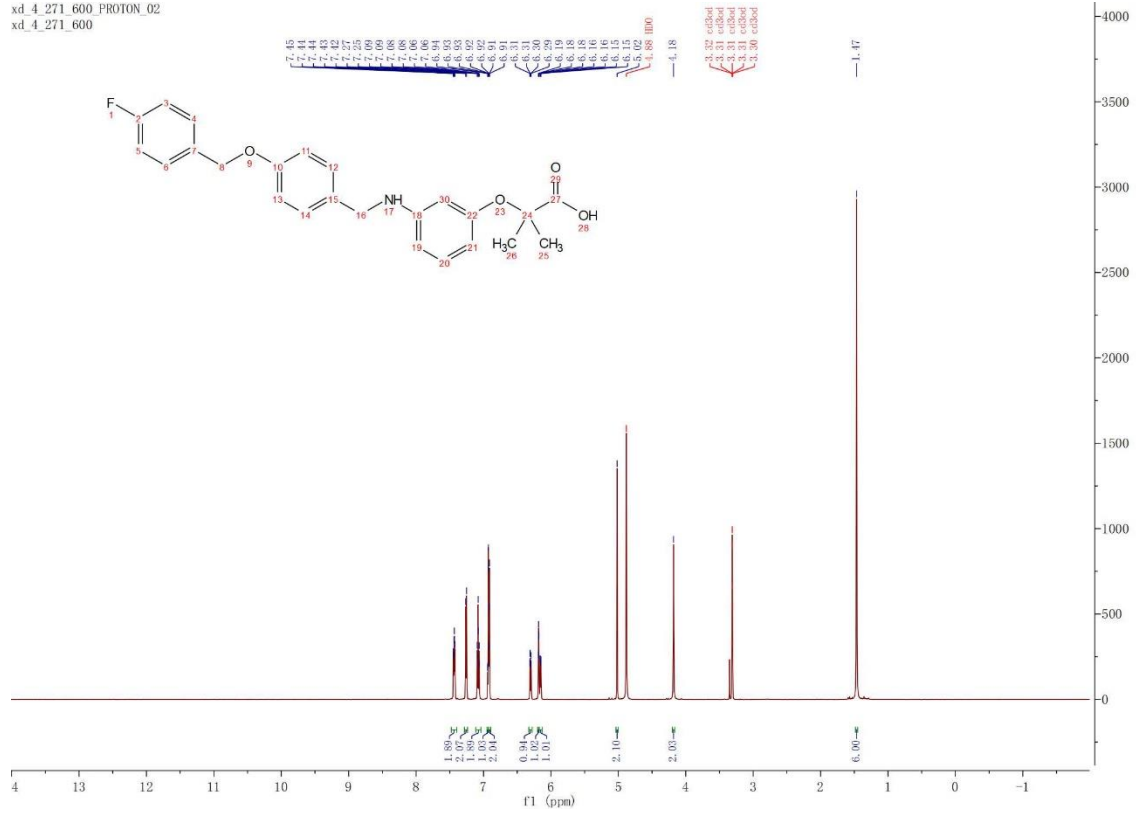


xd\_4\_211\_CARBON\_01  
xd\_4\_211

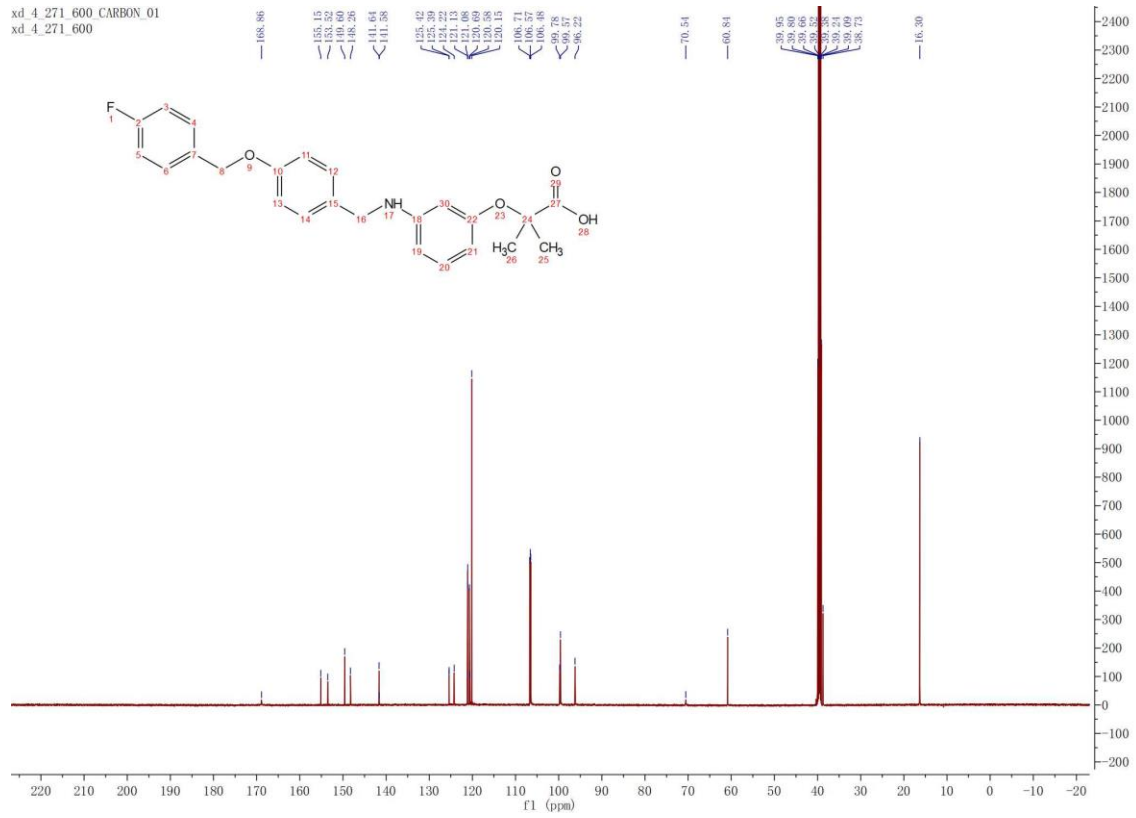


# 3.5b

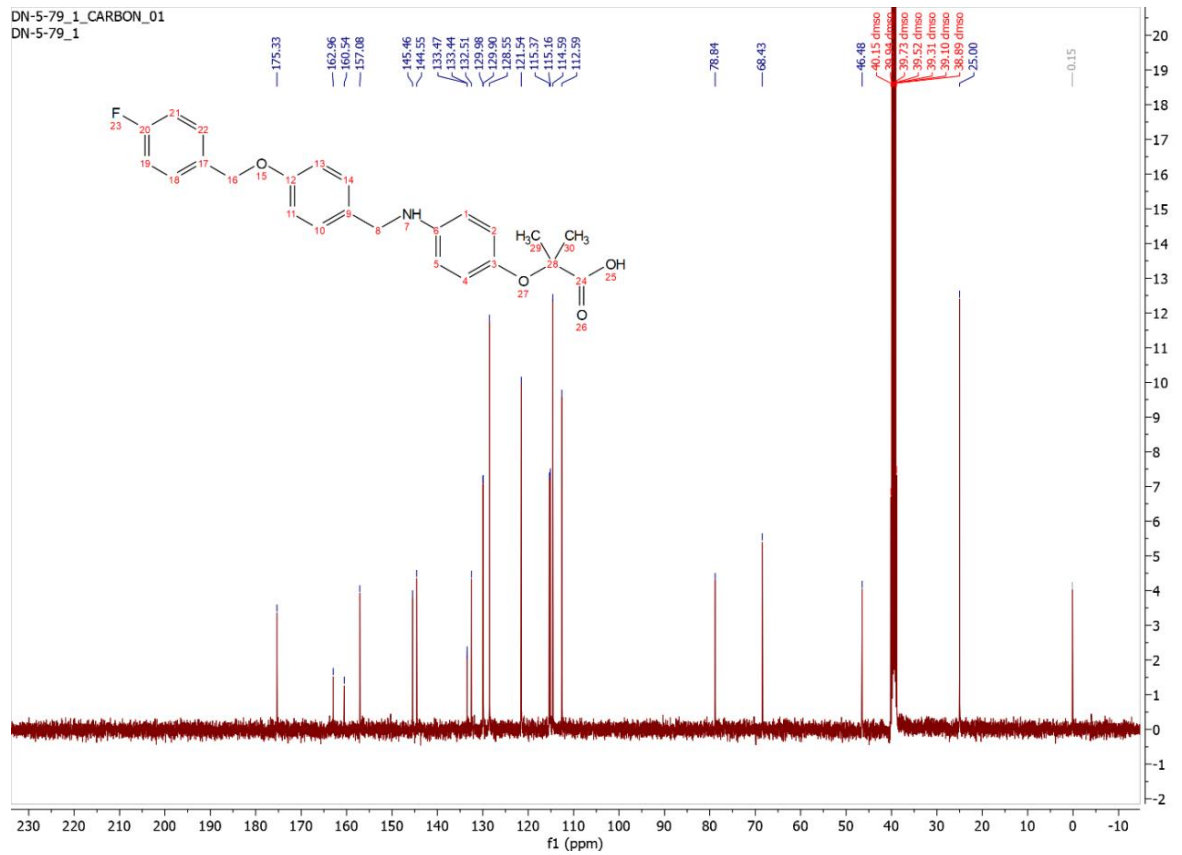
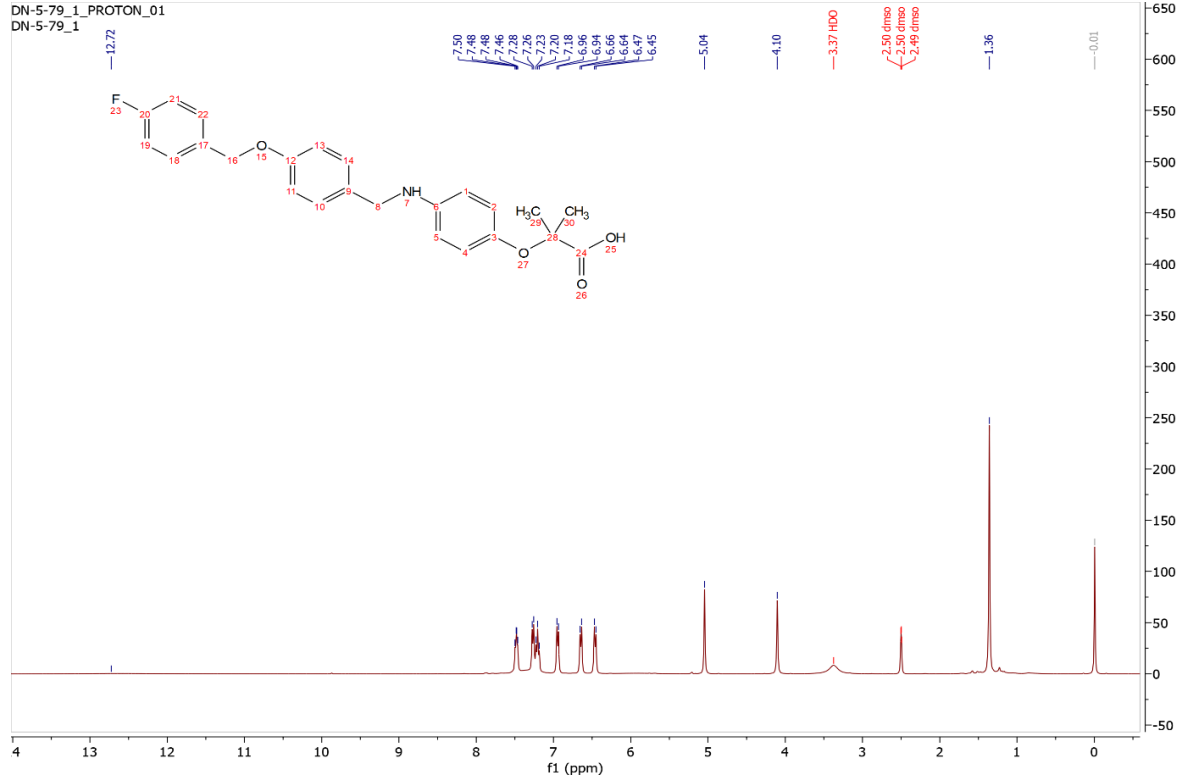
xd\_4\_271\_600\_PROTON\_02  
xd\_4\_271\_600



xd\_4\_271\_600 CARBON\_01  
xd\_4\_271\_600

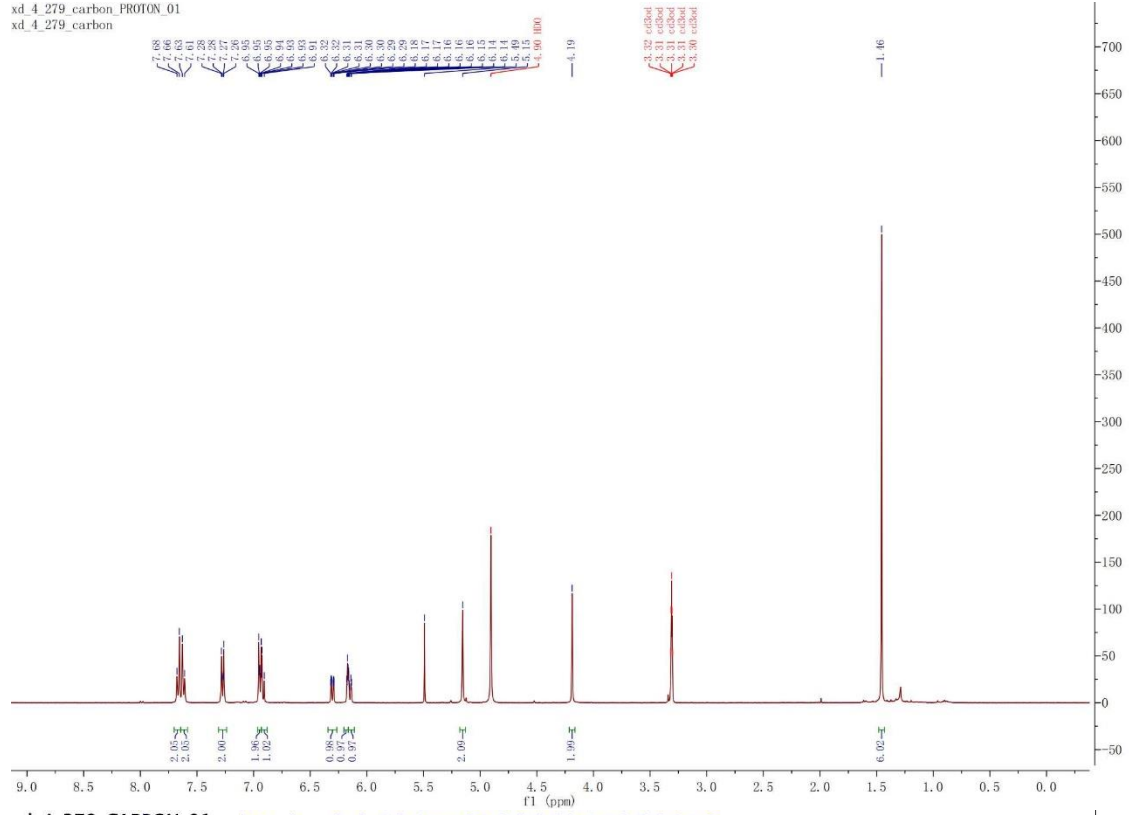


### 3.5b\*

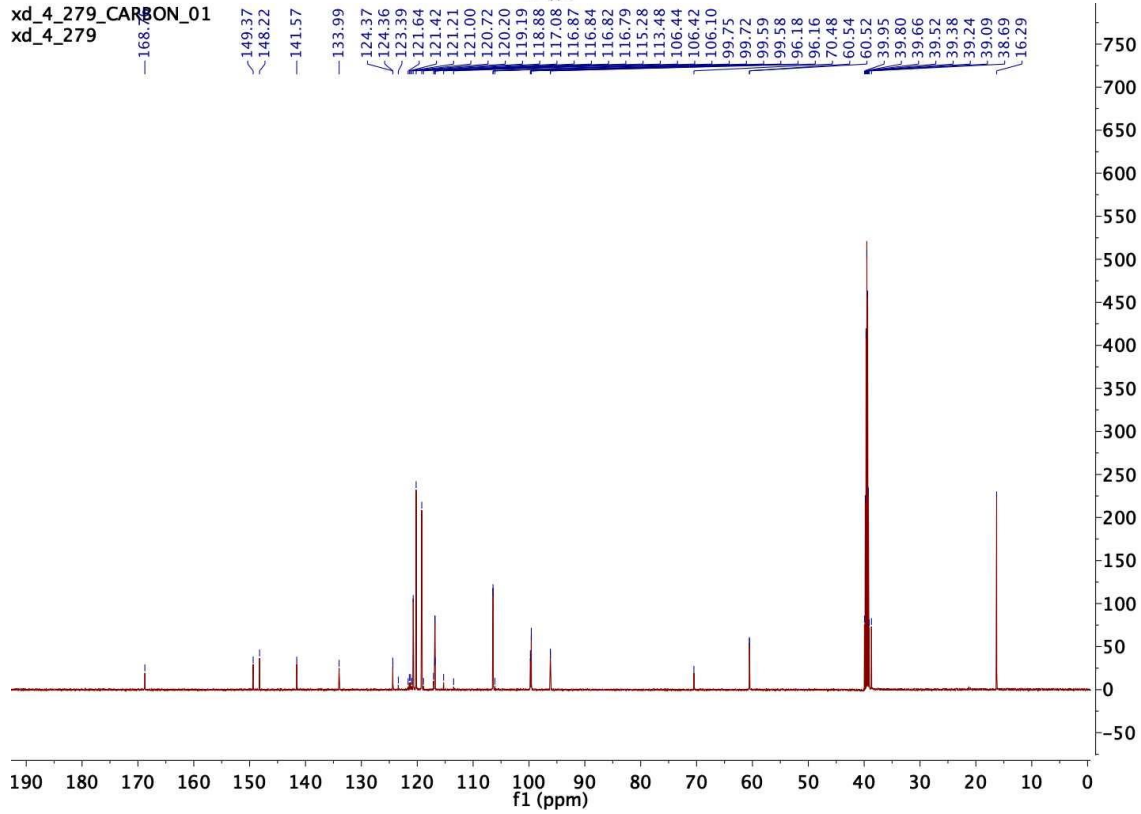


# 3.5f

xd\_4\_279\_carbon\_PROTON\_01  
xd\_4\_279\_carbon



xd\_4\_279\_CARBON\_01  
xd\_4\_279





















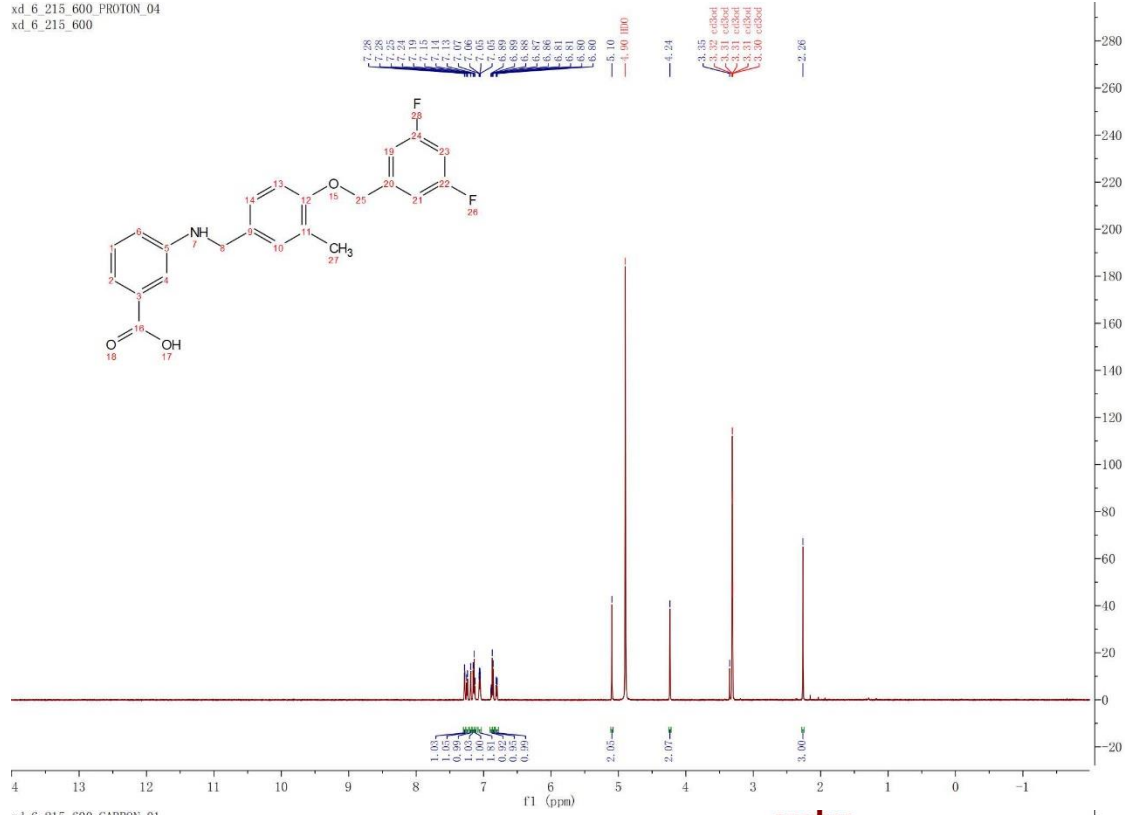




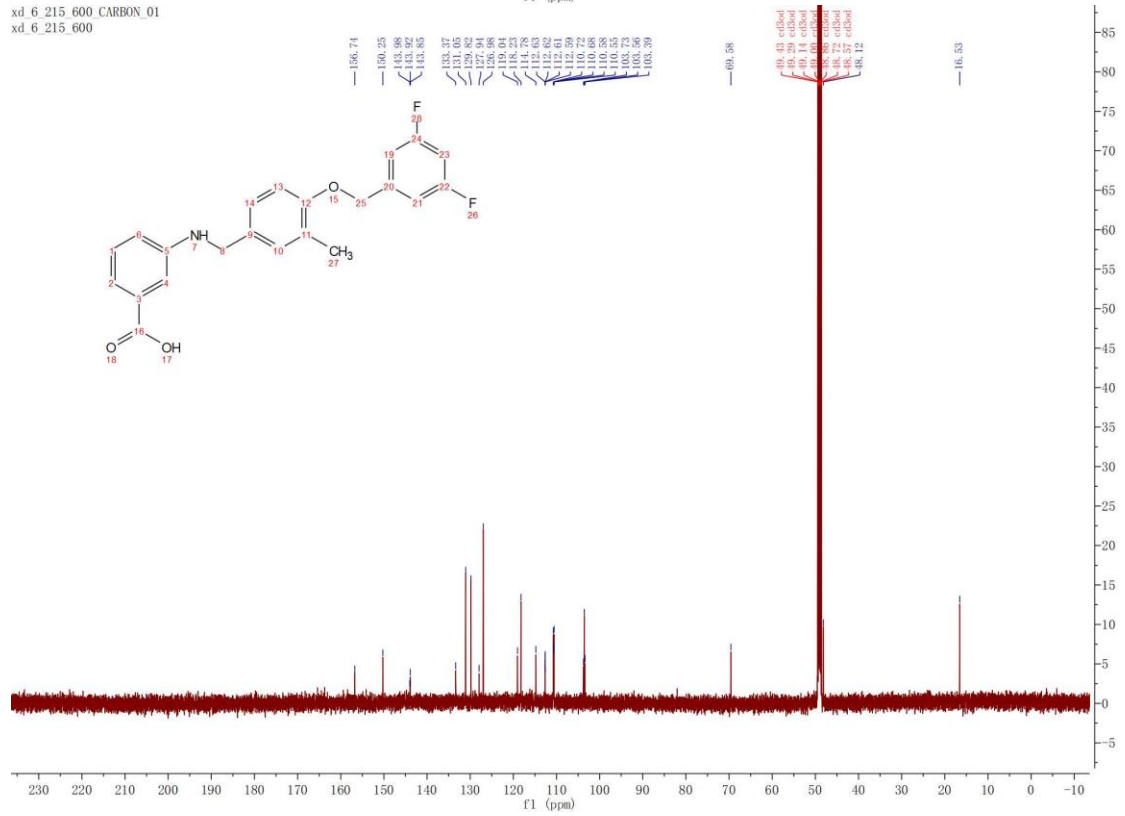


### 3.25

xd\_6\_215\_600\_PROTON\_04  
xd\_6\_215\_600



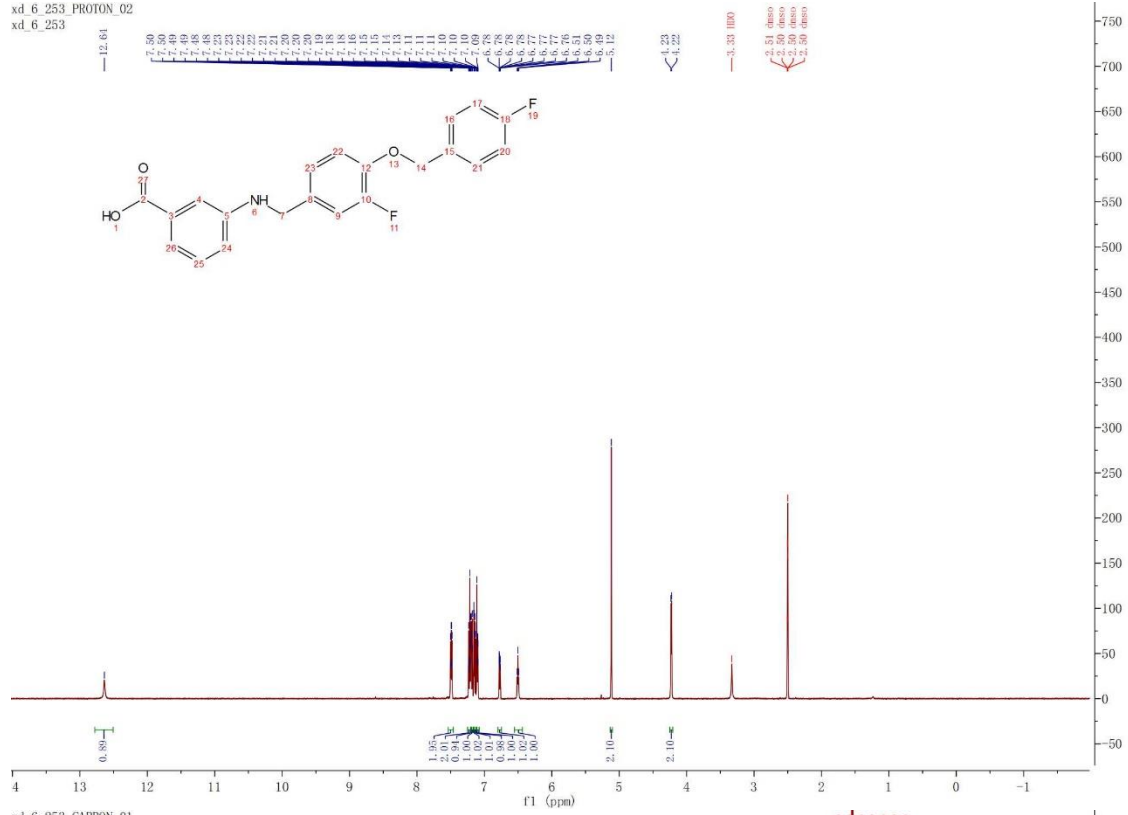
xd\_6\_215\_600\_CARBON\_01  
xd\_6\_215\_600



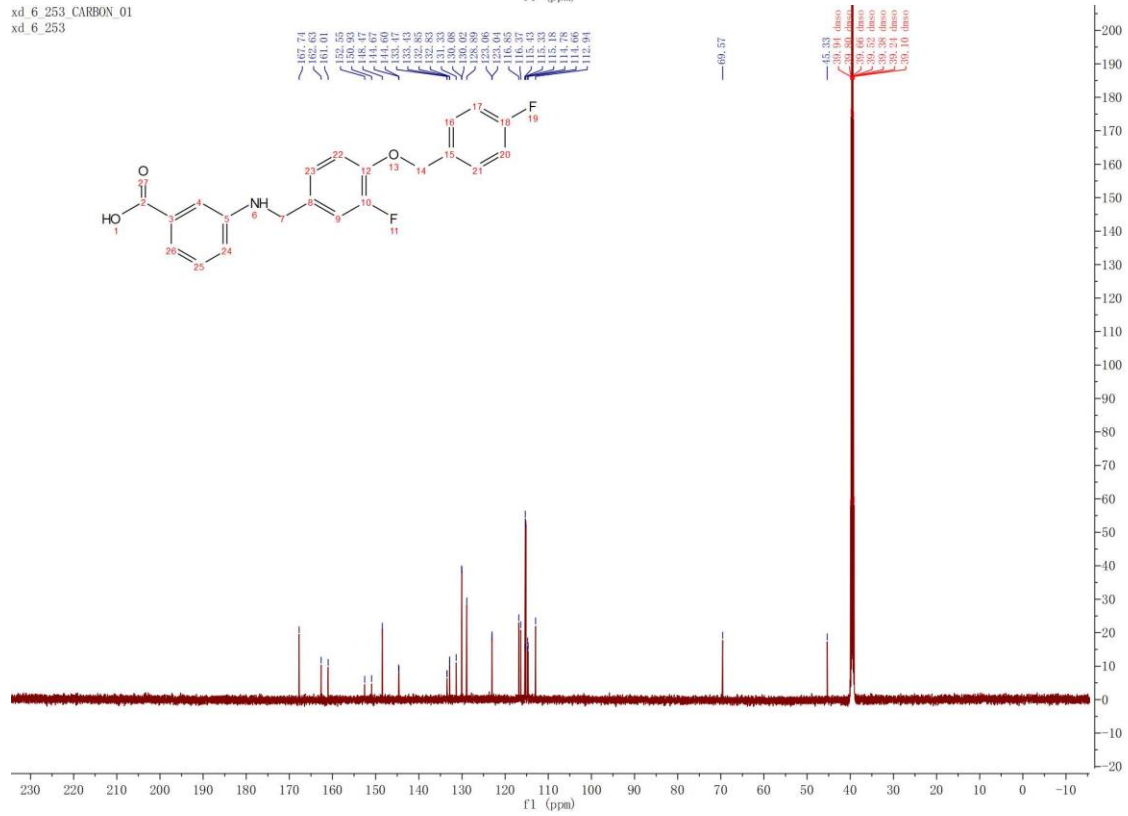


### 3.26

xd\_6\_253 PROTON\_02  
xd\_6\_253

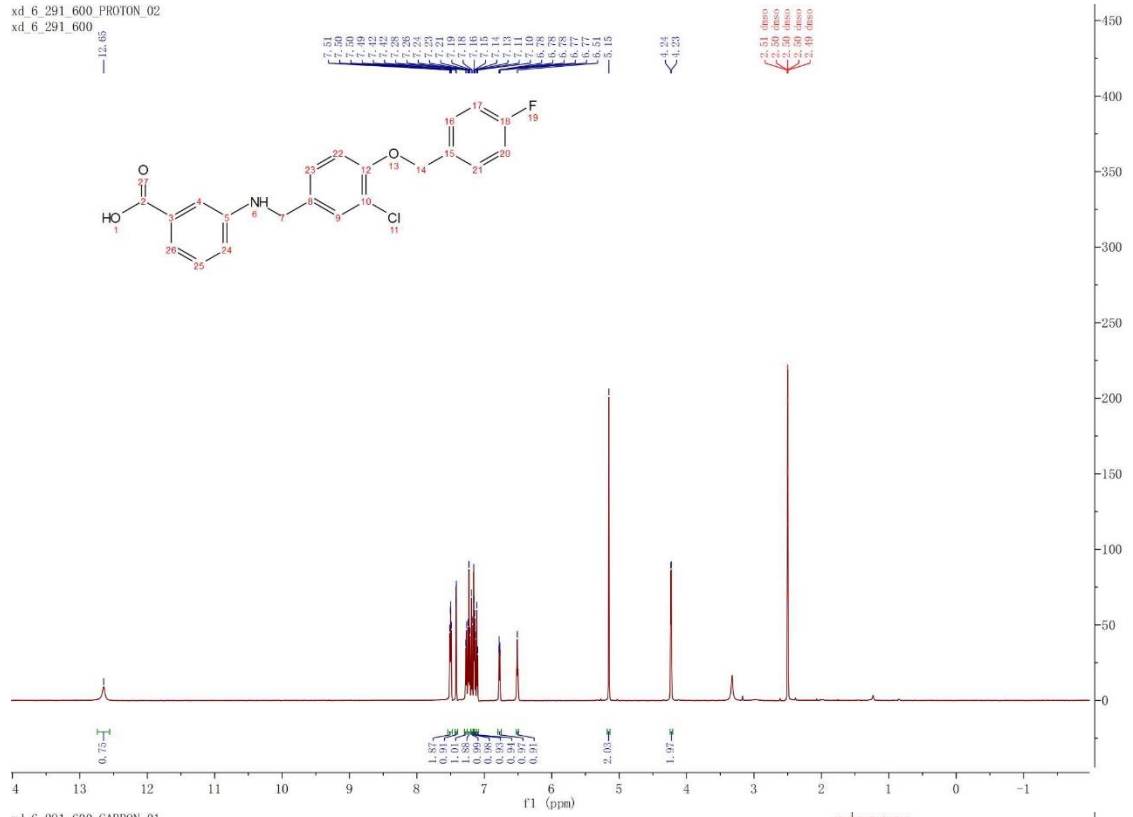


xd\_6\_253 CARBON\_01  
xd\_6\_253

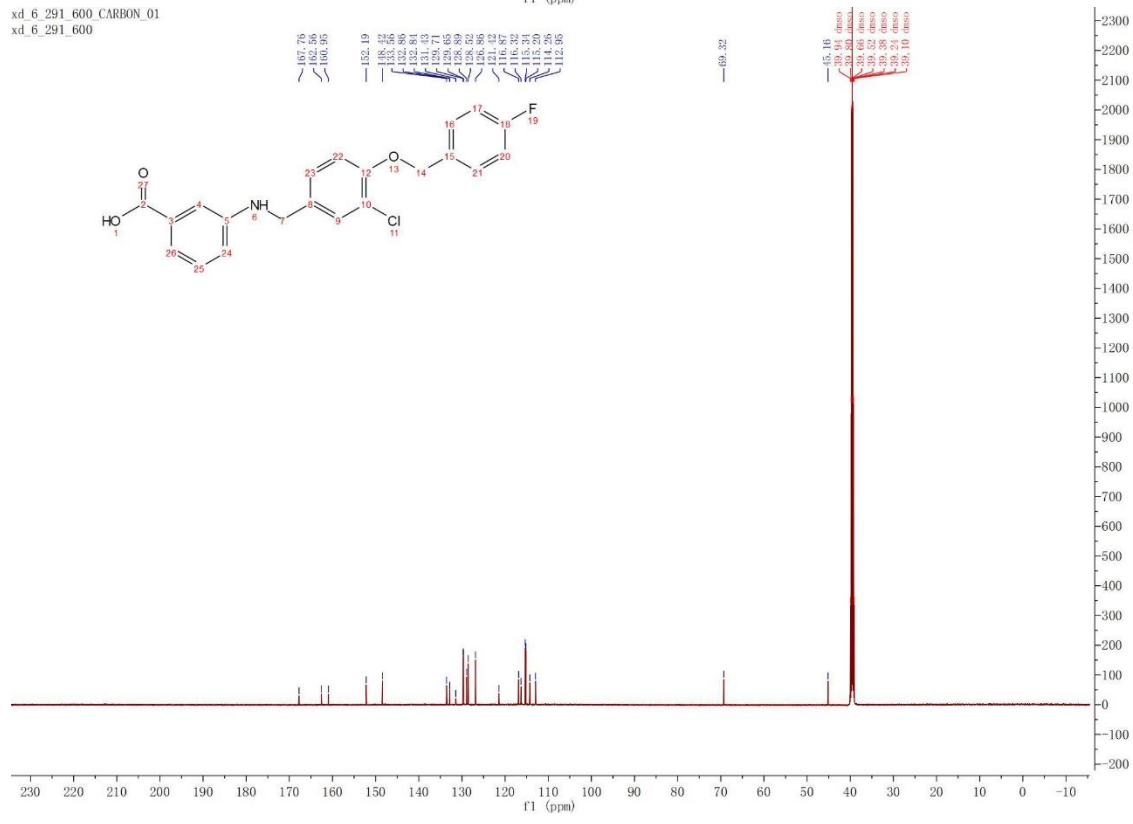


### 3.27

xd\_6\_291\_600\_PROTON\_02  
 xd\_6\_291\_600



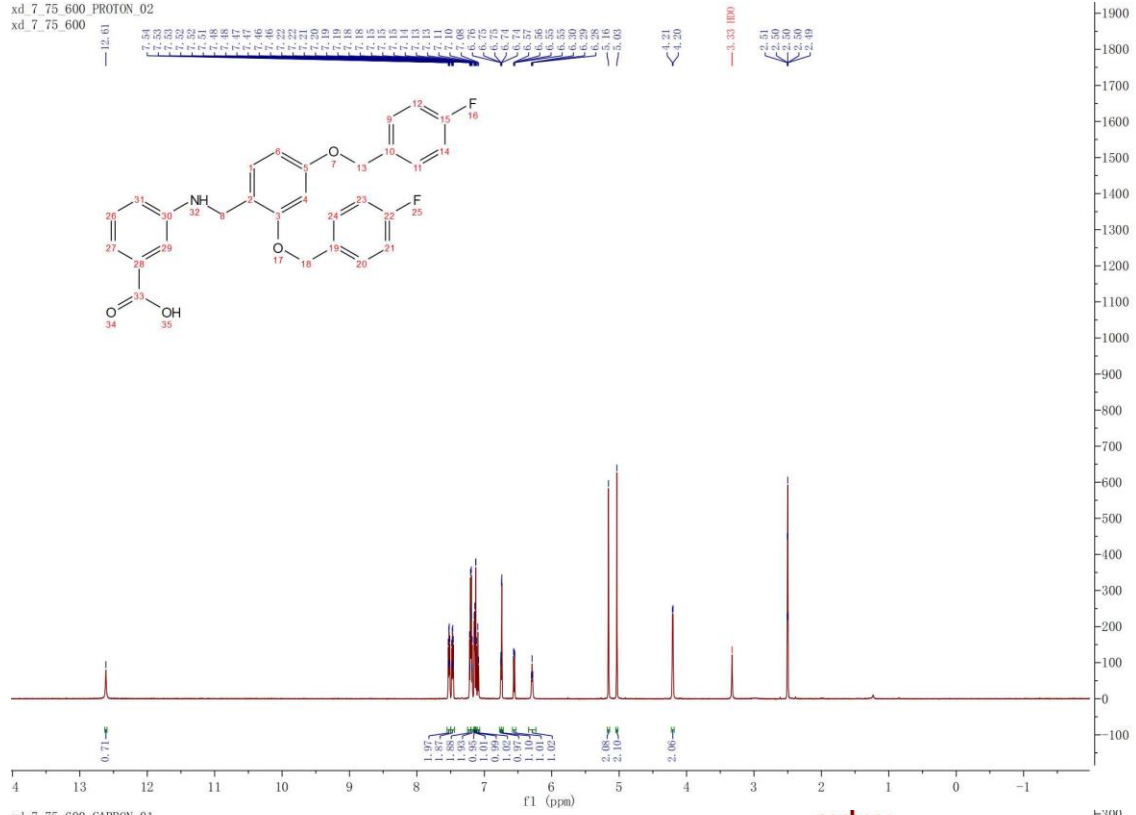
xd\_6\_291\_600\_CARBON\_01  
 xd\_6\_291\_600



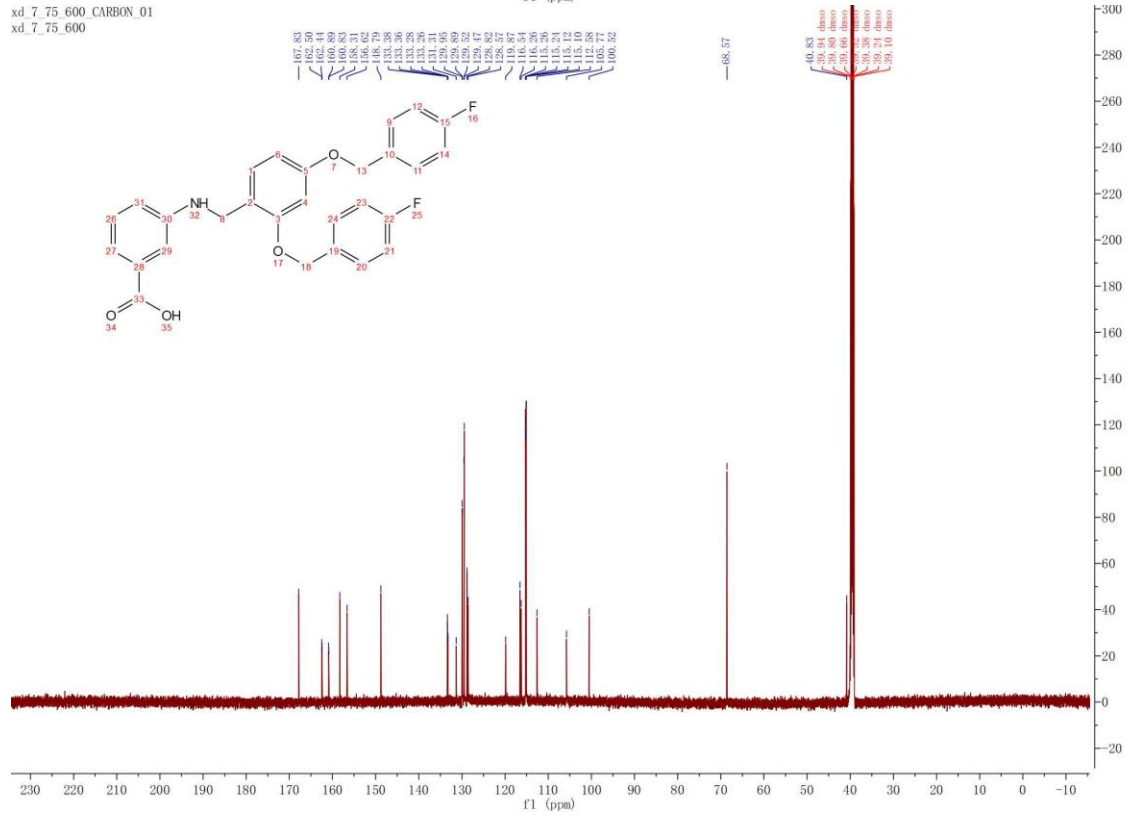


### 3.29

xd\_7\_75\_600 PROTON\_02  
 xd\_7\_75\_600



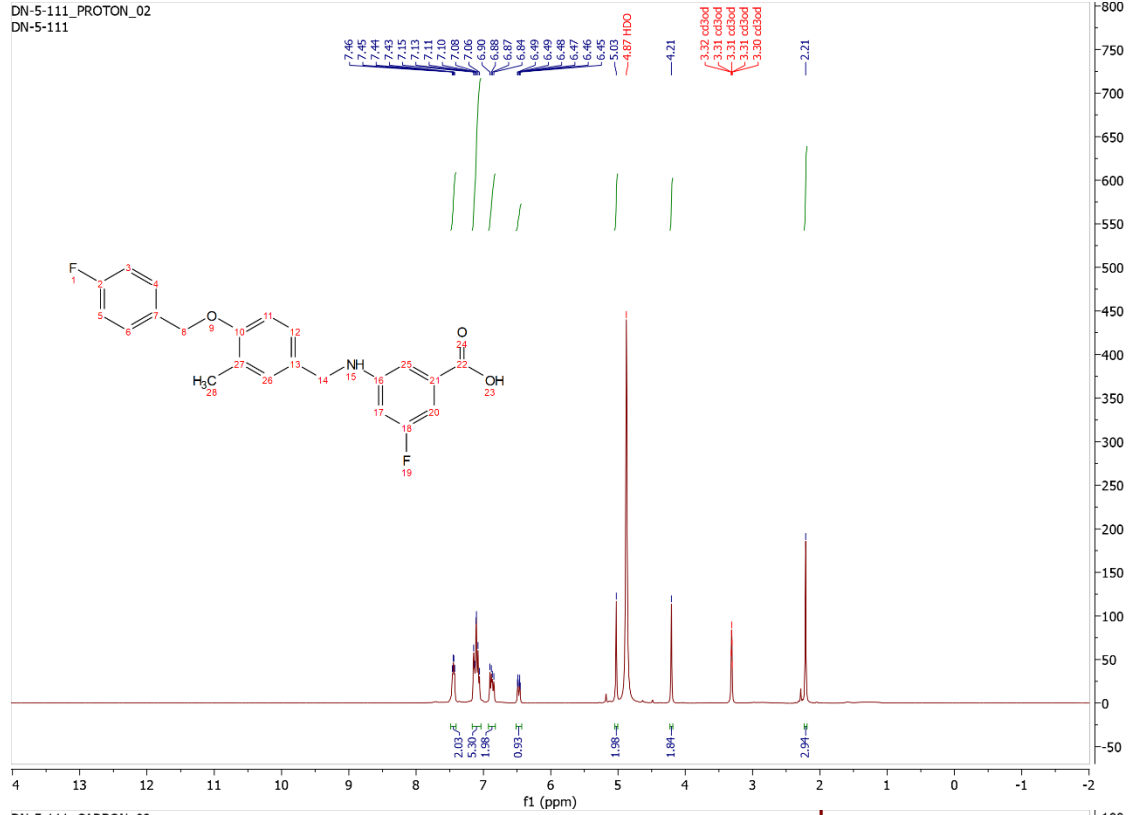
xd\_7\_75\_600 CARBON\_01  
 xd\_7\_75\_600



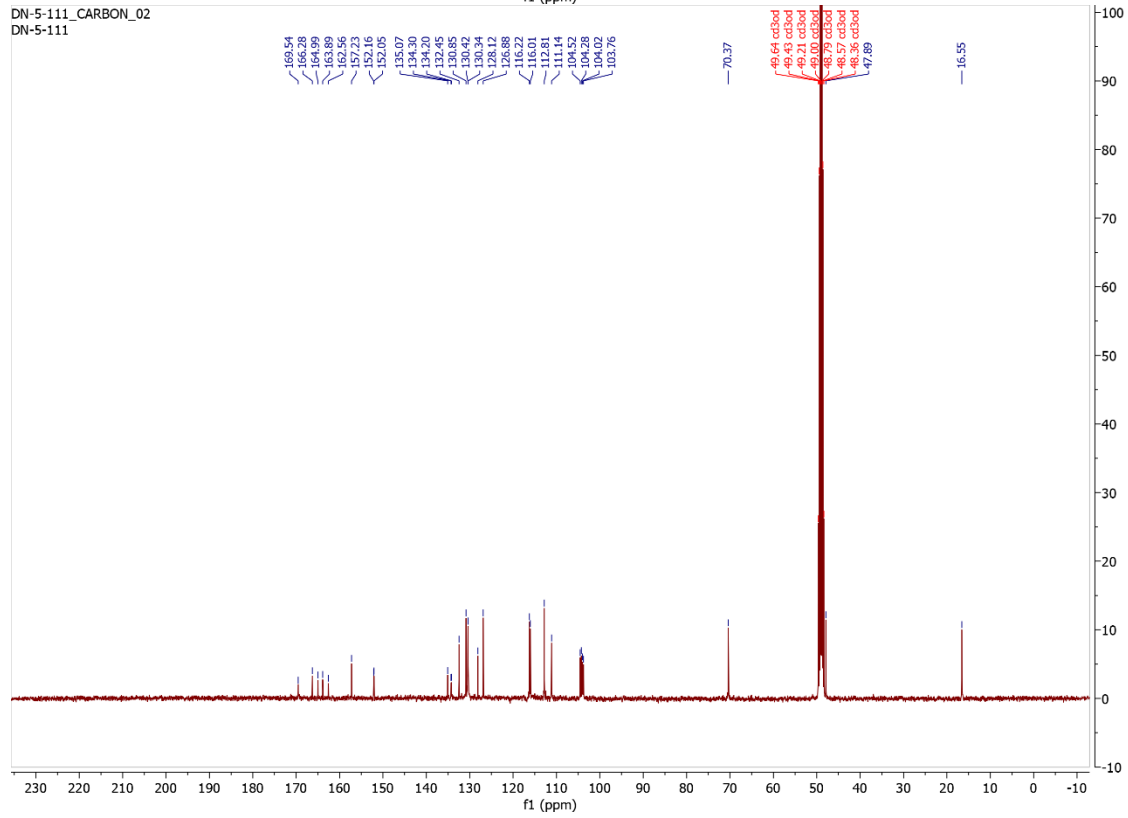


### 3.31

DN-5-111\_PROTON\_02  
DN-5-111

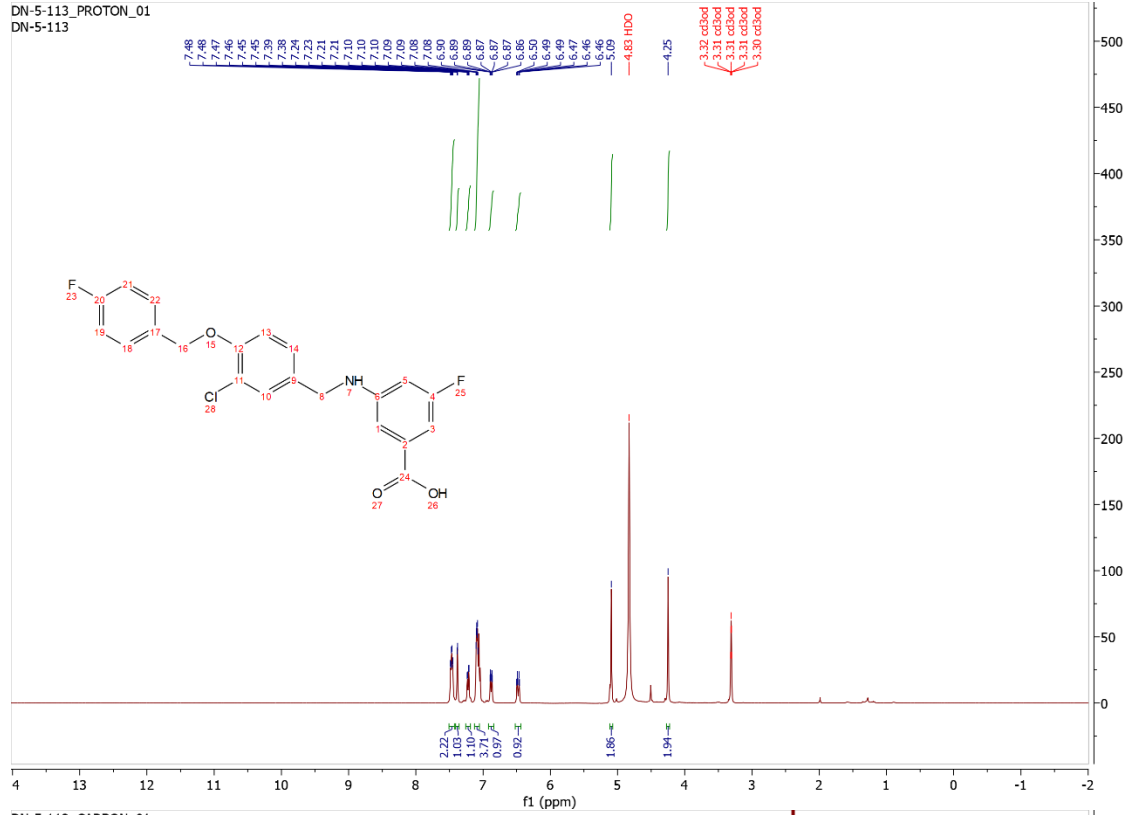


DN-5-111\_CARBON\_02  
DN-5-111

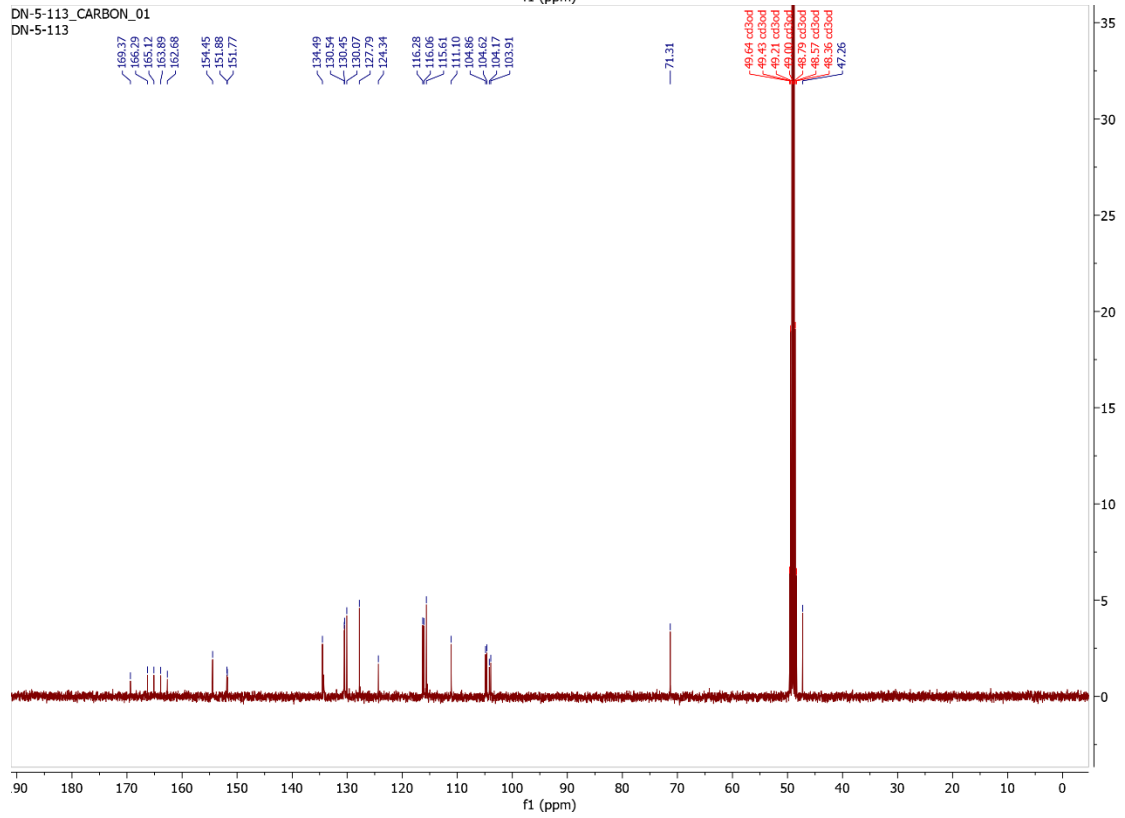


### 3.32

DN-5-113\_PROTON\_01  
DN-5-113

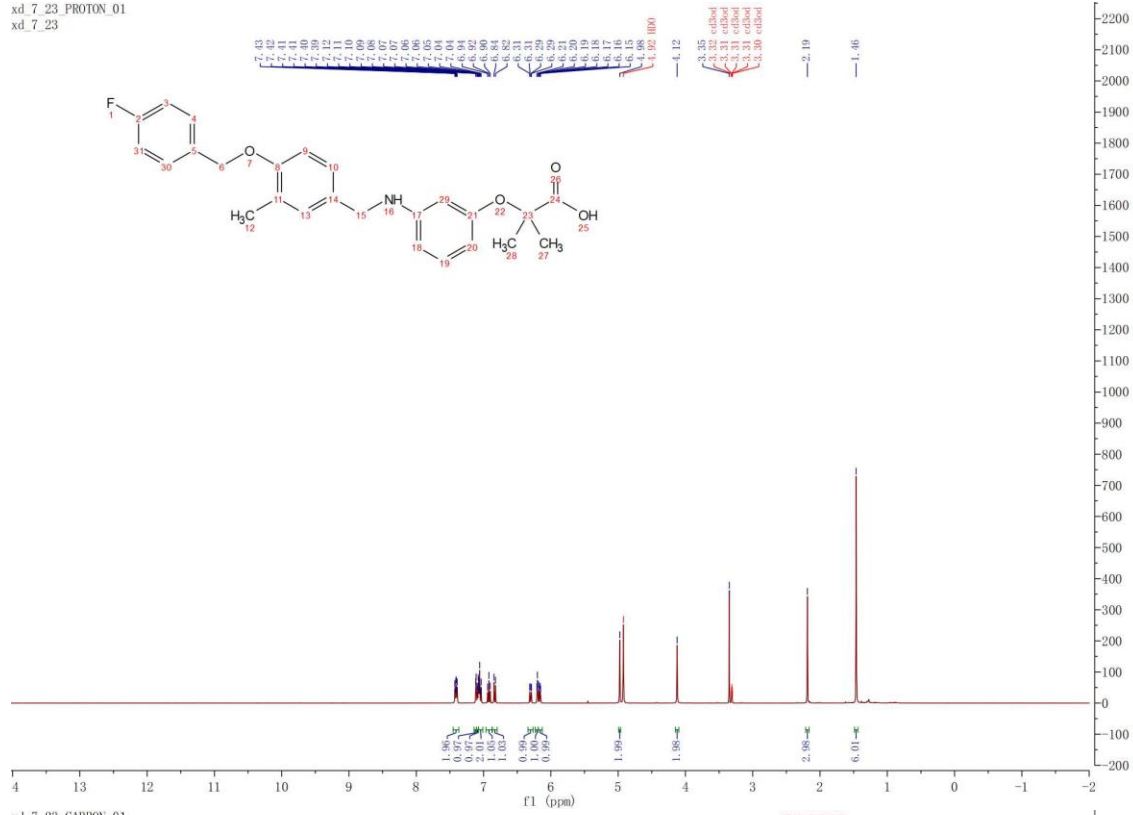


DN-5-113\_CARBON\_01  
DN-5-113



### 3.33

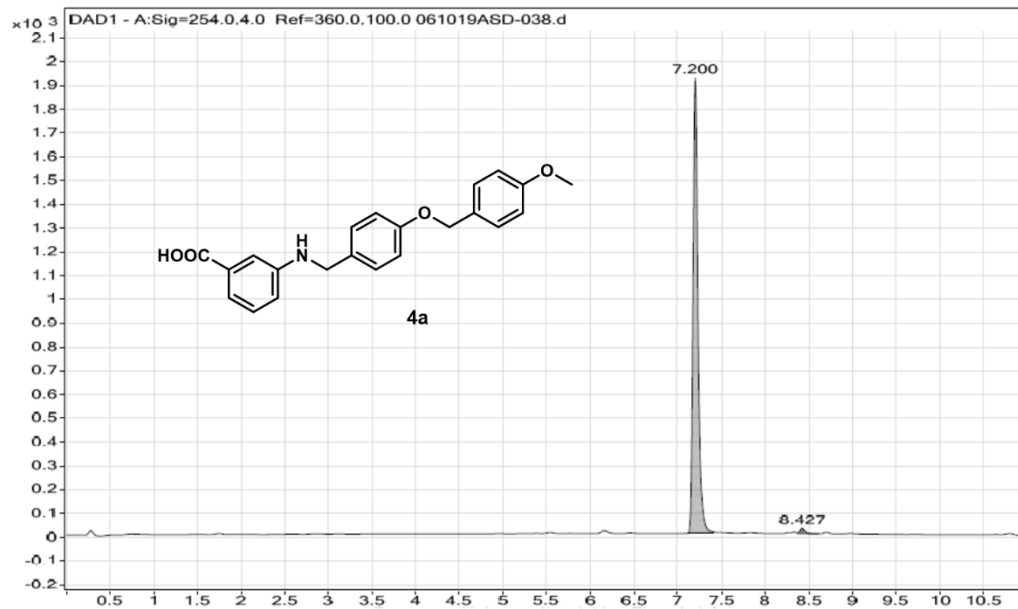
xd\_7\_23\_PROTON\_01  
xd\_7\_23



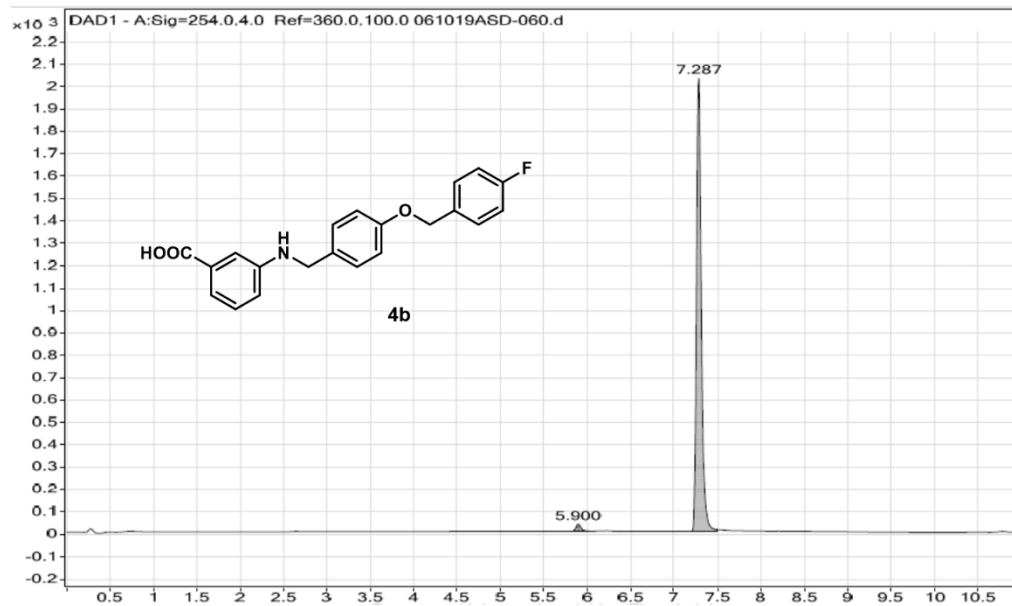


## HPLC Traces

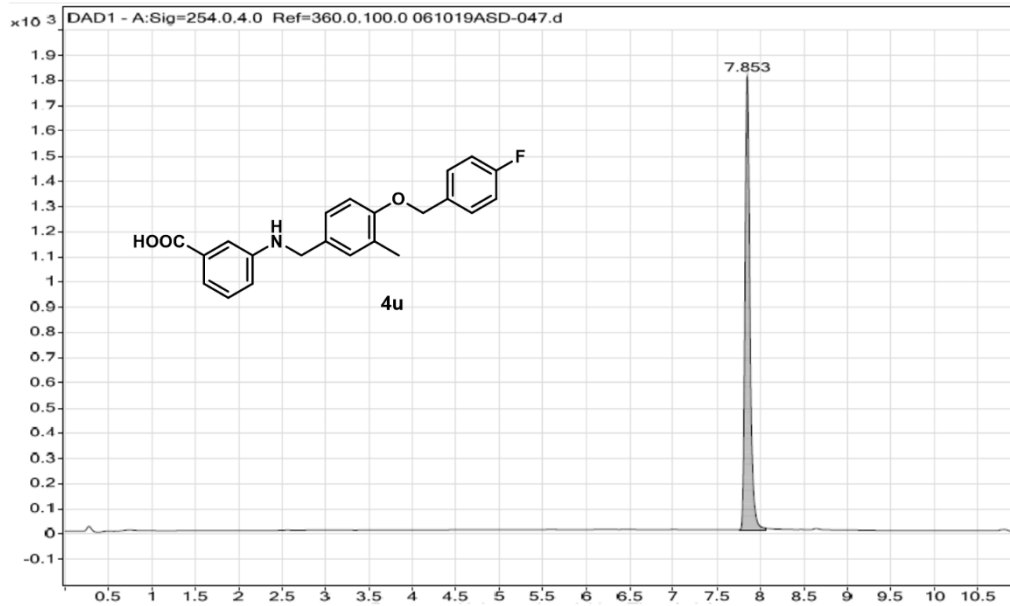
Peak	RT	Area	Height	Type	Saturated	Width	FWHM	SNR
1	7.2	7611.9	1917.3			0.293	0.059	
2	8.427	94.93	23.43			0.24	0.057	



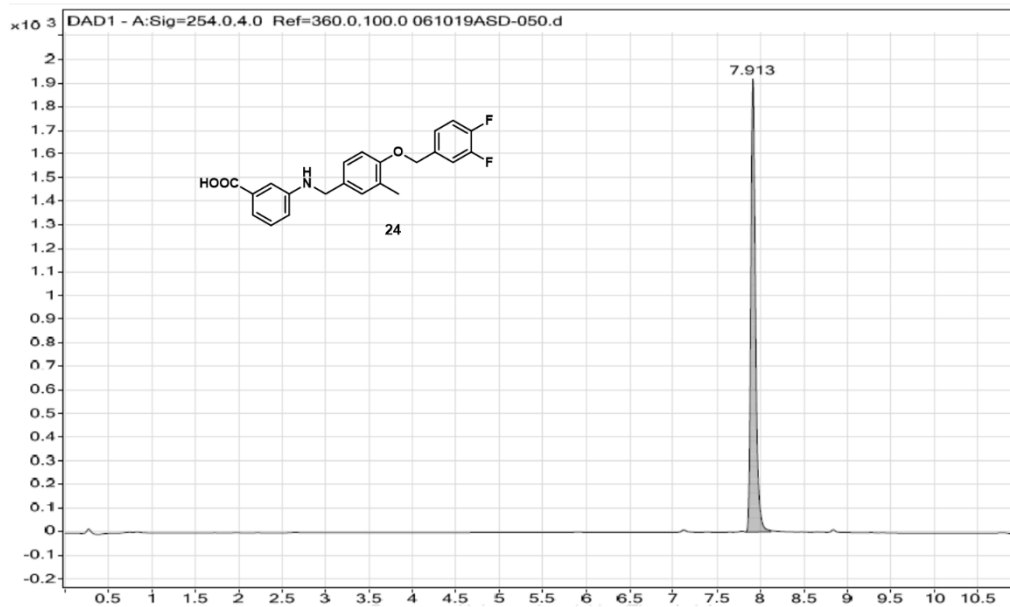
Peak	RT	Area	Height	Type	Saturated	Width	FWHM	SNR
1	5.9	135.02	32.58			0.247	0.061	
2	7.287	7833.3	2024.17			0.29	0.057	



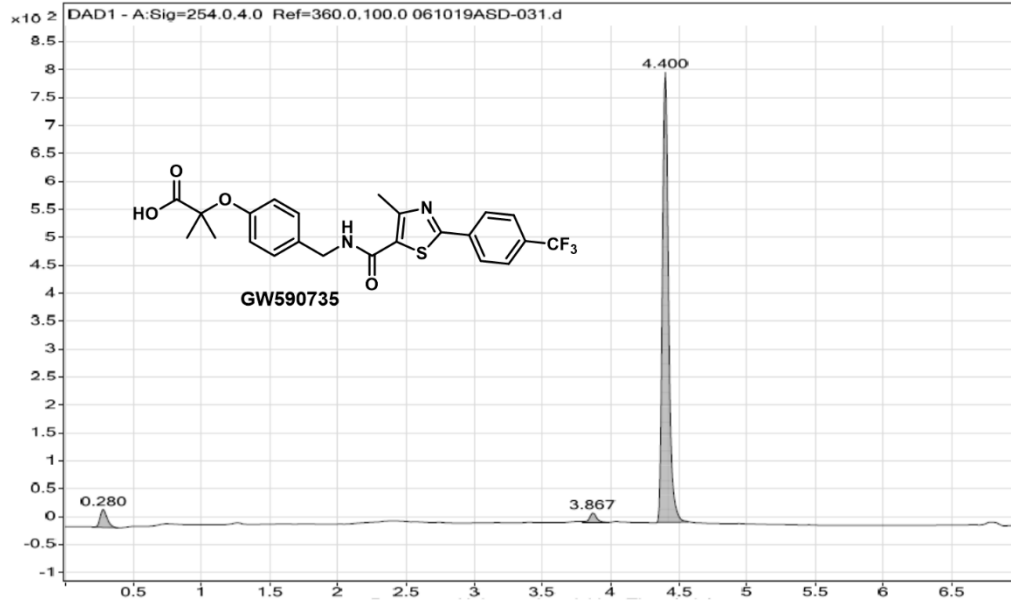
Peak	RT	Area	Height	Type	Saturated	Width	FWHM	SNR
1	7.853	7214.4	1803.97			0.3	0.059	



Peak	RT	Area	Height	Type	Saturated	Width	FWHM	SNR
1	7.913	7258.6	1920.86			0.287	0.056	



Peak	RT	Area	Height	Type	Saturated	Width	FWHM	SNR
1	0.28	115.51	32.09			0.189	0.054	
2	3.867	62.05	16.78			0.193	0.052	
3	4.4	2570.6	805.61			0.226	0.048	

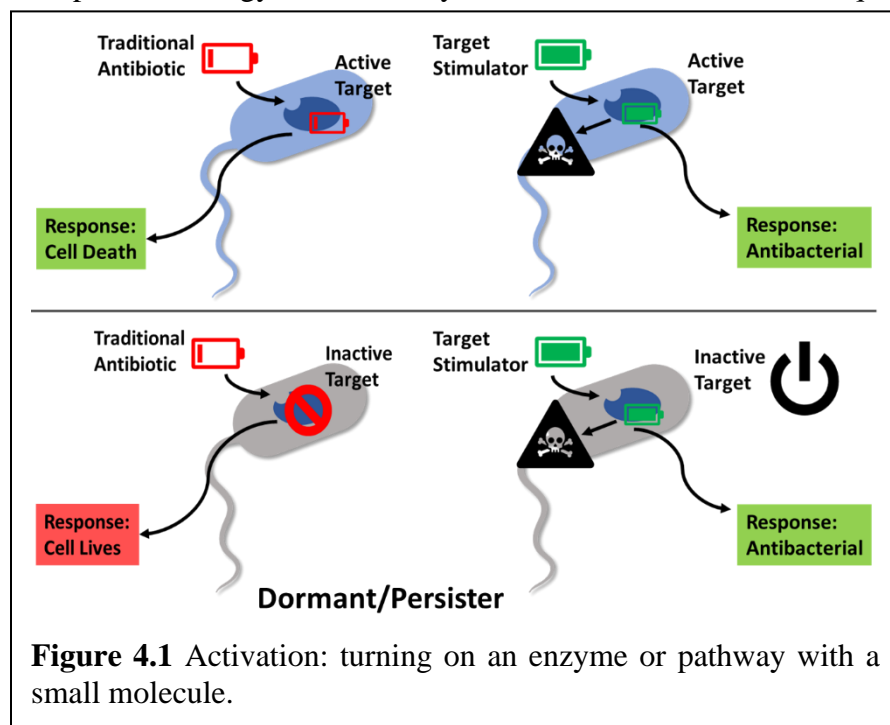


## Chapter 4 Design and Total Synthesis of a Methylene-linked ADEP Analog

### 4.1 Caseinolytic Peptidase Proteolytic Subunit (ClpP)

Antimicrobial resistance in human pathogens has drastically increased in recent years and there is an urgent need for antibiotics that operate through new mechanisms of action. In 2019, the Centers for Disease Control and Prevention (CDC) reported 18 completely drug-resistance bacteria and fungi that caused more than 2.8 million infections and more than 35,000 deaths in the U.S alone.<sup>1</sup> Currently, the *status quo* for antibiotic development is to inhibit essential processes in bacteria, resulting in cell death.<sup>2</sup> To avoid infections of pandemic proportions in the future and concomitant death tolls, it is necessary to discover significantly different therapeutic strategies for eradicating bacterial infections.<sup>3</sup> Specifically, the identification of antibacterial drugs that operate through the interaction with novel targets and/or disrupt bacterial pathogenicity is an important endeavor.

Small-molecule activation of bacterial pathways/enzymes provides a unique and clinically unexploited strategy that is clearly differentiated from the *status quo*. Compared to conventional



inhibition, enzyme-activation strategies have the potential to eradicate dormant persister cells, thus mitigating the development of drug tolerance (Figure 4.1).<sup>2</sup> Caseinolytic peptidase proteolytic subunit (ClpP),

a highly conserved serine protease with a canonical Asp-His-Ser catalytic triad, has emerged as a promising antibacterial target, and activation of this protease leads to bactericidal activity against a number of bacteria.<sup>4</sup> ClpP is one of two components in the Clp protease system, which is highly regulated by another component, the ATPase domain (i.e., ClpX and ClpA), in an ATP-dependent manner.<sup>5</sup> Clp proteases have been found in both bacteria and eukaryotes. Functions of ClpP in bacteria include the elimination of unnecessary and toxic proteins/peptides and the regulation of biological responses to environmental stressors including temperature fluctuation, macrophage attack, and UV exposure and cell cycle cues. ClpP plays important roles in the growth, survival, and virulence of a number of bacterial pathogens.<sup>6-10</sup>

ClpP is a cylindrical tetradecameric complex that is formed by two heptameric rings composed of ClpP monomers (**Figure 4.2A**).<sup>11</sup> The internal chamber is lined with 14 proteolytic active sites that degrade polypeptides (**Figure 4.2B**).<sup>5</sup> In the absence of ATP or cochaperones, only small unstructured polypeptides,  $\leq 51$  kDA ( $\leq 5-6$  amino acids), can be degraded by ClpP, which protects the organism from unregulated proteolysis.<sup>12</sup> Under normal physiological conditions, the ATPases recognize, unfold, and translocate tagged substrates into the ClpP proteolytic core for degradation.<sup>13</sup> Inhibition of this process by small molecules or gene knockouts of ClpP can result in accumulation of toxic substrates and often decreases bacterial virulence without causing cell death.<sup>13-15</sup> As such, the ClpP system represents a unique opportunity in antibacterial discovery as either inhibition or activation is detrimental to bacterial.

As mentioned previously, the activation of a bacterial enzyme to impart antibacterial effects is a more non-traditional approach and thus has captured our attention as a basic research laboratory. The physiological functions of ClpP can be activated by several small molecules yielding negative impacts to the bacterium ranging from inhibition of cell division to cell death

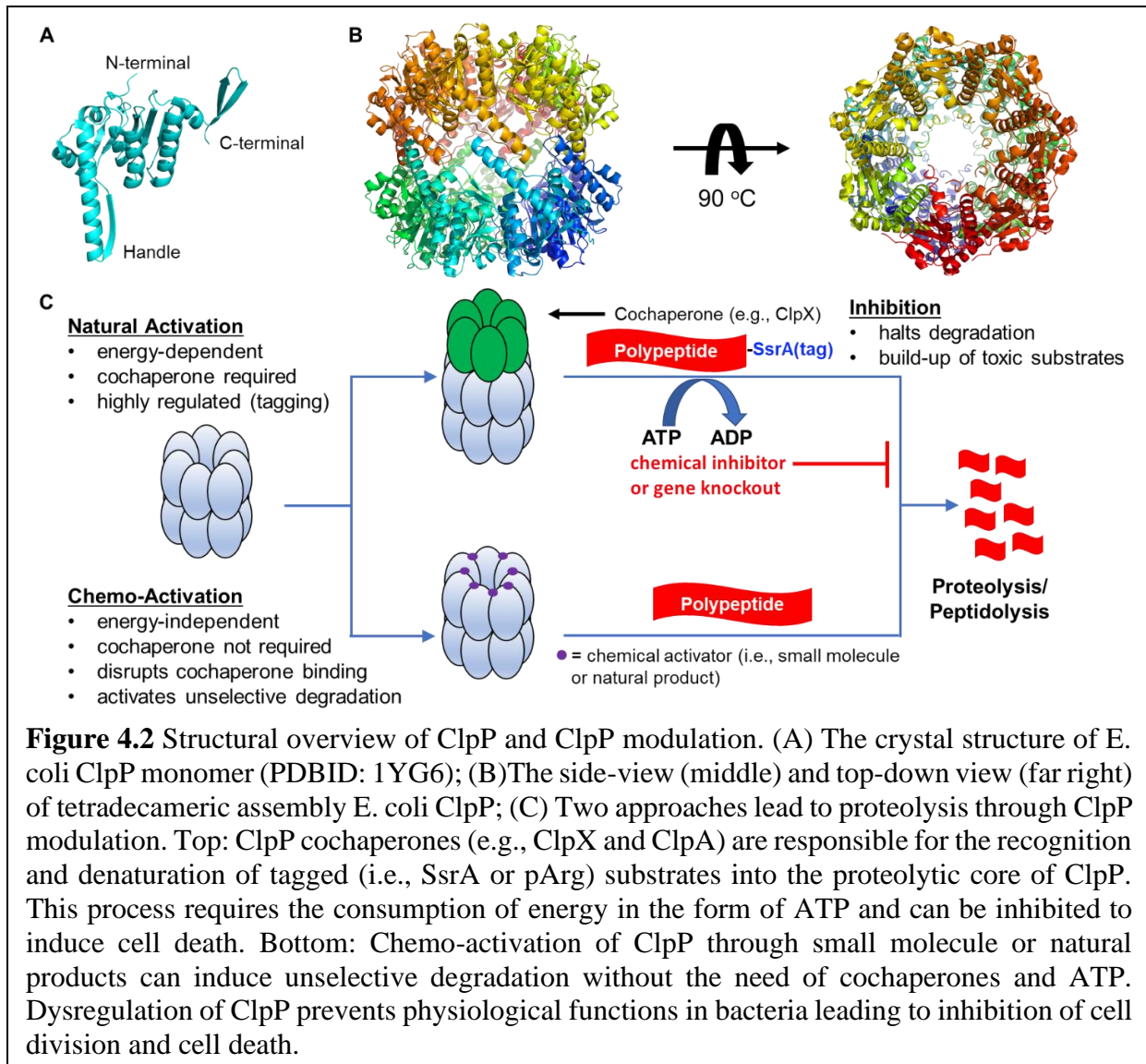
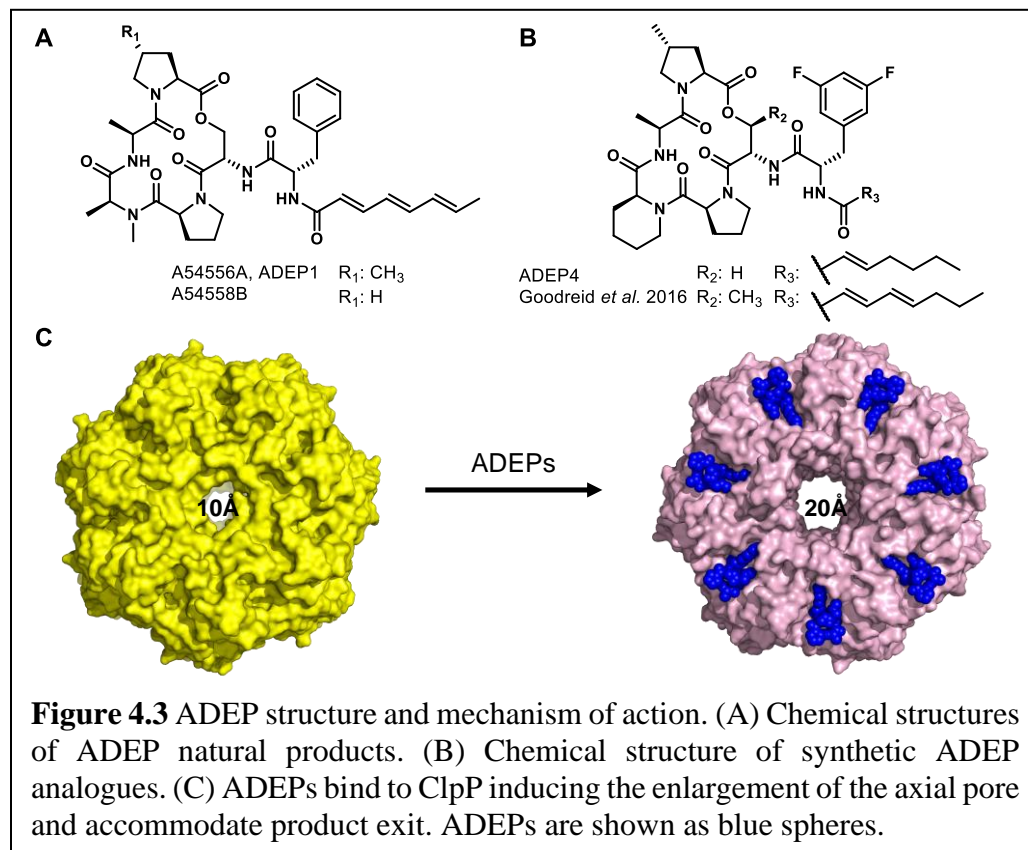


**Figure 4.2C).**<sup>13,14,16,17</sup> Activation of ClpP has been validated and proven safe *in vivo* as an antibacterial strategy against multiple infectious bacteria, including enterococci, staphylococci, and streptococci.<sup>17,18</sup> Moreover, the activation of ClpP kills the dormant state of persister cells, which prevents the formation of antibiotic tolerance.<sup>17</sup> Studies have shown that the activation of ClpP not only results in the degradation of non-specific polypeptides but also leads to the accumulation of proteins and peptides that are lethal to some pathogenic bacteria.<sup>19</sup> Therefore, “turning-on” ClpP provides a promising therapeutic strategy capable of addressing not only

actively growing and pathogenic bacterium but also the dormant persister phenotype that provide the population resistance.

## 4.2 Acyldepsipeptide (ADEP)



In the last decade, ADEPs have emerged as an promising ClpP activating chemotype.<sup>13</sup> The first ADEPs reported were A54556 A

(ADEP1, **Figure 4.3A**) and B from the fermentation broth of *Streptomyces hawaiiensis* NRRL 15010 and these two natural products demonstrate notable antibacterial activities against various antibiotic-resistant bacteria strains, including vancomycin-resistant *Enterococcus faecalis* (VRE), methicillin-resistant *Staphylococcus aureus* (MRSA), and penicillin-resistant *Streptococcus pneumoniae* (PRSP).<sup>20</sup> The antibacterial mechanism of action of ADEPs was later discovered to be the dysregulation of bacterial ClpP.<sup>16</sup> ADEP binds the hydrophobic pocket between two adjacent ClpP monomers, which mimics the interaction of the natural ATPases with ClpP. ADEP-bound ClpP undergoes a significant conformational reorganization to enlarge the entrance pore

and accommodate substrate entry, resulting in the non-selective degradation of polypeptides (**Figure 4.3B**).<sup>21,22</sup> Compared to Clp-ATPases, ADEP has a much higher affinity for ClpP.<sup>23</sup>

The crystal structure of ADEP1 and ClpP indicates that the N-acylphenylalanine of ADEP1 is embedded within the hydrophobic pocket of ClpP.<sup>24</sup> SAR studies reveal that 1) the (*E*)-2-heptenoic acid side chain is superior to other lengths and the introduction of polar substituents is not tolerated, 2) antibacterial activity is improved considerably by introduction of fluorine at 3 and 5 positions of the phenyl ring, and 3) introduction of a piperolate motif in the macrocycle increases rigidity of the macrocyclic core, thereby enhancing potency (ADEP4, **Figure 4.3B**).<sup>15</sup> Compared to the marketed antibiotic linezolid, ADEP4 exhibits a higher efficacy in mice infected with *S. aureus*, and its chemical stability is better than ADEP1.<sup>25</sup> Importantly, the combination of ADEP4 and rifampicin eradicates multi-drug resistant strains and persister cells in *S. aureus* biofilms in mouse models of chronic infection.<sup>17</sup> Further optimization of ADEP4 by Goodreid et. al demonstrates that introduction of an *allo*-threonine and an octanoyl aliphatic side chain, containing a diene functionality, improves activities against Gram-positive and -negative bacteria including a compromised *E. coli* strain (**Figure. 4.3A**).<sup>26</sup> Unfortunately, wild-type *E. coli* remained recalcitrant to ADEP treatment.<sup>26</sup>

Although the rational optimization of the ADEP chemotype has produced potent analogs against various bacteria, the clinical development of ADEPs has not advanced accordingly as pharmacokinetic and chemical liabilities persist.<sup>19,25</sup> One such example, published by Brotz-Oesterhelt and colleagues, demonstrates that preincubation of ADEP4 in Mueller-Hinton broth for nine days decreases minimal inhibitory concentration (MIC) against *Bacillus subtilis* from 0.13 µg/mL to 1 µg/mL, presumably due to ADEP degradation in experiment conditions.<sup>19</sup> Additionally, ADEPs failed to induce degradation of fluorogenic peptide substrates with any purified ClpPs of



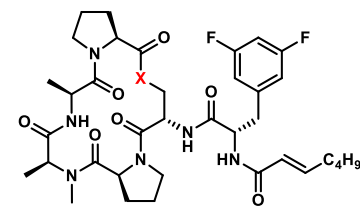
*Mycobacterium tuberculosis*.<sup>19</sup> Therefore, structural modification of the ADEP scaffold to address liabilities is necessary if this chemotype is to advance beyond animal studies and/or be developed into a broad spectrum antibacterial.

### 4.3 Addressing the Hydrolysis Issue of ADEP

One worry surrounding the ADEP scaffold is the stability of the depsipeptide core, as esters are known to undergo rapid hydrolysis in biological settings. One way to address the stability of the ester is to simply replace the ester with an amide or N-methyl amide. Goodreid et al. briefly reported that an -NH- substitution in ADEP4 decreases the activity against Gram-positive strains, including *S. aureus*, *S. aureus Newman*, *S. aureus ATCC 29213*, *E. faecalis V583*, *S. pneumoniae D39*, and *B. subtilis PY79*.<sup>26</sup>

In 2017, our group reported a systematic comparison of three ADEP analogs differing in only the macrocyclic linkage type (-O-, -NH-, -NMe-). The ability of these compounds to bind to ClpP and induce degradation of a self-quenching decapeptide is shown in **Table 4.1**. The -NH-substituted derivative (**4.2**) maintained target engagement but completely lost organismal activity.<sup>27</sup> The N-methyl amide analog (**4.3**) results in significant decreases in both potency and whole-cell activity. Through computational and spectroscopic analyses (**Table 4.1**), it was

**Table 4.1** Structure of designed ADEP analogs and activity comparison between ADEP analogs

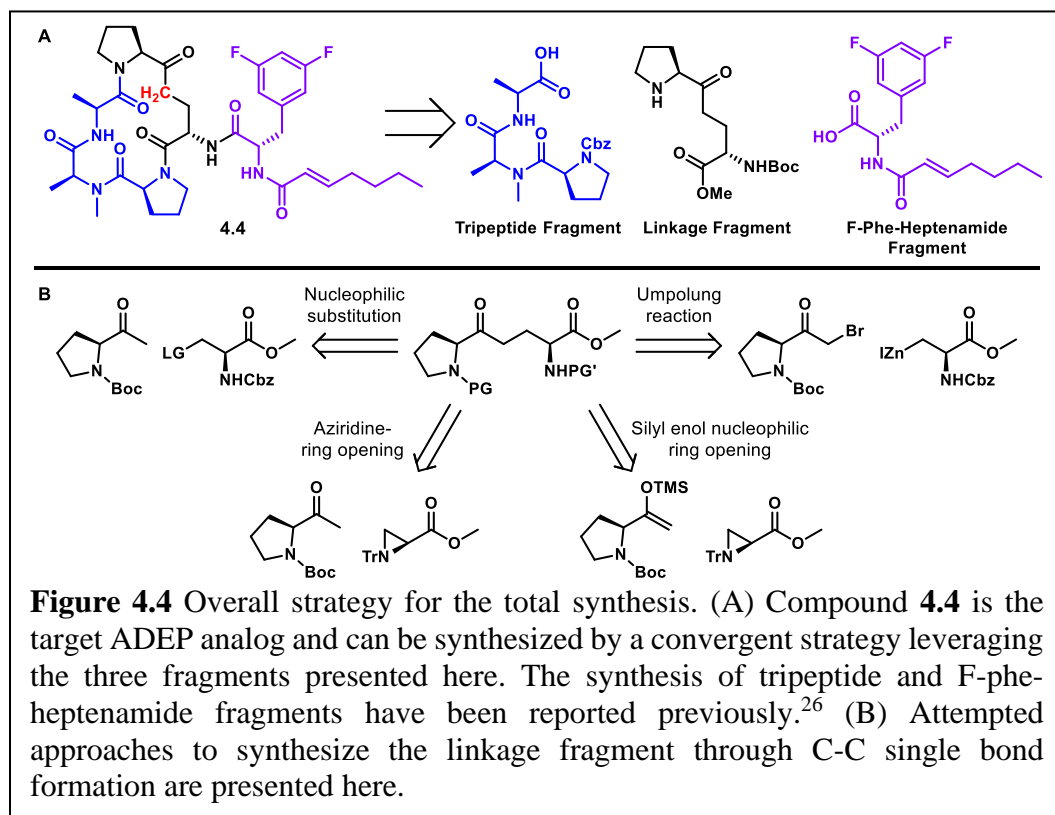
Structure	X	K <sub>app</sub> ( $\mu$ M)	MIC ( $\mu$ M: $\mu$ g/mL) <i>B. subtilis</i>	H/D exchange <i>t</i> <sub>1/2</sub> (min)
	-O- ( <b>4.1</b> , ADEP)	0.037	0.037:0.027	38
	-NH- ( <b>4.2</b> )	0.085	6.25:4.6	<4
	-NMe- ( <b>4.3</b> )	4.39	>25:>18.6	<4

concluded that a disruption of a key intramolecular hydrogen bond interaction is likely the reason for the discrepancy between target engagement and whole-cell activity for the -NH- linked derivative.<sup>27</sup> Thus, while the amide linkage may improve stability of the macrocycle, the concomitant negative affect on whole-cell activity limits this strategy.

#### 4.4 Total Synthesis of Designed Analog

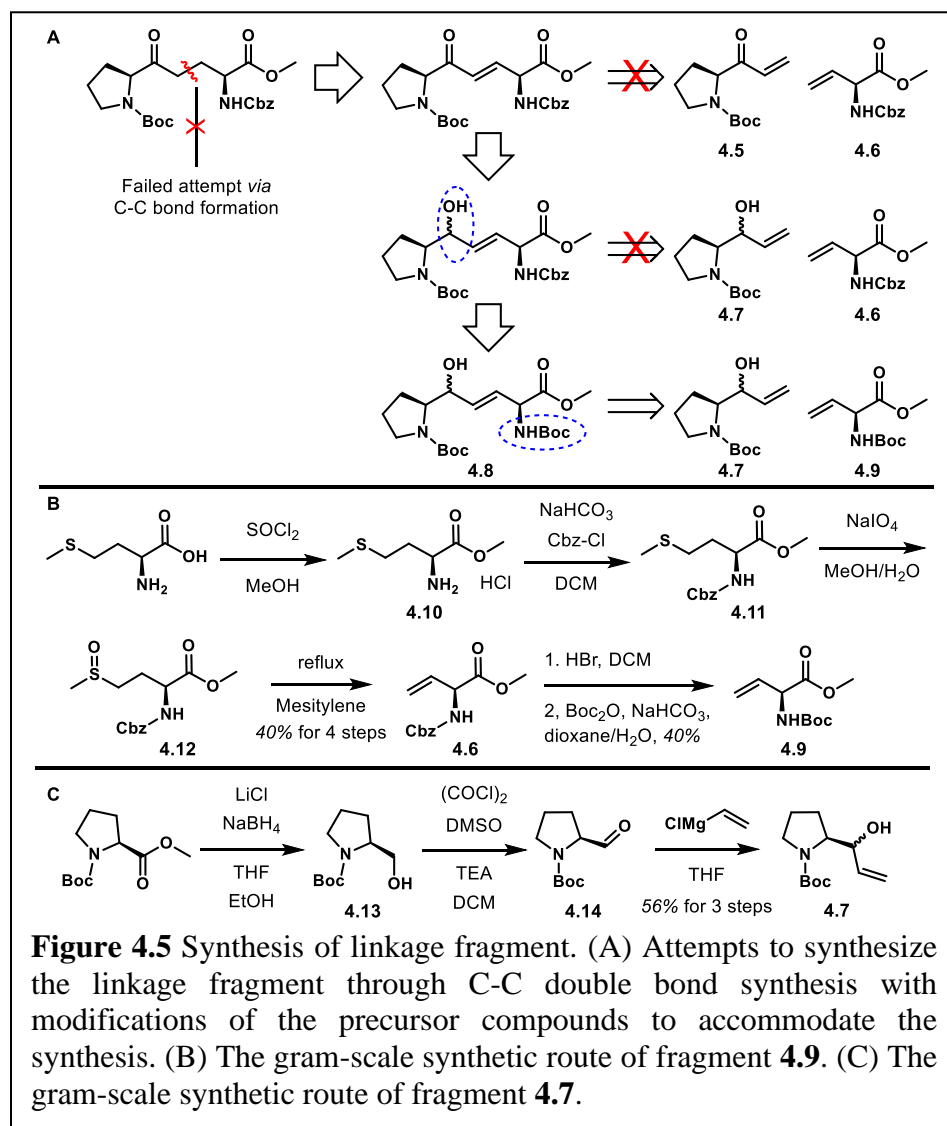
To provide more insight into the influence of the depsipeptide core on whole-cell activity, we hypothesized that replacing the -O- (**4.1**) linker with a -CH<sub>2</sub>- (**4.4**, **Figure 4.4A**) linkage would improve stability while maintaining the intramolecular hydrogen-bond interaction required for the

improved  
cell



permeability. This new ADEP analog (**4.4**) is only accessible through total synthesis and similar to the related derivatives synthesized by our group, we expected to access this derivative from a convergent synthetic approach comprised of tripeptide, linkage, and F-phe-heptenamide fragments (**Figure 4.4A**).

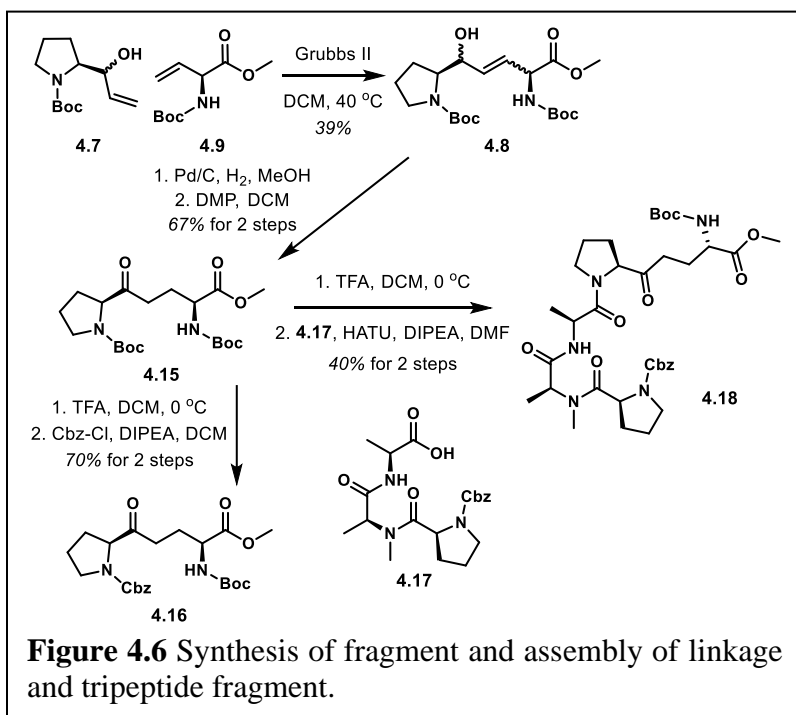
The primary challenge encountered in this work was in the synthesis of the linkage fragment. Initial retrosynthetic analysis of the linker fragment identified a C-C bond as an optimal disconnection and led to a number of attempts to form this bond directly (e.g., aldol reaction, aziridine opening, umpolung reaction, **Figure 4.4B**). All attempts were unsuccessful, in fact leveraging these methodologies failed to even produce trace amounts of product. Since direct formation of the C-C single bond failed, we sought to make this fragment through a metathesis reaction between compounds **4.5** and **4.6** (**Figure 4.5A**). These initial attempts failed under a variety of conditions including different catalysts, temperatures, and solvents.



Based on literature precedence, allylic alcohols are more reactive to cross metathesis than the corresponding allylic carbonyls.<sup>28</sup> Therefore, the oxidation state of fragment **4.5** was altered to the allylic alcohol **4.7**. Although the synthesis of allylic alcohol **4.7** required

a different route for preparation than the  $\alpha,\beta$ -unsaturated ketone **4.5**, this new fragment could be obtained using known procedures.<sup>29,30</sup> With this modification, a variety of conditions were evaluated in hopes of coupling **4.6** and **4.7**, but no desired product was formed. Therefore, we sought to modify the other fragment after determining that conversion of the benzyloxycarbonyl (Cbz) group (**4.6**) to a *t*-butylcarbamate (Boc) group (**4.9**) was reported to be more compatible with cross metathesis reactions.<sup>31</sup> After this second modification to the metathesis components, alkene **4.8** was successfully prepared from compounds **4.7** and **4.9** with the Second Generation Grubbs catalyst in dichloromethane at 40 °C for 12 h (**Figure 4.5A**).

It is worth noting that to complete the total synthesis, the linker fragment, arguably the most difficult to make, needed to be supplied in >1.0 g quantities. Fortunately, the vinyl glycine derivative **4.9** can be synthesized in gram-scale according to a reported procedure (**Figure 4.5B**).<sup>31</sup> To generate enough **4.9**,



L-methionine was converted into the methyl ester **4.10** using thionyl chloride in methanol. The amine was subsequently protected as the benzyloxycarbamate to give the derivative **4.11**, which was oxidized in the presence of NaIO<sub>4</sub> to obtain the sulfoxide **4.12**. A subsequent elimination reaction in mesitylene at 170 °C provided the desired terminal alkene **4.6** in a yield of 40% over

four steps. The Cbz group was removed with HBr and subsequent addition of (Boc)<sub>2</sub>O and NaHCO<sub>3</sub> provided the Boc-protected compound **4.9** in 40% yield.

The synthesis of allylic alcohol derivative **4.7** also required in gram-scale preparations and this was completed from L-Boc-Pro-OMe using a previously reported procedure (**Figure. 4.5C**).<sup>29</sup> The methyl ester was reduced to alcohol **4.13** with lithium chloride and sodium borohydride. A Swern oxidation provided aldehyde **4.14**, which was treated with vinyl magnesium chloride in a Grignard reaction to yield the allylic alcohol **4.7**. The overall yield was 56% and the NMR spectrum was identical to that previously described.<sup>29</sup> Since the alcohol will be converted to a

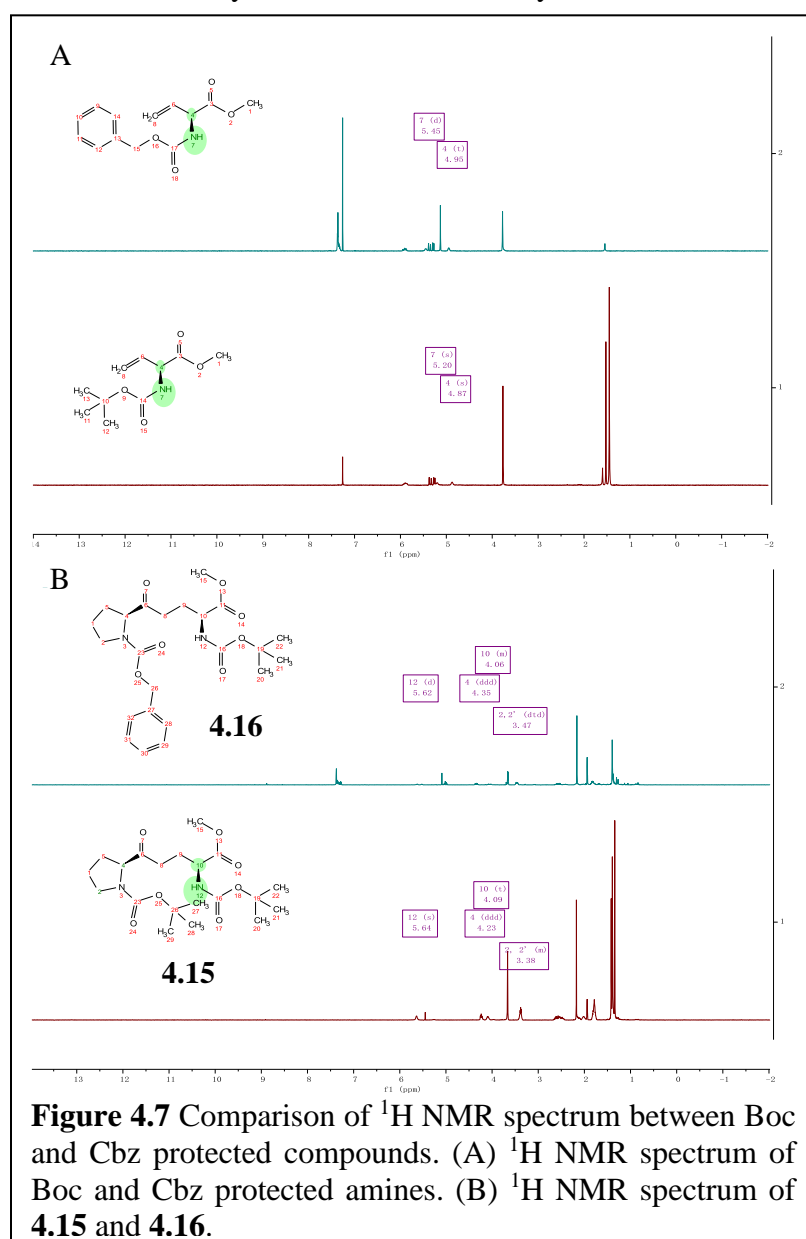
**Table 4.2** NMR Data (500 MHz, CD<sub>3</sub>CN) of **4.16**<sup>a</sup>

Atom	$\delta_C$ , type	$\delta_H$ (J in Hz)	COSY	HMBC <sup>b</sup>
1a	29.9, CH <sub>2</sub>	1.79 <sup>c</sup> , m	H-1b, H-2b, H-5a	2, 5
1b		1.79 <sup>c</sup> , m	H-1a, H-2a, H-5b	
2a	49.4, CH <sub>2</sub>	3.43, m	H-1b, H-2b	1, 5
2b		3.44, m	H-1a, H-2a	
4	67.5, CH	4.29 <sup>c</sup> , m	H-5a, H-5b	1, 5, 23 <sup>e</sup>
5a	30.8, CH <sub>2</sub>	2.12 <sup>c</sup> , m	H-1b, H-5b, H-4	1, 2, 4
5b		1.79 <sup>c</sup> , m	H-1a, H-5a, H-4	
6	170.1, C			
8a	36.1, CH <sub>2</sub>	2.52 <sup>c</sup> , m	H-8b, H-9b	9
8b		2.38 <sup>c</sup> , m	H-8a, H-9a	
9a	26.4, CH <sub>2</sub>	2.01 <sup>c</sup> , m	H-8b, H-9b, H-10	8, 10
9b		1.66 <sup>c</sup> , m	H-8a, H-9a, H-10	
10	55.4, CH	4.05, m	H-9a, H-9b	9
11	175.6, C			
15	54.2, CH <sub>3</sub>	3.63, d		11
16	155.0, C			
19	81.5, C			
20	29.0, CH <sub>3</sub>	1.38, s		19, 16
23	155.6, C			
26	68.9, CH <sub>2</sub>	5.08 <sup>d</sup> , m	H-28, H-29	23
27	139.7, C			
28	127.9, CH	7.28, m	H-26, H-29, H-30	26, 27, 30
29	127.8, CH	7.38, m	H-26, H-29, H-30	28, 30
30	127.6, CH	7.34, m	H-29, H-30	28, 29
NH(12)		5.58, m		

<sup>a</sup>c = 10 mg/mL. <sup>b</sup>HMBC correlations, optimized for 8.0 Hz, are from proton(s) stated to the indicated carbon. <sup>c</sup>Denotes values were taken from correlations observed in a <sup>1</sup>H-<sup>13</sup>C HSQC NMR experiment. <sup>d</sup>Protons are not solved. <sup>e</sup>HMBC correlation solved by 5.0 Hz.

ketone in a future step, both diastereomers were collected and advanced as a mixture. After sufficient amounts of **4.7** and **4.9** were in-hand, the focus moved towards the assembly of the fragments

into the macrocyclic core. A gram-scale cross metathesis reaction between **4.7** and **4.9** provided 400 mg of compound **4.8**. The alkene in **4.8** was reduced by exposure to Pd/C under an atmosphere of H<sub>2</sub> and then oxidation of the secondary hydroxyl group was accomplished with Dess-Martin periodinane (DMP) to give the desired fragment **4.15** (**Figure 4.6**). However, this intermediate posed a problem, as both amines were protected with Boc groups. In order to allow for us to use our previous synthetic route to establish the macrocycle, we needed to identify conditions that would selectively reveal the secondary amine. After several conditions were assessed, a



chemoselective method was developed to give an amine, which employs 15 equivalents of trifluoroacetic acid at 0 °C for two hours. To ensure the correct product was obtained, the resulting amine was protected with a Cbz group to give intermediate **4.16**, which was analyzed via NMR to directly confirm the chemoselective nature of the Boc deprotection.

The assignment of the  $^1\text{H}$  NMR spectrum of **4.16** was accomplished using a combination of 2D NMR techniques including COSY, NOESY, TOCSY, and HSQC (**Table 4.2**). The assignment of the  $^{13}\text{C}$  NMR spectrum of **4.16** utilized a combination of HSQC (for carbons with attached hydrogens) and HMBC spectra (for carbonyl carbons) (**Table 4.2** and **Figure 4.8**). The  $^1\text{H}$  NMR signals of the  $\beta$  hydrogen on C2 and C4 of **4.16** proved to be diagnostic in nature, as downfield shifts of 0.09 ppm and 0.12 ppm were observed, respectively, in comparison to **4.15**. A similar phenomenon was observed previously upon the Cbz to Boc conversion (**Figure 4.7**). All other hydrogen signals from **4.16** remained relatively unchanged, thus confirming the region of transformation. Moreover, correlations between H4 to C23 of **4.16** were found from the HMBC spectrum optimized by 5.0 Hz directly indicating the deprotection and protection on the secondary amine. It is assumed that the chemoselectivity of the deprotection arises from the inductive effect produced by a higher substitution of the secondary amine, making the appended carbamate more

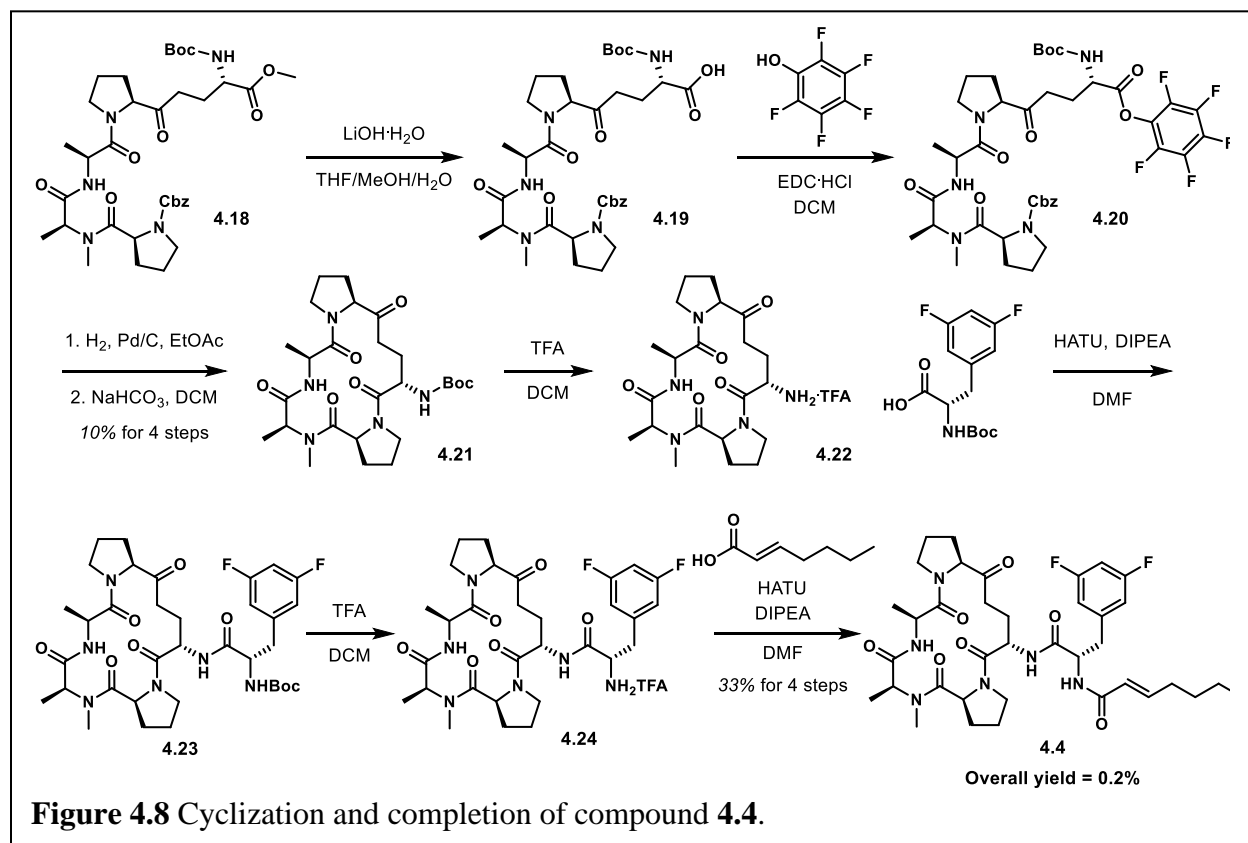


**Figure 4.8** Cyclization and completion of compound **4.4**.

reactive to the initial protonation step of the reaction. Once the selectivity of the deprotection was solved, **4.15** was deprotected and then coupled with the tripeptide fragment **4.17** to yield the requisite pentapeptide-like intermediate **4.18** (Figure 4.6).

To complete the synthesis, intermediate **4.18** was converted to macrocycle **4.21** (Figure 4.7). Although the four step yield was low (10%) it arises from a sequence that includes two protecting group removals, ester activation, and a base-catalyzed intramolecular cyclization (Figure 4.7) and provided enough material to progress.<sup>27</sup> As anticipated, the Cbz group protecting on the terminal proline was selectively removed via hydrogenolysis using Pd/C and H<sub>2</sub> in ethyl acetate. With the cyclized molecule **4.21** in hand, the final assembly of the ADEP analog was completed (Figure 4.7). Removal of the Boc protecting group under standard conditions provided the trifluoroacetic acid salt **4.22**, which was used without any further purification. Compound **4.22** was then coupled to *N*-Boc protected 3,5-difluoro-L-phenylacetic acid to produce **4.23**.

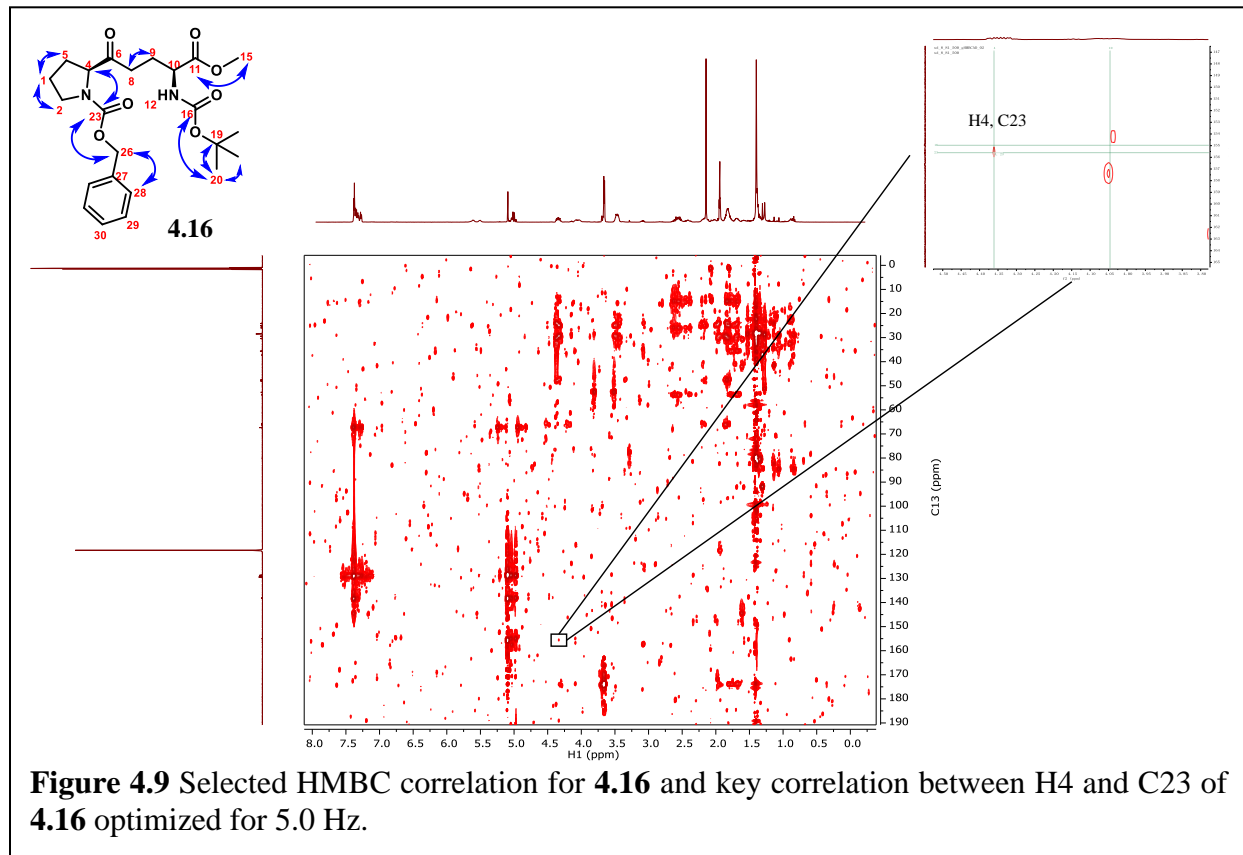


**Figure 4.9** Selected HMBC correlation for **4.16** and key correlation between H4 and C23 of **4.16** optimized for 5.0 Hz.



Subsequent Boc removal and exposure of **4.24** to (*E*)-hept-2-enoic acid under peptide coupling conditions provided the desired compound **4.4**. In the end, only 1~2 mg crude product was formed, which was confirmed by high resolution mass spectrometry (HRMS). While the low amount of crude product is not enough for us to run the requisite studies to confirm the structure, assess conformational properties, and determine biological activity the completion of the synthesis provides a means for future scale-up.

#### **4.5 Conclusion**

ClpP is a viable antibiotic target that can be activated by small molecules to achieve bactericidal effects. ADEPs represent a group of promising ClpP activators due to their excellent activity *in vitro* and *in vivo* against a number of multi-drug resistant pathogens. However, chemical and pharmacokinetic liabilities preclude the clinical development of this class. Herein, we designed and completed a 15-step total synthesis of an unnatural ADEP analog that contains a methylene linked macrocycle instead of the labile depsipeptide ester. Based on our previous work, the hypothesis is that this linkage will improve stability of the macrocycle while maintaining important conformational features responsible for tight binding and cell permeability. The highlight of the synthesis includes a metathesis reaction between two rationally modified segments, which enabled the synthesis of the critical linker fragment. Furthermore, this work includes the identification of chemoselective deprotection of a *t*-butylcarbamate to reveal the desired secondary amine. Based on this 15-step procedure, a new ADEP analog was synthesized and will be investigated with biochemical, microbiological, spectroscopic, and computational methods to determine if the hypothesis is correct. This work is expected to advance upon our previous studies on macrocyclic linker substitution and showcase the power of single atom substitution in molecular design.

## 4.6 Experimental Section

Methyl (S)-2-(((benzyloxy)carbonyl)amino)but-3-enoate (**4.6**): a solution of sulfoxide **4.12** (16.5 g, 50 mmol) in 1,3,5-trimethylbenzene (50 mL) was refluxed for overnight. After cooling to room temperature, the solvent was partially removed by rotary evaporator and the residue was purified on a silica gel column and eluted with hexanes to remove the remaining of 1,3,5-trimethylbenzene. Elution with hexanes/EtOAc 9:1 afforded **4.6** as a brown oil in 74% yield. <sup>1</sup>H NMR (400 MHz, Chloroform-*d*)  $\delta$  7.36 (s, 5H), 5.91 (ddd,  $J = 5.5, 10.3, 16.4$  Hz, 1H), 5.45 (d,  $J = 8.0$  Hz, 1H), 5.41 – 5.33 (m, 1H), 5.28 (dd,  $J = 1.7, 10.4$  Hz, 1H), 5.13 (s, 2H), 4.95 (t,  $J = 7.0$  Hz, 1H), 3.77 (s, 3H).

Methyl (S)-2-((tert-butoxycarbonyl)amino)but-3-enoate (**4.9**): a solution of **4.6** (2.49 g, 10.0 mmol) in an hydrobromic acid solution (4 mL) was stirred at room temperature for 2 h and then diluted with DCM. The resulting mixture was concentrated under reduced pressure to give the crude product as a brown oil. The crude product was dissolved in 1,4-dioxane (20 mL) and H<sub>2</sub>O (15 mL), and the pH of the solution was then slowly adjusted to pH = 9 by the addition of NaHCO<sub>3</sub> at 0 °C. A solution of Boc<sub>2</sub>O (4.36 g, 20.0 mmol) in 1,4-dioxane (10 mL) was added at the same temperature. The resulting mixture was stirred for 12 h at room temperature and then concentrated under reduced pressure. The residue was treated with H<sub>2</sub>O (15 mL), and the resulting solution was extracted with EtOAc (3 × 20 mL). The combined organic extracts were dried with Na<sub>2</sub>SO<sub>4</sub>, filtered, and concentrated. The residue was purified by chromatography on a silica gel column (hexanes/EtOAc, 10:1) to afford **4.7** (1.5 g, 70% over two steps) as a colorless oil; <sup>1</sup>H NMR (400 MHz, Chloroform-*d*)  $\delta$  5.90 (ddd,  $J = 5.4, 10.3, 16.4$  Hz, 1H), 5.35 (ddd,  $J = 0.7, 1.8, 17.1$  Hz, 1H), 5.28 – 5.21 (m, 1H), 5.20 (s, 1H), 4.87 (s, 1H), 3.77 (s, 3H), 1.45 (s, 9H).

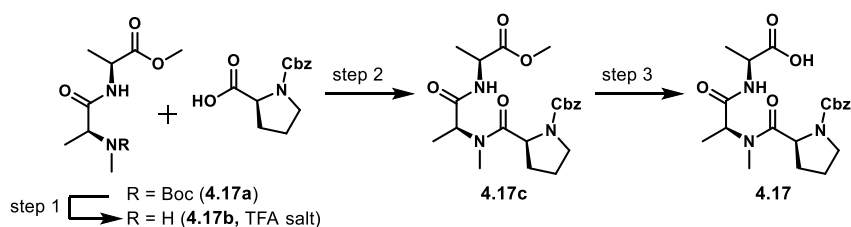
Tert-butyl (S)-2-(1-hydroxyallyl)pyrrolidine-1-carboxylate (**4.7**): crude aldehyde **4.14**<sup>29</sup> (5.00 mmol) was placed in a flask, which was capped with a rubber septum and flushed with N<sub>2</sub>.

Anhydrous THF (25 mL, 0.2 M) was added. The solution was cooled in a dry ice/acetonitrile bath (-40 °C), and vinylmagnesium chloride (1.6 M in THF, 6.30 mL, 10.0 mmol) was added. The solution was stirred (5 min), transferred to an ice bath (0 °C), stirred an additional 30 min, quenched with citric acid (10% aqueous, 60 mL), concentrated under reduced pressure, extracted with EtOAc (100 mL), washed with saturated aqueous NaHCO<sub>3</sub> solution (60 mL) and brine (60 mL), and dried with Na<sub>2</sub>SO<sub>4</sub>. Volatiles were removed under reduced pressure, and the crude materials was purified via a silica gel column (hexanes/EtOAc, 15:1), yielding pure and diastereomerically mixed fractions of the desired product **4.7** (681 mg, 60% yield overall). It was found most convenient to collect both diastereomers and used without further purification. <sup>1</sup>H NMR (400 MHz, Chloroform-*d*) δ 5.93 – 5.72 (m, 1H), 5.35 (dt, *J* = 1.5, 17.2 Hz, 1H), 5.24 (dtd, *J* = 1.1, 2.0, 10.3 Hz, 1H), 4.13 (d, *J* = 77.5 Hz, 2H), 3.92 – 3.11 (m, 3H), 2.09 – 1.68 (m, 4H), 1.57 (d, *J* = 4.5 Hz, 9H).

Tert-butyl (S)-2-((S,E)-4-((tert-butoxycarbonyl)amino)-1-hydroxy-5-methoxy-5-oxopent-2-en-1-yl)pyrrolidine-1-carboxylate (**4.8**): To a 50 mL round bottom flask were added allyl alcohol **4.7** (851 mg, 3.75 mmol), DCM (10 mL), and vinylglycinol **4.9** (1.20 g, 5.62 mmol) and Grubbs second generation catalyst (157 mg, 0.18 mmol). The flask was fixed with a reflux condenser and warmed in an oil bath (40 °C, 12 h). Additional vinylglycinol and catalyst (equal amounts to previous) were added, and the reaction was continued (additional 12 h). Volatiles were removed under reduced pressure, and the crude mixture was purified via a silica gel column (hexanes/EtOAc, 5:1 to 3:1 to 5:2), yielding diastereomerically mixed fractions of the desired product **4.8** (621 mg, 40% yield overall). The two diastereomers were not readily distinguished by <sup>1</sup>H NMR or TLC. <sup>1</sup>H NMR (400 MHz, Chloroform-*d*) δ 5.83 – 5.77 (m, 1H), 5.76 – 5.67 (m, 1H), 5.56 – 5.16 (m, 1H),

4.86 (d,  $J = 8.8$  Hz, 1H), 3.73 (d,  $J = 2.4$  Hz, 3H), 3.54 – 3.10 (m, 2H), 1.82 (d,  $J = 17.1$  Hz, 2H), 1.74 – 1.63 (m, 2H), 1.45 (d,  $J = 2.3$  Hz, 9H), 1.42 (d,  $J = 3.4$  Hz, 9H).

Tert-butyl (S)-2-((S)-4-((tert-butoxycarbonyl)amino)-5-methoxy-5-oxopentanoyl)pyrrolidine-1-carboxylate (**4.15**): To a 50 mL round bottom flask were added the compound **4.8** (621mg, 1.50 mmol) and MeOH (15 mL). The flask was capped with a septum and flushed with N<sub>2</sub>. The flask was quickly uncapped and 10% Pd/C (159 mg, 0.15 mmol) was added. The mixture was immediately capped and flushed with N<sub>2</sub> (5 min). A hydrogen-filled balloon was attached, the flask was flushed briefly with hydrogen by bubbling into the solution, and the reaction was stirred at room temperature under the balloon atmosphere for 12 h. The reaction was monitored by the TLC upon completion of the compound **4.8**. The balloon was removed, the flask was flushed with N<sub>2</sub>, the mixture was filtered through Celite, and volatiles were removed under reduced pressure. Due to cleanliness of the reaction, the crude compound was used without any further purification. The crude compound was dissolved into DCM (150 mL) and cooled to 0 °C. Dess-Martin periodinane (1.00 g, 2.37 mmol) was added and the solution was stirred vigorously for 3 h. The solution was quenched with aqueous 1M of Na<sub>2</sub>S<sub>2</sub>O<sub>3</sub> (30 mL) and saturated NaHCO<sub>3</sub> (70 mL). The organic phase was separated, and the aqueous phase was extracted with DCM (20 mL × 2). The combined organic layers were dried by Na<sub>2</sub>SO<sub>4</sub> and filtered. Volatiles were removed under reduced pressure, and the compound **4.15** was purified via a silica gel column (hexanes/EtOAc, 10:1). <sup>1</sup>H NMR (600 MHz, Acetonitrile-*d*<sub>3</sub>) δ 5.64 (s, 1H), 4.23 (ddd,  $J = 4.2, 8.4, 15.4$  Hz, 1H), 4.09 (t,  $J = 9.7$  Hz, 1H), 3.66 (s, 3H), 3.53 – 3.25 (m, 2H), 2.67 – 2.41 (m, 2H), 2.14 – 1.99 (m, 2H), 1.83 – 1.72 (m, 2H), 1.70 (dd,  $J = 4.9, 11.0$  Hz, 2H), 1.41 (d,  $J = 14.8$  Hz, 9H), 1.34 (s, 9H).

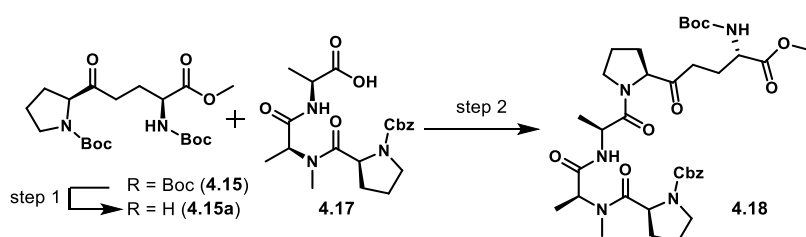


### Synthesis of compound **4.17**.

*Step 1:* Anhydrous TFA (5 mL) was added dropwise to a solution of a **4.17a** (500 mg, 1.74 mmol) in anhydrous DCM (20 mL) at 0 °C under an N<sub>2</sub> atmosphere and the reaction was stirred for 2 h. Upon completion of the reaction, as indicated via complete conversion of **4.17a** by TLC, the reaction was quenched by addition of solid NaHCO<sub>3</sub>. After vigorously stirring for 10 min, the solution was filtered through a filter funnel and filtrate was concentrated to yield crude **4.17b**, which was used without further purification.

*Step 2:* HATU (728 mg, 1.91 mmol) was added to a solution of a ((benzyloxy)carbonyl)-L-proline (434 mg, 1.74 mmol) in DMF (8 mL) at 0 °C under an N<sub>2</sub> atmosphere. A pre-mixed solution of **4.17b** and DIPEA (1 mL, 5.21 mmol) in DMF (8 mL) was then added to the reaction mixture by syringe. The reaction mixture was allowed to stir for 12 h at 25 °C under a N<sub>2</sub> atmosphere. The reaction mixture was diluted with EtOAc and washed three times with 1M aq. HCl, three times with saturated aq. NaHCO<sub>3</sub>, and one time with brine. The organic layer was collected, dried over Na<sub>2</sub>SO<sub>4</sub>, filtered, and concentrated *in vacuo*. The residue was purified by a silica gel column using a gradient of MeOH/DCM (1:50) to yield **4.17c** (82%, 596 mg). <sup>1</sup>H NMR (400 MHz, Acetonitrile-*d*<sub>3</sub>) δ 7.54 – 7.16 (m, 5H), 5.09 (dd, *J* = 3.7, 11.3 Hz, 2H), 5.04 – 4.84 (m, 1H), 4.81 – 4.49 (m, 1H), 4.41 (td, *J* = 4.3, 8.4 Hz, 1H), 3.65 (d, *J* = 4.0 Hz, 3H), 3.60 – 3.37 (m, 2H), 3.02 – 2.75 (m, 3H), 1.92 – 1.86 (m, 2H), 1.74 (d, *J* = 6.5 Hz, 2H), 1.28 (dd, *J* = 3.0, 8.0 Hz, 3H), 1.27 – 1.19 (m, 3H).

*Step 3:* To a stirred solution of a **4.17c** in THF/MeOH/H<sub>2</sub>O mixture (15 mL, 3:1:1) was added lithium hydroxide monohydrate (291 mg, 7 mmol) and the reaction mixture was stirred for 12 h at 25 °C. The reaction mixture was then concentrated to remove organic solvents and the aqueous layer was acidified to pH 2.0 with 1 N aq. HCl before extracting with EtOAc. The organic layer was washed with water and brine. The resulting organic layer was dried over anhydrous Na<sub>2</sub>SO<sub>4</sub>, filtered, and evaporated under vacuum. The crude compound **4.17** was used without any further purification.

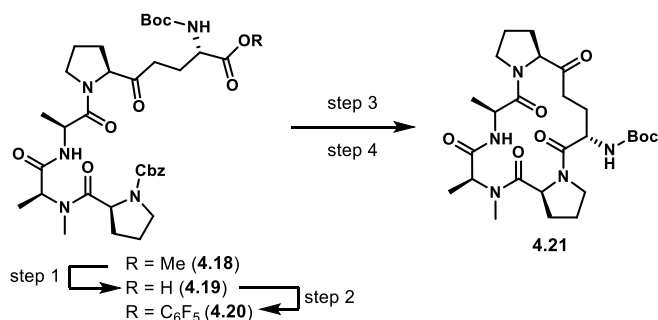


Synthesis of compound **4.18**.

*Step 1:* Anhydrous TFA (0.69 mL, 9 mmol) was added dropwise to a solution of a **4.15** (250 mg, 0.60 mmol) in anhydrous DCM (6 mL) at 0 °C under an N<sub>2</sub> atmosphere for 2 h. Upon completion of the reaction, as indicated via complete conversion of **4.15** by TLC, the reaction was quenched by addition of solid NaHCO<sub>3</sub> (3.78 g, 45 mmol). After vigorously stirring for 10 min, the solution was filtered through a filter funnel and the filtrate was concentrated in vacuo to yield crude **4.15a**, which was used without further purification.

*Step 2:* HATU (1.1 eq.) was added to a solution of a **4.17** (246 mg, 0.60 mmol) in DMF (3 mL) at 0 °C under an N<sub>2</sub> atmosphere. A pre-mixed solution of **4.15a** and DIPEA (0.32 mL, 1.80 mmol) in DMF ( mL) was then added to the reaction mixture by syringe. The reaction mixture was allowed to stir for 12 h at 25 °C under a N<sub>2</sub> atmosphere. Upon completion of the reaction, as indicated via complete conversion of **4.15a** by TLC, the reaction mixture was diluted with EtOAc (110 mL) and washed three times with 1M aq. HCl, three times with saturated aq. NaHCO<sub>3</sub>, and one time with

brine. The organic layer was collected, dried over Na<sub>2</sub>SO<sub>4</sub>, filtered, and concentrated *in vacuo*. The residue was purified by a silico gel column using a gradient of 0-20% acetone in EtOAc to yield **4.18** (15%, 64 mg). <sup>1</sup>H NMR (300 MHz, Acetonitrile-*d*<sub>3</sub>, 20 °C, major rotamer annotated) δ 7.39 – 7.27 (m, 5H), 5.07 (dt, *J* = 2.5, 7.7 Hz, 2H), 5.05 – 4.99 (m, 1H), 4.97 – 4.90 (m, 1H), 4.80 – 4.69 (m, 1H), 4.68 – 4.63 (m, 1H), 4.57 – 4.39 (m, 1H), 3.71 – 3.62 (m, 3H), 3.61 – 3.50 (m, 2H), 3.50 – 3.38 (m, 2H), 3.01 – 2.78 (m, 3H), 2.68 (s, 2H), 2.54 – 2.49 (m, 1H), 2.28 (dd, *J* = 4.5, 8.4 Hz, 2H), 2.16 – 2.07 (m, 2H), 1.88 (d, *J* = 3.4 Hz, 1H), 1.85 (s, 1H), 1.81 – 1.71 (m, 2H), 1.39 (d, *J* = 3.3 Hz, 9H), 1.26 (d, *J* = 4.1 Hz, 3H), 1.23 – 1.16 (m, 3H).

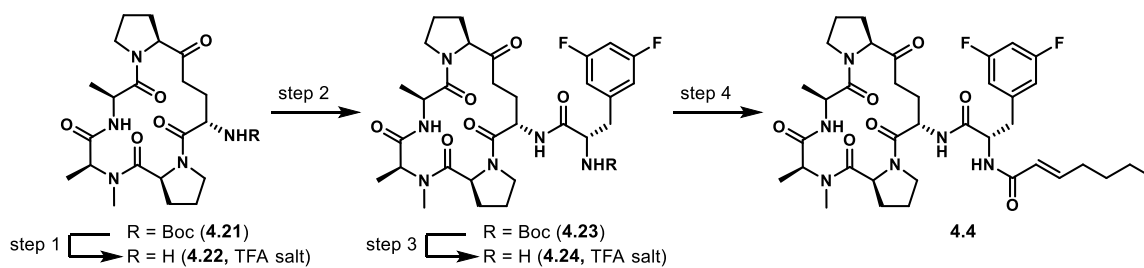


### Synthesis of compound **4.21**.

*Step 1:* To a stirred solution of a **4.18** (64 mg, 0.12 mmol) in THF/MeOH/H<sub>2</sub>O mixture (1.2 mL, 3:1:1) was added lithium hydroxide monohydrate (24.6 mg, 0.6 mmol) and the reaction mixture was stirred for 12 h at 25 °C. The reaction mixture was concentrated to remove organic solvents and the aqueous layer was acidified to pH 2.0 with 1 N aq. HCl before extracting with EtOAc. The organic layer was washed with water and brine then dried over anhydrous Na<sub>2</sub>SO<sub>4</sub>, filtered, and evaporated under vacuum.

*Step 2:* Compound **4.19** was dissolved in DCM (1.2 mL) and cooled to -20 °C. Neat pentafluorophenol (110 mg, 0.6 mmol) was added at once followed by EDC·HCl (37 mg, 0.19 mmol). The mixture was stirred for 12 h with gradual warming to RT. The solvent was removed *in vacuo* to reveal a pale-yellow oil residue **4.20**, which was used without further purification.

*Step 3 &4:* The crude pentafluorophenol ester **4.20** was dissolved in EtOAc (12 mL) The flask was capped with a septum and flushed with N<sub>2</sub>. The flask was quickly uncapped and 10% Pd/C (13 mg, 0.012 mmol) was added. The mixture was capped immediately and flushed with N<sub>2</sub> (5 min). A hydrogen-filled balloon was attached, the flask was flushed briefly with hydrogen by bubbling into the solution, and the reaction was stirred at room temperature under the balloon atmosphere for 12 h. The balloon was removed, the flask was flushed with N<sub>2</sub>, the mixture was filtered through Celite, and the volatiles were removed under reduced pressure. The crude residue was used without further purification. The crude residue was diluted with DCM (12 mL) and added dropwise at a rate of ~2 drops/second from an addition funnel into a flask containing a stirring solution of DCM (12 mL) and 1M aq. NaHCO<sub>3</sub> (24 mL). After complete addition, the reaction stirred for 12 h at 25 °C, after which, the solution was transferred to a separatory funnel and partitioned between H<sub>2</sub>O and DCM. The aqueous layer was subsequently washed with fresh DCM. The organic extracts were combined, dried over Na<sub>2</sub>SO<sub>4</sub>, filtered, and concentrated *in vacuo*. The residue was purified by a silica gel column using a gradient of 0-20% hexanes in EtOAc to yield **4.21** (7 mg, 14%). <sup>1</sup>H NMR (300 MHz, Chloroform-*d*) δ 7.12 (d, *J* = 8.2 Hz, 1H), 6.81 (d, *J* = 7.8 Hz, 1H), 5.11 (s, 0H), 4.89 – 4.77 (m, 1H), 4.70 – 4.49 (m, 1H), 4.31 (d, *J* = 9.3 Hz, 1H), 4.10 (s, 1H), 3.68 (t, *J* = 6.7 Hz, 2H), 3.59 (s, 2H), 3.34 – 3.13 (m, 3H), 3.13 – 2.68 (m, 1H), 2.27 (s, 1H), 2.21 – 2.08 (m, 2H), 2.09 – 1.99 (m, 2H), 1.98 – 1.94 (m, 2H), 1.93 – 1.88 (m, 2H), 1.86 – 1.79 (m, 2H), 1.45 – 1.39 (m, 9H), 1.35 (d, *J* = 7.0 Hz, 3H), 1.31 (d, *J* = 6.6 Hz, 3H).





Synthesis of compound **4.4**.

*Step 1:* Compound **4.21** was treated with TFA (0.5 mL) in DCM (0.5 mL) at 0 °C under an N<sub>2</sub> atmosphere. Upon completion of the reaction, as indicated via complete conversion of **4.21** by TLC, the reaction was concentrated with a stream of N<sub>2</sub> and the resulting residue (**4.22**) was then stored on the high vac. for 6 h prior to use without further purification.

*Step 2:* HATU (5 mg, 0.01 mmol) was added to a solution of Boc-difluorophenylalanine (4 mg, 0.01 mmol) in DMF (0.1 mL) at 0 °C under an N<sub>2</sub> atmosphere. A pre-mixed solution of **4.22** and DIPEA (7 mL, 0.04 mmol) in DMF (0.1 mL) was then added to the reaction mixture by syringe. The reaction mixture was allowed to stir for 12 h at 25 °C under an N<sub>2</sub> atmosphere. Upon completion of the reaction, as indicated via complete conversion of **4.22** by TLC, the reaction mixture was diluted with EtOAc and washed three times with 1 M aq. HCl, three times with saturated aq. NaHCO<sub>3</sub>, and one time with brine. The organic layer was collected, dried over Na<sub>2</sub>SO<sub>4</sub>, filtered, and concentrated *in vacuo* to reveal **4.23** as an amorphous white solid, which was used without further purification.

*Step 3:* Compound **4.23** was treated with TFA (0.5 mL) in DCM (0.5 mL) at 0 °C under an N<sub>2</sub> atmosphere. Upon completion of the reaction, as indicated via complete conversion of **4.23** by TLC, the reaction was concentrated with a stream of N<sub>2</sub> and the resulting residue (**4.24**) was then stored on the high vac. for 6 h prior to use without further purification.

*Step 4:* HATU (5 mg, 0.01 mmol) was added to a solution of (*E*)-2-heptenoic acid (1.3 mg, 0.01 mmol) in DMF (0.1 mL) at 0 °C under a N<sub>2</sub> atmosphere. A pre-mixed solution of **4.24** and DIPEA (7 mL, 0.04 mmol) in DMF (0.1 mL) was then added to the reaction mixture by syringe. The reaction mixture was allowed to stir for 12 h at 25 °C under a N<sub>2</sub> atmosphere. Upon completion of the reaction, as indicated via complete conversion of **4.24** by TLC, the reaction mixture was diluted

with EtOAc and washed three times with 1 M aq. HCl, three times with saturated aq. NaHCO<sub>3</sub>, and one time with brine. The organic layer was collected, dried over Na<sub>2</sub>SO<sub>4</sub>, filtered, and concentrated *in vacuo*. The crude residue was only characterized by HRMS. TOFMSESI m/z: 729.3796 (C<sub>37</sub>H<sub>50</sub>F<sub>2</sub>N<sub>6</sub>O<sub>7</sub> + H<sup>+</sup> requires 729.3743).

#### 4.7 References

1. CDC. Antibiotic Resistance Threats in the United States, 2019. Atlanta, GA: U.S. Department of Health and Human Services, CDC; **2019**.
2. Lewis, K., Platforms for Antibiotic Discovery. *Nat. Rev. Drug. Discov.* **2013**, *12*, 371-387.
3. Senior, K., Fda Approves First Drug in New Class of Antibiotics. *Lancet* **2000**, *355*, 1523.
4. Wong, P.; Houry, W. A., Chaperone Networks in Bacteria: Analysis of Protein Homeostasis in Minimal Cells. *J. Struct. Biol.* **2004**, *146*, 79-89.
5. Gottesman, S., Proteolysis in Bacterial Regulatory Circuits. *Annu. Rev. Cell Dev. Biol.* **2003**, *19*, 565-587.
6. Sauer, R. T.; Bolon, D. N.; Burton, B. M.; Burton, R. E.; Flynn, J. M.; Grant, R. A.; Hersch, G. L.; Joshi, S. A.; Kenniston, J. A.; Levchenko, I.; Neher, S. B.; Oakes, E. S.; Siddiqui, S. M.; Wah, D. A.; Baker, T. A., Sculpting the Proteome with Aaa(+) Proteases and Disassembly Machines. *Cell* **2004**, *119*, 9-18.
7. Gaillot, O.; Pellegrini, E.; Bregenholt, S.; Nair, S.; Berche, P., The Clpp Serine Protease Is Essential for the Intracellular Parasitism and Virulence of *Listeria Monocytogenes*. *Mol. Microbiol.* **2000**, *35*, 1286-1294.
8. Bottcher, T.; Sieber, S. A., Beta-Lactones as Specific Inhibitors of Clpp Attenuate the Production of Extracellular Virulence Factors of *Staphylococcus Aureus*. *J. Am. Chem. Soc.* **2008**, *130*, 14400-14401.

9. Bottcher, T.; Sieber, S. A., Structurally Refined Beta-Lactones as Potent Inhibitors of Devastating Bacterial Virulence Factors. *Chembiochem* **2009**, *10*, 663-666.
10. Compton, C. L.; Schmitz, K. R.; Sauer, R. T.; Sello, J. K., Antibacterial Activity of and Resistance to Small Molecule Inhibitors of the Clpp Peptidase. *ACS Chem. Biol.* **2013**, *8*, 2669-2677.
11. Flanagan, J. M.; Wall, J. S.; Capel, M. S.; Schneider, D. K.; Shanklin, J., Scanning Transmission Electron Microscopy and Small-Angle Scattering Provide Evidence That Native Escherichia Coli Clpp Is a Tetradecamer with an Axial Pore. *Biochemistry* **1995**, *34*, 10910-10917.
12. Woo, K. M.; Chung, W. J.; Ha, D. B.; Goldberg, A. L.; Chung, C. H., Protease Ti from Escherichia Coli Requires Atp Hydrolysis for Protein Breakdown but Not for Hydrolysis of Small Peptides. *J. Bio. Chem.* **1989**, *264*, 2088-2091.
13. Ye, F.; Li, J.; Yang, C. G., The Development of Small-Molecule Modulators for Clpp Protease Activity. *Mol. Biosyst.* **2016**, *13*, 23-31.
14. Raju, R. M.; Goldberg, A. L.; Rubin, E. J., Bacterial Proteolytic Complexes as Therapeutic Targets. *Nat. Rev. Drug. Discov.* **2012**, *11*, 777-789.
15. Malik, I. T.; Brotz-Oesterhelt, H., Conformational Control of the Bacterial Clp Protease by Natural Product Antibiotics. *Nat. Prod. Rep.* **2017**, *34*, 815-831.
16. Brotz-Oesterhelt, H.; Beyer, D.; Kroll, H. P.; Endermann, R.; Ladel, C.; Schroeder, W.; Hinzen, B.; Raddatz, S.; Paulsen, H.; Henninger, K.; Bandow, J. E.; Sahl, H. G.; Labischinski, H., Dysregulation of Bacterial Proteolytic Machinery by a New Class of Antibiotics. *Nat. Med.* **2005**, *11*, 1082-1087.

17. Conlon, B. P.; Nakayasu, E. S.; Fleck, L. E.; LaFleur, M. D.; Isabella, V. M.; Coleman, K.; Leonard, S. N.; Smith, R. D.; Adkins, J. N.; Lewis, K., Activated Clpp Kills Persisters and Eradicates a Chronic Biofilm Infection. *Nature* **2013**, *503*, 365-370.
18. Carney, D. W.; Schmitz, K. R.; Truong, J. V.; Sauer, R. T.; Sello, J. K., Restriction of the Conformational Dynamics of the Cyclic Acyldepsipeptide Antibiotics Improves Their Antibacterial Activity. *J. Am. Chem. Soc.* **2014**, *136*, 1922-1929.
19. Famulla, K.; Sass, P.; Malik, I.; Akopian, T.; Kandror, O.; Alber, M.; Hinzen, B.; Ruebsamen-Schaeff, H.; Kalscheuer, R.; Goldberg, A. L.; Brotz-Oesterhelt, H., Acyldepsipeptide Antibiotics Kill Mycobacteria by Preventing the Physiological Functions of the Clpp1p2 Protease. *Mol. Microbiol.* **2016**, *101*, 194-209.
20. Michel, K. H.; Kastner, R. E. A54556 Antibiotics and Process for Production Thereof. US patent 4492650, 1985.
21. Sass, P.; Josten, M.; Famulla, K.; Schiffer, G.; Sahl, H. G.; Hamoen, L.; Brotz-Oesterhelt, H., Antibiotic Acyldepsipeptides Activate Clpp Peptidase to Degrade the Cell Division Protein FtsZ. *Proc. Natl. Acad. Sci. U.S.A.* **2011**, *108*, 17474-17479.
22. Kirstein, J.; Hoffmann, A.; Lilie, H.; Schmidt, R.; Rubsamen-Waigmann, H.; Brotz-Oesterhelt, H.; Mogk, A.; Turgay, K., The Antibiotic Adep Reprogrammes Clpp, Switching It from a Regulated to an Uncontrolled Protease. *EMBO Mol. Med.* **2009**, *1*, 37-49.
23. Gersch, M.; Famulla, K.; Dahmen, M.; Göbl, C.; Malik, I.; Richter, K.; Korotkov, V. S.; Sass, P.; Rübnsamen-Schaeff, H.; Madl, T.; Brötz-Oesterhelt, H.; Sieber, S. A., Aaa+ Chaperones and Acyldepsipeptides Activate the Clpp Protease Via Conformational Control. *Nat. Commun.* **2015**, *6*, 6320.

24. Lee, B. G.; Park, E. Y.; Lee, K. E.; Jeon, H.; Sung, K. H.; Paulsen, H.; Rubsamens-Schaeff, H.; Brotz-Oesterhelt, H.; Song, H. K., Structures of Clpp in Complex with Acyldepsipeptide Antibiotics Reveal Its Activation Mechanism. *Nat. Struct. Mol. Biol.* **2010**, *17*, 471-478.
25. Hinzen, B.; Raddatz, S.; Paulsen, H.; Lampe, T.; Schumacher, A.; Habich, D.; Hellwig, V.; Benet-Buchholz, J.; Endermann, R.; Labischinski, H.; Brotz-Oesterhelt, H., Medicinal Chemistry Optimization of Acyldepsipeptides of the Enopeptin Class Antibiotics. *ChemMedChem* **2006**, *1*, 689-693.
26. Goodreid, J. D.; Janetzko, J.; Santa Maria, J. P., Jr.; Wong, K. S.; Leung, E.; Eger, B. T.; Bryson, S.; Pai, E. F.; Gray-Owen, S. D.; Walker, S.; Houry, W. A.; Batey, R. A., Development and Characterization of Potent Cyclic Acyldepsipeptide Analogues with Increased Antimicrobial Activity. *J. Med. Chem.* **2016**, *59*, 624-646.
27. Li, Y.; Lavey, N. P.; Coker, J. A.; Knobbe, J. E.; Truong, D. C.; Yu, H.; Lin, Y. S.; Nimmo, S. L.; Duerfeldt, A. S., Consequences of Depsipeptide Substitution on the Clpp Activation Activity of Antibacterial Acyldepsipeptides. *ACS Med. Chem. Lett.* **2017**, *8*, 1171-1176.
28. Chatterjee, A. K.; Choi, T. L.; Sanders, D. P.; Grubbs, R. H., A General Model for Selectivity in Olefin Cross Metathesis. *J. Am. Chem. Soc.* **2003**, *125*, 11360-11370.
29. Jakobsche, C. E.; Peris, G.; Miller, S. J., Functional Analysis of an Aspartate-Based Epoxidation Catalyst with Amide-to-Alkene Peptidomimetic Catalyst Analogues. *Angew. Chem. Int. Ed.* **2008**, *47*, 6707-6711.
30. Gross, U.; Nieger, M.; Brase, S., A Unified Strategy Targeting the Thiodiketopiperazine Mycotoxins Exserohilone, Gliotoxin, the Epicoccins, the Epicorazines, Rostratin a and Aranotin. *Chem. - Eur. J.* **2010**, *16*, 11624-11631, S11624/11621-S11624/11109.

31. Ghosh, A. K.; Lv, K., A Convergent Synthesis of Carbocyclic Sinefungin and Its C5 Epimer.  
*European J. Org. Chem.* **2014**, 2014, 6761-6768.